CHARACTERISATION OF SALINE GROUNDWATER BASED ON GROUND-BASED TIME-DOMAIN ELECTROMAGNETIC SOUNDINGS IN THE MACHILE RIVER BASIN, SOUTH-WESTERN ZAMBIA

BY

ALICE TEMBO

A thesis submitted to the University of Zambia in fulfillment of the requirements for the degree of Master of Science in Integrated Water Resources Management

THE UNIVERSITY OF ZAMBIA

LUSAKA

2014

Declaration

This dissertation was written and submitted in accordance with the rules and regulations governing the award of the degree of Master of Science in Integrated Water Resources Management of the University of Zambia. I, Alice Tembo, further declare that this dissertation has neither in part nor in whole been presented as substance of award of any degree, either to this or any other University. Where other people's work has been drawn upon, acknowledgement has been made.

Signature:…..... Date:…….....

Approval

This dissertation of Alice Tembo has been approved as fulfillment of the requirement for the award of the degree of Master of Science in Integrated Water Resources Management (IWRM) by the University of Zambia (UNZA).

Signature:

Chairperson……

1st Examiner……...

2nd Examiner……..……

External Examiner…….…

Abstract

Much of southern Africa is semiarid and heavily dependent on groundwater resources. However, access to safe and clean water is an important feature of the natural environment, a human right and a basic requirement for economic development. Like in other parts of the Kalahari Basin, parts of Sesheke and Kazungula districts have significant groundwater salinity problems which affect the use of groundwater as a freshwater resource. This study mapped the spatial distribution of saline groundwater in order to enhance the overall understanding of its existence. The study was undertaken in the Machile River Basin which is a topographic depression located partly in Sesheke District in the Western Province and partly in Kazungula District in the Southern Province of Zambia. The ground-based Time-Domain Electromagnetic (TDEM) method, based on the Maxwell's equations, was used in the study for data collection and the SiTEM-SEMDI software for data analysis. Other software used include ArcGIS and Geoscene3D for spatial data analysis and geological modelling, respectively. Research findings indicate that rock formation resistivities increase with depth as follows: 3,173Ωm at 10m, 10,616Ωm at 30m, 17,186Ωm at 50m and 19,738Ωm at 80m. The extent of saline groundwater with low resistivities of less than 35Ωm was less at 10m depth and more at 30, 50 and 80m and that salinity was concentrated around the depression bordering the two districts stretching from the Zambezi River going up in the northern direction, suggesting that 10m is generally the appropriate depth to drill for fresh groundwater. It was also observed that the subsurface formation of the Machile River Basin comprises the unconsolidated Kalahari sediments underlain by sandstones of the Barotse Formation of the Kalahari Supergroup which is also underlain by rocks of the Karoo (Batoka Basalts) and Basement Complex such as granites, gneisses and schists. It is therefore concluded that the increase in resistivities of formations with depth indicates the presence of formations ranging from sand, sandstone, basalts, granites and other rocks of the Undifferentiated Karoo and Basement Complex. It is also concluded that saline groundwater mostly exists in unconsolidated Kalahari sediments and sandstones.

Dedication

To my daughter: Blessed Hazel Mwanza, my parents: Mr. Alfred Tembo and Mrs. Alidess Stella Miti Tembo, my brothers: Dr Gelson Tembo, Nathan, Festus and Shadreck and to my sisters: Rachael and Aliness Tembo.

Your rare combination of excellence and humility always inspire me…….

Acknowledgements

First and foremost, I wish to thank God for his abundant love and protection during my two years stay in Lusaka to undertake this study.

I am immeasurably grateful to my Principal Supervisor, Prof. Imasiku. A. Nyambe who is also Director, Directorate of Research and Graduate Studies (DRGS) and Coordinator, IWRM Centre, UNZA. I am also thankful to Associate Prof. Peter Bauer-Gottwein of Denmark Technical University (DTU) for professional guidance during geophysical data analysis for this thesis. I am equally grateful to Mr. Mkhuzo Chongo, a PhD student at DTU for additional professional guidance. I also wish to acknowledge, with thanks Ms. Ingrid Mugamya Kawesha, IWRM Centre for helping with the accounts, logistics and ensuring progress in my studies.

The generosity of the Danish International Development Agency (DANIDA) and Ministry of Mines, Energy and Water Development (MMEWD) in collaboration with UNZA, IWRM Center cannot be overemphasized, for without them, I might not have had the opportunity to pursue this programme. Special thanks also go to the Acting Provincial Water Officer-Copperbelt, Mr. Moses Gondwe, for being extremely helpful.

I would like to extend my sincere gratitude to my elder brother Dr. Gelson Tembo and his wife Mrs. Doreen Goma Tembo for their immeasurable support. I also wish to thank my dear daughter, Blessed Hazel Mwanza for her patience and endurance during the period of the study.

Lastly, many more thanks go to my fellow IWRM students Mr. Wilson Mwandira for his tireless encouragement and support during the entire period of the study. More thanks go to all those individuals that played a part in my studies.

Table of Contents

List of Figures

List of Tables

List of Abbreviations and Acronyms

ABEM	Manufacturer of a WalkTEM equipment.
ArcGIS	Software for spatial data analysis
BGR	Bundesanstalt fur Geowissenschaften und Rohstoffe (Federal Institute for Geosciences and Natural Resources)
CSO	Central Statistical Office
CVES	Continuous Vertical Electrical Sounding
DANIDA	Danish International Development Agency
DNRM	Department of Natural Resources Mines
DTU	Denmark Technical University
EM	Electromagnetic
EMF	Electromagnetic Force
ET	Evapotranspiration
FAO	Food and Agricultural Organization
GIS	Geographical Information System
GPS	Global Positioning System
GRZ	Government of the Republic of Zambia
GSD	Geological Survey Department
HGG	Hydrogeophysics Group
HWSD	Harmonized World Soil Database
IDENT	Identity
I-GIS	Integrated Geographic Information System
IGRAC	International groundwater Resources Centre
IWRM	Integrated Water Resources Management
JICA	Japanese International Cooperation Agency
MEWD	Ministry of Energy and Water Development
MMEWD	Ministry of Mines, Energy and Water Development
MRB	Machile River Basin
NE	North East
NCSR	National Centre for Scientific Research
NW	North West
OKACOM	Okavango River Basin Commission
OKZ	Okavango Zambezi Axis

PET	Potential Evapotranspiration
RC	Receiver Coil
RO	Reverse Osmosis
SABONET	Southern Africa Botanical Diversity Network
SE	South East
SEMDI	Single Site Electromagnetic Data Inversion
SEBS	Surface Energy Balance System
SiTEM	Single site TEM data processing
SRTM	Shuttle Radar Topography Mission
SW	South West
STD	Standard Deviation
TDEM	Time-Domain Electromagnetic Method
TEM	Transient Electromagnetic
UK	United Kingdom
UNZA	University of Zambia
USEPA	United States Environmental Protection Agency
USGS	United States Geological Survey
UTM	Universal Transverse Mercator
ZFD	Zambia Forestry Department
ZMD	Zambia Meteorological Department

CHAPTER 1: INTRODUCTION

This chapter presents the background of the study, statement of the problem, objectives, significance of the study, description of the study area and the organization of the thesis.

1.1 Groundwater Usage

The distribution of groundwater is said to be uneven from areas of severe aridity like the Sahara in the north and the Kalahari in the south as the continent suffers from one of the most unstable rainfall regimes in the world (Donkor, 2003). Accessibility to clean, safe and affordable water is an important feature of the natural environment, a human right and a basic requirement for economic development because time is freed up to focus on income generating activities rather than fetching water. However, the safest and major world source of water supply is groundwater, which refers to all water below the surface in the layers of the earth's crust (Kirsh, 2006). About 50% of drinking water and the majority of irrigation water in the world is as a result of groundwater supplies. Conversely, the quality of these water resources is one of the major questions that face the world (Quevauviller, 2008). The International Groundwater Resources Assessment Centre (IGRAC) (2009) concluded that groundwater salinity is one of the most widespread water quality problems facing the world today. Much of Southern Africa is semi-arid and heavily dependent on groundwater resources. In the semi-arid to arid Kalahari Basin, water is a scarce resource as well as a valuable commodity and the only source of permanent water around central and southern Kalahari (Haddon, 2005). Similarly, in most parts of rural Zambia, groundwater is the most reliable source of drinking water and water for all other economic activities. Though replenished by precipitation, it is unevenly distributed in both quantity and quality depending on the local climate and the geology (MEWD-JICA, 1995).

1.2 Groundwater Salinity in Arid and Semi-Arid Zones

Arid and semi-arid regions cover about one third of the world’s land area and are inhabited by 400 million people (Williams, 1999). These arid and semi-arid regions are under increasing human pressure because water resources are in short supply. Poor quality of these water resources due to rising salinity is a critical factor limiting economic development (Harter, 2005). Groundwater salinity is a general term used to describe the presence of elevated levels of different salts such as sodium chloride,

magnesium and calcium sulphates and bicarbonates in groundwater (Department of Natural Resources and Mines (DNRM), 2004). About 1.1 billion people live in areas with groundwater salinity at shallow and intermediate depths from various generic sources and global groundwater regions (IGRAC, 2009). Salinity is defined as increase in the content of dissolved solids and these may vary from place to place and in terms of concentration levels. It is one of the significant groundwater supply problems which affect its use as a freshwater resource especially under arid climatic conditions (Kirsh, 2008). The accumulation of salt in groundwater in arid and semi-arid environments plays a major role in people's living conditions because the water becomes unsafe for human consumption (Christiansen, 2007). According to IGRAC (2009), saline groundwater is mostly present in stagnant conditions at greater depths and may have been there for thousands or millions of years. The rate of increase or decrease in salinity is much lower in deeper layers as compared to shallow layers in the aquifer. It is stored in geological layers that are not actively involved in the hydrological cycle. Based on this principle, IGRAC (2009) concluded that saline groundwater is comparatively old because it is not actively recharged.

1.3 Geophysical Investigations of Saline Groundwater in the Machile River Basin

Groundwater investigation is interdisciplinary in nature and is vital for provision of good quality water. Geomorphologists, hydrogeologists, social scientists, remote sensing specialists, geophysists and geologists all have potential roles to play in groundwater investigations (IGRAC, 2009). However, this study is concerned with the perspective of a geophysist to map the spatial distribution of saline groundwater in the Machile River Basin using the ground-based Time Domain Electromagnetic (TDEM) method. Chongo et al (2011) mapped part of the Machile River Basin which lies in Sesheke within the Barotse Basin using the same method, leaving the Kazungula side unmapped. The results indicated that the south-eastern part of the area was underlain by a saline aquifer which affected groundwater quality. This study, therefore, undertook a geophysical field campaign in Kazungula and combined the data with the existing Sesheke data in order to enhance the overall understanding of the existence of saline groundwater in the entire Machile River Basin.

1.4 Statement of the Problem

The occurrence of saline groundwater in the Machile River Basin has proved to be a limiting factor for water supply to the community. The area has a significant population of people in need of access to safe and affordable drinking water. Being in a semi-arid environment, streams and rivers are seasonal and do not flow all year round. In this regard, the rural population within the basin is dependent on groundwater through drilling of boreholes and/or construction of water wells. Since the rural population within the basin is hugely dependent on groundwater resources, it is of great significance to identify and understand the physical occurrence and distribution of groundwater salinity for the entire Machile River Basin. This knowledge is important as it gives a basis to determine the extent of saline groundwater problem in affected areas.

1.5 Objectives

The objectives of this study were:

(i) To map and interpret the distribution of electrical resistivities in the subsurface using the ground-based Time Domain Electromagnetic (TDEM) method on a regional scale in the Machile River Basin in South-Western Zambia;

(ii) To develop a spatial distribution map of saline groundwater based on electrical resistivities from ground-based TDEM measurements in the Machile River Basin in South-Western Zambia; and

(iii) To develop a geological model of the Machile River Basin based on existing borehole geological data in South-Western Zambia.

1.6 Research Questions

The research questions of this study were:

(i) What are the variations of electrical resistivities within the subsurface of the Machile River Basin in South-Western Zambia?

(ii) What is the distribution of saline groundwater from the perspective of electrical resistivities in the Machile River Basin in South-Western Zambia? and

(iii) What is the geological model of the Machile River Basin in South-Western Zambia based on existing borehole geological data?

1.7 Significance of the Study

The rationales for this study are:

(i) To provide information to government on the occurrence and distribution of saline groundwater in the Machile River Basin through the Ministry of Local government and housing and Ministry of Mines, Energy and Water Development in order to manage salinity problem efficiently;

(ii) To provide background information to researchers, water resources specialists, policy makers and the general public on the extent, distribution and severity of groundwater salinity in the basin covering parts of Sesheke and Kazungula districts;

(iii) To provide recommendations on the appropriate areas for and depths to fresh groundwater resources, and so doing help improve success rates of drilling for fresh supply of good quality drinking water for the rural populace in the basin; and

(iv) To provide information that will offer solutions for access to safe and clean drinking water for both the present and future generations.

1.8 Description of Study Area

This sub-section presents the location and description of the area where this study was undertaken. It includes the location, climate, geology, hydrology, soils and the vegetation type.

1.8.1 Location of the Study Area

The Machile River Basin is located on the southern plateau of the country between Latitude 16º0′0″S to 18º0′0″S and Longitude 24º0′0″E to 27º0′0″E with an elevation of 1310m above sea level (amsl) on the highest point and 882m amsl on the lowest point (Figure 1). The Machile River Basin is a topographic depression located partly in the Sesheke District in the Western Province and Kazungula District in the Southern Province of Zambia (Martinsen, 2012) within an area of approximately 16,000km^2. It is bounded on the south by the Zambezi River as far west as Katima Mulilo and the international boundary with the Caprivi Strip in Namibia. The basin was formed in response to down-warping of the interior of the Southern Africa terrain (Haddon, 2005). The topographic map was prepared based on Shuttle Radar Topography Mission (SRTM) data (United States Geological Survey (USGS), 2010).

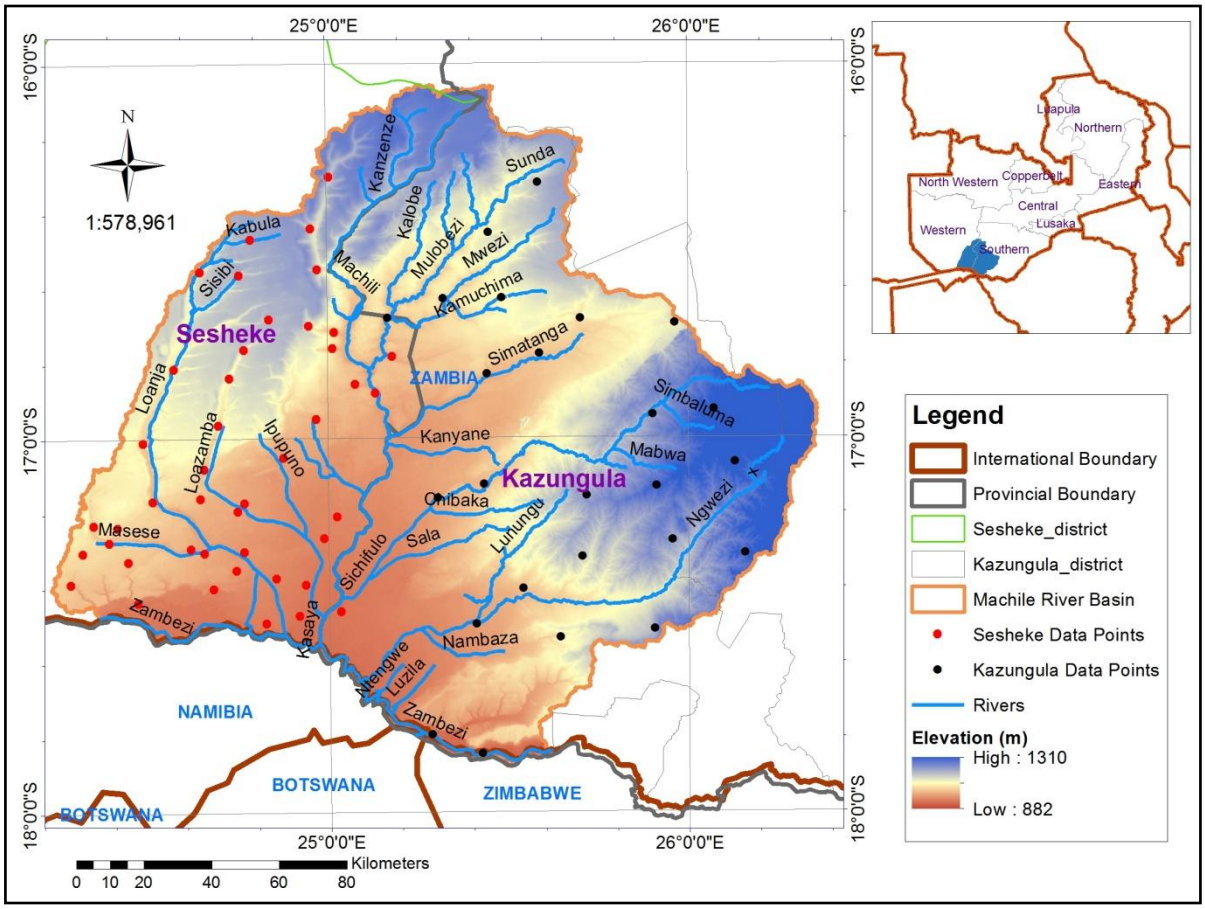

Figure 1: The elevation model over the study area between Sesheke and Kazungula districts, South Western Zambia (modified after USGS, 2010)

1.8.2 Climate

The climate in Zambia has three marked seasons: There is a cool dry season from May to August in the western part with a mean high monthly temperature of 18ºC or less during the coldest month of July followed by the hot dry season from September to November registering average high monthly temperatures of 24ºC or higher from October to November (Zambia Meteorological Department (ZMD), 2013) (Figure 2). Mean low monthly temperature range from 2°C in the coldest month of July to 20°C in the hottest month of October (Figure 2). Temperatures are very extreme from September to February with the absolute maximum of over 28ºC. During the winter nights, radiation from the sand gives rise to very low night temperatures (ZMD, 2013).

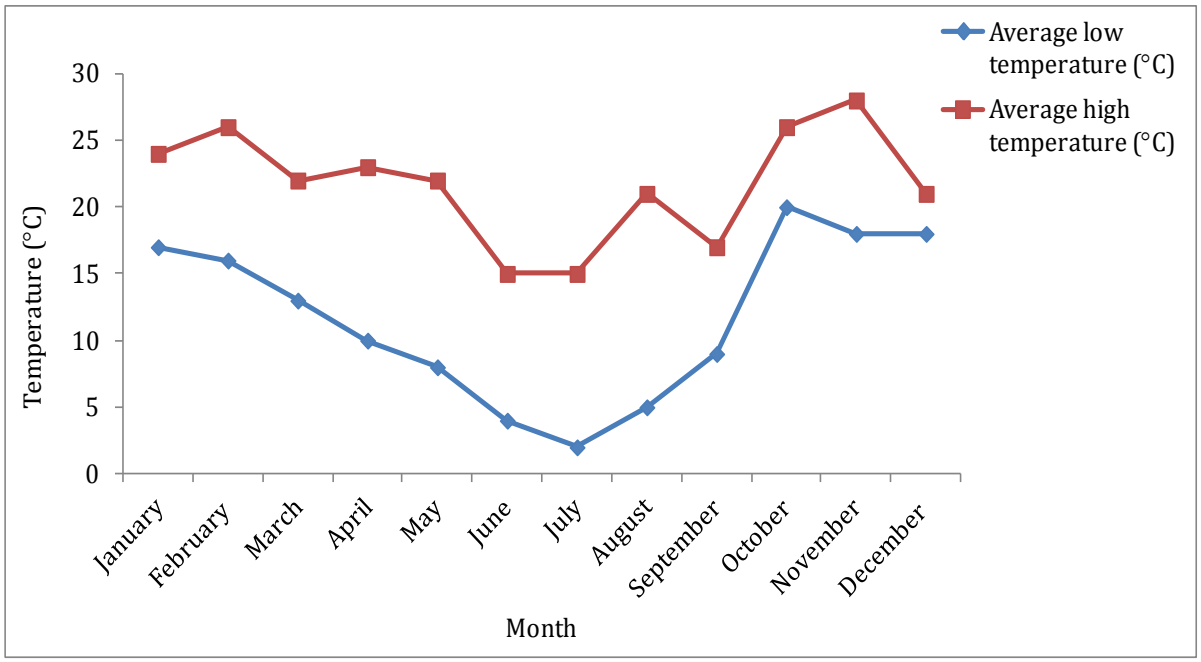

Figure 2: Annual low to high mean temperatures of the Machile River Basin in South-Western Zambia from 1963 to 2013 (after ZMD, 2013)

The three climatic or agro-ecological regions in Zambia are the low rainfall on the southern part, medium rainfall on the middle part of the country and high rainfall on the northern part (MEWD, 2009). The study area falls within the low rainfall region of the country with a dry sub-humid climate within the semi-arid climate of the Kalahari Basin in Southern Africa (Fanshawe, 2010). It is located in the 'Agro-ecological Region I' within the low rainfall region of Zambia with annual rainfall of approximately 600mm. The area receives erratic and high intensity rainfall causing frequent drought and moisture stress (Government of the Republic of Zambia (GRZ), 2010). The rainy season is generally spread over the period of October to April recording an average monthly precipitation of 18mm at the beginning of the season and 47mm at the end of the season (Figure 3). February has the highest average monthly precipitation of 120mm (ZMD, 2013) (Figure 3).

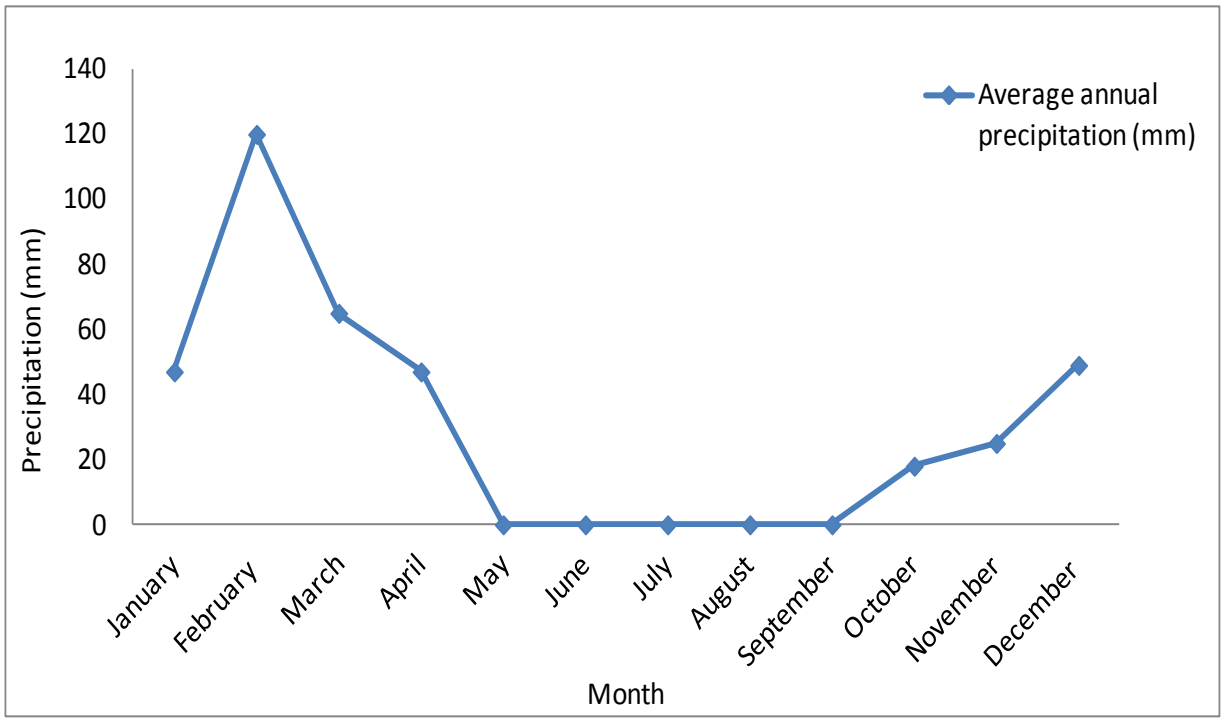

Figure 3: Annual precipitation of the Machile River Basin, South-Western Zambia from 1963 to 2013 (after ZMD, 2013)

1.8.3 Geology

This sub-section presents the description of the regional and local geology within which the Machile River Basin lies.

(i) Regional Geology of the Study Area: The study area lies within the Kalahari Basin of Sub-Saharan Africa which extends over Namibia, Botswana, Angola, Democratic Republic of Congo, Zambia, Zimbabwe and South Africa (FAO, 2010). The area is underlain by the Kalahari Group sedimentary rocks which were deposited in a large basin stretching for 2200km from South Africa in the south northwards through Botswana and Angola and across Zambia into the Democratic Republic of Congo (Haddon and McCarth, 2005; Money, 1972). The Kalahari Basin is believed to have been formed in the Late Cretaceous as a result of the down-warp of the terrain in Southern Africa. This down-warp movement of the interior terrain led to the formation of the Kalahari Basin and the deposition of the sediments of the Kalahari Supergroup. The sediments were predominantly deposited by rivers in the Late Cretaceous and Early Tertiary with later aeolian reworking of the uppermost unconsolidated sands occurring during the Pliocene and Quaternary. The deposited sediments included gravels, sand and other finer materials which later formed inter-beds. Sandstone and clays were also

deposited into the basin filling up lakes in the process. The Kalahari Supergroup and Karoo Supergroup sedimentary rocks were also exposed to erosion due to the uplift in the Pliocene. The eroded material was then washed into the Kalahari Basin where it was later re-transported and re-deposited by aeolian processes forming sand dunes during drier periods. The largest body of sand with maximum sediment thickness of 450m on earth is believed to have been formed from the unconsolidated sands of the Kalahari Supergroup (Haddon and McCarthy, 2005). The regional geology is characterized by sandstone which is overlain by sand and underlain by rock types of the Karoo and Basement Complex (Money, 1972). The Karoo comprises formations from bottom to top as Batoka Basalt, Mudstone, Sandstone, Luampa Coal and Gwembe Coal whereas the Basement Complex includes granites, gneisses, schist and migmatites (Money, 1972) (Figure 4).

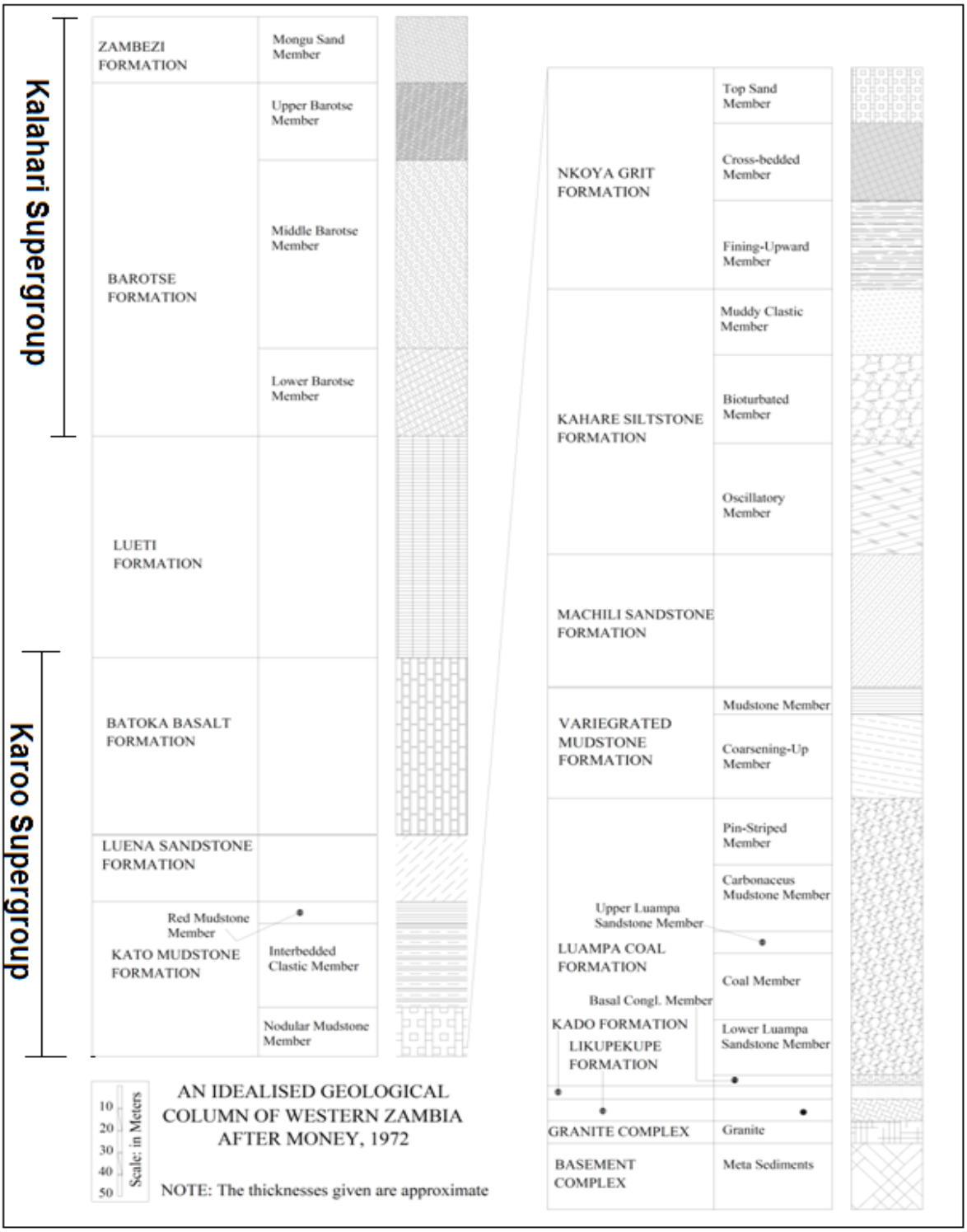

Figure 4: Stratigraphic log of Western Zambia (after Money, 1972)

(ii) Local Geology of the Study Area: The Machile River Basin contains rock formations ranging from alluvium, colluvium, laterite, fossil sief dunes, basalts, granite, igneous meta-igneous, undifferentiated granite gneiss and schists [Geological Survey

Department (GSD), 1981] (Figure 5). They are described based on the geology legend in Figure 5 and are not in a stratigraphic order.

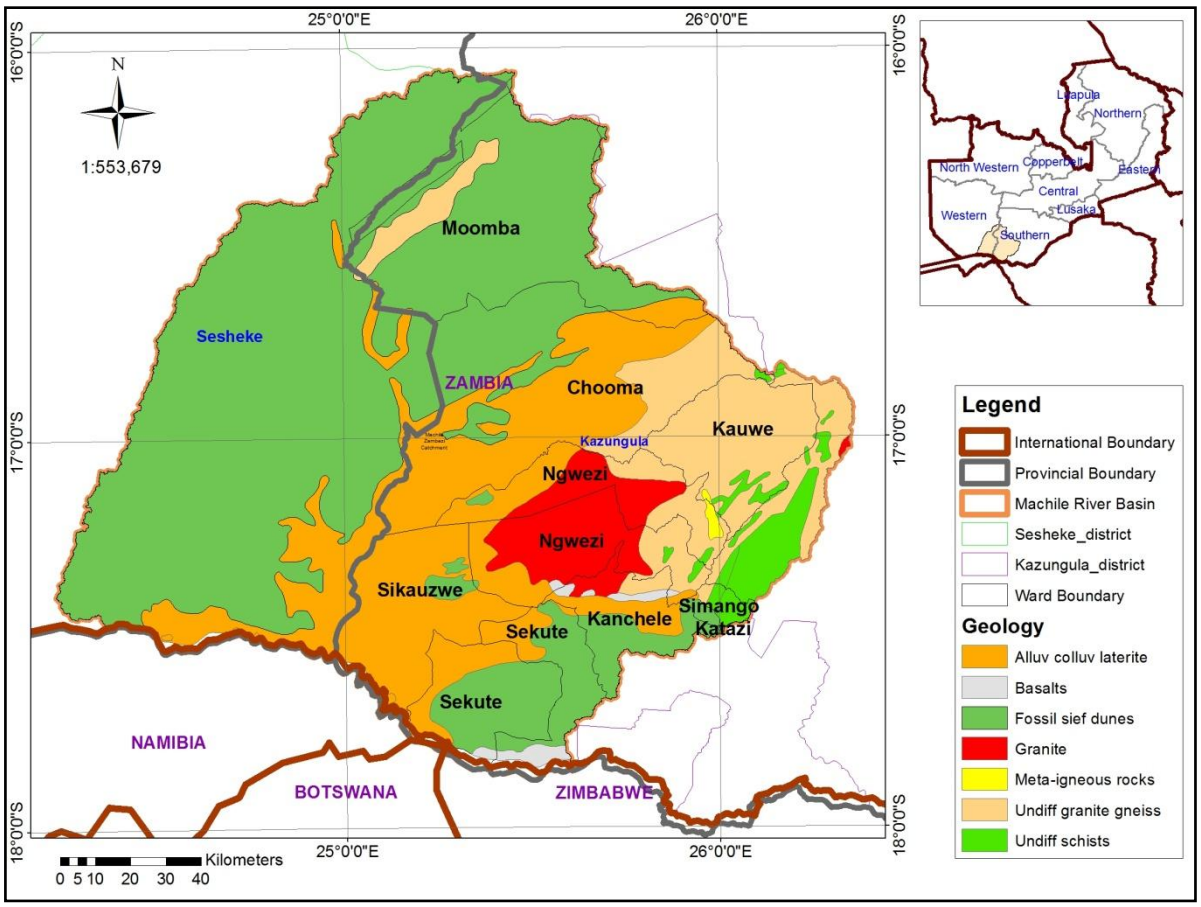

Figure 5: The geological map of the Machile River Basin in South-Western Zambia (after GSD, 1981)

(a) Alluvium, Colluvium and Laterite: These sediments cover the second largest area right from Simungoma through to Chooma wards (Figure 5). The alluvium and colluvium are unconsolidated or semi-consolidated clastic sediments of Cenozoic age (i.e. less than 20 Million years) (GRZ, 2007). These sediments come from the Kafue and Zambezi rivers and flood plain material in a large variety of grain size distribution. There are several local deposits of recent alluvium and lacustrine clays (Phiri, 2005). The DNRM (2004) defined alluvium as the surplus rock material (mainly sand and silt) deposited by rivers in their valleys. The laterite profile consists of clay, sandy clay and clayey sand (GRZ, 2007).

(b) Fossil Sief Dunes: Most parts of the western side of the study area are covered by Fossil Sief Dunes. To the south-west, west and north-west, Fossil Sief Dunes are present extending from the Zambezi River in the south-west to Luamuloba and Moomba areas in the north and parts of Sekute Ward in the south-east (Figure 5). These belong to the Kalahari Supergroup predominantly consisting of unconsolidated or consolidated sand that was eroded, transported and deposited mainly by winds to form fossil dunes (Money, 1972). The Kalahari Supergroup is overlain by a thick mantle of aeolian sands which are evident in the Western and Southern parts of the country (Phiri, 2005). Gravel, silt and clay are minor deposits within the sequence. The Fossil Sief Dunes, covering Western and parts of Southern Zambia, are of Quaternary and Cenozoic age (Money 1972; GRZ, 2007).

The Kalahari Supergroup, which is subdivided into sandstones and quartzites of the Barotse Formation, and the unconsolidated sands of the overlying Zambezi Formation are Post-Cretaceous in age (Money, 1972). The nature of the Tertiary-Quaternary deposits, according to Money (1972), suggests that the climate, over this part of Zambia, has been variable since the Miocene-Pliocene times, and that periods of heavy rainfall gave rise to fluviatile deposits in wider valleys. However during more arid periods loose sands were transported by wind to form a blanket over most parts of the region. Savory (1963), also, assumed a complex and multi-genetic origin for the surface sands and suggested that sands in Sesheke were as a result of Late Tertiary erosion of the Upper Karoo sediments deposited in shallow seasonal basins which were later reworked by the wind action during arid periods.

(c) Basalts: These belong to Batoka Basalt Formation which crop out in a small area around Kanchele and Ngwezi (Figure 5). They are within the Karoo Supergroup in the Early Jurassic and Triassic periods of the Mesozoic Era and the Permian Period of the Palaezoic Era. The Karoo formations are divided into the Lower and Upper Karoo on the lithostratigraphic basis (Money, 1972). The Upper Karoo Group comprises mainly the Batoka Basalts, sandstone, mudstone and other sedimentary formations which are overlain by the Batoka Basalt Formation and overly older rocks ranging in age from Precambrian to Lower Karoo (GRZ, 2007; Money, 1972). According to Nyambe (1999), the basalts are present in the southern part of the Barotse Basin to which the study area is a part. The Karoo Supergroup deposits are related to rifting

accompanied by the establishment of large scale graben systems. The basalts range in colour from reddish-purple to dark greyish-green and their origin is related to the break-up of the Gondwana Continent and the associated drift which started at the Carboniferous time (300 Million years ago) and continued until Early Jurassic. The age and character of the basalts suggest that they were erupted along fissures with little explosive activity. The Lower Karoo starts with sandstone followed by the Luampa Coal, and Mudstone Formation (Money, 1972). At the beginning of the Upper Karoo Group was deposited the sandstone, siltstone and mudstone. These clastic sediments are topped by the Early Jurassic Batoka Basalt Formation which is the youngest member of the Karoo Supergroup (GRZ, 2007; Money, 1972).

(d) Granite: Granites are presumed to be contained in the Basement Complex of the Palaezoic to Precambrian Era (Money, 1972). Granites are a kind of igneous rocks containing quartz, feldspar & mica. The granites crop out around Ngwezi Ward in the south-eastern part of the study area (Figure 5).

(e) Meta-Igneous Rocks: They are interpreted to be the metamorphic rocks that were once igneous and changed form due to heat and pressure. They cover the smallest stretch of the study area around Ngwezi (Figure 5). Igneous rocks could be granite, diorite, gabbro, periodotite or pegmatite in nature (GRZ, 2007).

(f) Undifferentiated Granite-Gneiss: These are a mixture of granite and gneiss which are contained in the rocks of the Basement Complex of Precambrian age (Money, 1972). These overlie the Kauwe Ward and parts of the surrounding areas. A stripe of the undifferentiated granite-gneiss was also observed in Moomba Ward up north (Figure 5).

(g) Undifferentiated Schists: The undifferentiated schists only occur in few patches on the southeastern corner of the study area (Figure 5). These are Neoproterozoic rocks between 900 and 543 Million years old (GRZ, 2007) in the Basement Complex of Precambrianage (Money, 1972). Due to major tectonic events after their deposition, they have undergone metamorphism of different degrees. The Kafue Rhyolith and the Nazingwe Formation are the earliest volcanic deposits within a rift environment and are metamorphosed up to amphibolites facies (GRZ, 2007).

1.8.4 Hydrology

The Machile River Basin is a sub-catchment within the Zambezi River Basin of Zambia. It was formed out of combination of three sub-catchments namely Machile, Loanja and Ngwezi river basins (Figure 6).

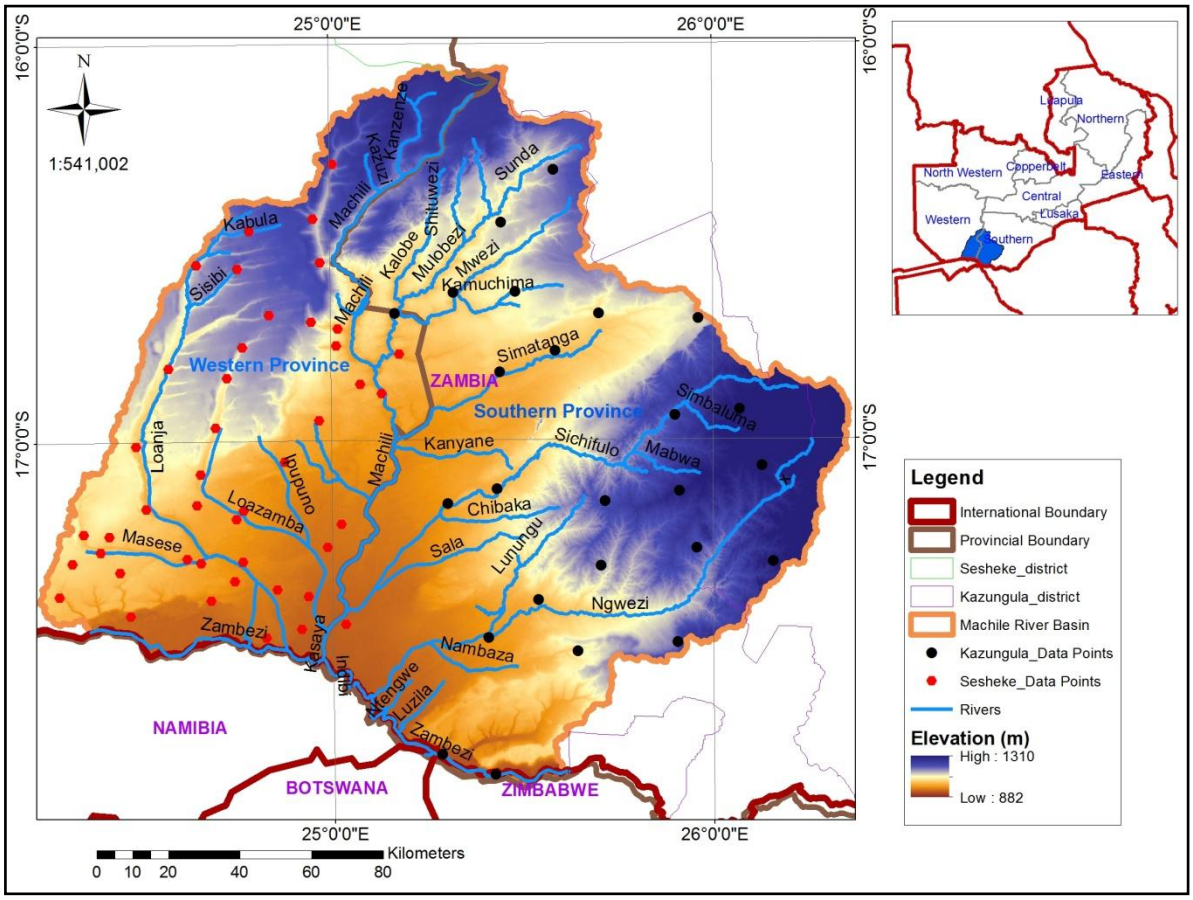

Figure 6: The hydrology of the Machile River Basin in South-Western Zambia

The hydrology of the Machile River Basin is determined by the annual variation of summer rainfall, which is influenced by the movement of the Intertropical Convergence Zone (Coppinger and Williams, 1991). It is controlled mainly by Machile, Mulobezi, Simatanga, Kanyane, Loazamba, Sichifulo, Loanja and Ngwezi rivers (Figure 6). Summer rainfall is further influenced by man through draining of wetlands for agricultural and domestic landuse and evaporation during warm seasons (Coppinger and Williams, 1991). The development of the drainage system that led to the formation of saline groundwater in South-Western Zambia is briefly described below.

(i) The Post Cretaceous Development of the Drainage System in Southern Africa: During the Upper Jurassic to Cretaceous, the Palaeo-Okavango, Cuando and Zambezi-Luangwa rivers formed headwaters of the Limpopo River System (Moore and Larkin, 2001) (Figure 7). The upper Zambezi River System formerly emptied into the Indian Ocean via the Limpopo River (Moore and Larkin, 2001).

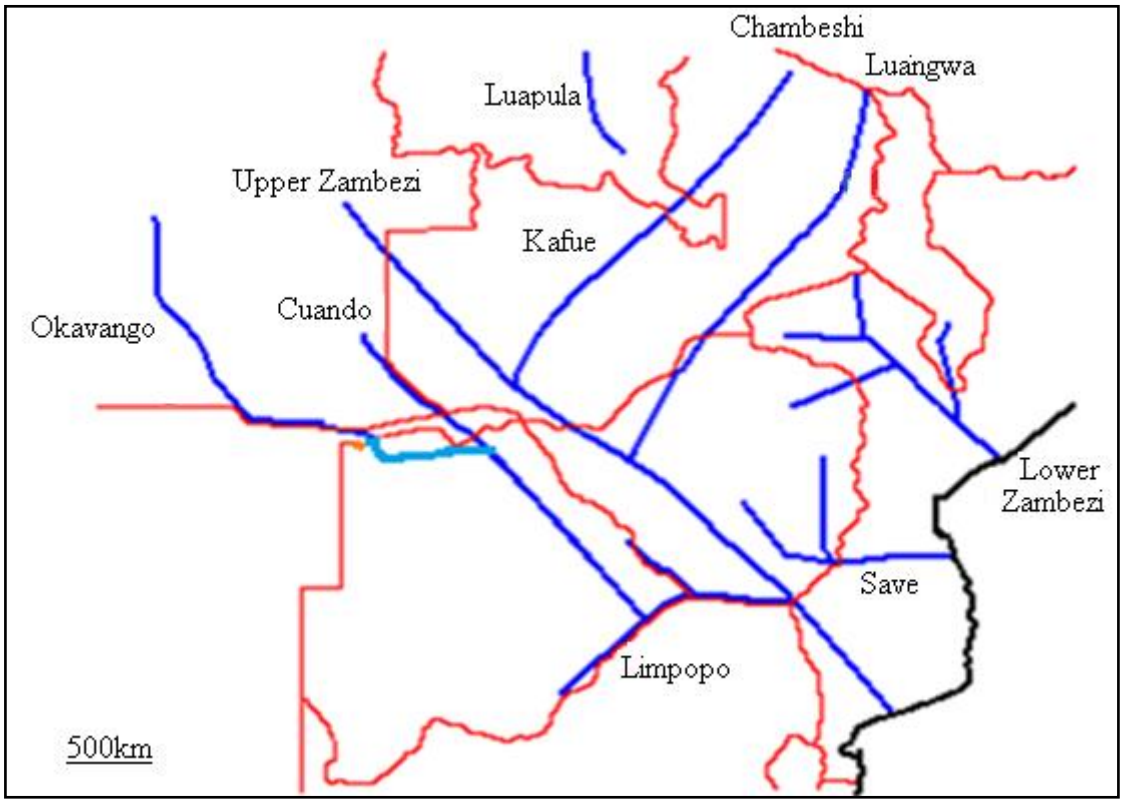

Figure 7: The Palaeo-Okavango River as a part of the Limpopo River system and the Upper Zambezi Catchment during the Late Cretaceous Period in Southern Africa (Moore and Larkin, 2001)

From the end of the Cretaceous to Mid Pleistocene, the Palaeo-Okavango, Cuando and the upper Zambezi rivers were cut off from the Limpopo River (Moore and Larkin, 2001), sustaining the palaeo-lake system (Moore et. al., 2012) (Figure 8). This link was disrupted by the uplift of the Okavango-Kalahari Zimbabwe axis in the Late Palaeogene, which severed the links between the Limpopo and the Okavango, Cuando and Zambezi-Luangwa resulting in a senile endoreic drainage system which supplied sediments to the Kalahari Basin (Moore and Larkin, 2001). The initiation of the endoreic drainage system led to the deposition of the fluvitile and lacustrine Kalahari Supergroup formations into the Kalahari Basin (Moore et al., 2012). The dramatic

decrease in the sediment supply to the Kalahari Basin followed the diversion of the Upper Zambezi drainage network into the Mid Zambezi River (Moore et. al, 2012) (Figure 8).

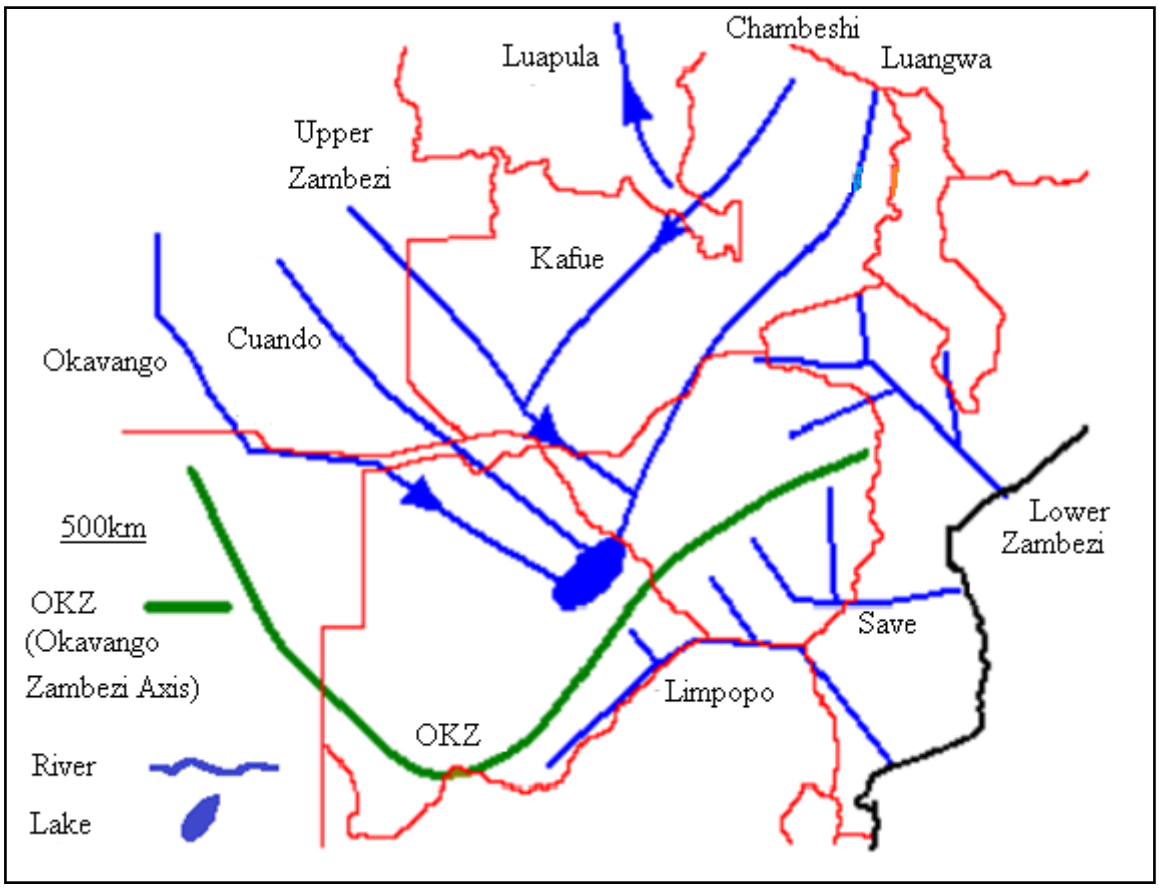

Figure 8: Palaeo-Okavango River and the Upper Zambezi Catchment cut-off from the Limpopo River system during the Palaeogene to Mid Pleistocene Periods in Southern Africa (after Moore and Larkin, 2001)

The uplift, however, rejuvenated the Lower Zambezi initiating capture of the Luangwa, Upper Zambezi and Kafue (Figure 9). The Lower Zambezi-Shire formed a separate graben-bound river system with a discharge point into the Indian Ocean through the mouth of the present day Zambezi. During the Pleistocene period, the Okavango Basin was detached from the Zambezi River (Figure 9) as the influence of the East African Rift System spread westwards (Moore and Larkin, 2001).

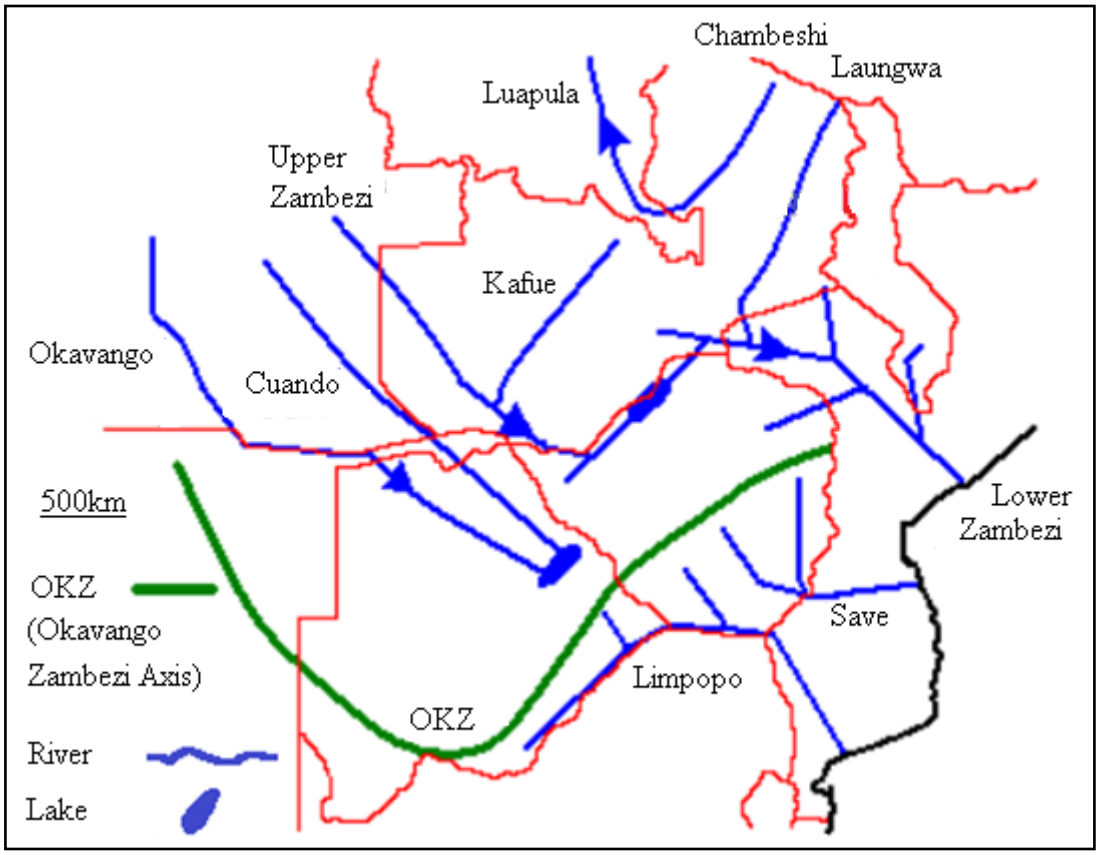

Figure 9: The Okavango Basin detached from the Zambezi River during the Mid-Late Pleistocene Period in Southern Africa (after Moore and Larkin, 2001)

According to FAO (2010), the present day situation is that the Cuando River is detached from the Okavango River System and attached to the Zambezi River (Figure 10).

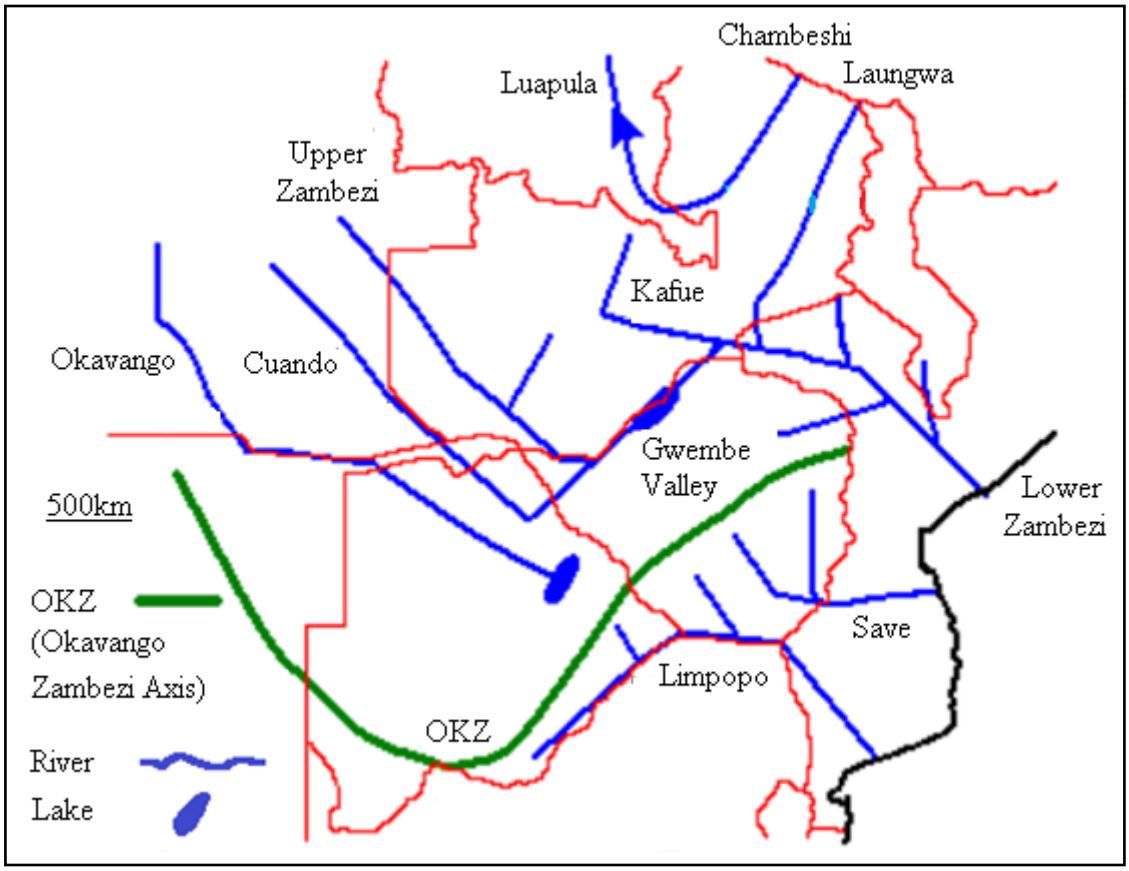

Figure 10: The Cuando River detached from the Okavango River system and attached to the Zambezi River in Southern Africa (Moore and Larkin, 2001)

As the hydrological regime became seasonal, it was predicted that large parts of the palaeo-drainage system became ephemeral and fragmented into a series of closed (endorheic) basins in some places (Moore and Larkin, 2001). A Palaeo-Lake system is believed to have been formed due to the disrupted flow of the Okavango, Cuando and Upper Zambezi rivers into the Indian Ocean through the Limpopo River System in the Mid Pleistocene Period (Moore et al., 2012). According to Money (1972), even if many present landscape features point to an arid climate in the recent past, the geomorphological characteristics such as rapids, retreating waterfalls, wide valleys with misfit streams, river terraces and abrupt changes in river courses indicated the fluctuations on rainfall and minor tectonic adjustments.

(ii) The Zambezi River Basin: The Zambezi River Basin extends over a territory of eight countries (Zambia, Angola, Namibia, Botswana, Zimbabwe, Malawi, Tanzania and Mozambique) covering a catchment area of 1,320,000km^2 with a cumulative mean annual flow of 97km^3 making the Zambezi River the largest to discharge into the Indian

Ocean from the African Continent and the largest in Southern Africa (Gupta, 2007; Coppinger & Williams, 1991). The part of the Zambezi River which falls within Zambia is divided in to three river basins i.e. the Zambezi, Kafue and Luangwa. These three are further sub-divided into sub-catchments. One example of such sub-catchments is the Machile River sub-basin, which is part of the Zambezi River Basin.

1.8.5 Soils

The area is mostly covered by sand of the Kalahari type, probably underlain by Karoo rocks and patches of silty grey alluvium in plains. Soils of the Kalahari Basin are deep sands presumed to be of aeolian origin (Phiri, 2005). Much of the sand was deposited in lakes formed by the ponding of the Upper Zambezi and subsequently reworked by wind action. These sands are of Pleistocene age and are not very fertile but where they are well drained, they support excellent growth of trees. The sands have the ability to conserve the entire season's rainfall to such an extent that damp soil is found, locally within 1m of the sub-surface around September and October (Fanshawe, 2010). Soil units such as podzols, planosols, acrisols, arenosols, leptosols and luvisols are predominant in the study area with podzols covering most parts of Sesheke and the rest covering parts of Kazungula (Figure 11). The less predominant soil types are gleysol, vertisol, lixisols and cambisols. Gleysols are mostly found around water bodies (Figure 11).

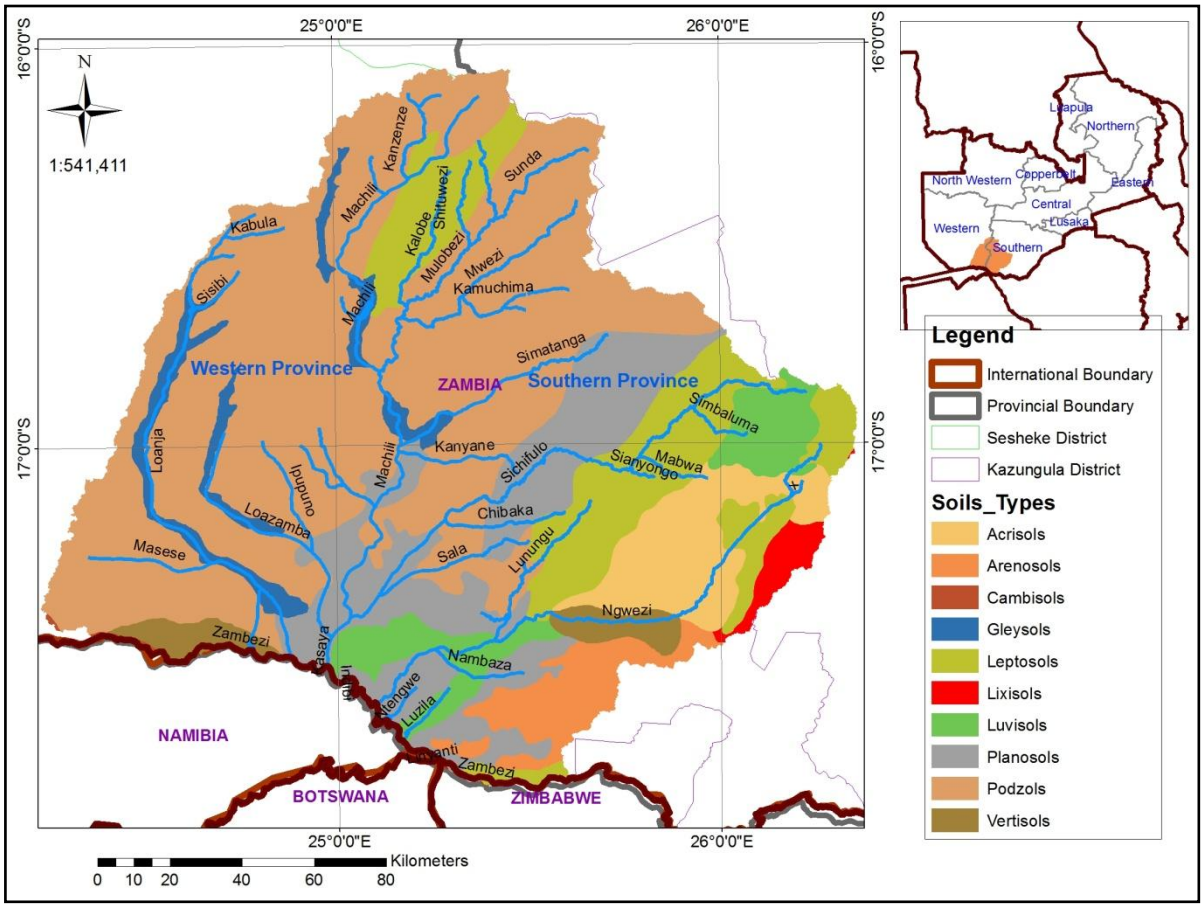

Figure 11: Map showing soil units of the Machile River Basin, South-Western Zambia (after GSD, 1981)

(i) Podzols (PZ): Podzols have a largest coverage of the study area. They are predominant on the western part (across the Machile River on the south-west and Simatanga Stream on the north-eastern parts) (Figure 11). They contain mostly loose sandy soils with a sub-horizon continuously cemented by organic matter with iron or aluminium (FAO, 2009). They are somewhat excessively drained, very deep and are present around Sesheke area in western Zambia.

(ii) Planosols (PL): Planosols are temporary water saturated topsoil on slowly permeable subsoil (FAO, 2009). They are poorly drained, very deep, dark grey, clayey to fine clayey soils abruptly underlying a sandy loam to silty clay loam soil. These are present on the southern middle part of the study area and beyond Sichifulo River in the south-eastern part. (Figure 11).

(iii) Acrisols (AC): Acrisols are fine loamy to clayey soils. They are soils with subsurface accumulation of low activity clays and low base saturation (FAO, 2009), in the subsoil than in the topsoil as a result of pedogenetic processes (especially clay migration). They are found in Kazungula covering the area between Ngwezi and Sichifulo rivers (Figure 11).

(iv) Arenosols (AR): Arenosols are sandy soils with little or no soil development (FAO, 2009). It includes soils developed in residual sands after in-situ weathering of quartz-rich sediments or rocks. It also includes soils developed in recently deposited sands such as dunes in arid environments (FAO, 2009). Arenosols are commonly known as Kalahari sands, extending to at least 1m deep with a sand content of more than 70%, with a clay and silt content of less than 10%, low nutrient content, low water retention capability due to the porous structure. They are present in Kazungula near Livingstone (Figure 11).

(v) Leptosols (LP): Leptosol are very shallow soils over hard rock or in unconsolidated very gravelly material (FAO, 2009). They are a product of mechanical weathering with only superficial chemical weathering of the field spars and ferrol-magnesium silicate accessory mineral surfaces. They are transported under arid and semi arid conditions. They are well drained and range from friable, rocky, stony and gravely to fine loamy and clayey soils (FAO, 2009). They are found mostly in northern and eastern parts of the study area (Figure 11).

(vi) Luvisols (LV): These are soils with subsurface accumulation of higher activity clays and higher base saturation than in the topsoil as a result of pedogenetic processes (especially clay migration) (FAO, 2009). Unlike acrisols, these have high activity clays throughout the subsoil horizon and base saturation at certain depths (FAO, 2006). It is limited to areas immediately adjacent to major rivers and drainage lines. They are deposited by flood water and are characterized by rich organic and nutrient content accumulated over long periods along edges of rivers. These are present in patches on the Kazungula side from Kasaya to the area around the effluent of Lunungu Stream and around the source of Simbaluma Stream in the eastern part (Figure 11).

(vii) Gleysols (GL): These are wetland soils saturated with groundwater for long enough periods to develop a grey horizon with a characteristic colour pattern (FAO, 2006). According to FAO (2009), these are soils with permanent or temporary wetness near the surface. They are formed as a result of prolonged saturation in the presence of organic matter at shallow depths for some months or all of the year resulting in grey, olive or blue-coloured layers beneath the surface (Figure 11).

(viii) Vertisols (VR): Vertisols are heavy dark coloured soils with clay soils with a high proportion of swelling clays. The soils tend to form deep and wide cracks from the surface downwards when they dry out (FAO, 2009). Vertisols are present in two patches within the study area, along the Zambezi River in the south-west and Ngwezi River in the south-east (Figure 11).

(ix) Lixisol (LX): Lixisols are soils with subsurface accumulation of low activity clays and high base saturation (FAO, 2009). They are deep to moderately deep with a dark red to dark reddish brown colour. Lixisols were observed in the far south-east end of the Machile River Basin (Figure 11).

(x) Cambisols (CM): Cambisols are weakly to moderately developed soils. These are deep, well drained coarse loamy soils (FAO, 2009). They are only present in a very small area along the Zambezi River in Sesheke (Figure 11).

1.8.6 Vegetation

Despite its aridity, the Kalahari Basin supports a variety of fauna and flora on soils known as the Kalahari sands. According to the vegetation map of Zambia (Zambia Forestry Department (ZFD), 1976) the main vegetation types in Sesheke and Kazungula districts comprise Closed Forest, Open Forest, Termitaria and Grasslands (Figure 12). These are described below.

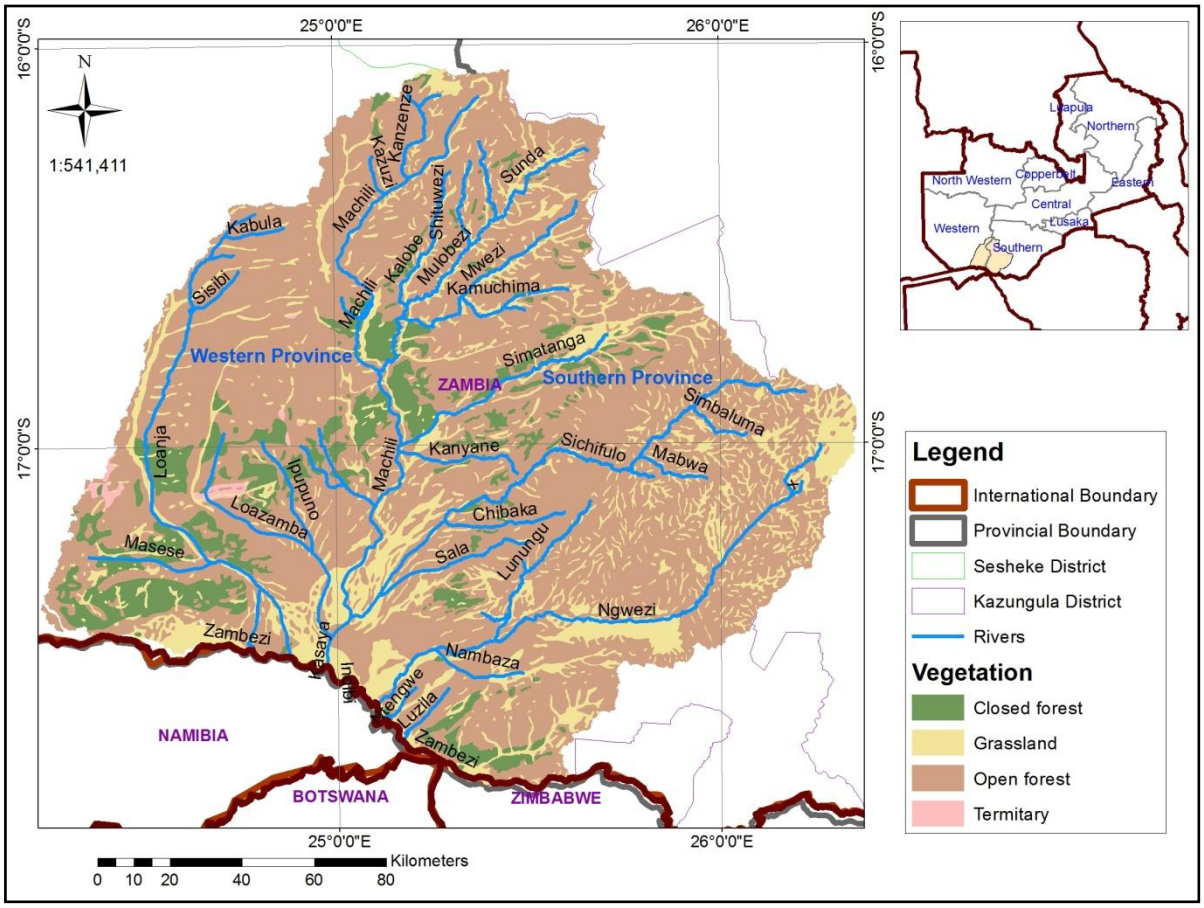

Figure 12: Map showing the vegetation type of the Machile River Basin, South-Western Zambia (after ZFD, 1976)

(i) Closed Forest

Closed Forest comprises the Dry Evergreen Forest such as Cryptosepalum and Kalahari Sand Chipya and the Dry Deciduous Forest such as the Baikiaea Forest (dwarf and secondary) and Riparian woodlands. Closed Forest appears in isolated patches concentrated around the western part of the study area (Figure 12). These are as described below.

(a) Cryptosepalum Forest: Cyptosepalum forests are outliers of the Dry Evergreen Forest type (Fanshawe, 2010) and are in most cases partially distributed (ZFD, 1976). The partial destruction of Cyptosepalum Forest leads to the formation of Miombo or Kalahari woodlands whereas its total destruction leads to the formation of Kalahari Sand Chipya (ZFD, 1976). Cryptosepalum is strongly dominated by *Brachystegia longifolia, Brachystegia spiciformis* and *Julbernardia paniculata* from the surrounding Kalahari Woodland. It is also dominated by shrubs and sub-shrubs. The woodland has a

more or less closed canopy of 9.1 to 11.6 m high (ZFD, 1976). Cryptosepalum Forests are present within the closed forests symbolized by green colour in the legend (Figure 12).

(b) Kalahari Sand Chipya: The Kalahari Sand Chipya is specific to Kazungula and comes as a result of total destruction of Cryptosepalum Forest. It is characterized by canopy species such as *Burkea africana, Combretum collinum, Dialium engleranum, Erythrophlem africanum, Gulbourtia coleosperma, Peltophorum africanum, Pterocarpus angolensis* and *Terminalia sericea*. These are equally present within the closed forests indicated by the green legend (Figure 12).

(c) Baikiaea Forest: This is a two storeyed forest with an open or closed, usually deciduous canopy of 9 to 18 meters high. The original dominants of the Baikiaea Forest are composed of *Baikiaea phirijuga* and *Pterocarpus antunesii* in varying proportions (ZFD, 1976). The Pterocarpus is more fire sensitive than Baikiaea. Below the canopy is a well defined deciduous thicket (called Mutemwa) composed of shrubs and scramblers 3 to 6 meters high. Close to the Sesheke-Kazungula Boundary exists the Baikiaea Forest in dwarf form with a canopy of 1.3 meters high and occasional emergents up to 3 meters high (ZFD, 1976). Partial destruction of Baikiaea Forest and the clearing of the "Mutemwa" for cultivation lead to Kalahari woodlands. Total or almost total destruction of Baikiaea Forest results in a secondary Baikiaea dominated by *Acacia giraffae, Acacia nigrescens, Combretum collinum, Combretum imberbe, Combretum mechowianum, Peltophorum africanum* and *Terminalia sericea* (Fanshawe, 2010). These were also observed within the closed forests indicated by the green legend (Figure 12).

(d) Riparian Woodland: The woodland is largely evergreen with occasional anthills and often carrying evergreen thicket. Dominant species like *Diospyros mespiliformis, Kigelia africana* and *Strychnos potatorum* growing up to 18m high. The woodland is also dominated by common shrubs, climbers and scramblers (ZFD, 1976). Like the vegetation types presented above these were also observed within the closed forests indicated by the green colour in the legend (Figure 12).

(ii) Open Forest

Open Forest (Figure 12) includes the Kalahari Woodlands such as the Miombo Woodland, Kalahari Sand Woodland, Mopane and Munga woodlands. Open Forest cover most parts of the study area. These are as described below.

(a) Miombo Woodland: This is two-storeyed woodland with an open or partially closed canopy of semi-evergreen trees of about 15 to 21 meters high. It is characterized by species of *Brachystegia*, and *Julbernardia paniculata, Manguesia macroura, Erythrophleum africanum, Parinari curatellifolia* and *Pericopsis angolensis* (ZFD, 1976). Most Miombo woodlands are secondary re-growth as a result of extensive cultivation in the past. In the west, the Miombo has invaded the Kalahari sands to become Kalahari Woodland which extends beyond the borders of Zambia (Phiri, 2005). The typical grasses and trees of the Miombo Woodland are mainly adapted to the base-poor, residual sandy soils developed by the in-situ weathering over the crystalline Basement and certain Karoo formations (FAO, 2010). Adding to this, FAO (2010) also observed a close correlation between the occurrence of the arenosols and leptosols soils and the distribution of the Miombo Woodland. Miombo Woodland is present within the open forests indicated by the brown vegetation in the legend (Figure 12).

(b) Kalahari Sand Woodland: Kalahari Sand Woodland is derived from the destruction of Baikiaea Forest by fire. It embraces most woodland on Kalahari sands. It is two storeyed woodland with an open or partially closed, deciduous or semi-deciduous of about 18 to 24 meters high (ZFD, 1976). It is mainly characterized by *Amblygonocarpus andongensis, Burkea africana*, *Combretum collinum, Cryptosepalum exfoliatum ssp., Dialium engleranum, Erythrophleum africanum, Gulbourtia coleosperma, Parinari curatellifolia, Pterocarpus angolensis, Ricinodendron rautaneni* and *Terminalia sericea*. Important shrubs may also include such species as *Baphia massaiensis, Bauhinia urbaniana, Copaifera baumiana* and *Kotschya strobilantha*. Climbers are rare because they are fire sensitive (ZFD, 1976). These are also present within the open forests indicated by the brown vegetation in the legend (Figure 12).

(c) Mopane Woodland: This is a one-storeyed woodland with an open deciduous canopy of 6 to 18 meters high. The dominant Colophospermum Mopane is pure or almost pure scattered elements of Munga woodlands represented mainly by *Acacia*

nigrescens, Adansonia digitata, Combretum imberbe, Kirkia acuminate and *Lannea stuhlmannii.* Mopane-Munga acotones are more common than pure Mopane woodlands in the basin (ZFD, 1976). Mopane Woodlands though not visible are equally present within the open forests indicated by the brown vegetation in the legend (Figure 12).

(d) Munga Woodland: This is an invented term for Savanna woodlands. It is an open park-like of 1 to 2 storeyed deciduous woodlands with scattered or grouped emergents up to 18 meters high characterized particularly by *Acacia combretum* and *Terminalia ssp* (ZFD, 1976). Munga Woodlands are also present within the open forests indicated by the brown vegetation in the legend (Figure 12).

(iii) Termitaria

Termitaria (Figure 12) includes all types of vegetation i.e. forest, woodlands, thicket, shrub and grassland can be found around bases of Termitaria. Termitaria are divided into Miombo Termitaria, Kalahari Termitaria (whose mounds occur on Kalahari sands of the Karoo type where the silt and clay content is high), Mopane Termitaria, Munga Termitaria and Riparian Termitaria (ZFD, 1976). Termitaria are present in small and few patches on the Sesheke side mostly surrounded by Open Forests (Figure 12).

(iv) Grasslands

Grasslands (Figure 12) comprise of all naturally treeless and grassy areas. They are divided into dambo, riverine and floodplain grassland. These are associated with streams and rivers, flood plains, seasonally flooded freshwater swamps, and mountain grassland and watershed plains (ZFD, 1976).

CHAPTER 2: LITERATURE REVIEW

2.1 Groundwater Resources

About 97% of all available freshwater resources in the world are from groundwater sources which constitutes the underground part of the hydrological cycle for maintenance of wetlands and river flows acting as buffer through dry periods (Quevauviller et al., 2007). However, groundwater vary from arid to semi-arid to humid zones. It plays a major role in supplementing water supply to meet the ever-increasing demands, as water is a scarce and therefore very valuable commodity in semi-arid to arid zones within the Kalahari Basin (Haddon, 2005). Groundwater is closely related to other water resources such as surface water, springs and wetlands where it naturally discharges. According to Wayland (1953) recharge of groundwater in many areas of the Kalahari Basin is usually low because of low rainfall and high evapotranspiration which lead to subsiding water tables. Subsiding water tables were observed and described as far back as the 1950s (Wayland, 1953), with complete drying-up of boreholes observed in some areas of the Northern Cape Province during dry periods (Levin, 1980). Though groundwater is an overlooked resource, many rural populations rely on groundwater for the supply of safe drinking water and water for all other economic activities, aquatic and terrestrial ecosystems in both developed and developing countries (Quevauviller et al., 2007). This makes the appropriate management of the groundwater resource an important task for administrators and legislators in order to ensure that there are significant quantities and high quality groundwater resources [Integrated-Geographic Information System (I-GIS), 2010]. Deterioration of groundwater due to salinity is one of the causes of poor quality groundwater resources. Therefore, in order to manage saline groundwater, researchers, water resources specialists, policy makers and politicians need information on its distribution, dynamics and severity (IGRAC, 2009). This study therefore aims at providing information to these groups of people and enhances the general understanding of groundwater salinity and widens the inspiration for selecting effective measures for interventions in the semi-arid Machile River Basin.

2.2 General Sources of Groundwater Salinity

Globally, saline groundwater occurrence and genesis is mostly observed in arid climates and is as a result of several sources. These can be generally categorized under the following themes.

2.2.1 Evaporation

Saline groundwater may develop when climatic conditions favour evaporation or evapotranspiration, especially when linked to shallow water-table conditions which are prevail in semi-arid to arid areas (IGRAC, 2009). In semi-arid to arid environments, rainfall is significantly less than evaporation rates and groundwater discharge becomes a major component of salt balance in wetlands. However, salinity in these environments varies as a result of high evaporative conditions. Wetlands are generally at risk of salinity because of their lower elevation in the landscape, which exposes them to increased saline groundwater inflows and evaporation (Jolly et al., 2008). Saline groundwater may also originate from large-scale irrigation which occurs as a result of shallow groundwater tables rising. Evaporation from the water table may leave a residue of relatively mineralized water in the soil, which percolates into the aquifer and increases groundwater salinity (IGRAC, 2009). According to Haddon (2005), salinity in the Okavango Delta is as a result of evaporation of near surface which over a period of time leads to concentration of salts in groundwater. Water being evaporated does not necessarily have to be saline because the evaporation of freshwater can equally result in salinity over time. Sometimes water accumulates in a hollow and when it evaporates salinity would increase. The process of evapotranspiration also concentrates salts in groundwater and soils (Haddon, 2005).

2.2.2 Dissolution

Groundwater may be enriched in mineral content by dissolution of naturally occurring soluble salts as it flows through such bodies underground. Even when groundwater is flowing through ordinary aquifers with a small fraction of easily dissolvable materials it may become brackish to saline if time and other conditions favour dissolution. This is common in arid regions including among others Western and Eastern Australia, Saharan and Sub-Saharan basins (IGRAC, 2009). Similarly, Fetter (2001) described high saline groundwater in inland aquifers as occurring through mineralization due to stagnation or slow circulation of water. Murphy (1999) noted that vast groundwater salinity in Australia originates from weathering of rocks and sediments. Salts may accumulate in groundwater by water soaking through sediments and sedimentary rocks that originally formed in salty marine environments.

2.2.3 Agriculture

The natural pollution of surface and groundwater by inorganic salts, mostly chlorides (Cl^-), sulphates (SO_4^{2-}), sodium (Na^+), magnesium (Mg^{2+}) and calcium ($Ca^{2+)}$ in arid zones is a consequence of the dry climate and extensive agricultural practices (Barica, 1972). Salinity has overwhelmed crop production in irrigated regions of the world (Hanson et al., 2006). In Australia, dryland salinity and irrigation salinity are two major types of salinization problems caused by agricultural practices (Podmore, 2009; Hart et al., 1990).

Dryland salinity occurs in non-irrigated areas, principally caused by clearing of native deep rooted vegetation for farming purposes. Big trees are replaced by shallow rooted crops and pasture plants which need less water from the groundwater. As less water is taken from the system, the water table rises bringing with it dissolved salts to the root zone, resulting in dryland salinity (Murphy, 1999; DNRM, 2004).

Irrigation salinity is particularly common in arid and semi-arid areas where evapotranspiration exceeds annual precipitation and where irrigation is necessary to meet crop water needs (Hanson et al., 2006). The accumulation of salts in soil and water to levels that impact on human and natural assets such as plants, animals, aquatic ecosystems, water supplies, agricultural and infrastructure (Podmore, 2009). Groundwater is enriched in salt content by irrigation as a result of crop evapotranspiration. Water vapour leaving the crops during evapotranspiration is almost without dissolved solids making it less concentrated than irrigation water supplied (IGRC, 2009). Irrigation increases the quantity of water draining below the root zone which is the dominant cause of irrigation salinity. Water then moves upwards from the water table to replace the evapotranspired water causing water logging and salinity, which in the process reduces productivity (DNRM, 2004). The presence of salts in irrigation water is primarily as a result of chemical weathering of chloride and carbonate containing sedimentary rocks. Therefore, irrigation salinity occurs due to increased leakage and groundwater recharge rates causing the water table of dissolved salts to rise into the plant root zone as well. The salt remains behind in the soil and into aquifers when water is taken up by evapotranspiration or lost to evaporation (Podmore, 2009). Similarly, the underlying groundwater system may also be salinized by saline

water tables, saline drainage water, fertilizers, irrigating with waste water and soil amendments such as gypsum and lime (Hanson et al., 2006).

2.2.4 Saline Groundwater of Marine Origin

According to IGRAC (2009) saline groundwater of marine origin includes:

(i) Connate Saline Groundwater: Connate saline groundwater is typical in sedimentary formations of marine origin. Geological formations made from sedimentary rocks of marine origin are particularly major contributors of salinity (IGRAC, 2009; Hanson et al., 2006). When seawater is deposited together with a rock medium it stays there, unless it is flushed afterwards. Under natural boundary conditions, migration of connate saline groundwater tends to be extremely slow (IGRAC, 2009);

(ii) Saline Groundwater Originating from Marine Transgressions: Throughout geological history, the sea level tends to change over time. Consequently, it is common that coastal lowlands became flooded by the sea during marine transgression periods. During the transgression period, seawater flows downwards because of density differences and may have turned originally fresh coastal aquifers into brackish and saline groundwater reservoirs (IGRAC, 2009; Post, 2004). This process is relatively fast. Within hundreds of years, aquifers of hundreds of meter thickness may turn saline due to this process. It has also been established that intensive agricultural activities, usually, increase the risk of groundwater quality degradation through high groundwater pumping rates (IGRAC, 2009). Such uncontrolled groundwater extraction modifies natural flow systems and induces seawater intrusion from the coast into groundwater bodies reducing quality of the water (Kouzana et al., 2009);

(iii) Saline Groundwater Originating from Incidental Flooding by Seawater: A similar mechanism of salinization may occur at a much smaller time basis. When sea levels are exceptionally high, e.g. during a tsunami, or when coastal defense systems fail during high tides, low-lying coastal plains may become regularly flooded by seawater. Although the period of flooding is much shorter than in the case of a marine transgression, large extents of coastal aquifers nevertheless may become salinized due to the infiltration of seawater ponding on land surface. The effect is particulate in and

mostly limited to the shallow (first meters) domains of these aquifers. Temporal submersion of unprotected wellheads during the flooding may lead to introduction of saline water to greater aquifer depths via the well screens (IGRAC, 2009);

(iv) Saline Groundwater Originating from Laterally Intruded Seawater: Intruded seawater is saline groundwater which is as a result of the interaction between the seas and hydraulically connected aquifers. It is controlled by migration and mixing of saline water bodies with groundwater resources. The strong adherence between freshwater and saline water/brine or seawater) indicates the importance of mixing under natural and/or anthropogenic influences (Han et al., 2013). Lateral seawater intrusion in coastal areas may be enhanced by surface water bodies connected to the sea, such as estuaries and rivers (greatly increasing the coastline length) if conditions allow seawater to travel inland through these bodies. When the shallow fresh groundwater resources are abstracted for human productive use and when land use changes, groundwater replenishment and shallow fresh groundwater head decreases. This can cause up-coning of deeper, often more saline groundwater and an inland movement of the fresh/saline groundwater interface. Also decreased estuarine river discharge may increase seawater intrusion because of upstream water allocation. This anthropogenic induced intrusion is a relatively fast process depending on the hydraulic pressure changes and the transmissivity of the coastal aquifers (IGRAC, 2009).

Under certain circumstances, depending on the extent of seawater intrusion due to hydrodynamic dispersion and aquifer properties the portion of the aquifer occupied by seawater to that occupied by freshwater takes the form of a transition zone, which may be narrow or wide depending on the aquifer thickness (IGRAC, 2009). However, once seawater has invaded beyond a tolerable distance, restoration of water quality in the invaded zones is generally expensive; it requires a large amount of freshwater flushing for a long period of time (Bear et al., 1999);

(v) Groundwater Enriched in Mineral Content by Seawater Sprays: The lower areas in coastal zones may be rich in salt particles, originating from the sea. These salt particles will be dissolved by rains and be incorporated in groundwater recharge water, thus contributing to groundwater salinization (IGRAC, 2009).

2.3 General Impacts of Salinity

Whatever the cause, salinity has significant economic, social and environmental impacts (Williams, 1999). Economic impacts of salinity include reduced productivity of crops and agricultural land, reduced income and water quality for livestock, humans and irrigation purposes. It also leads to poor animal health, farm structures and infrastructure such as roads, buildings and bridges being damaged (Murphy, 1999). Environmental impacts include decreased biodiversity, and changes in the natural character of aquatic ecosystems, reduced ecological productivity, reduced aesthetic, recreational and tourism values of landscape (Williams, 1999). Generally, agricultural practices also impact the subsurface part of the hydrologic cycle by flushing salts into the underlying aquifers potentially degrading groundwater quality (Scanlon et al., 2005). Salinity can also kill crops and vegetation as well as increase sediment and chemical pollution of rivers and dams, distorting water supplies for drinking and irrigation (DNRM, 2004). Social impacts may include reduced aesthetic, recreational and tourism values of landscape and reduced agricultural incomes due to productivity losses (Podmore, 2009).

2.4 Groundwater studies in Okavango Delta in proximity to the study area

In southern Africa, many authors have written about salinity and their sources. This is due to the presence of dry lands that characterize the semi arid to arid regions. In Botswana, Bauer et al. (2010) undertook a study which suggested that salinity in the Okavango Delta was a result of an evaporative salt enrichment. However, Christiansen (2007) attributed the accumulation of salts in groundwater of the Okavango Delta to evapotranspiration, which later lead to poor living conditions for plants, animals and humans. A groundwater salinization study by Bauer et al. (2006) in the Okavango Delta in Botswana indicated that soil and groundwater salinization were a major problem in a natural evaporative aquatic system, which accumulates about 300,000 tons of dissolved solids per year. As a result, shallow groundwater in the centre of the islands, was found to be highly saline. The study by Linn et al. (2002) on the impacts of groundwater development on shallow aquifers in the lower Okavango Delta in northwestern Botswana indicated that when rivers stop flowing due to climatic aridity, the water quality in the freshwater aquifers begins to deteriorate through upward migration of saline water from underlying saline aquifers. The study also indicated that the high rate

of evapotranspiration in the area was reflected by the presence of brackish and saline water aquifers as water quality controlled groundwater development.

2.5 Previous Groundwater Studies in the Machile River Basin

There are only three previous pieces of literature on groundwater studies in the Machile River Basin. These have been reviewed below.

Firstly, Wibroe and Thomsen (2009) undertook a geophysical study to monitor and model the salt and freshwater dynamics in the Upper Zambezi, of which Sesheke District is a part. The findings identified a saline aquifer with resistivity of less than 10Ωm corresponding with the sandy clay sediments observed in lithological profiles of the area. A shallow freshwater lens of up to 20m deep was also observed with resistivities of 20-50Ωm. The model with a recharge of 5.10^{-10}m/s corresponding to 2% of annual precipitation and a maximum of evaporation and transpiration rate of $2.5X10^{-8}$m/s was obtained. It resulted in a replacement of the initial salt concentration of $6kg/m^3$ with freshwater to a depth of 20m within a period of 1000 years. The spatially distributed data were interpolated with existing data whose interpretation revealed increased salinity towards the South-Eastern corner of Sesheke District. They further observed from literature that the area was located in an alluvial, lacustrine belt formed by prehistoric tectonic events. The belt goes as far as the Okavango Delta and the Makgadikgadi salt pans in Botswana. Wibroe and Thomsen (2009), attributed the source of salinity to evapo-concentration from large and isolated old lakes as observed in other semi-arid areas such as the Okavango.

Secondly, a study by Chongo (2011) and Chongo et al. (2011) in Sesheke, Western Zambia indicated that groundwater salinity occurrence at a regional scale varied from fresh to saline groundwater. Salinity was observed to increase with depth; at 5m, groundwater salinity was restricted to the extreme south-eastern end of Sesheke and the extent became larger at greater depths. For example, at 30m depth almost the entire area was affected by saline groundwater and only interrupted by isolated brackish and fresh groundwater anomalies. They further associated the origin of saline groundwater to evapo-concentration of soluble salts in interdune deposits during semi-arid conditions and that it could as a result of the linkages to the former endorheic lake system (Lake Palaeo Makgadikgadi) covering large parts of Southern Africa.

Recently, Phiri (2013) studied the spatial and temporal variability of actual evapotranspiration using Surface Energy Balance System (SEBS) algorithm in the semi-arid Barotse sub-basin in South-western Zambia. He found out that water bodies and regularly flooded vegetation had the highest rates of evapotranspiration (ET) of 6.9 and 5.9mm per day on warm-wet days respectively. The lowest rates of ET occurred over mosaic vegetation/croplands and closed to open grassland with respective high variation of up to 64.1 and 71.1% between warm-wet and hot-dry days. Therefore, the systematic lack of physical agreement on cool-dry, hot-dry and warm-dry days implied that SEBS estimates were not doubtful, but that the assumptions on which potential evapotranspiration (PET) was based differed from the surface conditions. The study concluded that the SEBS model can be used successfully to estimate evaporative fluxes in heterogeneous areas in order to improve water resources management (Phiri, 2013).

2.6 Present Study

No previous study has considered mapping the distribution of saline groundwater over the entire Machile River Basin. Therefore, this study was undertaken in order to map Kazungula District and combine the field campaign soundings with the existing soundings for Sesheke to enhance the overall understanding of the existence of saline groundwater in the basin.

CHAPTER 3: METHODOLOGY

This chapter gives a description of the methods and materials used such as geophysical methods for groundwater mapping using the WalkTEM equipment, software for data analysis and limitations. Geophysical data used were a combination of survey data (captured on the Kazungula side) and existing data captured by Chongo (2011) on the Sesheke side. The two data sets were merged in order to form a complete data set for the entire Machile River Basin (Appendix 1). Some of the material that are Literature Review in nature (e.g. sections 3.2.1 and 3.2.2 are included here instead of Chapter 2-Literature Review because they describe the processes that take place in the instruments during field work and in the software during data analysis.

3.1 Desk and Field Studies

The desk study involved reviewing books, journal articles and reports around studies focusing on groundwater and salinity undertaken in South-Western Zambia and other countries. The information from desk review was also very useful in describing the Machile River Basin, presented in the description of the study area in this thesis. Fieldwork involved geophysical surveys using ground-based Time-Domain Electromagnetic (TDEM) technique.

3.2 Geophysical Methods for Groundwater Salinity Mapping

Geophysical methods obtain or estimate physical properties of the subsurface directly or indirectly by measuring geophysical signals such as electric, magnetic and electromagnetic fields (ABEM Instrument, 2012). The Time-Domain Electromagnetic (TDEM) method was the geophysical method used in the field campaign to collect electromagnetic data. The TDEM data was the primary dataset for this salinity spatial distribution study.

3.2.1 Time Domain Electromagnetic (TDEM) Method

Electromagnetic (EM) methods have been one of the primary geophysical methods used in hydrogeological investigations because of its ability to distinguish between formations of different resistivities. The method has been proven highly efficient in detecting saline groundwater (Goldman and Neubauer, 1994; Goldman et al, 1994). The TDEM measurements have increasing applications in the mapping of saline-freshwater interfaces (Reynolds, 1997). The first application of the ground-based TDEM method

was described by Ward (1938). It has been developed and refined most intensively since the mid 1980s making it younger than the frequency domain and the geoelectric methods (Christiansen et al., 2006). Kafri and Goldman (2005) used the method for salt water boundary mappings. Recently, Bauer et al. (2010) described the ground-based TDEM method as a method well known for measuring ground electric conductivity which is strongly correlated with groundwater salinity. The application of the methods was therefore mostly focused on studying the relationship between salinity and electrical resistivity. In this study, the application of the TDEM method was based on its cost-effectiveness, its ability to detect good conductors, such as saline water environment and that it was recently modified leading to the improvement of its electronics and signal processing allowing the acquisition of high quality data for the interpretation (ABEM Instrument, 2012). The Aarhus University in collaboration with ABEM Instrument made a significant contribution to the advancement of the technology. The advancement of the technology resulted in solutions capable of resolving slight changes in fine detail with better penetration of depth (ABEM Instrument, 2012).

According to Bauer et al. (2010), the method offers a cheap and non invasive option for mapping groundwater salinization. The successful use of TDEM in arid environment was also demonstrated earlier by the work of Young et al. (1998) in Oman where over 30% of the population rely on groundwater extracted from alluvium aquifers on the Batinah Plain on the coast of the Gulf of Oman. Similarly, Taylor et al. (1992) showed the use of TDEM with simple 1D, closely spaced soundings to define local hydrogeology in an arid alluvial environment. The results were used to reduce the total number of wells required to characterize the groundwater system. For this study, the method was used because it was quick and easy to implement as long as there was enough space to lay the cables and away from any form of interference.

The TDEM method gives indirect information about the hydrogeological properties such as electrical conductivity or electrical resistivity of the subsurface and uses the transmitter to induce time varying ground current. The two hydrogeological properties are related as presented in equation 1 (Archie, 1942).

$\rho = {}^{1}/_{\sigma}$ ……Equation 1

Where

ρ = electrical resistivity (Ohm.m or Ωm)

σ = electrical conductivity (S/m)

3.2.2 The Principle behind TDEM Sounding

Generally, the TDEM is a time-domain controlled method that uses transient electromagnetic field diffusion. A direct current is alternatively turned on and off in a rectangular loop of wire laid on the ground as a transmitter (TX) source. The time varying currents create primary magnetic fields that propagate in the earth and generate secondary electrical currents (the eddy currents) (Figure 13). The weak secondary magnetic field is produced in proportion to the waving strength of the eddy currents. The longer the time period between pulses of the current, the deeper the eddy currents penetrate into the earth (Fetter, 2001). Being an active method, a time varying magnetic field which induces eddy currents in the subsurface is generated by abruptly switching off an electric current in a loop.

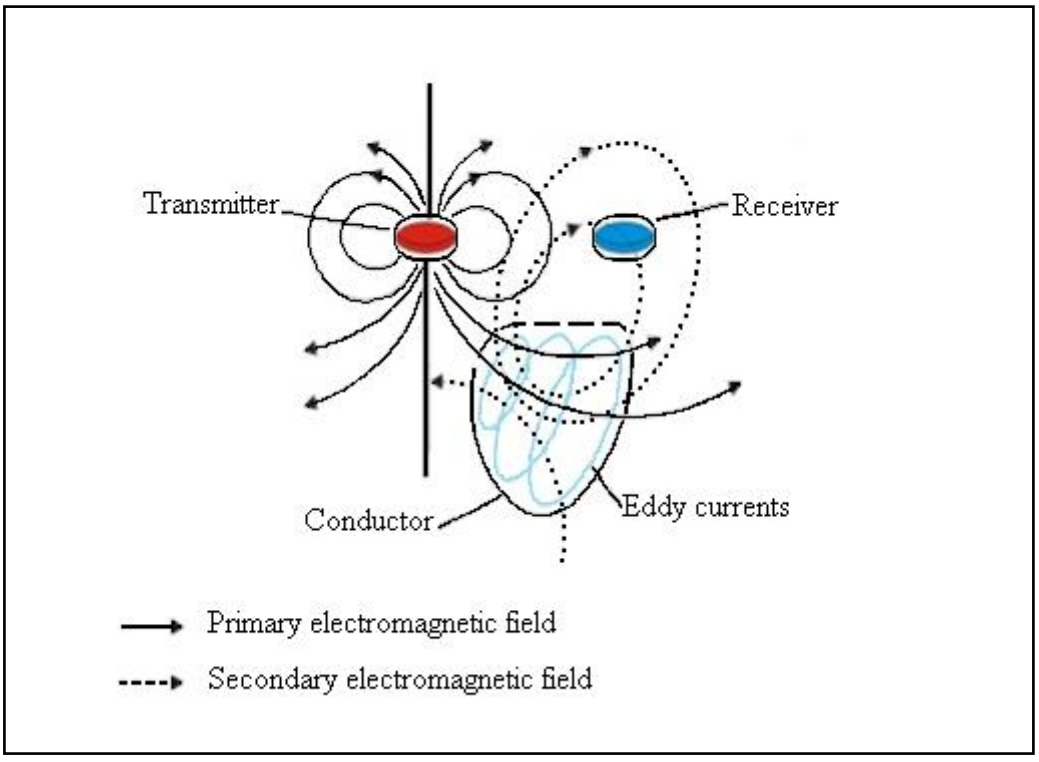

Figure 13: Principle behind the electromagnetic (EM) method (after Klein and Lajoie (1980)) used in the Time–Domain Electromagnetic (TDEM) sounding during data collection in the Machile River Basin, South-Western Zambia

The four Maxwell's first order linear differential equations (2 to 5) which describe the vector functions of an electromagnetic field govern the electromagnetic theory (Kirsh, 2006). The equations express the relations between the vector function of an electromagnetic field such as D, E, B, H and J written as:

$\nabla . \mathrm{D} = \rho$…….. Equation 2

$\nabla \times \mathrm{E} + \frac{\partial \mathrm{B}}{\partial t} = 0$…… Equation 3

$\nabla . \mathrm{B} = 0$…… Equation 4

$\nabla \times \mathrm{H} = \mathrm{J} + \frac{\partial \mathrm{D}}{\partial t}$……..... Equation 5

Where the equations express the relations between

D= electrical displacement ($\mathrm{C/m^2}$);

E= electrical field ($\mathrm{V/m}$);

B= magnetic flux density (T or $\mathrm{Wb/m^2}$), T for Telsa;

H = magnetic field intensity ($\mathrm{A/m}$);

J = electrical current density ($\mathrm{A/m^2}$);

ρ =electrical charge density ($\mathrm{C/m^3}$); and

t = time (msec).

Two fundamental electromagnetic principles required to derive the physics behind TDEM surveys are; the Faraday's Law of induction on which equation 3 is based and Lenz's Law (Fetter, 2001). According to Faraday's law of induction an impulsive electromotive force (EMF) induced in the ground by decaying primary magnetic field at the current turn-off time produce secondary or eddy currents in conductive bodies (Figure 13). These induced currents penetrate into the ground and create a secondary magnetic field with amplitude that decreases over time.

The voltages are measured at the surface by a receiver (Rx) coil or loop at several preset times during the turn-off period. By increasing the period over which the decaying voltages are observed, information is obtained about deeper formations (Al-Garni and El-Kaliouby, 2009). The eddy currents are therefore produced by Faraday's Law, which states that any change in the magnetic field will cause an electric field or voltage or electromotive force (EMF) to be induced (Tsourlos et al., 2004) which also according to Maxwell's Law generate varying electric fields. When electrical current is flowing in a

conductor, there is an associated magnetic field created around the wire (Figure 13). Similarly, when a wire is moved inside a magnetic field an electric current is generated in the wire (Fetter, 2001). This is expressed in Faraday's Law (equation 6);

$$Voltage\ Generated\ (EMF) = -N\frac{\Delta(BA)}{\Delta t} \quad \text{.....Equation 6}$$

Where

EMF = Electromotive Force or Voltage (volts);

N = the number of turns of coil;

BA = Magnetic flux; and; and

t = Time (milliseconds).

A minus sign (-) in the Faraday's Law denotes "Lenz's Law", which states that the polarity of the induced EMF is such that it produces a current whose magnetic field opposes the change that produces it (opposes the original magnetic flux change). It is related with the direction of the induced EMF which keeps the magnetic flux in the loop constant; if the magnetic flux through the circuit increases, the direction of the induced current opposes this change by trying to reduce the magnetic flux and vice versa. Therefore, Faraday's law is a mathematical law that relates the changing magnetic field to the induced current (Fetter, 2001).

The transmitter current is a modified symmetrical square wave (Figure 14). After every second quarter period, the transmitter current is abruptly reduced to zero for one quarter period. The process of abruptly reducing the transmitter current to zero induces, in accord with Faraday's Law, a short duration voltage pulse in the ground, which causes a loop current to flow in a transmitter wire (United States Environmental Protection Agency (USEPA), 2011). As soon as the transmitter current is turned off, the amplitude of the current starts to decay because of the infinite ground resistivity. The net result is a downward and outward diffusion of currents in the subsurface (Figure 14). The decaying current similarly induces a voltage pulse that causes more current to flow for a long distance and depth from the transmitter loop (USEPA, 2011). The time after the transmitter current has been switched off determines the depth of investigation. The induced currents concentrated in the upper layers cause early measurements of the electromagnetic fields from these currents to be sensitive to the electrical conductivity

of the shallow structures. As time increases, the maximum current migrates to greater depths causing the measured signal to depend more on the conductivities of deeper layers. However, when the current density in the near surface layers decreases, the electrical conductivity of near-surface structures only has a minor influence on the measured signal at later times (Goldman and Neubauer, 1994).

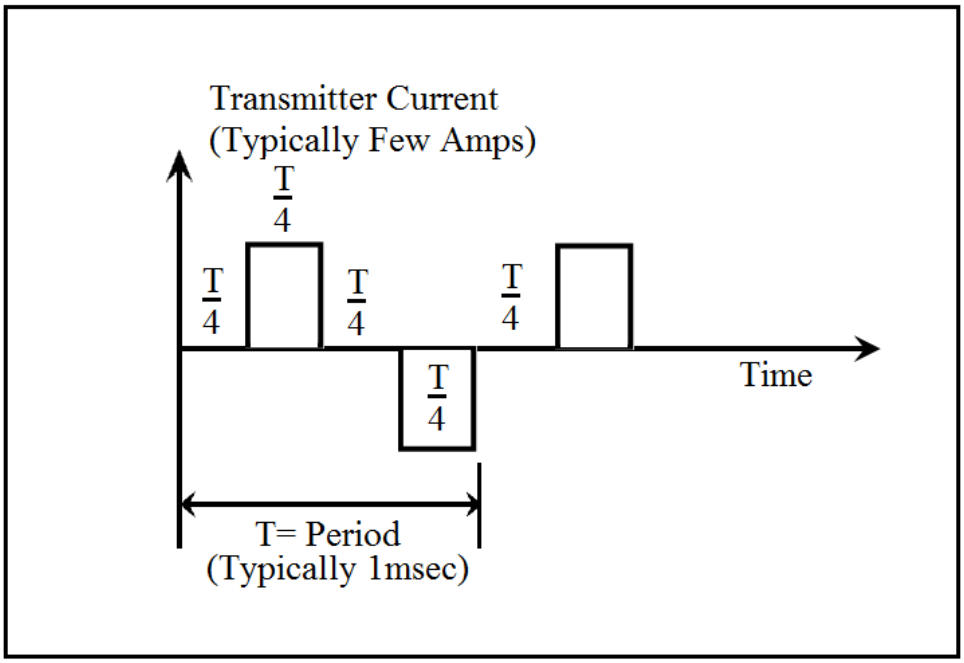

Figure 14: Movement of a periodic transmitter current during the TDEM sounding–method (after USEPA (2011)) used during data collection in the Machile River Basin in South Western Zambia

Figure 15 shows the output voltage of the receiver coil together with the transmitter current. The measured data consist of a series of values of receiver output voltages at each of the successions of time gates. These gates are located in time from a few microseconds after the transmitter current has been turned off. The receiver coil measures the time rate of change of the magnetic field $e(t)=dB/dt$, as a function of time during the transient. Where $e(t)$ is in nanovolts per square meter (nV/m^2) of the receiver coil area. Measured decays typically range from many thousands of nanovolts per square meter at early times to less than 0.1 nV/m^2 at late times (Al-Garni and El-Kaliouby, 2009).

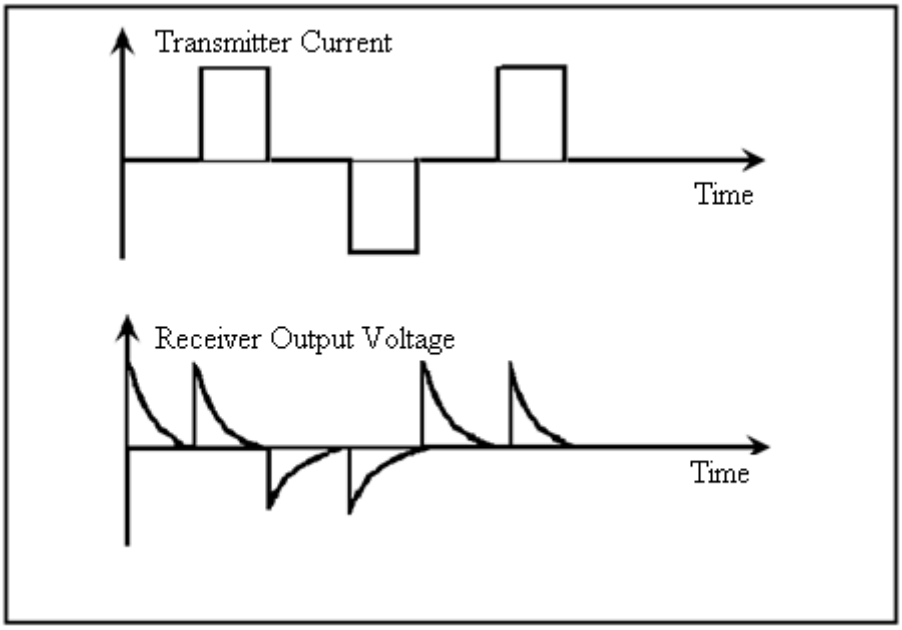

Figure 15: Transmitter current and receiver output voltage during a TDEM sounding method (after USEPA, (2011)) used during data collection in the Machile River Basin in South Western Zambia

The receiver contains 20 narrow gates which open one after another in order to measure and record the amplitude of the decaying voltage. Figure 16 is a linear plot of a transient response from the earth showing the measuring gates. The early gates (1 to 5) which are located where voltage is changing rapidly are narrow (Figure 16) in order to minimize distortions as measurement of transient voltage is going on (USEPA, 2011). The later gates (e.g. 19 and 20) are broader and are located where the transient voltage is changing much slower (Figure 16). The wider gates which become smaller with time enhance the signal to noise ratio because the accuracy of measurement is not affected by small errors in the location of the receiver coil (USEPA, 2011). USEPA (2011) further added that, the sounding data consist of a series of values of receiver output voltage at each of the succession of gate times. The gates are located in time from a few microseconds up to tens or even hundreds of milliseconds after the transmitter current have been turned off depending on the desired depth of investigation. The receiver coil measures the time rate of change of the magnetic field as a function of time during the transient.

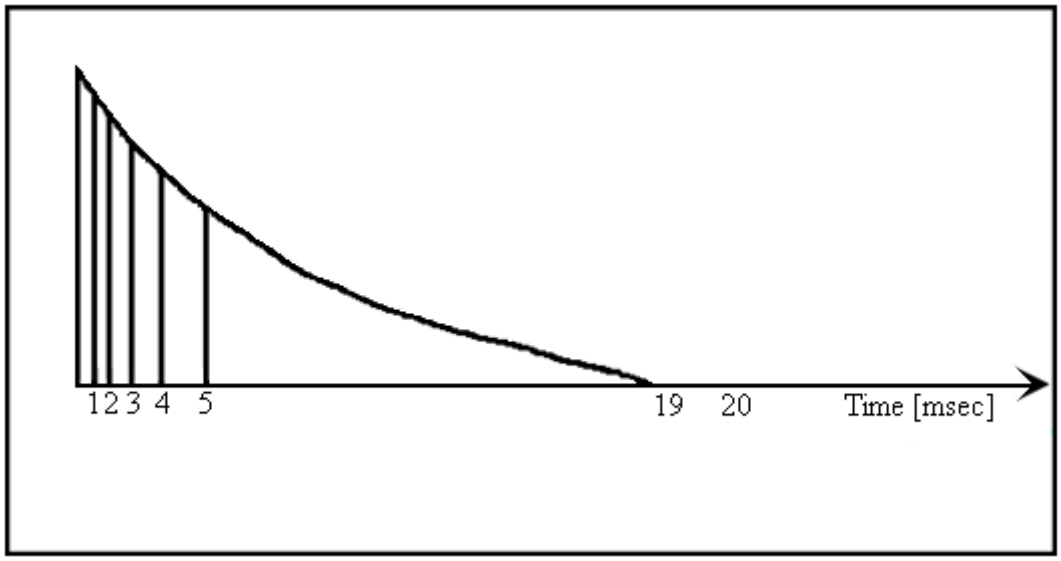

Figure 16: Measurement gates during the TDEM sounding–method (after USEPA, (2011)) used during data collection in the Machile River Basin in South Western Zambia

In time-domain method, the response from the earth is measured in the absence of the primary field generated by the instrument transmitter. The response measured at different times after current switch-off is used to obtain information about the conductivity of the subsurface at different depths (Christiansen et al., 2006).

3.3 Site Selection

The area was subdivided into 25 by 25km square grids so that soundings are collected in 25km spacing. However, non or impassable roads made the plan non realistic. Soundings were collected in every square kilometer grid but not at exactly 25km spacing. The main requirements for selection of sounding points were distance from signal interference such as wire fences, electric power lines, buildings, vehicles and other structures that could cause coupling problems (Herckenrath and Bauer, 2013). Consequently, for this study, the sites for TDEM soundings were selected away from such interference (at about 150m away).

3.4 Data Capture

Twenty five (25) TDEM soundings were captured on the Kazungula side and were merged with the 44 soundings captured by Chongo (2011) on the Sesheke side in order to provide a spatial distribution of saline groundwater over the entire Machile River

Basin (Figure 17). This came to a total of 69 soundings considered for this study (Figure 17 and Appendix 1). The TDEM survey campaign on the Kazungula side was carried out during the month of July 2013.

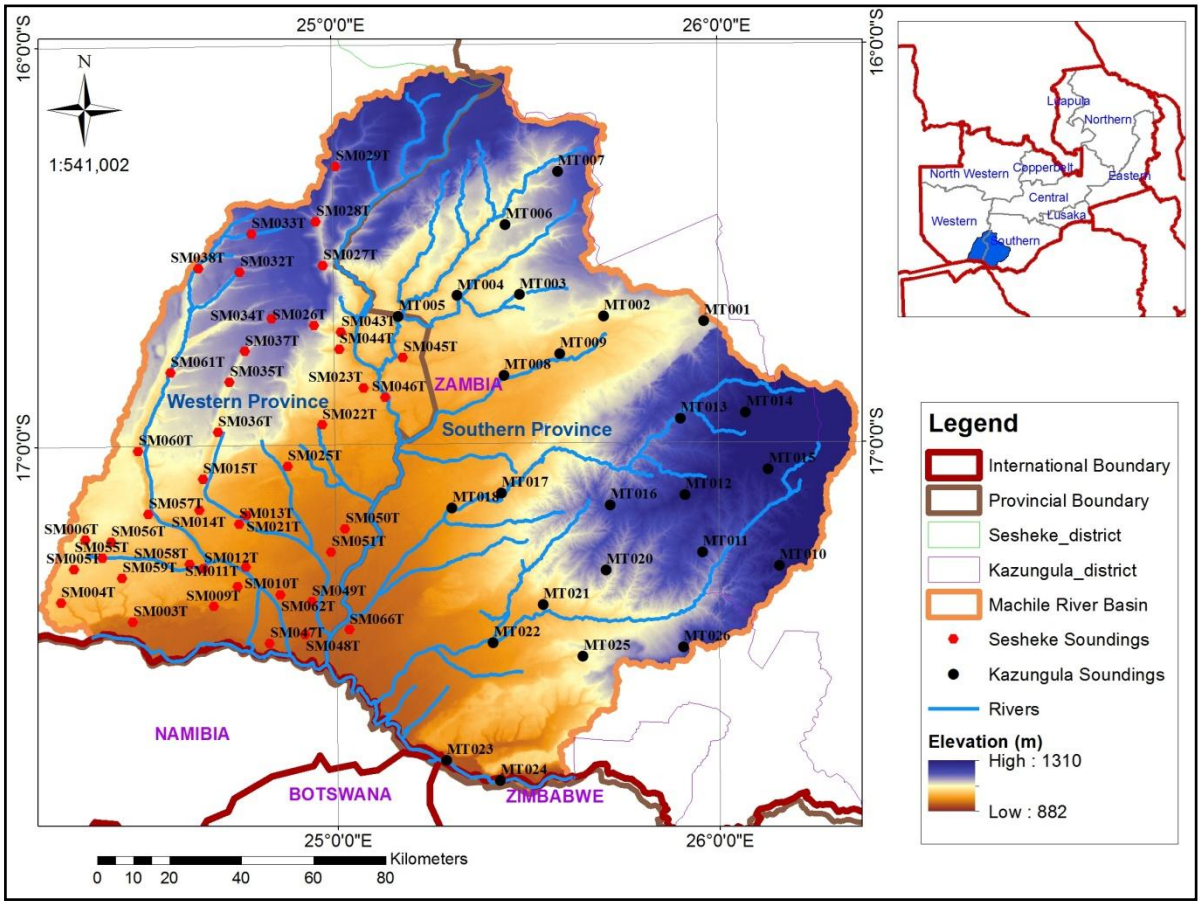

Figure 17: Map showing location of the 25 TDEM survey soundings on the Kazungula side and 44 existing soundings by Chongo (2011) on the Sesheke side in Machile River Basin, South-Western, Zambia

A survey configuration consisting of a single square turn loop with a horizontal receiver coil located at the centre was used. An electric current was applied through a 40 by 40m^2 transmitter loop at the land surface into the subsurface. The size of the transmitter loop is a function of the desired depth of investigation (Fetter, 2001). However, the depth of investigation is dependent on the intensity of the applied electric current and the time after the transmitter current has been switched off. When the electric current was turned off, the primary magnetic field decay and that decay induces an eddy current in the ground which in the process produces secondary magnetic fields. The secondary magnetic fields created an electromotive force measured in time by a Receiver Coil

(RC-5) placed in the middle of the transmitter loop (Figure 18). The receiver coil measured the time rate of change of the decaying secondary magnetic field (Tsourlos et al., 2004). It is the secondary magnetic field that creates a measurable voltage in the receiver. The primary magnetic field at the centre of the transmitter loop is very high and the presence of any metal including the receiver coil can cause sufficient transient response to seriously distort the measured signal from the ground (USEPA, 2011). To avoid this distortion, the receiver coil was placed about 10m away from the nearest transmitter edge (Figure 18). The process of applying the current, shutting it down and measure the magnetic field strength was repeated severally in order to improve the signal to noise ratio of the sounding (Fetter, 2001). The square single turn transmitter loop laid on the ground was connected to the WalkTEM equipment (Figure 19). The WalkTEM equipment was significantly important as it was used to collect all primary data. As the TDEM data were collected, the Global Positioning System (GPS) coordinates were also picked at each sounding point (Appendix 1).

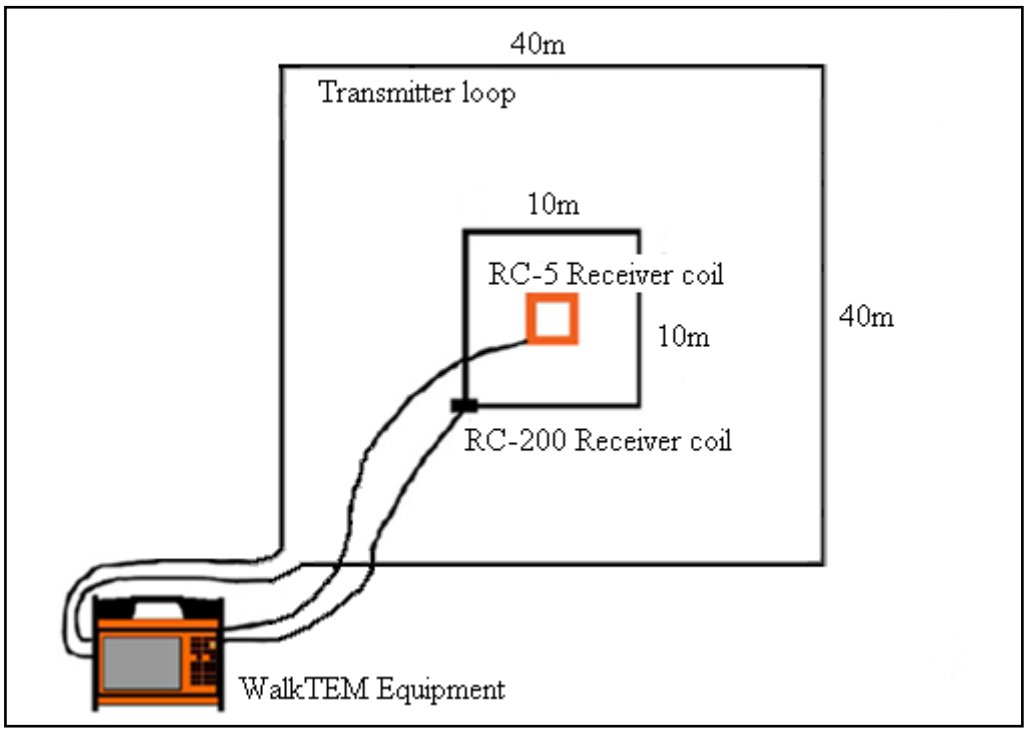

Figure 18: Principle layout of the WalkTEM equipment (WalkTEM user guide by ABEM Instrument, 2012) used during TDEM soundings in the Machile River Basin, South-Western Zambia

Figure 19: WalkTEM equipment being used during TDEM soundings in the Machile River Basin, South-Western Zambia

3.5 Noise Measurement

The data uncertainty can be determined from noise measurements. Every measurement recorded was either data/sounding or noise measurement (Hydrogeophysics Group (HGG), 2001). Therefore, to avoid coupling problems measurements were taken about 150m away from man-made installations such as power lines. Power lines hinder data collection because of electromagnetic noise. During data capture for this study noise was recorded in both the early moment (shallow depths) and late moment (deeper depths). For some data, the high moment curves were recorded as noise throughout the measurement. Such data were totally removed during processing in Singlesite Transient Electromagnetic (SiTEM) data processing software, ending up with the low moment data curves only and over processed high moment curves for some instances. In addition, sounding point MT019 on the Kazungula side of the Machile River Basin was not included in the data set because it recorded noise throughout the measurement due to high resistive sub-surface. Most high level noise contamination of data was caused by the nature of the formation in the subsurface which was highly resistive in some places. This is an indication that the TDEM sounding method can provide accurate information in a highly conductive environment (Tsourlos et al., 2004). Such factors as noise in inversion of data impacted on the interpretation. However, the data that was

difficult to interpret after inversion was taken back to SiTEM for further processing. The 1-D inversion method was the best method employed for this data.

3.6 WalkTEM Equipment

The WalkTEM equipment (Figure 19) was developed by Arhus University in close collaboration with ABEM Instrument (ABEM Instrument, 2012). It is a Time Domain Electromagnetic (TDEM) system designed for studying the geological sub-surface. The technology is designed to meet demanding requirements for groundwater investigations, salinity studies, civil engineering, mineral exploration and environmental investigations. The system connects to an external transmitter loop and a single or dual receiver coils (RC-5 and/or RC-200) (Figure 18). It has the ability to simultaneously collect and correlate data from its high frequency RC-5 receiver coil for shallow soundings and low frequency RC-200 receiver coil suitable for deeper soundings (ABEM Instruments, 2012).

The system includes external devices such as storage devices, keyboard and mouse, an integral battery charger, a 20 channel Global Positioning System (GPS) receiver, wired and wireless network interfaces as well as an integrated field PC running Windows XP. The integrated PC helps to evaluate and process data on-site. The system is powered by internal rechargeable batteries or by external power for extended operation time and enhances transmitter performance (ABEM Instruments, 2012).

3.7 Geophysical Data Analysis

Geophysical data were analysed using Singlesite Transient ElectroMagnetic (SiTEM) processing software and Singlesite ElectroMagnetic Data Inversion (SEMDI) software. These are two different software but are often used together hence referred to as SiTEM-SEMDI. SiTEM-SEMDI is a tool for processing, inversion and interpretation of ground-based Time-Domain Electromagnetic (TDEM) soundings. The software were developed by the HydroGeophysics Group (HGG) at the University of Aarhus in Denmark (HGG, 2001). The geological data were visualized in GeoScene3D software whereas all spatial data analysis and maps were done in ArcGIS software.

3.7.1 Geophysical Data Processing, Inversion and Interpretation

There are many ways in which TDEM data can be processed and these are largely dependent upon the instrument system used to acquire raw data (Reynolds, 1997). For the WalkTEM instrument system data were processed using the SiTEM software. The general data analysis procedure ranged from uploading the project file containing raw data from the equipment to the computer, checking the raw data curves in DataChecker software, processing the data in SiTEM and inversion and interpretation of the data in SEMDI (summarized in Figure 20). However, the main analysis software used for the TDEM data was the SiTEM-SEMDI software package (Version 3.1.22.101) which does a one-dimension (1-D) forward modeling and inversion of the data (HGG, 2001).

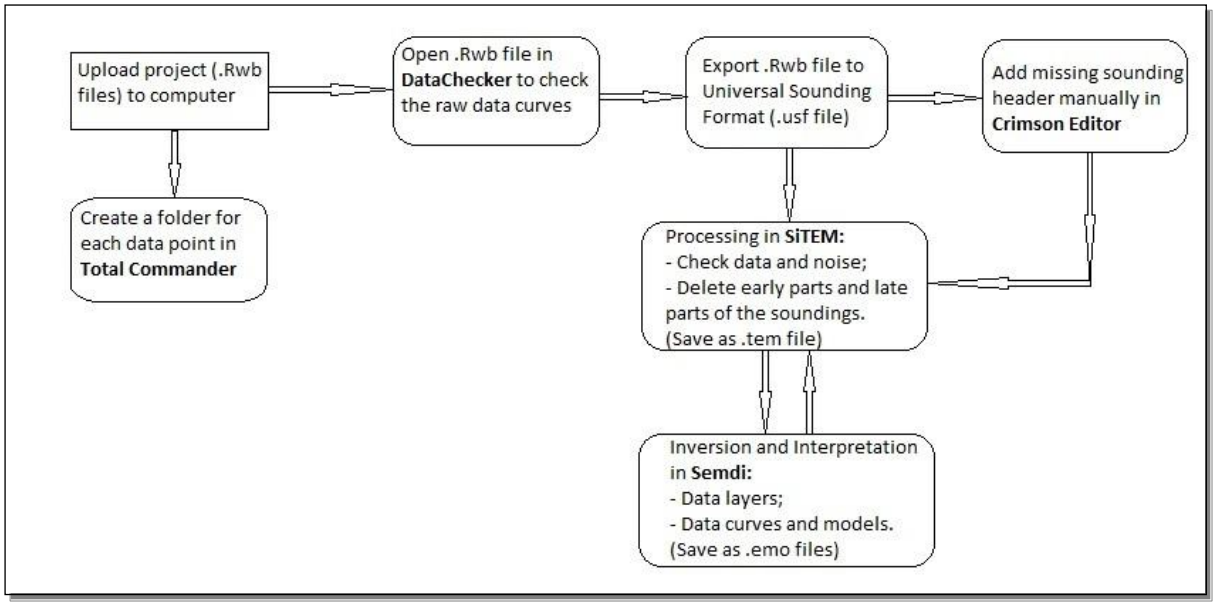

Figure 20: Ground-based Time-Domain Electromagnetic (TDEM) data analysis procedure (Processing, Inversion and Interpretation) followed in the Machile River Basin, South-Western Zambia (Modified from HGG, 2001)

(i) Data preparation for Processing (DataChecker-Version 16-2-2009)

Data (.Rwb) was imported into the computer from raw data files recorded in the TDEM field campaign equipment receiver (called WalkTEM from ABEM Instruments). Then, individual folders for each of the point data were created in Total Commander. In DataChecker, point raw data curves plotted as noise, high and low moment in Nanovolt as a function of time (us), with file extension .Rwb were checked and exported to a universal sounding format (.usf file) which was read in SiTEM. However, some .usf files generated by DataChecker had missing information on the sounding header (Table

1, left column), which had to be added manually in Crimson Editor SVN286 (Table 1, right column). The data in italics on the right column (Table 1) was the missing information which was manually added.

Table 1: Missing information on sounding header manually added in Crimson Editor SVN 286 during the data processing of the Machile River Basin, South-Western Zambia

DATACHECKER	**MANUALLY EDITED IN CRIMSON EDITOR**
!----------SOUNDING HEADER----------	!----------SOUNDING HEADER----------
/ARRAY: CENTRAL LOOP TEM	/ARRAY: CENTRAL LOOP TEM
/DATE: 20130307	/DATE: 20130307
/DAYTIME: 14.4317	/DAYTIME: 14.4317
/INSTRUMENT: "WalkTEM"	/INSTRUMENT: "WalkTEM"
/VOLTAGE_UNITS: V/M2	/VOLTAGE_UNITS: V/M2
/POINTS: 86	/POINTS: 86
/SOUNDING_NUMBER: 1	/SOUNDING_NUMBER: 1
/SOUNDING_NAME: 20130307 142554 024	/SOUNDING_NAME: 20130307 142554 024
/SWEEPS: 32	/SWEEPS: 32
/COIL_LOCATION: -1655.5150 2604.2747	/COIL_LOCATION: -1655.5150 2604.2747
	/LOOP_SIZE: 40.0 , 40.0
	/LOOP_TURNS: 1
	/LOW_PASS: 300000 , 1, 450000, 1
	/RAMP_TIME: 5.5E-06
	/RAMP_ON_TIME: 700E-06
	/TIME_DELAY: -1.7e-6
	/FIELD_SHIFT_FACTOR: 1.02
	!----------

(ii) SiTEM (Singlesite TEM Data Processing)

The TDEM data processing involves editing which includes deleting complete soundings of poor quality data, deleting or disabling bad data points from soundings and/or undeleting or enable previously disabled noise to data points (HGG, 2001). Editing is done in the data plot window in SiTEM. Data were trimmed in areas where noise was assumed to have too much influence on the data. In SiTEM the .usf file is opened as new project if being opened for the first time or as existing project. The data were also checked whether it was noise or signal. All the data with zero current were considered to be noise and the rest as data to be used (Herckenrath and Bauer, 2013). After processing, data were saved as .tem file, a format that opens in SEMDI for inversion in SEMDI. The processed data were easily accessed through a graphical user

interface. Multiple data plots can be viewed in different ways such as without a normalized moment (dB/dt:V/(m^2)) plotting raw data values, average normalized with moment (dB/dt (V/(Am^4)) which is an apparent resistivity or Rhoa (Ohm.m) to assist in the processing procedure. The dB/dt:V/Am^4 improves the overview of data making it easy to recognize and eliminate problems. All these graphical user interfaces were displayed as logarithmic plots of voltages as a function of decay time (milliseconds) (HGG, 2001). Raw data were transformed from voltages to average normalized moment (dB/dt) which were also calculated to apparent resistivity and plotted as a function of time (s) (Kirsch, 2006). SiTEM is project based because it uses data from the project database which contains raw data from a receiver instrument (HGG, 2001).

(iii) SEMDI (Singlesite Electromagnetic Data Inversion) and Interpretation

All TDEM soundings were interpreted using 1-D inversion method in Semdi software. Christiansen et al. (2006) describe the interpretation of TDEM data as approximately 50-100 times more computer intensive compared to interpretation of frequency and geoelectric data. SEMDI is a graphical user interface to the inversion engine which performs the actual inversion. The inversion in em1dinv.exe produces .emo files that contain the inverted models and forward data (HGG, 2001). The processed data that was saved as .tem file in SiTEM Software were opened in SEMDI for inversion and interpretation. Therefore, to invert the soundings processed earlier in SiTEM, a batch job was prepared. Starting models with 2 to 5 layers were set up and tested for each sounding. The job for the inversion was set up in the "Standard Batch Editor". After the inversion, the soundings were inspected in relation to estimated models and the varying number of layers. Three, four and five layer models were used. Where there was a need, modifications were made in SiTEM and inversions rerun.

After inversion and interpretation, the model with the best fit was selected and saved as .emo file. The data files were kept in two different libraries such as a library containing both the processed (.tem) files from SiTEM and that containing the generated optimum or best fit model files (emo.files) which passed quality control. The files that pass quality control constituted the results. When there was need for reinterpretation, the inverted model was reopened in SiTEM for further editing. After editing the file is resubmitted to an em1dinv.exe engine for further inversion. The inversion program attempts to create a better fit to the observed data. In contrast to SiTEM, SEMDI is file

based (it uses data that was saved as .tem files after processing in SiTEM Software). The optimum model parameters, line models and data plots for three sounding points are described below to illustrate how the results in the following chapter were arrived at.

3.7.2 The TDEM Measured and Interpreted Optimum Data Models

This sub-section is part of the data analysis process describing the interpreted apparent resistivity models obtained from the TDEM data inversion. This is the data that was used for interpolation in order to get the final results. The description was done using 3, 4 and 5 layered earth models from SM060T, MT021 and SM059T sounding points respectively. The measured apparent resistivity or Rhoa (Ωm) data plots as a function of time (s) (in error bars) give a fit between measured and theoretical data whereas the model response curve or line model (right panel) is a plot of apparent resistivity (Ωm) as a function of depth (m) after the inversion. The fit between the data and the model shows the accuracy of the survey data. The interpretation of each line model is given in Tables 2 to 4.

(i) Model Parameters and Analysis Tables

After inversion the parameters were displayed in a model parameters and analysis window in table formats (Tables 2, 3 and 4). Therefore, presented in Table 2, is the 3-layered parameters and analysis model with respective standard deviations for a sounding point SM060T.

Table 2: Apparent resistivity data for a 3-layered model at sounding point SM060T in Machile River Basin in South-Western Zambia

SM060T: 3-Layered Model						
	Res	**Thk**	**Dep**	**ResSTD**	**ThkSTD**	**DepSTD**
Layer 1	140.4	22.9	22.9	1.16	1.13	1.13
Layer 2	31.6	32	54.8	1.11	1.19	1.05
Layer 3	2417.5			2.41		

The parameters are defined and explained below:

Res = resistivity (Ωm);

Thk = thickness (m);

Dep = depth (m);
ResSTD = resistivity standard deviation (no unit);
ThkSTD = thickness standard deviation (no unit); and
DepSTD = depth standard deviation (no unit).

Layer 1 (Table 2) shows a resistivity of 140.4Ωm at 22.9m depth whose thickness is 22.9m. The resistivity in layer 1 has a standard deviation (STD) of 1.16 while thickness and depth each have an STD of 1.13. This implies that from the surface up to the depth of 22.9m resistivity was at 140.4 Ωm which reduced to 31.6Ωm at 54.8m then short up to 2417.5Ωm at an indefinite depth. Layer 2, whose thickness is 32m at 54.8m depth has a resistivity of 31.6Ωm. The STDs for layer 2 are 1.11 for resistivity, 1.19 for thickness and 1.05 for depth. The differences in resistivity at various depths and thickness showed the presence of different materials in the subsurface. Standard deviation indicates the certainty of the equipment about the measurement obtained. The recommended standard deviation according to HGG (2001) is 2 or less. The resistivity standard deviation of 1.11 in layer 2 means that the instrument was very certain about the resistivity obtained. If STD is greater than 2, then the equipment is less certain about the measurement whereas the STD of 99 means the equipment is not certain at all. This and other 3 layered model parameter tables are presented in Appendix 2.

The parameters and analysis model for a 4-layered earth model of a sounding point MT021 indicate that layer 1 is 6.8m thick, 6.8m deep with a resistivity of 64.4Ωm (Table 3). It shows a resistivity STD of 8, thickness STD of 2.81 and depth STD of 2.81 which imply that the equipment was less certain about the 3 parameters obtained. Layer 3 has a thickness STD of 99 indicating that the equipment was not certain at all. Note that the depth of the top layer (6.8) is the same as the layer thickness (6.8), hence the standard deviation for the two parameters on this layer happens to be the same as well. The same interpretation applies to all the other 4-earth layered models (Appendix 3).

Table 3: Apparent resistivity data for a 4-layered model at sounding point MT021 in Machile River Basin in South-Western Zambia

MT021: 4-Layered Model						
	Res	**Thk**	**Dep**	**ResSTD**	**ThkSTD**	**DepSTD**
Layer 1	64.4	6.8	6.8	8	2.81	2.81
Layer 2	15.3	16.9	23.7	1.3	2.12	1.29
Layer 3	105.4	38.5	62.1	5.82	99	3.18
Layer 4	189.3			1.48		

A 5-layered model of the subsurface (Table 4) indicate a resistivity of 426.2Ωm at 21m depth and a resistivity STD of 99 in layer 1 indicating that the equipment was not certain about the resistivity obtained. Layer 3 has the lowest resistivity of 11.8Ωm at 58.3m depth with a thickness of 15m. The model indicates that resistivity was reducing with depth up to 58.3m, and then started increasing beyond this depth. Similar 5-layered earth models for all the other soundings are presented in Appendix 4.

Table 4: Apparent resistivity data for a 5-layered model at sounding point SM059T in Machile River Basin in South-Western Zambia

SM059T: 5-Layered Model						
	Res	**Thk**	**Dep**	**ResSTD**	**ThkSTD**	**DepSTD**
Layer 1	426.2	21	21	99	4.93	4.93
Layer 2	48.4	22.3	43.3	3.58	3.17	1.26
Layer 3	11.8	15	58.3	2.22	4.14	1.54
Layer 4	64.8	84.7	143	1.61	2.08	1.55
Layer 5	186.6			1.71		

There are the data used for the interpolation of resistivities and salinity at 10m, 30m, 50m and 80m depths in the results chapter. Resistivity plots, as a function of depth, are presented in a line model window while resistivity plots, as a function of time, are presented in a data plot window. Only the models which gave satisfying fit between observed data and the model were used in the interpretation of the data.

(ii) Data Plots and Line Models

The calculated apparent resistivity (Ohm.m) displayed as a function of time (s) (Figure 21, left panel) plotted in error bars is a best fit 3-layered earth model for sounding SM060T indicating the three channels of data measurement. The red, green and blue

curves in error bars indicate the channels through which apparent resistivity of the subsurface was measured with time. The layered model (right panel) (Figure 21) represents the vertical delineation of calculated apparent resistivity plotted as an inverse or line model or model response curve. The parameters in this model are presented in a model parameter and analysis table (Table 2) where the line model indicates that at 22.9m depth, there was a formation resistivity of 140.4Ωm which reduced to 31.6Ωm at 54.8m, then increased to 2417.5Ωm at depth beyond 54.8m. The resistivities and depths in Table 2 essentially give an interpretation of the line model. The best fit 3-layered data plots and the inverse models for all the soundings in the Machile River Basin are presented in Appendix 5.

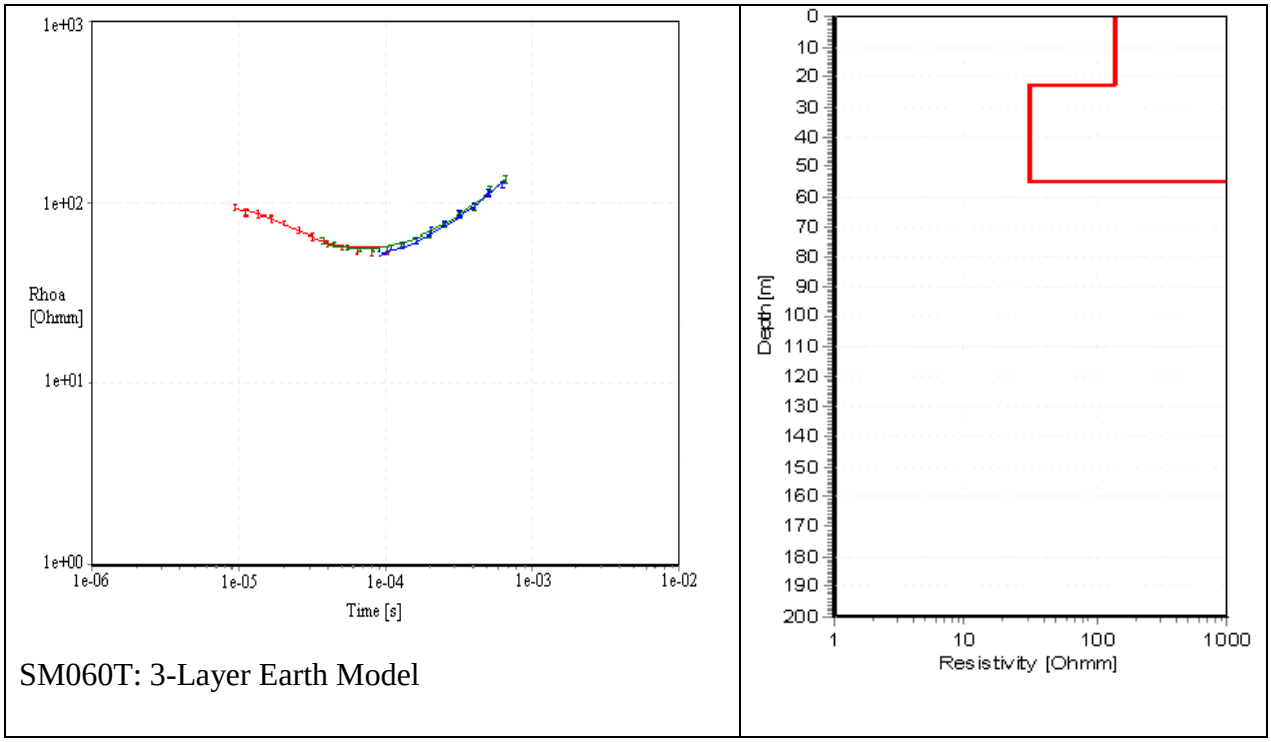

Figure 21: Apparent resistivity data (in error bars) and model response curve for a 3-layered model at sounding point SM060T in Machile-Zambezi Basin, South-Western, Zambia

The curves (Figure 22) are plots of 4-layer models for sounding point MT021. The plots in error bars have two channels of resistivity measurement with time. The inverse model presents the parameters indicated in Table 3 where the subsurface at 6.8m depth had a resistivity of 64.4Ωm which reduced to 15.3Ωm at 23.7m. At 62.1m depth, resistivity increased to 105.4Ωm and to 189.6Ωm at an indefinite depth. This is the data that is used to show the distribution of salinity. The parameters (Table 3) are the

interpretation of the line model (Figure 22). The 4-layered inverse models and data plots for all the other soundings are given in Appendix 6.

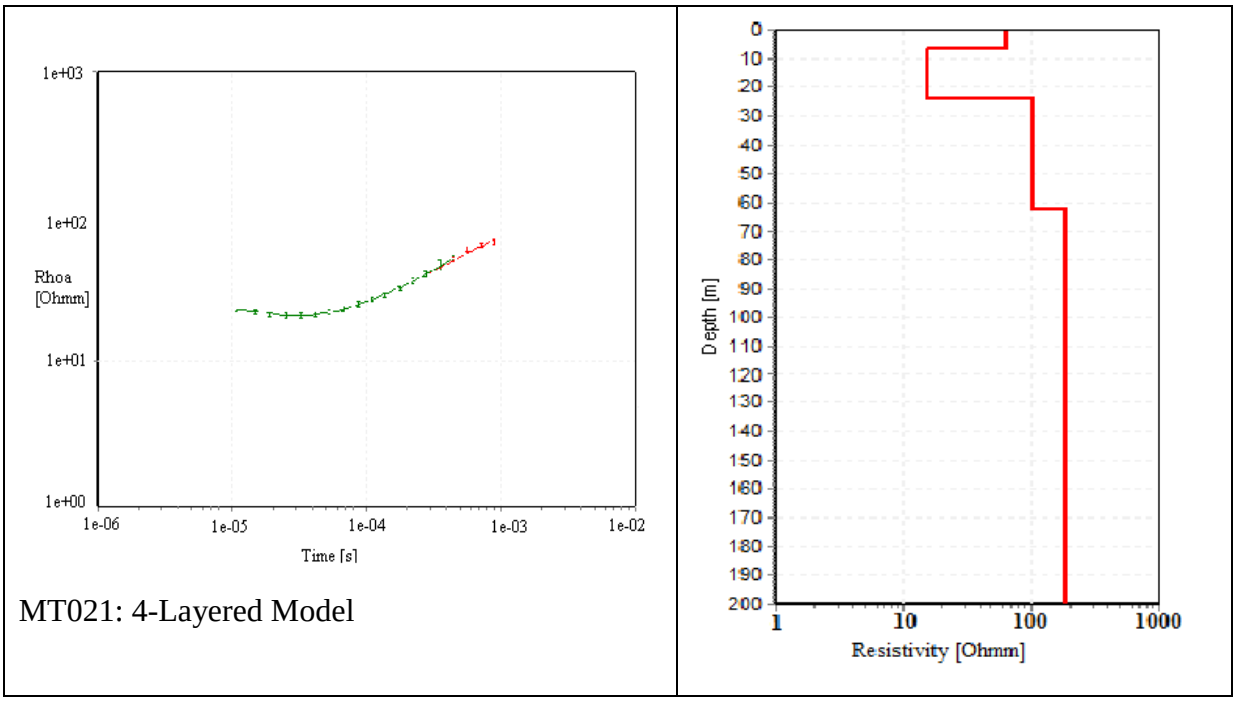

Figure 22: Apparent resistivity data (in error bars) and model response curve for a 4-layered model at sounding point MT021 in Machile-Zambezi Basin, South-Western, Zambia

The 5-layer earth model (Figure 23) shows the resistivity data measurement plot (left panel) and the line model (right panel). The line model indicates resistivity of 426.2Ωm at 21m depth which reduced to 48.4Ωm at 22.3m and further reduced to 11.8Ωm at 15m. At 84.7m, resistivity had increased to 64.6Ωm and to 186.6Ωm at an indefinite depth (as interpreted in Table 4). Similarly, the 5-layered line models and data plots for all the other soundings are presented in Appendix 7.

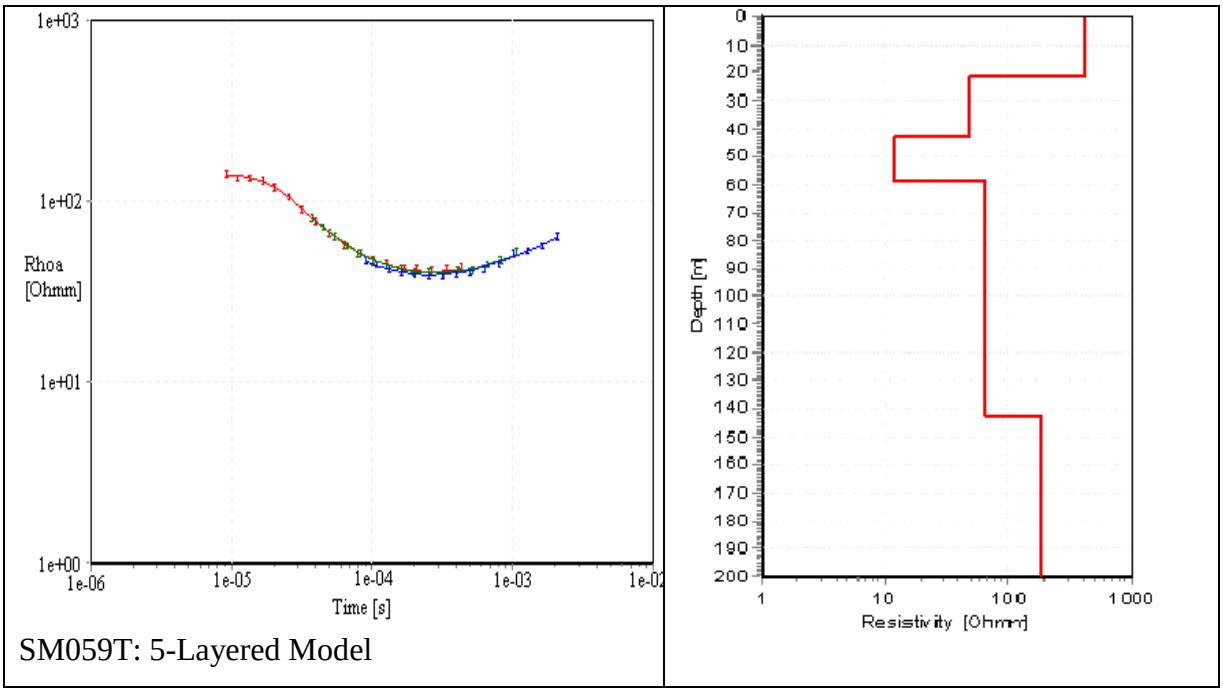

Figure 23: Apparent resistivity data (in error bars) and model response curve for a 5 layered model at sounding point SM059T in Machile-Zambezi Basin, South-Western, Zambia

Based on the relationship between the formation electrical resistivity and electrical conductivity, and assuming a constant formation factor of 5, Flemming (2009) classified formation resistivities in terms of saline, brackish and fresh groundwater (Table 5).

Table 5: Classification of groundwater salinity in terms of formation resistivities assuming a constant formation factor of 5 (after Flemming, 2009)

Class name	**Formation resistivity (Ωm)**
Saline water	< 35
Brackish water	35 – 70
Freshwater	> 70

These were the classifications adopted for this study in order to show the spatial distribution of saline, brackish and fresh groundwater in the Machile River Basin.

3.7.3 Spatial Data Analysis

All spatial data were analyzed in ArcGIS. The analysis included interpolation of sub-surface apparent electrical resistivities and mapping of groundwater salinity over the Machile River Basin. Measurements were strategically collected at dispersed sample locations and predicted values were assigned to all other locations using kriging method.

(i) Interpolation using Kriging in ArcGIS

Subsurface electrical resistivities captured at spatial locations in the Machile River Basin were interpolated in ArcGIS using Ordinary Kriging method. Ordinary Kriging is a general and widely used interpolation method. Kriging is a geostatistical procedure that generates an estimated surface from a scattered set of points with z-values (ESRI, 2012). Visiting every location in the study area to take measurements would be expensive and typically not practical. However, sample points were used to derive the prevailing values using Spatial Analyst extension in ArcGIS which creates the surface in the native grid format (Childs, 2004). Kriging assumes that the distance or direction between sample points reflects a spatial correlation that can be used to explain variation in the surface (meaning that things that are close together tend to have similar characteristics (Kumar, 2006). The Kriging tools fit a general mathematical function (Equation 7) to all points within a specified radius in order to determine the output value for each location.

$$Z(s_0) = \sum_{i=1}^{N} \lambda_i Z(s_i) \quad \text{.....Equation 7}$$

Where,

$Z(s_0) =$ the predicted value for location s_0;

$\lambda_i =$ an unknown weight for the measured value at the *i*th location;

$s_0 =$ the prediction location;

$Z(s_i) =$ the observed value at the location s_i; and

$N =$ the number of measured values (ESRI, 2012).

(ii) Conceptual Outline of Kriging

In Kriging every known data value and every missing data has an associated variance. Variance, also referred to as a measure of the uncertainty of a value, is a statistical parameter of a quantitative measure of confidence in a data value. Conceptually, variance plays a role of a weighting function. With the points further away, you are less certain of their value. Therefore, the uncertainty increases with distance from the known value. Variance for each known data value should be set to the uncertainty of that value. This means that each known value has a variance function associated with it, which is used to determine the variance of the data values around the known location. The curves have the minimum value, usually zero (0) at any known data location and the maximum value of one (1) at some specified distance (range) away from that point. In addition to variance and range, Kriging allows for a variance discontinuity at the known data value called the nugget. The effectiveness of Kriging depends on the correct specification of several parameters that describe the semivariogram. However, Kriging is forceful, even with a naive selection of parameters the method still works well (El-Sheimy, 1999).

3.8 Geological Modeling

The lithological data of the study area were modeled in 2-dimensional (2D) vertical cross sections using the GeoScene3D version 9.5.0.377 software. GeoScene3D is a geodata visualization and geological modelling tool. The software was used because it is suited for groundwater use providing visualization, interpretation of the data (I-GIS, 2010). The data were visualized in two profile lines (the SE-NW and NE-SW) across the Machile River Basin.

3.8.1 Geological Data Preparation

Geological data were collected from existing borehole logs in Sesheke and Kazungula mostly drilled by JICA under Department of Water Affairs, Ministry of Mines, Energy and Water Development and by Ministry of Local Government and Housing. The elevation at which the lithological data were collected was calculated as top and bottom elevation. The depth of investigation was also presented as top and bottom depths for all the points. Lithologies were coded and rock values indicated in preparation for geological modelling. The lithological data of the Machile River Basin used to create a geological model are presented in Appendices 8 to 24. The area in the northern part of the Machile River Basin that did not have real boreholes had pseudo boreholes

(Appendix 24) created based on TDEM data. The lithological data from the pseudo boreholes were counter-checked with the nearest boreholes and rock outcrops in some places. The pseudo boreholes lithological data were used in locations with missing real borehole data.

3.8.2 Procedure for Creating a Geological Model

The procedure for creating a geological model was as followed:

(i) An excel sheet containing lithological information extracted from 160 boreholes in Sesheke and Kazungula was create (Appendices 8 to 24);

(ii) Seven pseudo boreholes were created in the northern part of the Machile River Basin based on TDEM data and they were counter-checked with the nearest boreholes and rock outcrops in some places (Appendix 24);

(iii) The data from the real boreholes and pseudo boreholes were combined in one excel sheet;

(iv) The lithological data were imported into GeoScene3D on the basis of point information for the top and bottom elevations for each layer type. For example, an import was made for all points containing the top elevation of sandstone only and a separate import was made for all points containing the bottom elevation of sandstone only;

(v) Lithological surfaces were then created in GeoScene3D by interpolating the respective lithological points using Inverse Distance Weigting (IDW) (Equation 8). An export of 2.0 was used with zero (0) smoothing factor. For the most dominant (with large extent) lithologies such as sand and sandstone, a search radius of 25km was used whereas for minor (limited extent) lithologies, the search radius was reduced to 15km. A copy of the geological model data to be opened in GeoScene 3D have been served on a Computer Disc (CD) for submission alongside the thesis (Appendix 25); and

(vi) The respective geological layers were then defined by creating new layer objects bounded by respective top and bottom surfaces created above.

Inverse distance weighted methods are based on the assumption that the interpolating surface should be influenced more by the nearby points and less by the more distant points. The interpolating surface is a weighted average of the scatter points and the weight assigned to each scatter point diminishes as the distance from the interpolation

point to the scatter point increases (Shepard, 1968). The general equation used to interpolate is as follows:

$F(x, y) = \sum_{i=1}^{n} w_i f_i$……..…….……..Equation 8

Where,

$F =$ *weighted average;*

$n =$ number of scatter points in a set;

$fi =$ function values at the scatter points (e.g. the data set values); and

$wi =$ weight functions assigned to each scatter point.

The weight function is expressed in equation 9 as

$w_i = \frac{h_i^{-p}}{\sum_{j=1}^{n} h_j^{-p}}$ ……Equation 9

Where,

$p =$ power parameter (typically, $p = 2$); and

$hi =$ distance from the scatter point to the interpolation point (Equation 10).

$h_i = \sqrt{(x - x_i)^2 + (y - y_i)^2}$……..……Equation 10

Where,

$(x, y) =$ coordinates of the interpolation point

$(x_i, y_i) =$coordinates of each scatter point.

The weight function varies from a value of unity at the scatter point to a value approaching zero as the distance from the scatter point increases. The effect of the weight function is that the surface interpolates each scatter point and is influenced most strongly between scatter points by the points closest to the point being interpolated (Shepard, 1968). All these equations run behind the software.

CHAPTER 4: RESULTS AND DISCUSSION

This chapter presents and discusses the results in order to address the three objectives of this study.

4.1 The Distribution of Electrical Resistivities in the Subsurface Obtained from Ground-Based TDEM Method on a Regional Scale

The subsurface of the Machile River Basin is characterized by electrical resistivities ranging from 1 to 19,738Ωm. Interpolated resistivities were only considered at the following depths:10, 30, 50 and 80m in order to obtain the spatial distribution pattern of the subsurface resistivities.

4.1.1 Subsurface Electrical Resistivity Distribution at 10m Depth

The subsurface electrical resistivities at 10m ranged from 1 to 645Ωm (in the first range) covering a cone shaped area from Lusu and Mushukula in the south-west to Sekute and Kanchele in the south-east through to Moomba wards in the north-east (Figure 24). The different colours show classes of resistivities in different places at this particular depth. Resistivities ranging from 645 to 1,277Ωm only cover parts of Luazamba, Sichili, Moomba, Chooma, Ngwezi and Simango wards whereas other sections of Sichili, Moomba, Kamanga, Chooma, Ngwezi, Kauwe and Simango have resistivities of 1,277 to 1,909Ωm. Resistivities of 1,909 to 2,541Ωm were also observed in small areas around Nawinda, Sichili, Luamuloba and Kauwe wards whereas some areas in Nawinda and Luamuloba had resistivities ranging from 2,541 to 3,173Ωm.

The area within 10m depth is overlain by unconsolidated Kalahari sediments such as unconsolidated sands (Money 1972). Nawinda, Sichili, Luamuloba and Kauwe have quite high electrical resistivities whereas areas stretching from Lusu and Mushukula to Sekute up north in Moomba have relatively low resistivities (Figure 24). The resistivities range found in the Machile River Basin are consistent with the resistivities of sediments according to Geonics (1980) and Telford (1976) where they found out that the resistivity of sand ranges from 500 to 5000Ωm (Table 6). The occurrence of groundwater salinity cannot be determined at this point, however, the resistivity range from 1 to 645Ωm is of great importance because salinity is identified by its low resistivity.

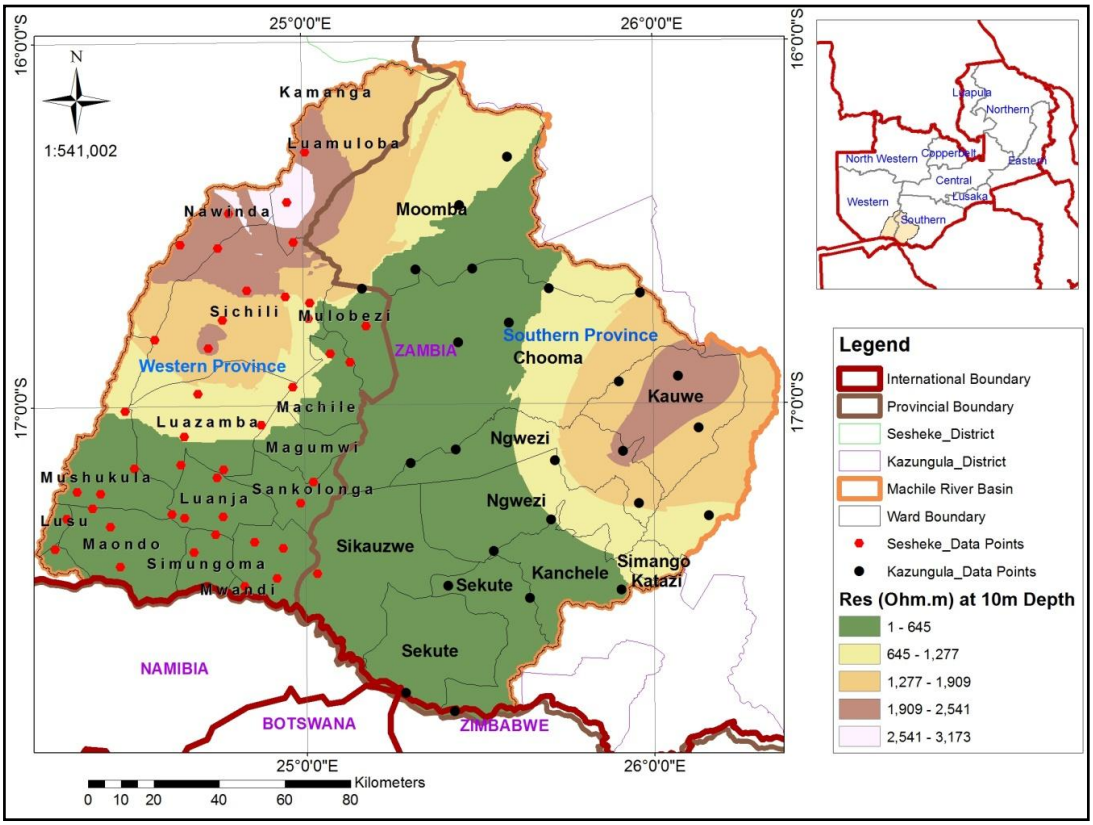

Figure 24: Subsurface resistivities at 10m depth from 44 existing TDEM soundings by Chongo (2011) and 25 survey soundings in the Machile River Basin, South-Western Zambia

Table 6: Resistivities of rocks and sediments in a sedimentary environment (modified from Geonics, 1980 after Telford, 1976).

Rocks and Sediments	Resistivity Range (Ohm.m)
Rocks	
Granite	300 – 1,000,000
Basalt	10 – 13,000,000
Gneiss	3,000,000
Dolomite	350 – 5,000
Schists	20 – 10,000
Slates	600 – 40,000,000
Sediments	
Alluvium and sands	10 – 800
Sand	500 – 5,000
Limestone	50 – 10,000,000
Consolidated shale	20 – 2,000
Quartzites	10 – 200,000,000
Sandstones	1 – 640,000,000
Clays	1 – 100

4.1.2 Sub-Surface Electrical Resistivity Distribution at 30m Depth

Subsurface resistivities at 30 meter depth ranged from 1 to 10, 616Ωm, with the highest covering parts of Simango, Katazi, Kanchele, Sekute, Ngwezi, Sichili, Nawinda and Kamanga wards (Figure 25). In terms of salinity, it cannot be determined at this point because the TDEM technique is not suitable to define resistive layers (Schmutz et al., 2001). However, resistivities ranging from 1 to 1,883Ωm (in green) are relatively significant because it is within this area that saline groundwater would exist. The area at this depth is overlain by unconsolidated sand and sandstone in some areas. Sandstone is also observed covering parts of Katazi, Kanchele and Simango wards with resistivities of 6,249 to 10, 616Ωm which are within the sandstone ranges (Geonics, 1980). Sandstone, according to Geonics (1980), has resistivity values ranging from 1 to 640,000,000Ωm (Table 6).

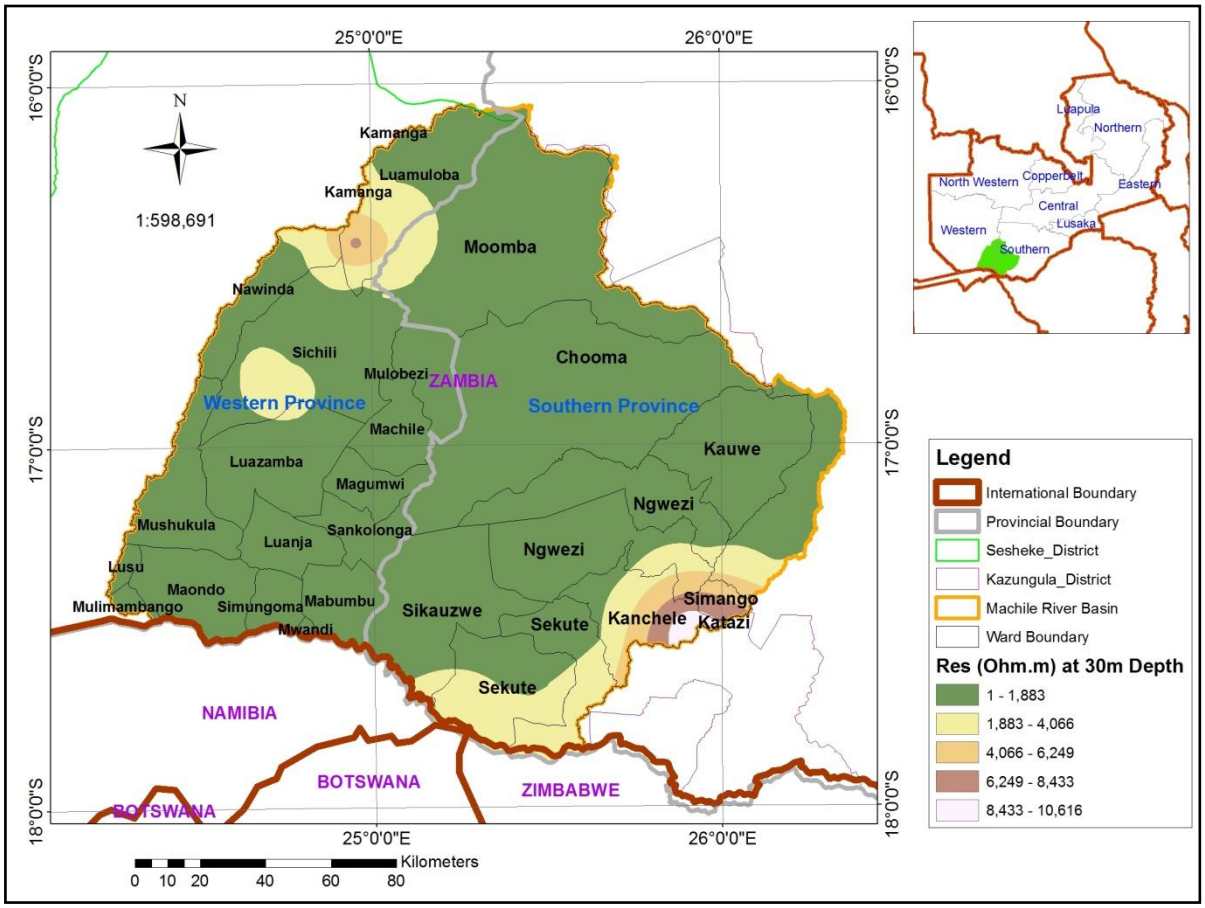

Figure 25: Ground resistivities at 30m depth in the Machile River Basin, South-Western Zambia

4.1.3 Subsurface Electrical Resistivity Distribution at 50m Depth

At 50m depth, subsurface resistivities covering all the layers range from 1 to 17,186Ωm. Salinity, at this point is expected to exist within the range 1 to 2,821Ωm which covers over three quarters of the study area. The geology overlying the 50m depth range from unconsolidated sands to sandstone and basalt to granite in some areas (Money, 1972). Sand and sandstone, as outlined by Geonics (1980), have resistivities ranging from 1 to 640,000,000Ωm. The resistivity variations of between 1 and 17,186 Ωm at 50m depths are consistent with those observed by Boucher et al. (2009) at 5 to 55m with a resistivity of about 1000Ωm. The basalt and granite were also observed outcropping in the south-east around a small area covering Kanchele, Simango, Ngwezi and Katazi (Figure 26). Using the basalts and granites resistivity values that range from 10 to 13,000,000Ωm and 300 to 1,000,000Ωm respectively (Table 6; Geonics, 1980) in the Machile River Basin, it is observed that the results (1 to 17,186 Ωm) could have been produced by these rock types. For example, basalts have been observed to occur in a

small area bordering Sichili and Luamuloba wards in the north. The source of the measured resistivities could be due to basalts which occur in the area as mapped by Money (1972).

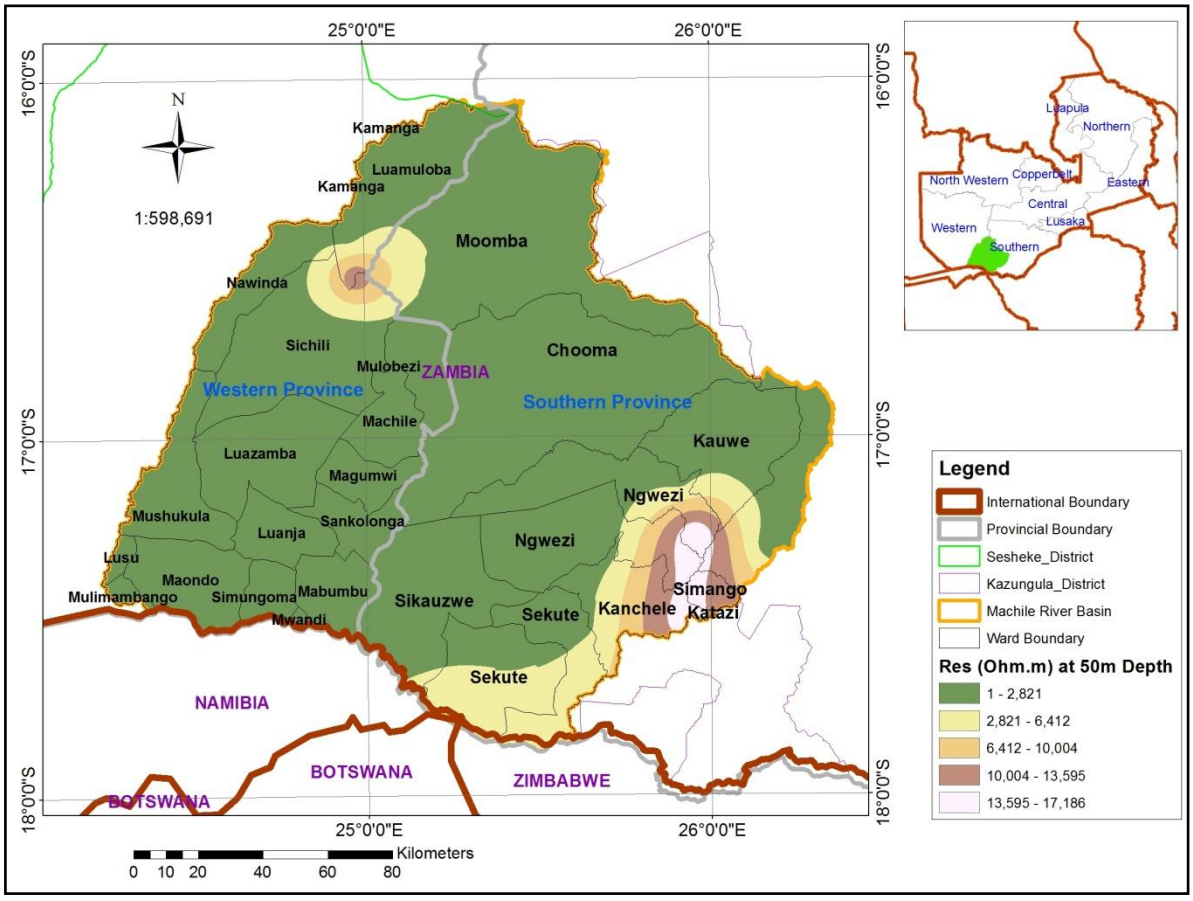

Figure 26: Ground resistivities at 50m depth in the Machile River Basin, South-Western Zambia

4.1.4 Subsurface Electrical Resistivity Distribution at 80m Depth

Subsurface resistivities at 80m depth range from 1 to 19,738Ωm (Figure 27). The major formation in this depth range is the sandstone. The sandstone, in the eastern and south-eastern parts of the study area is underlain by basalt, granite and other rocks of the Karoo formations. The occurrence of granite around Sichili is consistent with the mapping by Money (1972). These rocks exist at depths beyond 80m. Like at other depths above, resistivities ranging from 1 to 2,987Ωm and covering the largest part of the study area at 80m are important because saline groundwater would exist at such depths. The existence of the basalt at this depth is confirmed by the findings of Margane et al. (2005) in the Eastern Caprivi at 3 locations beneath and beyond 80 to 120m depth,

which indicates that basalts extend beyond Zambian borders and form part of the Batoka Basalt Formation of the Upper Karoo Group (Nyambe, 1999).

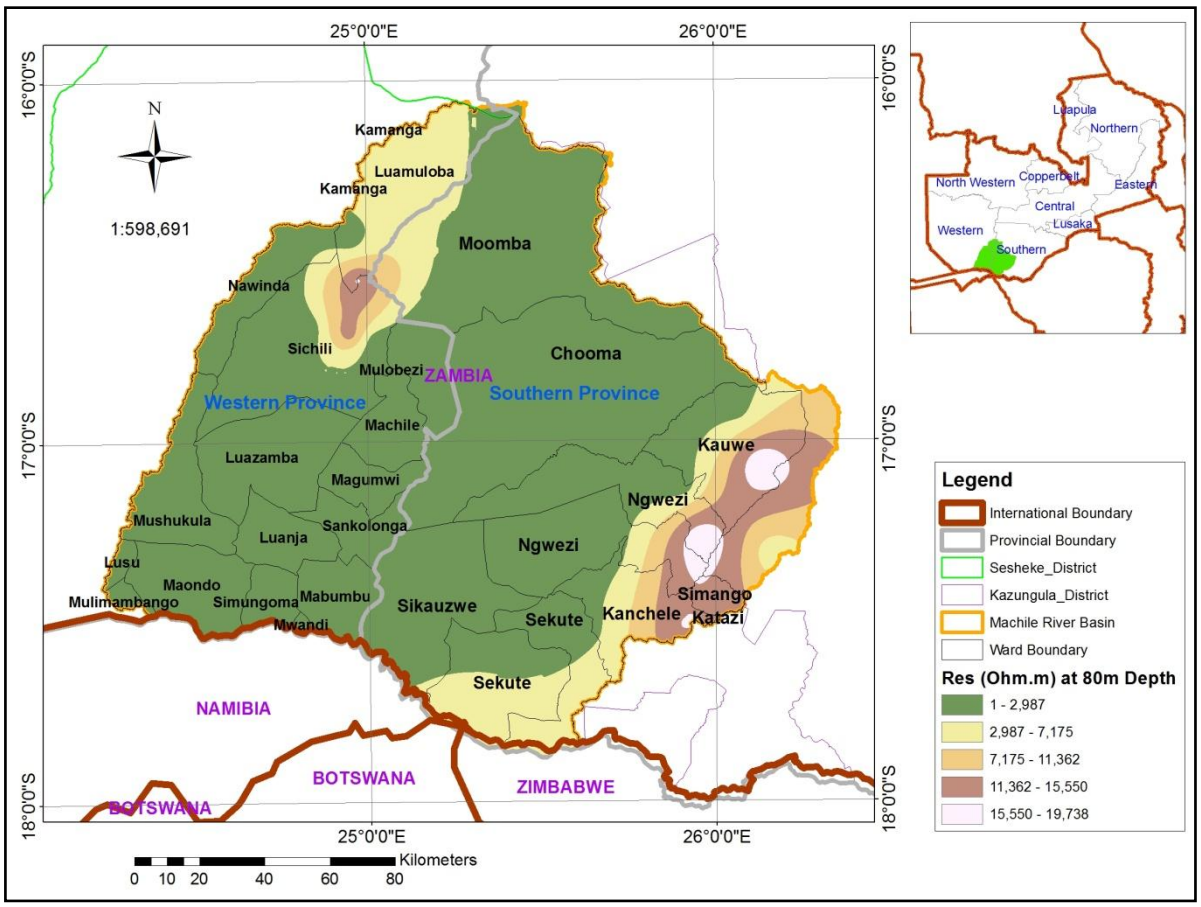

Figure 27: Ground resistivities at 80m depth in the Machile River Basin, South-Western Zambia

4.2 The Spatial Distribution of Saline Groundwater Based on Electrical Resistivities from Ground-Based TDEM Measurements

This sub-section presents the spatial distribution of saline groundwater at 10, 30, 50 and 80m depths. Three zones, with respect to resistivity values corresponding to groundwater types such as saline, brackish and freshwater, were detected. Ordinary Kriging interpolation method was used in order to obtain these results. Saline groundwater classification by Flemming (2009) is used in the interpretation of the data for 10m, 30m, 50 and 80m depths.

Generally, groundwater contaminants such as soluble salts significantly reduce resistivity. At 10 m depth, using Table 5 (Flemming, 2009), saline groundwater was

typically identified by the presence of low resistivity of less than 35Ωm around a small area bordering Mabumbu and Sikaunzwe wards in Sesheke and Kazungula districts, respectively (Figure 28). In Figure 28, red indicates saline groundwater, whereas yellow and blue indicate brackish water and freshwater, respectively. Boucher et al. (2009) equally observed the saline water pocket from the transient electromagnetic results with a slight decrease of resistivity (up to 32Ωm) between 5 and 15m depth. Chongo et al. (2011) similarly observed electrical resistivities of less than 20Ωm up to 10m depth predominant in the South-Eastern part of the Barotse Basin indicating the presence of saline water. However, Batayneh (2006) using electrical resistivity methods for detecting subsurface fresh and saline water, detected three water bearing formations including (i) strata saturated with fresh to slightly brackish groundwater, (ii) brine mixed with fresh to brackish groundwater and (iii) water bearing formation containing brine. This study does not agree with Batayneh (2006) because water is unlikely to be a mixture of brine with fresh to brackish water but can be fresh, brackish, saline or brine. Brackish groundwater in the Machile River Basin existed outside the saline water body stretching up to the Zambezi River in the south-west and to Chooma Ward in the south-east part of the basin. The rest of the study area, at 10m depth, is underlain by freshwater (Figure 28). Saline groundwater exists within the resistivity category of 1 to 645Ωm (Figure 24) within the unconsolidated Kalahari sediments and not in the other categories.

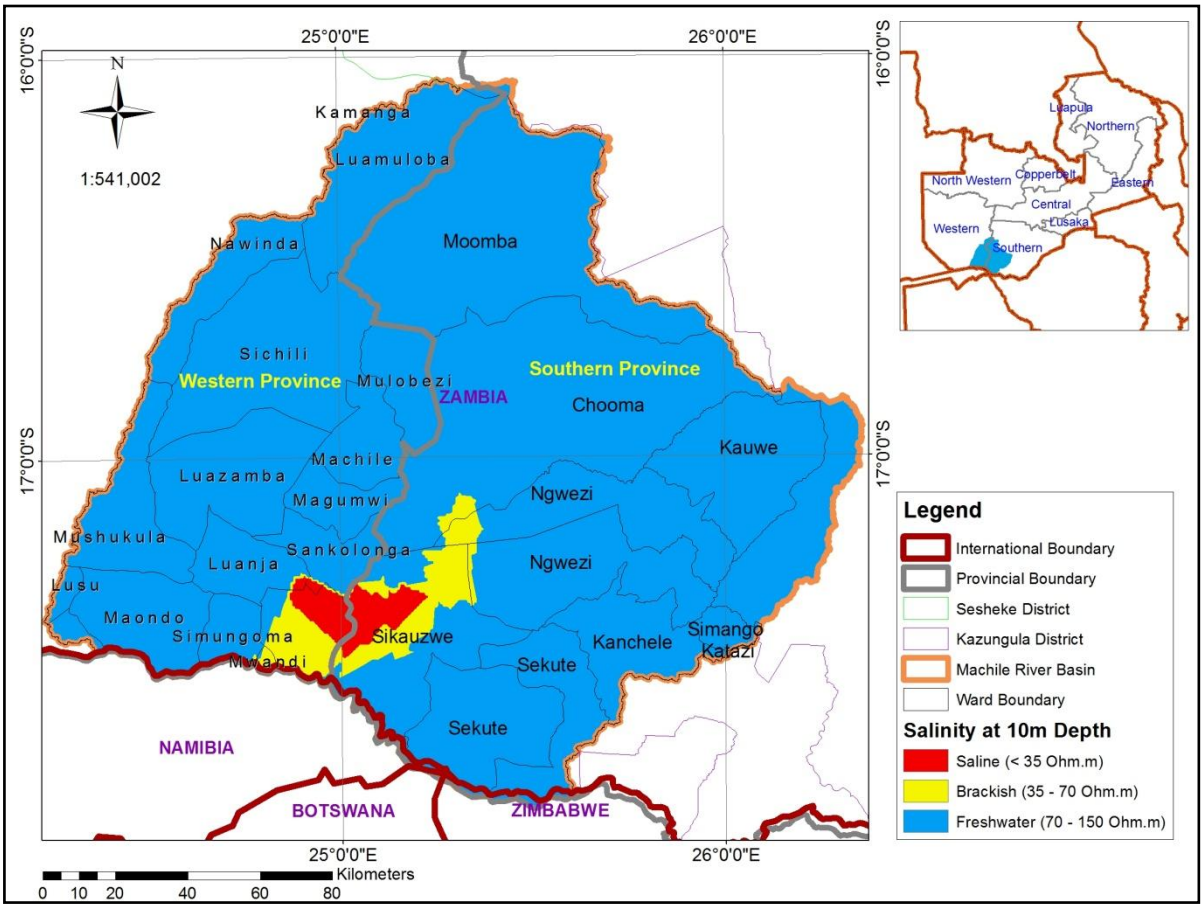

Figure 28: Groundwater salinity map at 10m depth in the Machile River Basin, South-Western Zambia

At 30m depth, the saline groundwater (Figure 29) is overlain by freshwater (Figure 28). It forms a tick-like shape of saline water stretching from Mushukula in the south-west, curving around Simungoma and Mwandi wards and going further in the north-east direction to Chooma Ward and across the Machile River. Similarly, results obtained by Chongo et al. (2011) on the Sesheke side, indicate the presence of a saline aquifer with resistivity values of less than 35Ωm overlain by an unconfined freshwater aquifer with resistivity of values greater than 70Ωm. In Luanja Ward, a freshwater pocket is observed to be surrounded by brackish groundwater which is in turn surrounded by saline water on the eastern through southern to western parts of the ward (Figure 29). Parts of Ngwezi Ward are also observed to be underlain by saline water. Generally, there is a correlation between resistivity and salinity in groundwater. It shows that salinity is one of the factors controlling subsurface resistivity. Saline groundwater at this depth occurs within the unconsolidated Kalahari sediments and sandstones.

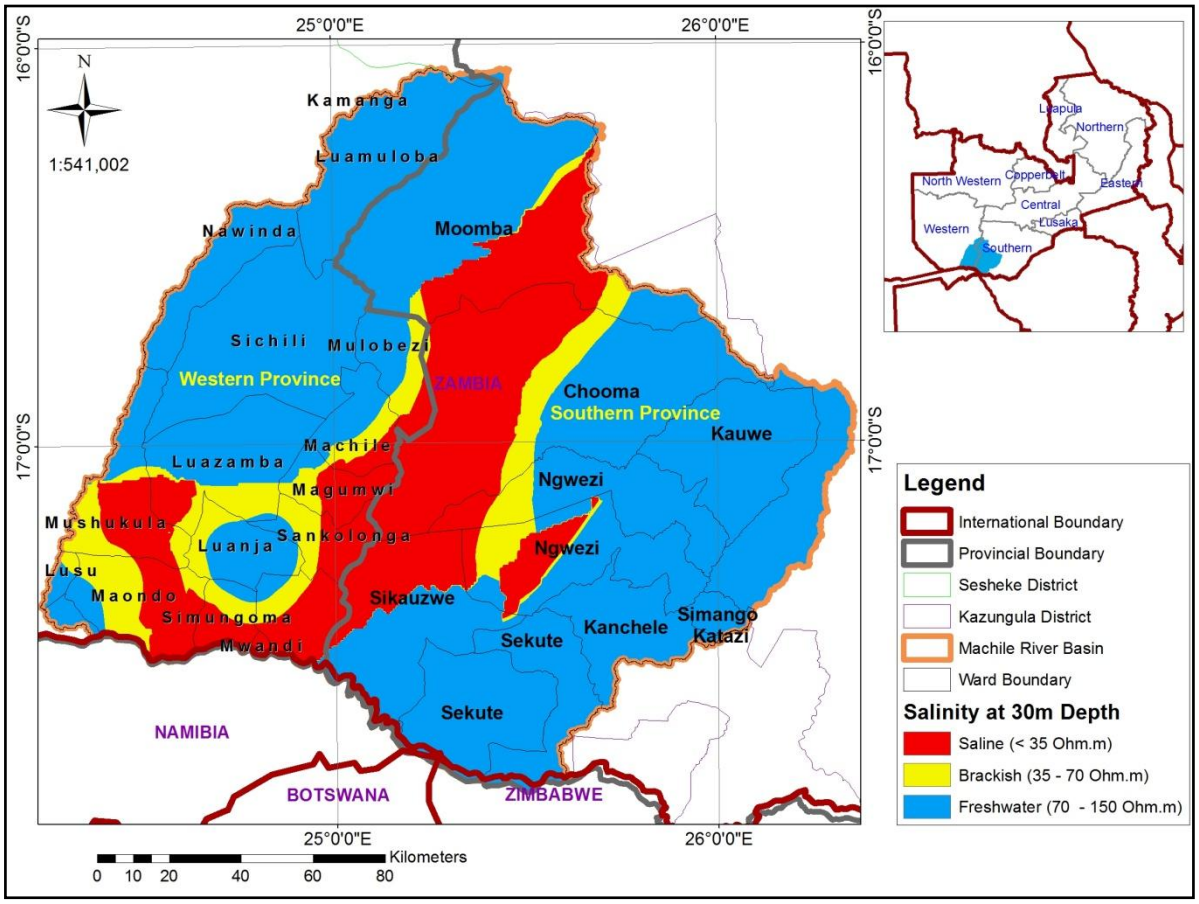

Figure 29: Groundwater salinity map at 30m depth in the Machile River Basin, South-Western Zambia

Further observations, show that the extent of occurrence of saline groundwater at 50m depth (Figure 30) was higher than at 30m depth which was also a lot higher than at 10m depth. Saline groundwater meanders from Mushukula and Lusu wards through Simungoma and Mwandi in the south-west and towards the north-east direction up to Moomba Ward which further curves into Kamanga Ward. Brackish water was observed on the edges of saline water whereas the rest of the area is overlain by freshwater. A stretch of saline groundwater cutting through Ngwezi Ward in the granite formation (Figure 5) into Chooma Ward leaving a stripe of freshwater on the left hand side bounded by brackish groundwater on the further left hand side was also observed (Figure 30). Most of the saline groundwater at 50m depth exists within the unconsolidated Kalahari sediments and sandstones. The isolated pocket of saline groundwater in the eastern part of the study area east of Kauwe Ward seems to have a different source and exist in undifferentiated granites (Figure 5). The isolated salinity pocket could be as a result of dissolution (Appello and Postma, 2005). Similarly, the

saline aquifer was observed by Bauer et al. (2006) along a profile in the Tshwene Island of the Okavango Delta at depths shallower than 50m. Similar results were obtained in the Thata Island where resistivity below 5Ωm was identified at shallow depths.

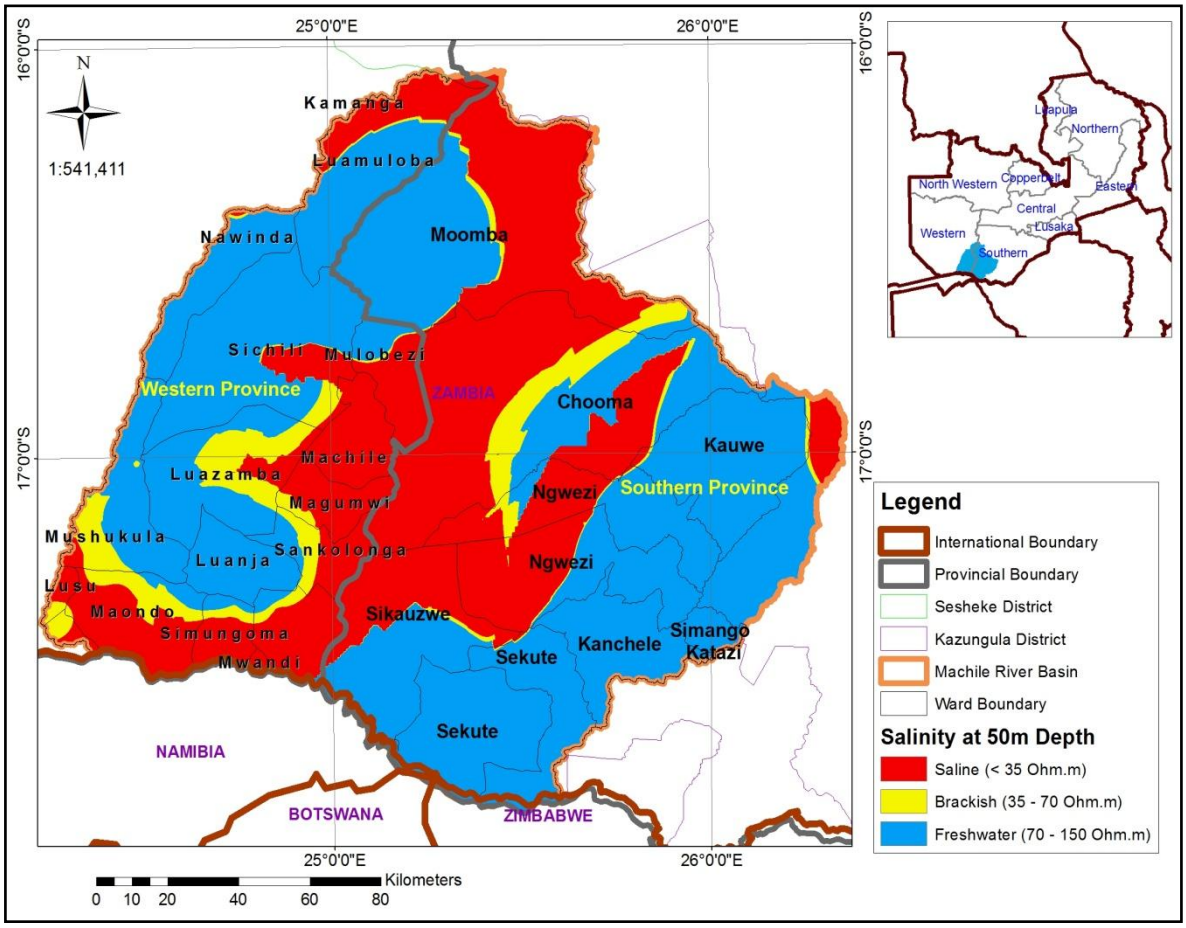

Figure 30: Groundwater salinity map at 50m depth in the Machile River Basin, South-Western Zambia

The extent of saline groundwater distribution at 80m (Figure 31) is lower than at 50m (Figure 30). A reduction in the extent of saline groundwater distribution observed at 80m depth in the western part of the study area indicates that freshwater could exist at depths deeper than 80m. These results were consistent with those obtained in a study by Kafri et al. (1997), where the TDEM measurement detected high resistivity units of freshwater underlying the brines of resistivities less than 1Ωm. This interpretation is also consistent with Choudhury (2001) in a geophysical study of the saline water intrusion in a coastal alluvial terrain where he showed that fresh groundwater existed at 128 and 210m depths. Furthermore, results obtained by Margane et al. (2005) in a groundwater investigations study using ground-based TEM method in Eastern Caprivi

indicated that fresh groundwater resources existed beyond 80 to 120 meters. In their study, brackish water was also observed above the freshwater aquifer. Margane et al. (2005) further indicated that four boreholes out of 6 drilled in Eastern Caprivi penetrated a high yielding rock beyond 125 to 135 meters depth encountering high quality freshwater. In addition, Bauer et al. (2006) recognized a freshwater aquifer with resistivities above 100Ωm below a low resistivity anomaly of the salt pan in Tshwene Island in the Okavango Delta. However, IGRAC (2009) argued that fresh groundwater is stored at shallow depths of the geological layers that are most actively involved in the hydrological cycle. They further added that saline groundwater on earth is mostly present in stagnant conditions at deeper depths and that it may have been there for thousands or millions of years. Based on this principle, IGRAC (2009) concluded that fresh groundwater is comparatively young because it is actively recharged.

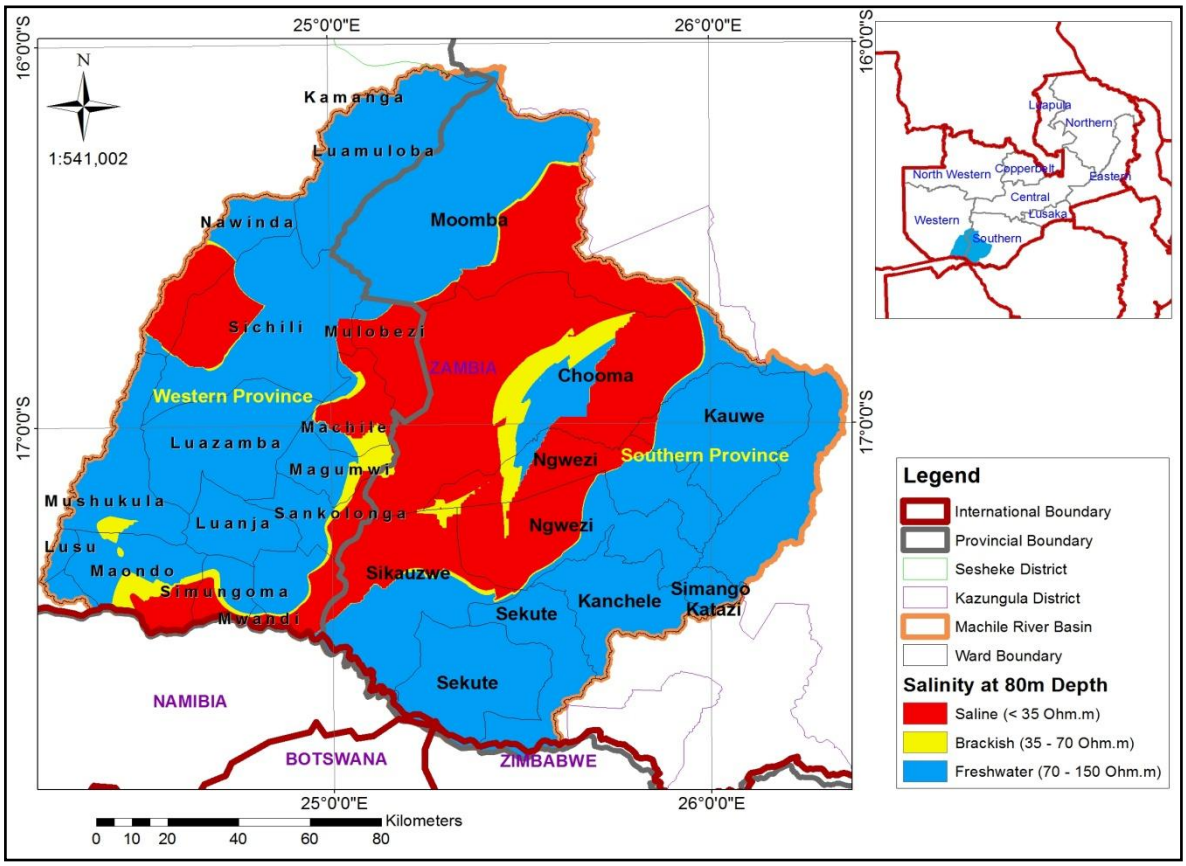

Figure 31: Groundwater salinity map at 80m depth in the Machile River Basin, South-Western Zambia

Based on the resistivity distribution in the Machile River Basin, saline groundwater is found in larger parts of the subsurface, at 30, 50 and 80m. However, in as much as

freshwater has been accessed at greater depths in some areas, this study, according to its findings, agrees with IGRAC (2009) that fresh groundwater is generally present at shallow depths because it is in proximity to the other parameters of hydrologic cycle, accessed and replaced when depleted. The terrain of the study area, as observed in the field and topographic map, discharges groundwater from upstream into the depression. This process leads to water logging in the area thereby increasing the evaporation rate which further results in the formation of groundwater salinity due to increased concentration of salts. The saline groundwater then percolates into deep layers leaving the layer less saline. This qualifies the findings that the extent of the distribution of saline groundwater at 10m depths is less than that at deeper depths.

4.3 The Geological Model of the Machile River Basin

The geology of the Machile River Basin, visualized in GeoScene3D software across two vertical cross sections along the profile lines south-east to north-west (SE-NW) and north-east to south-west (NE-SW) directions, are indicated over the topographic image (Figure 32). The light grey colour on the topographic image (Figure 32) indicates the lowest relief, whereas dark-grey indicates the highest relief of the study area.

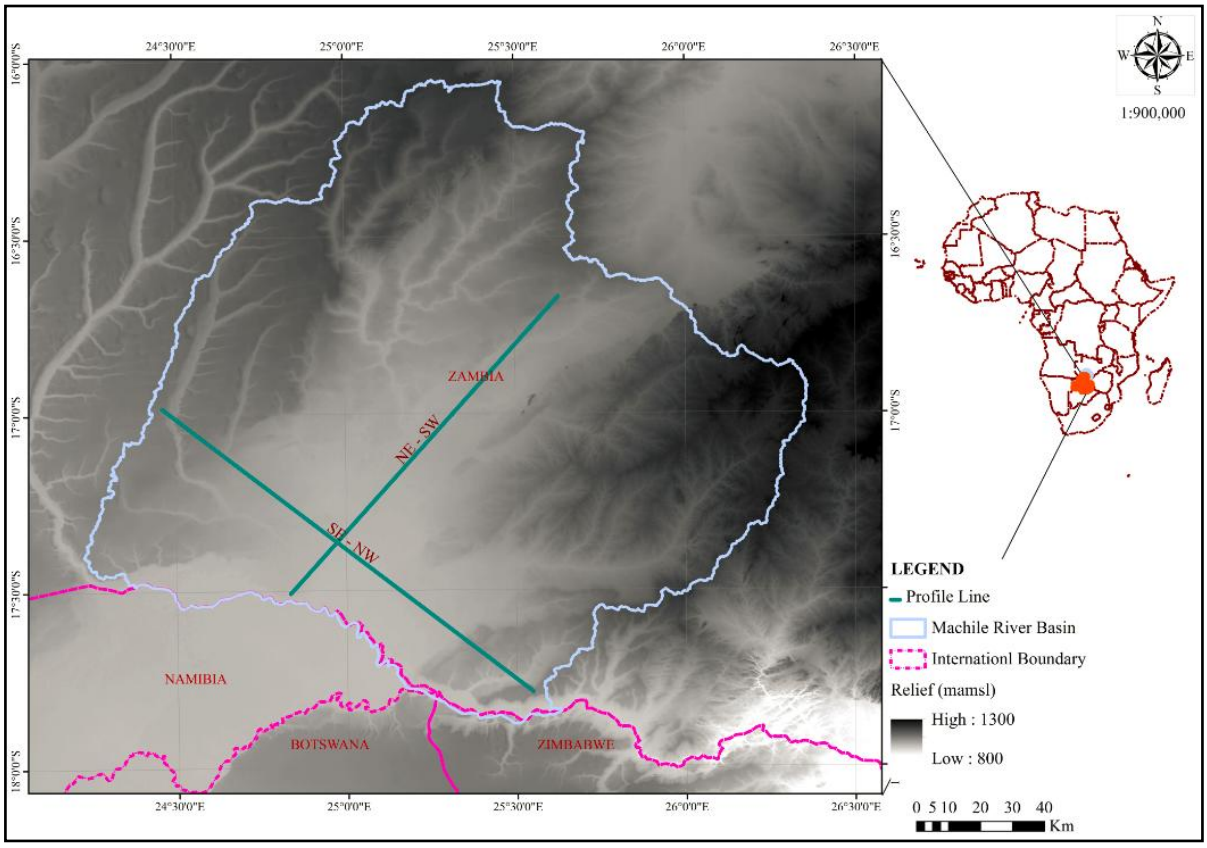

Figure 32: Topographic image of the Machile River Basin showing southeast-northwest (SE-NW) and northeast-southwest (NE-SW) profile lines across which geological cross sections were taken in South-Western Zambia

The regional geological models for the Machile River Basin along the two profiles lines SE-NW and NE-SW were generated and visualized in 2-dimensional (2-D) format in order to show the vertical variations in topography and lithology. The left panel of the profile corresponds to NW whereas the right panel to SE (Figure 33). This line was visualized across a topographic depression of the Machile River Basin (Figure 33). The geology of the profile line SE-NW on a 140,000m stretch with the highest elevation being 1,060m above mean sea level and the lowest being 950m above mean sea level is characterized by the unconsolidated Kalahari sediments, sandstone and rocks of the Undifferentiated Karoo and Basement Complex. The sequence of the unconsolidated Kalahari sediments thin out towards the middle and thereafter thickens at the middle of the profile. The middle part (from 62,500m to 107,500m stretch) probably cuts the sequence of the other lithologies abruptly due to the geological graben. The unconsolidated Kalahari sediments which extend over a large area is about 5m to 60m thick at the middle. Sandstone, from the middle of the profile thins out towards the SE

whereas rocks of the Undifferentiated Karoo and Basement Complex thicken out. Also observed are two valleys on both ends of the profile which could be interpreted as river channels or gullies (Figure 33).

The geological relationship of this model generally indicates that the area is underlain by the Kalahari sediments which are mostly underlain by sandstone. The sandstone, belonging to the Barotse Formation of the Kalahari Supergroup, is only a few cm thick around the valley in the SE and about 40m thick in the far NW (Figure 33). Sandstone overlie rocks of the Undifferentiated Karoo and Basement Complex which are about 35m to 100m thick (Figure 33). Rocks of the Undifferentiated Karoo and Basement Complex form the base of the geological model and could be thicker than shown here (Figure 33).

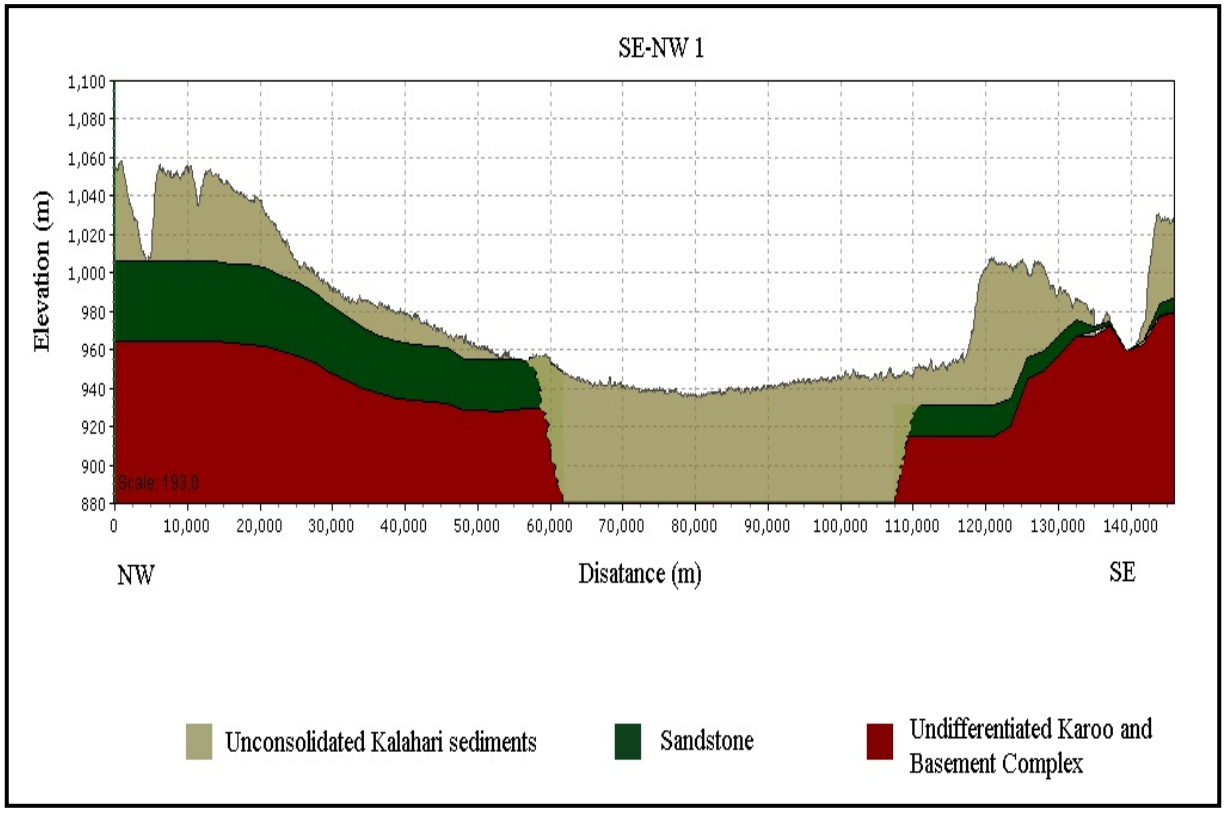

Figure 33: Geological model of the Machile River Basin across SE to NW profile in South-Western Zambia

The NE-SW geological profile cut along a topographical depression of the basin from the Zambezi River in the NE and away from the Zambezi River in the SW direction. This profile is about 125,000m long with elevation of about 1,070m above mean sea

level in the NE and 940m above mean sea level in the SW. The model is characterized by the unconsolidated Kalahari sediments, sandstone and rocks of the Undifferentiated Karoo and Basement Complex. The unconsolidated Kalahari sediments stretch across the entire profile with thickness ranging from 5m to 60m (Figure 34). The occurrence of unconsolidated Kalahari sediments was due to deposition probably from upland into the depression by either streams and/or wind. The sandstone is observed below the unconsolidated Kalahari sediments. It is about 15m to 40m thick and only covers the NE part of the depression. In this model, the sandstone overlie rocks of the Undifferentiated Karoo and Basement Complex which thins out towards the SW. Rocks of the Undifferentiated Karoo and Basement Complex range in thickness from 10m to 100m.

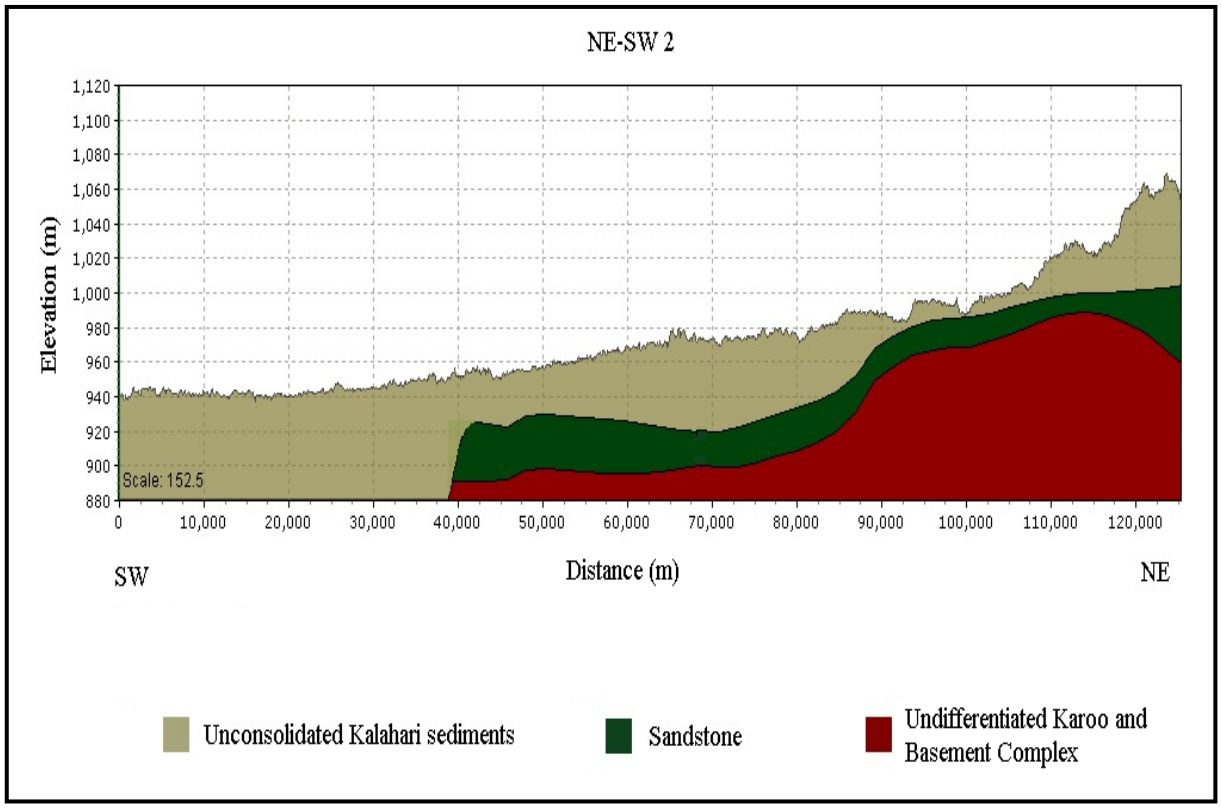

Figure 34: Geological model of the Machile River Basin across a NE to SW profile in South-Western Zambia

The geological sequence in the model is similar to the findings by Money (1972) where rocks ranging from Undifferentiated Karoo and Basement Complex underlie the sandstone which is overlain by sand. The thickness of the unconsolidated Kalahari sediments is consistent with the findings by Haddon and McCarthy (2005) that the

unconsolidated sands at the top of the Kalahari Group sequence extend over a larger area than the underlying formations and vary in thickness from a few cm to over 200 m in northern Namibia. Haddon (2005) added that the unconsolidated sands cover an area of over 2.5 million km^2, stretching from the Orange River in the south to as far north as the Democratic Republic of Congo, and that it forms the largest continuous body of sand on earth. Money (1972) too, observed that the dominant landform (over 85%) associated with the unconsolidated sand deposits is the dune fields. Similarly, as observed by Money (1972), the sands in western Zambia are related to fluctuations in the water table and climate as it is transported from one point to another by flooding water during flood periods. These are primarily loose sands of the Zambezi Formation which rests on the Barotse Formation and older rocks. These sands, when cemented by silica, give rise to sandstone of the Barotse Formation. Money (1972) divided the Karoo rocks into Lower and Upper Karoo and indicated that since the beginning of the Karoo times, much of western Zambia was a sedimentary basin. He further observed rocks of the Basement Complex referred to as the pre-Karoo crystalline rocks cropping out in an arc along the north-eastern and eastern rim of the basin and as isolated inliers within the region.

Saline groundwater along the topographic depression exists within the unconsolidated Kalahari sediments. Moving away from the depression towards the west and the east saline groundwater exists in sandstone formations and partly in rocks of the Undifferentiated Karoo and Basement Complex as well (Figures 5, 33 and 34). Money (1972) similarly recorded a number of saline evaporite horizons from a number of pans west of the Zambezi. These were generally less than 2cm thick and represented soluble salts precipitated by evaporation.

CHAPTER 5: CONCLUSIONS AND RECOMMENDATIONS

This chapter gives the conclusions and recommendations of this study.

5.1 Conclusions

The ground-based Time-Domain EM is an effective technique to use in conductive environments to determine the distribution groundwater salinity implying that the method is less effective in highly resistive areas. However, with respect to the use of the TDEM method, the conclusions of the study are:

(i) Resistivities were observed to be increasing with depth from the most resistive formation being 3,173Ωm at 10m, 10,616Ωm at 30m, 17,186Ωm at 50m to 19,738Ωm at 80m depth. This is an indication of the presence of formations ranging from sands, sandstones, basalts to granites in some places and rocks of the Karoo and Basement Complex;

(ii) Groundwater salinity increased with depth and was mainly restricted to the depression. Generally, the extent of groundwater salinity at 10m depth is less than that at 30, 50 and 80m across the entire Machile River Basin;

(iii) Most of the saline groundwater in the basin exists within the unconsolidated Kalahari sediments and sandstone;

(iv) The geological model of the Machile River Basin, as indicated by borehole data is characterized by the unconsolidated Kalahari sediments, sandstone and rocks of the Undifferentiated Karoo and Basement Complex; and

(v) TDEM soundings can help to anticipate required drilling depths for freshwater resources. It is a quick and low-cost method because it is used where borehole drilling is impractical or impossible.

5.2 Recommendations

The recommendations provided are focused on achieving access to safe and clean drinking water for both the present and future generations:

(i) Generally, from the depths considered in this study, drilling for freshwater resources along the depression is recommended at 10m depth This is so because the extent of groundwater salinity at 10m depth is less than at greater depths;

(ii) Drilling for freshwater resources away from the depression should be considered at deeper depths as well though in consultation with geophysical data in some areas;

(iii) Integrated Water Resources Management (IWRM) Centre in collaboration with the Department of Water Affairs to consider undertaking a study in order to determine the quantities of this saline water and the extent of the aquifers;

(iv) Integrated Water Resources Management (IWRM) Centre to consider undertaking a Continuous Vertical Electrical Sounding (CVES) on the Kazungula side of the Machile River Basin in order to compare results with the TDEM findings; and

(v) Similar TDEM surveys to be undertaken in Luapula Province where salt extends up to the surface in order to determine the extent to which groundwater is affected.

REFERENCES

ABEM Instruments 2012. "WalkTEM User Guide". Sweden, 19 pages.

Al-Garni, M. A. and M. H. El-Kaliouby, 2009. "Delineation of saline groundwater and sea water intrusion zones using transient electromagnetic (TEM) method, Wadi Thuwal area, Saudi Arabia". Saudi Society for Geosciences 4, 655–668.

Appello, C. A. J. and D. Postma, 2005. "Geochemistry, groundwater and pollution". Taylor and Francis 2nd Edition. ISBN: 978-1-4398-3354-4, 634 pages

Archie, G. E. 1942. "Electrical resistivity log as an aid in determining some reservoir characteristics". Trans Am. Inst. Mech. Eng 146, 54-62.

Barica, J. 1972. "Salinization of groundwater in arid zones". Water research Pergamon Press 6, 925-933.

Batayneh, A. T. 2006. "Use of electrical resistivity methods for detecting subsurface fresh and saline water and delineating their interfacial con*fi*guration: a case study of the eastern Dead Sea coastal aquifers, Jordan". Springer, Hydrogeology Journal 14, 1277–1283.

Bauer, P., R. Supper, S. Zimmermann and W. Kinzelbach, 2006. "Geoelectrical imaging of groundwater salinization in the Okavango Delta, Botswana". Journal of Applied Geophysics. Elsevier (60), 126–141.

Bauer, P., B. N. Gondwe, L. Christiansen, D. Herckenrath, L. Kgotlhang and S. Zimmermann, 2010. "Hydrogeological exploration of 3-dimensional salinity anomalies with the TDEM". Elsevier (380), 318-329.

Bear, J., A. H. Cheng, S. Sorek, D. Ouazar and I. Harrera, 1999. "Sea water intrusion in coastal aquifers, concepts method and practices". Kluwer Academic Publishers, 630 pages.

Boucher, M., G. Favreau, M. Descloitres, J. Vouillamoz, S. Massuel, Y. Nazoumou, B. Cappelaere and A. Legchenko, 2009. "Contribution of geophysical surveys to groundwater modelling of a porous aquifer in semiarid Niger: An overview". Journal of Applied Geophysics. Elsevier (341), 800-809.

Childs, C. 2004. "Interpolating surfaces in ArGIS spatial analyst". Esri Education Services, 4 pages. http://www.esri.com/news/arcuser/0704/files/interpolating.pdf. (Date accessed: 05/07/2014).

Chongo, M. 2011. A geophysical Study of the Spatial Distribution of Saline Groundwater in the Kalahari Sand Aquifer in the Sesheke Area. Masters Thesis. University of Zambia, 184 pages.

Chongo, M., J. Wibroe, K. Staal-Thomsen, M. Moses, I. A. Nyambe, F. Larsen and P. Bauer, 2011. "The use of Time Domain Electromagnetic method and Continuous Vertical Electrical Sounding to map groundwater salinity in the Barotse Sub-Basin, Zambia". Elsevier (36), 798-805.

Choudhury, K., D. K. Saha and P. Chakraborty, 2001. "Geophysical study of saline water intrusion in a coastal alluvial terrain". Journal of Applied Geophysics, Elsevier 46, 189-200.

Christiansen, A. V., E. Auken and K. Sorensen, 2006. "The transient electromagnetic Method". In: Kirsh R. (Ed), chapter 6. "Groundwater geophysics-A tool for hydrogeology". Springer, ISBN: 3-540-29383-3, 179-225.

Christiansen, L. 2007. "Salinization of groundwater in the Okavango Delta, Botswana". Masters Thesis, University of Copenhagen, 149 pages.

Coppinger, M. and J. Williams, 1991. "Zambezi: River of Africa". 1st edition, Struik, Cape Town, 176 pages.

Department of Natural Resources and Mines (DNRM) 2004. "The Saltwatch Resources Book". Part A: What is salinity? Queensland, 29 pages.

Donkor, S. M. K. 2003. "Development challenges of water resources management in Africa". African Water Journal, Pilot Edition. United Nations Water/Africa, 1-19.

El-Sheimy, N. 1999. "Digital Terrain Modelling". Lecture Notes for the ENGO 573 Course [1998-2005], Department of Geomatics Engineering, The University of Calgary.

ESRI 2012. "How kriging works. Notes". ArcGIS Resource Center. http://help.arcgis.com/en%20/arcgisdesktop/10.0/help/index.html#//009z000000 76000000.htm. (Online notes: Date accessed: 05/07/2014)

Fanshawe, D. B. 2010. "Vegetation descriptions of the Upper Zambezi District of Zambia". Occasional Publications in Biodiversity No. 22, Bulawayo, 239 pages.

Fetter, C. W. 2001. "Applied Hydrogeology". Prentice Hall, Inc. New Jersey, 621 pages.

Flemming L. 2009. "Note about saline water in aquifers". Hanoi, Vietnam: Geological Survey of Denmark and Greenland (GEUS).

Food and Agriculture Organization (FAO) 2006. "World reference base for soil resources". A framework for international classification and communication. World Soil Resources Report 103, Rome.

Food and Agriculture Organization (FAO) 2009. "Harmonized World Soil Database (HWSD) documentation". (Version 1.1) Rome, 43 pages.

Food and Agriculture Organization (FAO) 2010. "The groundwater hydrology of the Okavango Basin". Okavango River Basin Transboundary Diagnostic Analysis Technical Report. OKACOM, Botswana, 83 pages.

Geological Survey Department (GSD) 1981. “Geological Map of Zambia”. Scale 1:1,000,000, Edition 2; Government of the Republic of Zambia; Lusaka.

Geonics 1980. “Electrical conductivity of soils and rocks”. Technical Note TN-5. Ontario, Canada, 20 pages.

Goldman, M. and F. M. Neubauer, 1994. “Groundwater exploration using integrated geophysical techniques”. Kluwer Academic Publishers, Surveys in Geophysics 15, 331-361.

Goldman, M., B. Rabinovich, M. Rabinovich, D. Gilad, I. Gev and M. Schirov, 1994. “Application of the integrated NMR-TDEM method in groundwater exploration in Israel”. Elsevier, Journal of Applied Geophysics, 31, 27-52.

Government of the Republic of Zambia (GRZ) 2007. “Groundwater Resources for Southern Province”. Technical Report. First Edition. Department of Water Affairs/Federal Institute for Geosciences and Natural Resources, Lusaka, 58 pages.

Government of the Republic of Zambia (GRZ) 2010. “National Water Policy 2010”. Ministry on Energy and Water Development, Lusaka, 40 pages.

Gupta, A. 2007. [editor] “Large rivers: geomorphology and management”. John Wiley and Sons, England, 433 pages.

Haddon, I. G. 2005. “The Kalahari geology and tectonic evolution of the Kalahari Basin, Southern Africa”. PhD thesis, University of Witwatersrand, 360 pages.

Haddon, I. G. and T. S. McCarthy, 2005. “The Mesozoic-Cenozoic interior sag basins of Central Africa: The Late-Cretaceous-Cenozoic Kalahari and Okavango basins”. Journal of African Earth Sciences, Elsevier. 43, 316-333.

Han, D. M., X. F. Song, M. J. Currell, J. L. Yang and G. Q. Xiao, 2013. "Chemical and isotopic constraints on evolution of groundwater salinization in the coastal plain aquifer of Laizhou Bay, China", Journal of Hydrology. Elsevier 508, 12-27.

Hanson, B. R., S. R. Grattan and A. Fulton, 2006. "Agricultural Salinity and Drainage. Division of Agriculture and Natural Resources", Publication 3375, University of California.

Hart, B. T., P. Bailey, R. Edwards, K. Hortle, K. James, A. McMahon, C. Meredith and K. Swadling, 1990. "Effects of salinity on river, stream and wetland ecosystems in Victoria, Australia", Elsevier Vol 24, Issue 1, 1103-1117.

Harter, T. 2005. "Aquifers. Water Encyclopedia". John Wiley and Sons, 5, 9-11.

Herckenrath, D. and P. Bauer, 2013. "Operation manual-WalkTEM Equipment". Version 1.3, Technical University of Denmark, Lynby, 11 pages.

Hydrogeophysics Group (HGG) 2001. "Getting started with SiTEM/Semdi". Aarhus University. Aarhus, 22 pages.

Integrated Geographic Information System (I-GIS) 2010. "Geoscene3D-modelling and visualization of geological data", Denmark. www.i-gis.dk. (Online data: Date accessed: 26/06/2014).

International Groundwater Resources Assessment Centre (IGRAC) 2009. "Global Overview of saline groundwater occurrence and gnessis". Report nr. GP 2009-1, 107 pages.

Jolly, I. D., K. L. McEwan and K. L. Holland, 2008. "A review of groundwater-surface water interactions in arid/semi-arid wetlands and the consequences of salinity for wetland ecology". Ecohydrology, John Willey & Sons 1, 43-58.

Kafri, U., M. Goldman and B. Lang, 1997. “Detection of sub-surface brines, freshwater bodies and the interface configuration in-between by the time-domain electromagnetic method in the Dead Sea Rift, Israel”. Springer, Environmental Geology 31, 42-49.

Kafri, U. and M. Goldman, 2005. “The use of the Time Domain Electromagnetic Method to delineate saline groundwater in granular and carbonate aquifers and to evaluate porosity”. Applied Geophysics 57, 167-178.

Kirsh, R. 2006. “Groundwater geophysics: A tool for hydrogeophysics”, Springer (Ed), 155-178.

Kirsh, R. 2008. “Groundwater geophysics: A tool for hydrogeophysics”. Springer Science and Business Media (Illustrated Version), pages 568.

Klein, J. and J. J. Lajoie, 1980. “Electromagnetic prospecting for minerals: Practical geophysics for the exploration geologists”. Northwest Mining Association, Spokane, WA, 239-290.

Kouzana, L., A. B Mammou and M. S. Felfoul, 2009. “Seawater intrusion and associated processes: Case of the Korba Aquifer (Cap-Bon, Tunisia)”. C. R. Geoscience, Elsevier 341, 21-35.

Kumar, V. and J. Remadevi, 2006. "Kriging of groundwater levels: a case study”. Journal of Spatial Hydrology 6 (1), 81-94.

Levin, M. 1981. “The geology, hydogeology and hydrochemistry of an area between the Kuruman and Orange Rivers, North-Western Cape.” Transactions Geological Society of South Africa, 84, 177-190.

Linn, F., M. Masie and A. Rana, 2002. “The impacts on groundwater development on shallow aquifers in the lower Okavango Delta, northwestern Botswana”. Environmental Ecology, Springer 44, 112-118.

Margane, A., R. Baeumle and F. Schildknecht, 2005. "Investigations groundwater resources and Airborne Geophysical investigation of selected mineral targets in Namibia: Groundwater investigations in the Eastern Caprivi Region". Main hydrogeological report vol IV. GW. 2. 1, DWA Namibia and BGR Hannover.

Martinsen, G. 2012. "Global Positioning System (GPS) for groundwater resources assessment in Zambia". Masters Thesis, Technical University of Denmark, 73 pages.

MEWD-JICA 1995. "The study on the National Water Resources Master Plan in the Republic of Zambia". Hydrogeology Supporting Report (D), Lusaka, 132 pages.

MEWD 2009. "Water in a changing world: Zambia-National Water Resources Report for World Water Development Report (WWDR) 3", Lusaka, 218 pages.

Money, N. J. 1972. "An outline of the geology of Western Zambia". Drysdal, A. R. & Johnson, R L. (eds.): Geological Survey Department, Records of the Geological Survey Volume 12, Lusaka, Zambia, 25 pages.

Moore, A. E. and P. A. Larkin, 2001. "Drainage evolution in South-Central Africa since the breakup of the Gondwana". South African Journal of Geology 104 (1), 47-68.

Moore, A. E., F. P. D. Cotterill and F. D. Eckardt, 2012. "The evolution and ages of Makgadikgadi Palaeo-Lakes: Consilient evidence from Kalahari drainage evolution report", South Africa, 29 pages.

Murphy, J. 1999. "Salinity-our silent disaster". Murphy's report on salinity, Australia Broadcast Corporation, 6 pages. http://abc.net.au/science/slab/salinity (Date accessed: 26/06/2014).

Nyambe, I. A. 1999. "Tectonic and climatic controls on sedimentation during deposition of the Sinakumbe Group and Karoo Supergroup in the Mid-Zambezi Valley Basin, Southern Zambia". Journal of African Earth Sciences 28 (2), 443-463.

Phiri, P. S. M. 2005. "A checklist of Zambian vascular plants: Southern Africa Botanical Diversity". Network Report No. 32, SABONET, Pretoria, 183 pages.

Phiri, W. K. 2013. "Remote sensing estimation of spatial and temporal variability of actual evapotranspiration using SEBS algorithm in the semi-arid Barotse Sub-Basin in South-Western Zambia". Master thesis, University of Zambia, 154 pages.

Podmore, C. 2009. "Irrigation salinity-causes and impacts". Primefact 937, 4 pages. www.industry.nsw.gov.au. (Date accessed: 26/06/2014).

Post, V. E. A. 2004. "Groundwater salinization processes in the coastal area of the Netherlands due to transgressions during the Holocene". PhD thesis, Vrije University.

Quevauvillller, P., A. M. Fouillac, D. Muller and P. Negrel. 2007. "Groundwater science and policy: An international overview". Royal Society of Chemistry (RSC). 1st Edition, 766 pages.

Quevauvillller, P. 2008. "Groundwater Science and Policy: An international Overview". Royal Society of Chemistry, Illustrated Edition, 754 pages.

Reynolds, J. M. 1997. "An introduction to applied and environmental geophysics". John Wiley and sons. England, 796 pages.

Savory, B. M. 1963. "Site quality and tree root morphology in Northern Rhodesia". Rhodesian Journal of Agricultural Research 1, 55-64.

Scanlon, B. R., R. C. Reedy, D. A. Stonestrom. D. E. Prudic. and K. F. Dennehy, 2005. "Impact of land use and land cover change on groundwater recharge and quality in the southwestern US". Global Change Biology, Blackwell Publishing 11, 1577-1593.

Schmutz, M, Y. Abouy, R. Guerin, O. Maquaire, J. Vassal, J. J. Schott and M. Descloitres, 2001. "Joint electrical and Time Domain Electromagnetism (TDEM) data inversion applied to the super sauze earthflow in France". Kluwer Academic Publishers 21, 371–390.

Shepard, D. 1968. "A two-dimensional interpolation function for irregularly-spaced data". Proceedings of the 1968 23rd ACM national conference, 517-524. www.emsi.com/smshelp/Data_Module/Interpolation/Inverse_Distance_Weighted.htm. (Date accessed: 10/08/2014).

Taylor, K., M. Widmer and M. Chesley, 1992. "Use of Time-Domain Electromagnetics to define local hydrogeology in an arid alluvial environment". Geophysics, Vol. 57, 343-352.

Telford, W. M., L. P. Geldart, R.E. Sheriff and D. A. Keys, 1976. "Applied Geophysics".Ch. 5. Cambridge University Press, New York, 860 pages.

Tsourlos, P., I. Papapolouslos, P. Karmis, G. Vargemezis and G. N. Tsokas, 2004. "A TDEM survey to define local hydrogeological structure in Anthemountas Basin", 7 (1), 1-11.

United States Environmental Protection Agency (USEPA) 2011. "Environmental Geophysics". http://www.epa.gov/esd/cmb/GeophysicsWebsite/pages/reference/methods/Surface_Geophysical_Methods/Electromagnetic_Methods/TimeDomain_Electromagnetic_Methods.htm. (Online notes: Date accessed: 02/06/2014).

United States Geological Survey (USGS), 2010. "Shuttle Radar Topography Mission (SRTM)". (Online). http://seamless.usgs.gov/2010. (Date accessed: 17/05/2013)

Ward, S. S. 1938. “Electrical prospecting with non-sinusoidal alternating currents in geophysics”, 306-314.

Wayland, E. J. 1953. “More about the Kalahari”. Geographical Journal, 119, 49-56.

Wibroe, J. and S. Thomsen, 2009. “Geophysical monitoring and modeling of salt and freshwater dynamics in the Upper Zambezi”. Master Thesis. Technical University of Denmark, 165 pages.

Williams, W. D. 1999. “Salinization: A major threat to water resources in the arid and semi-arid regions of the world”. Lakes and reservoir: Research and Management 4, 85-91.

Young, M. E., R. G. M. de Bruijn and A. S. Al-Ismaily, 1998. “Exploration of an alluvial aquifer in Oman by Time-Domain Electromagnetic Sounding”. Hydrogeology Journal v. 6, 383-393.

Zambia Forestry Department (ZFD) 1976. “The vegetation of Zambia”. Vegetation Map 1:500000, sheet No 4, Frankfurt: Institute for Angewandte Geodasie.

Zambia Meteorological Department (ZMD). 2013. “Annual Report. Ministry of Works and Supply and Communication”, Lusaka, Zambia.

APPENDICES

Appendix 1: Location of Sounding Points (1 to 69) and Inversion Residual or Iteration for Machile River Basin in South-Western Zambia

No	Point	Latitude X	Longitude Y	Elevation (m)	Residuals
1	MT001	389625.15	8123959.06	1072.9424	0.65
2	MT002	361638.93	8155106.97	1023.6732	0.47
3	MT003	338322.21	8161028.89	1029.6000	0.21
4	MT004	321029.5	8160758.14	1017.9188	0.64
5	MT005	304736.5	8154904.34	992.8436	0.55
6	MT006	334406.75	8180397.73	1038.8662	0.73
7	MT007	348943.97	8195154.69	1102.3260	0.23
8	MT008	334091.51	8138587.15	989.1952	0.28
9	MT009	349523.1	8144623.09	1008.0172	0.73
10	MT010	410478.56	8085888.49	1219.7800	5.42
11	MT011	389116.61	8089711.83	1151.0984	0.61
12	MT012	384307.78	8105541.02	1212.2507	24.32
13	MT013	383060.92	8126755.88	1137.9900	0.9
14	MT014	401114.01	8128497.45	1242.5516	1.38
15	MT015	407424.68	8112760.39	1246.3800	1.69
16	MT016	363590.67	8102714.82	1145.8800	5.59
17	MT017	333339.59	8105956.8	998.5988	0.32
18	MT018	319679.79	8101835.84	975.3200	0.32
19	MT020	362435.36	8084603.84	1093.2340	5.77
20	MT021	344937.73	8075072.11	1004.2600	0.48
21	MT022	331128.31	8064492.51	973.2684	0.27
22	MT023	318160.63	8031784.24	930.5239	0.84
23	MT024	333040.34	8026281.44	921.2599	0.48
24	MT025	356025.53	8060701.24	1039.9436	0.4
25	MT026	383877.22	8063381.43	1138.7200	0.78
26	SM003T	231197.7	8070088.64	944.0000	0.49
27	SM004T	211211.82	8075362.89	992.0000	0.55
28	SM005T	214846.65	8084639.68	1026.0000	0.8
29	SM006T	218021.28	8092834.67	1013.0000	0.41
30	SM009T	253603.61	8074425.42	961.0000	0.49
31	SM010T	260267.91	8079896.89	968.0000	0.32
32	SM011T	262511.78	8085348.09	967.0000	0.54
33	SM012T	250753.14	8084997.87	984.0000	0.79
34	SM013T	260596.46	8097293.92	979.0000	0.7
35	SM014T	249568.62	8101038.04	998.0000	0.98

No	Point	Latitude X	Longitude Y	Elevation (m)	Residuals
36	SM015T	250570.86	8109730.58	1007.0000	0.63
37	SM021T	262568.84	8099741.33	979.0000	0.49
38	SM022T	283644.58	8124813.26	992.0000	0.25
39	SM023T	295167.09	8135101.36	999.0000	0.6
40	SM025T	274052.41	8113331.75	976.0000	0.71
41	SM026T	281409.45	8152364.01	1076.0000	0.76
42	SM027T	283812.54	8168947.91	1094.0000	0.94
43	SM028T	281831.87	8181092.74	1105.0000	2.42
44	SM029T	287257.31	8196454.66	1117.0000	1.22
45	SM032T	260759.84	8167164.41	1100.0000	0.74
46	SM033T	264028.52	8177717.4	1113.0000	1.1
47	SM034T	269654.55	8154188.17	1114.0000	0.95
48	SM035T	257958.24	8136632.58	1054.0000	1.2
49	SM036T	254687.72	8122733.36	1027.0000	0.81
50	SM037T	262190.9	8145149.9	1075.0000	0.35
51	SM038T	249313.02	8168151.78	1065.0000	0.72
52	SM043T	288884.32	8150535.75	997.0000	0.63
53	SM044T	288377.57	8145737.87	1045.0000	0.67
54	SM045T	306046.82	8143439	1007.0000	0.54
55	SM046T	301138.81	8132513.33	990.0000	0.67
56	SM047T	269111.57	8064200.61	941.0000	0.61
57	SM048T	278964.71	8066624.4	937.0000	0.68
58	SM049T	280799.85	8075744.05	939.0000	0.69
59	SM050T	289966.31	8096009.24	952.0000	0.8
60	SM051T	286151.08	8089483.16	947.0000	1.26
61	SM055T	222654.26	8087847.83	1007.0000	0.56
62	SM056T	225063.23	8092281.14	1017.0000	0.66
63	SM057T	235477.37	8100020.72	998.0000	0.72
64	SM058T	246867.58	8086134.92	978.0000	1.17
65	SM059T	228197.53	8082230.1	1011.0000	0.55
66	SM060T	232559.26	8117467.86	1013.0000	0.88
67	SM061T	241527.65	8139238.63	1053.0000	3.62
68	SM062T	272073.89	8077596.65	955.0000	0.74
69	SM066T	291221.24	8067972.12	936.0000	0.37

Appendix 2: Apparent Resistivity Data for 3-layers Models at various Sounding Points in Machile River Basin, South-Western Zambia

MT002: 3-Layered Model

	Res	Thk	Dep	ResSTD	ThkSTD	DepSTD
Layer 1	96.6	19.6	19.6	1.26	1.1	1.1
Layer 2	16.5	84.5	104.1	1.07	1.24	1.16
Layer 3	172.1			99		

MT010: 3-Layered Model

	Res	Thk	Dep	ResSTD	ThkSTD	DepSTD
Layer 1	153.8	55.5	55.5	1.04	1.38	1.38
Layer 2	4083.4	124.7	180.1	99	99	4.43
Layer 3	16.2			99		

MT012: 3-Layered Model

	Res	Thk	Dep	ResSTD	ThkSTD	DepSTD
Layer 1	7336.2	23.1	23.1	99	99	99
Layer 2	785.8	128.5	151.5	99	99	99
Layer 3	45.5			99		

MT014: 3-Layered Model

	Res	Thk	Dep	ResSTD	ThkSTD	DepSTD
Layer 1	6773.4	18.4	18.4	99	99	99
Layer 2	1399.5	72.4	90.8	99	99	9.39
Layer 3	502.4			1.56		

MT015: 3-Layered Model

	Res	Thk	Dep	ResSTD	ThkSTD	DepSTD
Layer 1	486.5	53.8	53.8	1.1	1.63	1.63
Layer 2	20000	153.7	207.6	99	1.32	1.09
Layer 3	95.3			99		

MT016: 3-Layered Model

	Res	Thk	Dep	ResSTD	ThkSTD	DepSTD
Layer 1	126.3	35.3	35.3	1.03	1.2	1.2
Layer 2	398.1	198.9	234.2	1.54	1.67	1.45
Layer 3	87.2			99		

MT018: 3-Layered Model

	Res	Thk	Dep	ResSTD	ThkSTD	DepSTD
Layer 1	212.9	7	7	99	2.96	2.96
Layer 2	10	13.1	20.1	1.41	2.51	1.24
Layer 3	19.5			1.04		

MT026: 3-Layered Model

	Res	Thk	Dep	ResSTD	ThkSTD	DepSTD
Layer 1	81	9.4	9.4	99	1.69	1.69
Layer 2	6.7	10.3	19.6	1.62	2.14	1.15
Layer 3	15884.5			99		

SM005T: 3-Layered Model

	Res	Thk	Dep	ResSTD	ThkSTD	DepSTD
Layer 1	100.2	3.5	3.5	99	6.4	6.4
Layer 2	21.7	51.9	55.4	1.03	1.16	1.06
Layer 3	287.6			1.75		

SM009T: 3-Layered Model

	Res	Thk	Dep	ResSTD	ThkSTD	DepSTD
Layer 1	26.8	13.3	13.3	1.39	1.18	1.18
Layer 2	6.8	57.1	70.4	1.03	1.13	1.08
Layer 3	23.2			1.36		

SM011T: 3-Layered Model

	Res	Thk	Dep	ResSTD	ThkSTD	DepSTD
Layer 1	52.1	15.9	15.9	1.1	1.06	1.06
Layer 2	3.4	6.6	22.5	1.33	1.39	1.06
Layer 3	562.8			1.8		

SM012T: 3-Layered Model

	Res	Thk	Dep	ResSTD	ThkSTD	DepSTD
Layer 1	773	13.3	13.3	99	1.16	1.16
Layer 2	10.9	17.3	30.7	1.1	1.18	1.04
Layer 3	272.9			1.24		

SM023T: 3-Layered Model

	Res	Thk	Dep	ResSTD	ThkSTD	DepSTD
Layer 1	141.8	17.1	17.1	1.32	1.06	1.06
Layer 2	15.7	57.7	74.8	1.03	1.11	1.07
Layer 3	47.6			1.28		

SM027T: 3-Layered Model

	Res	Thk	Dep	ResSTD	ThkSTD	DepSTD
Layer 1	183.8	21.4	21.4	2.08	1.71	1.71
Layer 2	42.3	22.8	44.2	1.54	2.07	1.13
Layer 3	16217			99		

SM034T: 3-Layered Model

	Res	Thk	Dep	ResSTD	ThkSTD	DepSTD
Layer 1	64.6	11.7	11.7	2.51	2.03	2.03
Layer 2	16.3	14.2	25.9	1.59	2.36	1.16
Layer 3	126.7			1.11		

SM036T: 3-Layered Model

	Res	Thk	Dep	ResSTD	ThkSTD	DepSTD
Layer 1	127.8	10.2	10.2	5.51	3.66	3.66
Layer 2	48.3	48.8	59	1.09	1.44	1.1
Layer 3	367			1.55		

SM045T: 3-Layered Model

	Res	Thk	Dep	ResSTD	ThkSTD	DepSTD
Layer 1	45.9	24.2	24.2	1.02	1.06	1.06
Layer 2	7.5	12.3	36.5	1.25	1.4	1.08
Layer 3	35.2			1.08		

SM049T: 3-Layered Model						
	Res	**Thk**	**Dep**	**ResSTD**	**ThkSTD**	**DepSTD**
Layer 1	9.5	6.7	6.7	1.04	1.03	1.03
Layer 2	2.4	69.9	76.6	1.01	1.18	1.15
Layer 3	5.3			1.77		
SM060T: 3-Layered Model						
	Res	**Thk**	**Dep**	**ResSTD**	**ThkSTD**	**DepSTD**
Layer 1	140.4	22.9	22.9	1.16	1.13	1.13
Layer 2	31.6	32	54.8	1.11	1.19	1.05
Layer 3	2417.5			2.41		

Appendix 3: Apparent Resistivity Data for 4-layers Models at various Sounding Points in Machile River Basin, South-Western Zambia

MT001: 4-Layered Model

	Res	Thk	Dep	ResSTD	ThkSTD	DepSTD
Layer 1	71	5.5	5.5	99	99	99
Layer 2	17.4	7.8	13.3	99	99	1.98
Layer 3	37.8	77.3	90.6	1.07	1.35	1.05
Layer 4	56.3			1.14		

MT004: 4-Layered Model

	Res	Thk	Dep	ResSTD	ThkSTD	DepSTD
Layer 1	114.3	19.5	19.5	1.27	1.16	1.16
Layer 2	10.5	10.1	29.7	1.61	3.5	1.33
Layer 3	15.7	65.3	95	1.06	1.27	1.02
Layer 4	7.1			1.18		

MT006: 4-Layered Model

	Res	Thk	Dep	ResSTD	ThkSTD	DepSTD
Layer 1	306.4	8.2	8.2	99	1.58	1.58
Layer 2	13.1	27.9	36.1	1.09	1.53	1.39
Layer 3	8.9	24.5	60.6	1.48	3.15	1.31
Layer 4	21.6			1.21		

MT007: 4-Layered Model

	Res	Thk	Dep	ResSTD	ThkSTD	DepSTD
Layer 1	153.5	13.3	13.3	4.15	1.24	1.24
Layer 2	10.2	15.9	29.3	1.21	1.79	1.23
Layer 3	16.1	67.3	96.6	1.09	1.75	1.43
Layer 4	25			1.68		

MT008: 4-Layered Model

	Res	Thk	Dep	ResSTD	ThkSTD	DepSTD
Layer 1	204.4	7.3	7.3	99	99	99
Layer 2	15.6	9.3	16.6	99	99	8.66
Layer 3	18.1	44.1	60.7	1.11	99	3.18
Layer 4	21.7			1.13		

MT009: 4-Layered Model

	Res	Thk	Dep	ResSTD	ThkSTD	DepSTD
Layer 1	201.5	11.4	11.4	99	99	99
Layer 2	9	5.3	16.7	99	99	2.07
Layer 3	23.4	166.2	182.8	1.05	1.56	1.45
Layer 4	40.1			7.89		

MT011: 4-Layered Model

	Res	Thk	Dep	ResSTD	ThkSTD	DepSTD
Layer 1	177.9	43.7	43.7	2.15	99	99
Layer 2	20000	37	80.7	99	99	99
Layer 3	583.3	7.9	88.6	99	99	99
Layer 4	0.1			99		

MT013: 4-Layered Model

	Res	Thk	Dep	ResSTD	ThkSTD	DepSTD
Layer 1	231.6	9.5	9.5	99	99	99
Layer 2	87.1	20.2	29.8	99	99	7.78
Layer 3	414.4	206.6	236.4	99	99	6.21
Layer 4	19.3			99		

MT020: 4-Layered Model

	Res	Thk	Dep	ResSTD	ThkSTD	DepSTD
Layer 1	230.1	13.6	13.6	99	99	99
Layer 2	83.3	32.5	46.1	8.04	99	2.56
Layer 3	734.2	236.2	282.3	99	99	8.54
Layer 4	45.6			99		

MT021: 4-Layered Model

	Res	Thk	Dep	ResSTD	ThkSTD	DepSTD
Layer 1	64.4	6.8	6.8	8	2.81	2.81
Layer 2	15.3	16.9	23.7	1.3	2.12	1.29
Layer 3	105.4	38.5	62.1	5.82	99	3.18
Layer 4	189.3			1.47		

MT022: 4-Layered Model

	Res	Thk	Dep	ResSTD	ThkSTD	DepSTD
Layer 1	314.9	3.6	3.6	99	1.69	1.69
Layer 2	6.9	27.1	30.6	1.04	99	3.75
Layer 3	6.6	33.3	64	1.36	99	1.31
Layer 4	231.9			99		

MT023: 4-Layered Model

	Res	Thk	Dep	ResSTD	ThkSTD	DepSTD
Layer 1	14.2	1.3	1.3	99	99	99
Layer 2	1.8	5.6	6.8	3.32	9.56	1.79
Layer 3	460.4	8.9	15.7	99	99	99
Layer 4	6115.5			99		

MT024: 4-Layered Model

	Res	Thk	Dep	ResSTD	ThkSTD	DepSTD
Layer 1	191.2	13.9	13.9	99	99	99
Layer 2	47.7	20.6	34.5	99	99	2.97
Layer 3	5084.7	160.1	194.6	99	99	4.01
Layer 4	14.5			99		

MT025: 4-Layered Model

	Res	Thk	Dep	ResSTD	ThkSTD	DepSTD
Layer 1	286.6	12.1	12.1	99	5.87	5.87
Layer 2	32	25.4	37.6	1.62	3.63	1.33
Layer 3	1874.9	269.6	307.1	99	99	8.07
Layer 4	58.5			99		

SM003T: 4-Layered Model

	Res	Thk	Dep	ResSTD	ThkSTD	DepSTD
Layer 1	48.9	14.6	14.6	1.17	1.14	1.14
Layer 2	12.3	27.6	42.2	1.09	1.35	1.16
Layer 3	31.6	68.9	111	1.44	2.01	1.48
Layer 4	187.3			99		

SM004T: 4-Layered Model

	Res	Thk	Dep	ResSTD	ThkSTD	DepSTD
Layer 1	199.6	35.2	35.2	1.14	1.36	1.36
Layer 2	48.9	24.8	59.9	2.03	3.78	1.38
Layer 3	228.9	84.8	144.7	2.79	1.43	1.16
Layer 4	17.4			1.28		

SM013T: 4-Layered Model

	Res	Thk	Dep	ResSTD	ThkSTD	DepSTD
Layer 1	41.4	20.3	20.3	1.04	5.22	5.22
Layer 2	33.4	18.5	38.8	2.48	99	2.64
Layer 3	57.9	28.5	67.3	9.31	3.46	1.56
Layer 4	231.9			1.57		

SM014T: 4-Layered Model

	Res	Thk	Dep	ResSTD	ThkSTD	DepSTD
Layer 1	391.9	8	8	99	1.64	1.64
Layer 2	23.8	34.5	42.6	1.06	1.26	1.13
Layer 3	328.9	20.6	63.2	99	99	2.57
Layer 4	179.4			1.3		

SM015T: 4-Layered Model

	Res	Thk	Dep	ResSTD	ThkSTD	DepSTD
Layer 1	128.8	9.3	9.3	99	2.5	2.5
Layer 2	5.4	3.9	13.2	99	99	1.46
Layer 3	51.3	63.4	76.6	1.31	1.32	1.28
Layer 4	1090			99		

SM021T: 4-Layered Model

	Res	Thk	Dep	ResSTD	ThkSTD	DepSTD
Layer 1	75.8	10.3	10.3	4.07	2.23	2.23
Layer 2	19	23.1	33.5	1.29	2.09	1.28
Layer 3	122.3	61.5	95	4.77	99	2.74
Layer 4	497.1			99		

SM025T: 4-Layered Model

	Res	Thk	Dep	ResSTD	ThkSTD	DepSTD
Layer 1	839.8	24.8	24.8	99	3.25	3.25
Layer 2	53.8	14	38.8	99	4.61	1.31
Layer 3	20.2	36.2	75	1.13	1.56	1.35
Layer 4	345			2.39		

SM028T: 4-Layered Model

	Res	Thk	Dep	ResSTD	ThkSTD	DepSTD
Layer 1	13173.1	38.3	38.3	99	1.62	1.62
Layer 2	402.1	3.4	41.7	99	99	1.24
Layer 3	105.7	69.7	111.4	1.24	1.23	1.04
Layer 4	0.5			1.69		

SM029T: 4-Layered Model

	Res	Thk	Dep	ResSTD	ThkSTD	DepSTD
Layer 1	82.7	8.1	8.1	99	6.55	6.55
Layer 2	11.1	8.1	16.2	4.28	99	1.68
Layer 3	23.7	38.5	54.7	1.18	1.25	1.26
Layer 4	6491.6			99		

SM032T: 4-Layered Model

	Res	Thk	Dep	ResSTD	ThkSTD	DepSTD
Layer 1	1225.4	16	16	99	99	99
Layer 2	363.3	25.2	41.2	99	99	1.31
Layer 3	73.7	78.4	119.7	1.07	1.28	1.36
Layer 4	2871			99		

SM033T: 4-Layered Model

	Res	Thk	Dep	ResSTD	ThkSTD	DepSTD
Layer 1	35	6.3	6.3	99	99	99
Layer 2	8.8	6.8	13	9.15	99	1.73
Layer 3	117.7	61.8	74.8	3.28	4.24	2.29
Layer 4	1007.7			99		

SM035T: 4-Layered Model

	Res	Thk	Dep	ResSTD	ThkSTD	DepSTD
Layer 1	8579.3	15.4	15.4	99	99	99
Layer 2	7604.2	28.9	44.3	99	99	1.04
Layer 3	27.5	28.5	72.7	1.1	1.18	1.05
Layer 4	161.8			1.21		

SM037T: 4-Layered Model

	Res	Thk	Dep	ResSTD	ThkSTD	DepSTD
Layer 1	906.3	11.9	11.9	99	99	99
Layer 2	868.8	41.3	53.2	99	6.86	1.2
Layer 3	104.5	89.5	142.7	1.11	1.53	1.23
Layer 4	247			2.76		

SM038T: 4-Layered Model

	Res	Thk	Dep	ResSTD	ThkSTD	DepSTD
Layer 1	183.5	1.5	1.5	99	99	99
Layer 2	2280.9	56.9	58.5	99	1.25	1.13
Layer 3	51.7	59	117.5	1.16	1.44	1.14
Layer 4	172.4			1.75		

SM043T: 4-Layered Model

	Res	Thk	Dep	ResSTD	ThkSTD	DepSTD
Layer 1	109.3	14.6	14.6	2.48	1.4	1.4
Layer 2	16.4	18.6	33.1	1.27	1.74	1.17
Layer 3	38.4	99.8	132.9	1.1	1.2	1.07
Layer 4	13			1.48		

SM044T: 4-Layered Model

	Res	Thk	Dep	ResSTD	ThkSTD	DepSTD
Layer 1	1746.2	35	35	99	1.42	1.42
Layer 2	38.9	25.1	60.2	1.71	1.57	1.07
Layer 3	1.5	1.8	62	99	99	1.11
Layer 4	24.7			1.08		

SM046T: 4-Layered Model

	Res	Thk	Dep	ResSTD	ThkSTD	DepSTD
Layer 1	33	13.6	13.6	1.14	1.46	1.46
Layer 2	4.1	2.3	16	99	99	1.3
Layer 3	29	192	192	1.04	1.29	1.23
Layer 4	353.8			99		

SM047T: 4-Layered Model

	Res	Thk	Dep	ResSTD	ThkSTD	DepSTD
Layer 1	200	8	8	99	1.15	1.15
Layer 2	7.2	38.3	46.3	1.03	1.08	1.07
Layer 3	4.1	85.5	131.8	1.11	1.19	1.11
Layer 4	1.7			2.05		

SM051T: 4-Layered Model

	Res	Thk	Dep	ResSTD	ThkSTD	DepSTD
Layer 1	16.6	7.6	7.6	1.07	1.04	1.04
Layer 2	2.9	27.6	35.2	1.03	2.24	1.63
Layer 3	6	14.9	50.1	99	99	2.33
Layer 4	21.8			2.17		

SM055T: 4-Layered Model

	Res	Thk	Dep	ResSTD	ThkSTD	DepSTD
Layer 1	2049.2	15.4	15.4	99	99	99
Layer 2	837.4	10.4	25.8	99	99	1.29
Layer 3	65.3	56	81.9	1.07	1.24	1.2
Layer 4	191.9			1.11		

SM056T: 4-Layered Model

	Res	Thk	Dep	ResSTD	ThkSTD	DepSTD
Layer 1	63.1	16	16	1.21	1.32	1.32
Layer 2	18.1	18.7	34.6	1.35	2.2	1.31
Layer 3	47	49.7	84.3	1.61	1.37	1.29
Layer 4	994.2			4.55		

SM057T: 4-Layered Model

	Res	Thk	Dep	ResSTD	ThkSTD	DepSTD
Layer 1	40.4	18.2	18.2	1.04	1.23	1.23
Layer 2	22.9	30.1	48.3	1.14	1.38	1.13
Layer 3	210	120.1	168.4	2.4	1.38	1.19
Layer 4	32.4			1.4		

SM058T: 4-Layered Model

	Res	Thk	Dep	ResSTD	ThkSTD	DepSTD
Layer 1	38.1	6.8	6.8	1.1	99	99
Layer 2	37.5	34.5	41.3	1.06	4.7	1.57
Layer 3	68.3	35.4	76.6	3.37	1.79	1.52
Layer 4	360.3			1.33		

SM061T: 4-Layered Model

	Res	Thk	Dep	ResSTD	ThkSTD	DepSTD
Layer 1	511.4	3.1	3.1	99	99	99
Layer 2	534	74	77.1	1.69	1.34	1.04
Layer 3	1.9	0.6	77.7	99	99	1.04
Layer 4	153.1			1.05		

SM062T: 4-Layered Model

	Res	Thk	Dep	ResSTD	ThkSTD	DepSTD
Layer 1	1238.4	5	5	99	1.1	1.1
Layer 2	13.9	40.9	46	1.02	1.05	1.04
Layer 3	1.4	9.3	55.2	1.64	1.74	1.06
Layer 4	1826.8			99		

SM066T: 4-Layered Model

	Res	Thk	Dep	ResSTD	ThkSTD	DepSTD
Layer 1	7.8	5.2	5.2	1.07	1.1	1.1
Layer 2	2.6	12.8	17.9	1.05	1.42	1.23
Layer 3	3.3	76.9	94.8	1.04	1.38	1.24
Layer 4	2.2			1.51		

Appendix 4: Apparent Resistivity Data for 5-layers Models at various Sounding Points in Machile River Basin, South-Western Zambia

MT003: 5-Layered Model

	Res	Thk	Dep	ResSTD	ThkSTD	DepSTD
Layer 1	154.1	7.1	7.1	99	2.78	2.78
Layer 2	17.1	27	34.1	1.18	2.91	2
Layer 3	12.1	21.6	55.6	2.42	99	2.27
Layer 4	22.2	45.3	100.9	8	99	99
Layer 5	22.4			1.94		

MT005: 5-Layered Model

	Res	Thk	Dep	ResSTD	ThkSTD	DepSTD
Layer 1	362.8	16.4	16.4	99	99	99
Layer 2	70.4	3.9	20.3	99	99	99
Layer 3	15.8	19	39.3	4.43	99	99
Layer 4	20.4	66.9	106.3	1.14	1.8	99
Layer 5	33.8			1.52		

MT017: 5-Layered Model

	Res	Thk	Dep	ResSTD	ThkSTD	DepSTD
Layer 1	171.6	10.9	10.9	99	99	99
Layer 2	9.1	7.7	18.6	99	99	4.97
Layer 3	25.5	27.1	45.7	7.19	99	4.54
Layer 4	20.4	229.2	274.9	1.16	3.05	1.64
Layer 5	9.2			5.12		

SM006T: 5-Layered Model

	Res	Thk	Dep	ResSTD	ThkSTD	DepSTD
Layer 1	293	13.8	13.8	99	99	99
Layer 2	113.2	8.3	22.1	99	99	1.73
Layer 3	33.2	30.4	52.4	1.26	2.27	1.37
Layer 4	102.9	86.8	139.2	1.69	2.29	1.61
Layer 5	654.6			99		

SM010T: 5-Layered Model

	Res	Thk	Dep	ResSTD	ThkSTD	DepSTD
Layer 1	88.3	11.9	11.9	99	7.91	7.91
Layer 2	14.4	17.4	29.2	2.44	3.41	1.14
Layer 3	3.2	17.1	46.3	1.3	2.99	1.54
Layer 4	8.5	24.6	70.9	7.52	3.87	1.72
Layer 5	101.7			99		

SM022T: 5-Layered Model

	Res	Thk	Dep	ResSTD	ThkSTD	DepSTD
Layer 1	145.7	14	14	99	3.73	3.73
Layer 2	11.8	10	24	8.97	99	2.29
Layer 3	40.2	18	42	99	99	1.76
Layer 4	13.9	49.4	91.4	1.51	3.05	1.33
Layer 5	160.4			9.68		

SM026T: 5-Layered Model

	Res	Thk	Dep	ResSTD	ThkSTD	DepSTD
Layer 1	2475.7	19.1	19.1	99	2.41	2.41
Layer 2	217.3	2.7	21.8	99	99	1.11
Layer 3	16.8	36.5	58.3	1.04	1.12	1.1
Layer 4	394.3	5.7	64	99	99	1.57
Layer 5	14152			99		

SM048T: 5-Layered Model

	Res	Thk	Dep	ResSTD	ThkSTD	DepSTD
Layer 1	101.6	3.8	3.8	99	2.56	2.56
Layer 2	11.2	22.4	26.2	1.08	1.66	1.35
Layer 3	26.1	23.9	50.1	2.91	1.8	1.08
Layer 4	5	142.7	192.8	1.09	1.44	1.25
Layer 5	20.6			99		

SM050T: 5-Layered Model

	Res	Thk	Dep	ResSTD	ThkSTD	DepSTD
Layer 1	27.2	10.1	10.1	1.08	1.03	1.03
Layer 2	2.4	14.8	24.9	1.05	1.29	1.15
Layer 3	7	26.1	51	2.06	3.11	1.64
Layer 4	54.4	35.8	86.8	99	99	3.17
Layer 5	317.6			99		

SM059T: 5-Layered Model

	Res	Thk	Dep	ResSTD	ThkSTD	DepSTD
Layer 1	426.2	21	21	99	4.93	4.93
Layer 2	48.4	22.3	43.3	3.58	3.17	1.26
Layer 3	11.8	15	58.3	2.22	4.14	1.54
Layer 4	64.8	84.7	143	1.61	2.08	1.55
Layer 5	186.6			1.71		

Appendix 5: Apparent Resistivity Data (in error bars) and Line Model (right panel) for a 3-layered Model in the Machile River Basin, South-Western, Zambia

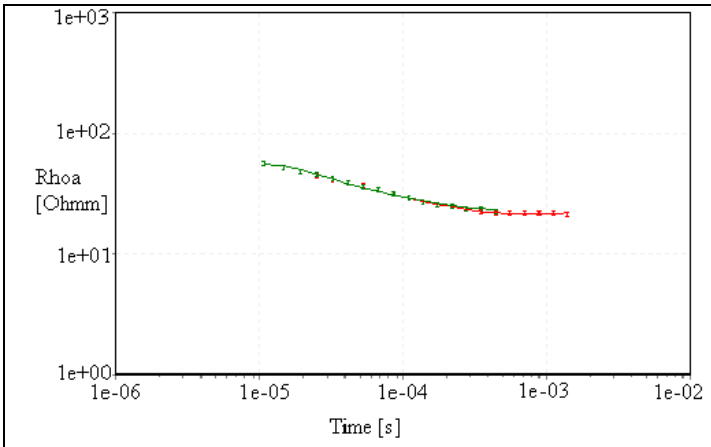

MT002: 3-Layered Model

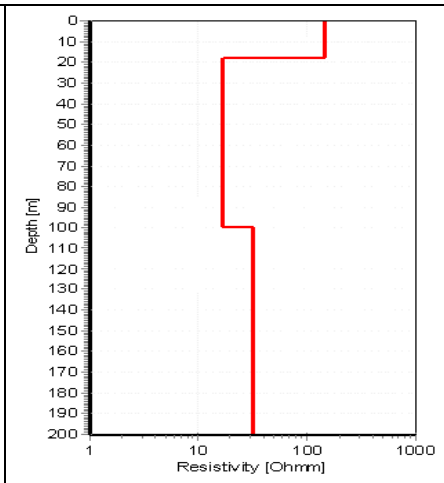

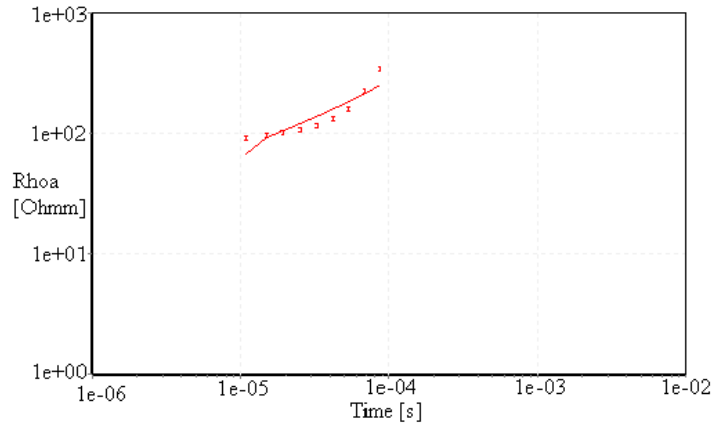

MT010: 3-Layered Model

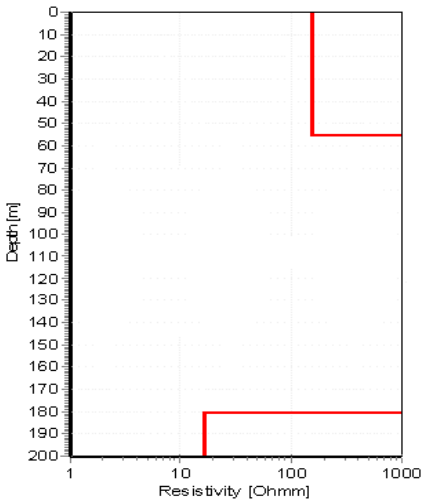

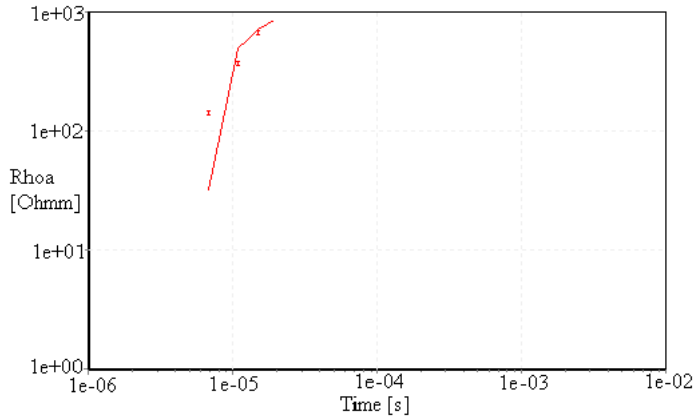

MT012: 3-Layered Model

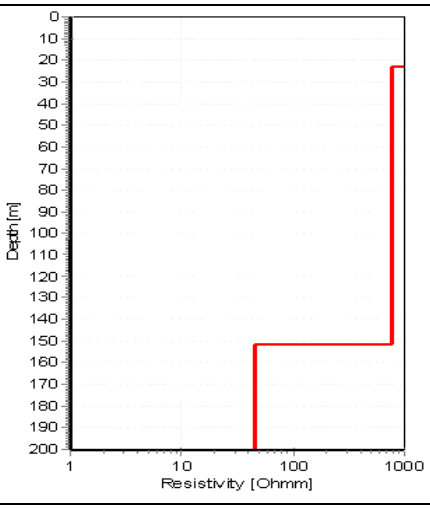

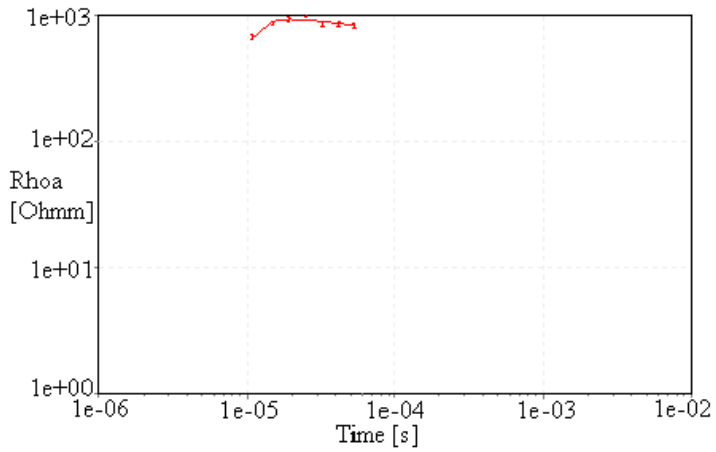

MT014: 3-Layered Model

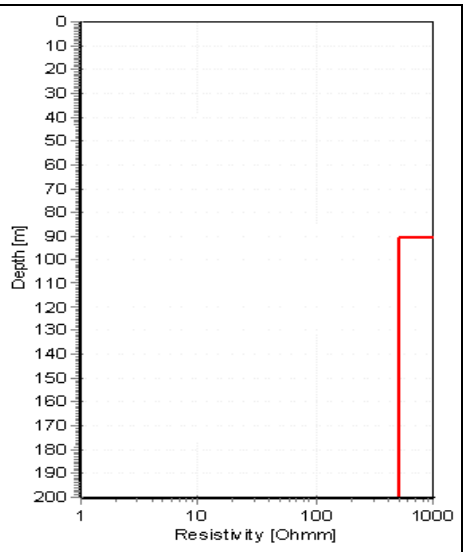

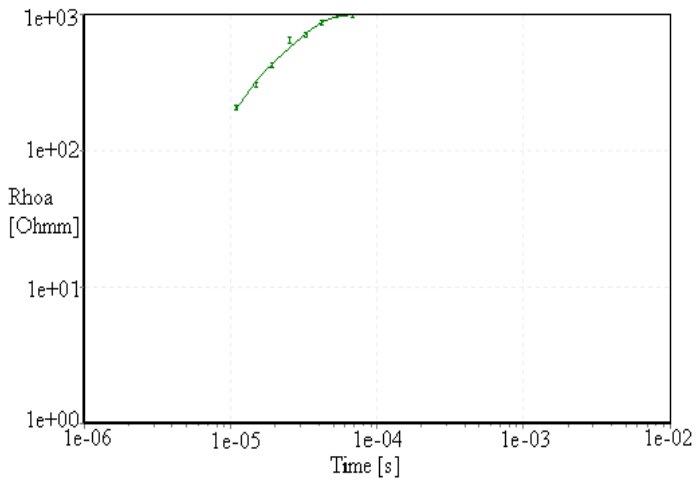

MT015: 3-Layered Model

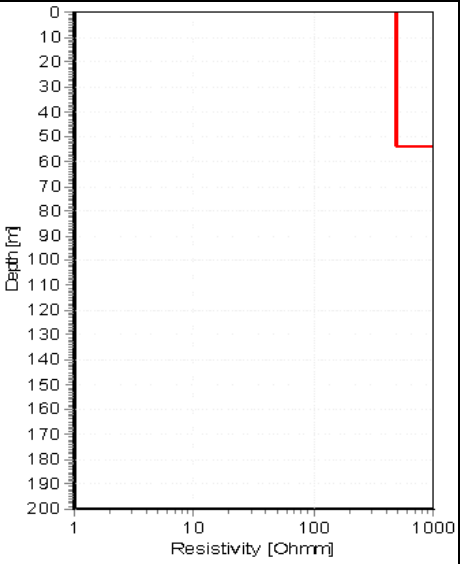

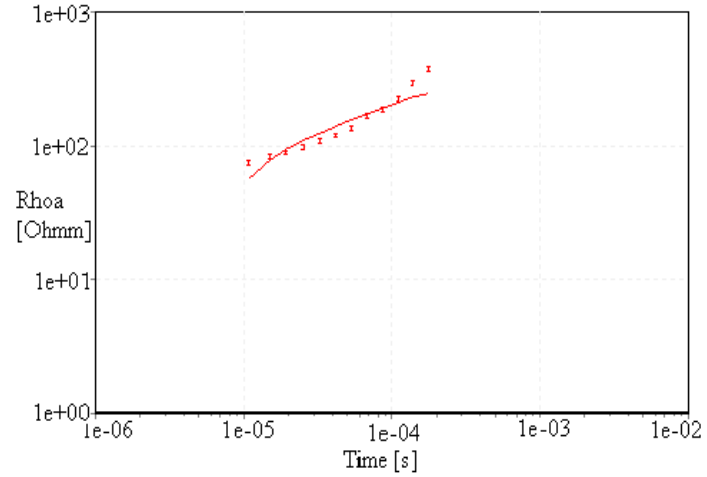

MT016: 3-Layered Model

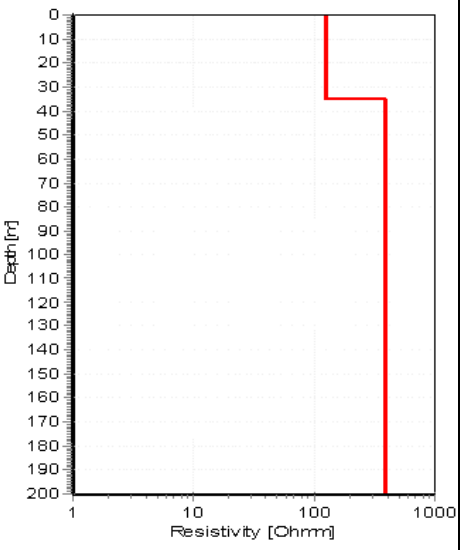

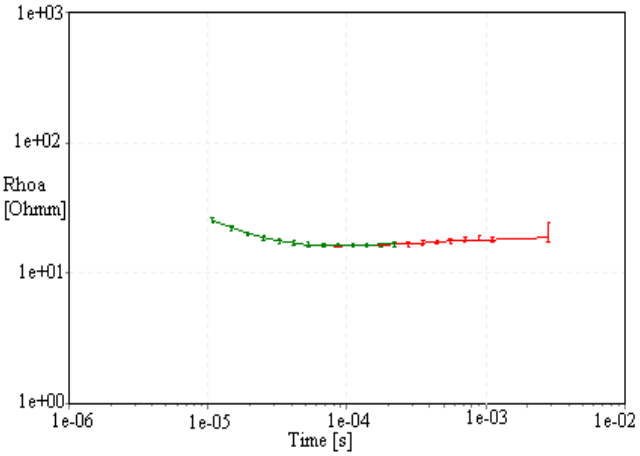

MT018: 3-Layered Model

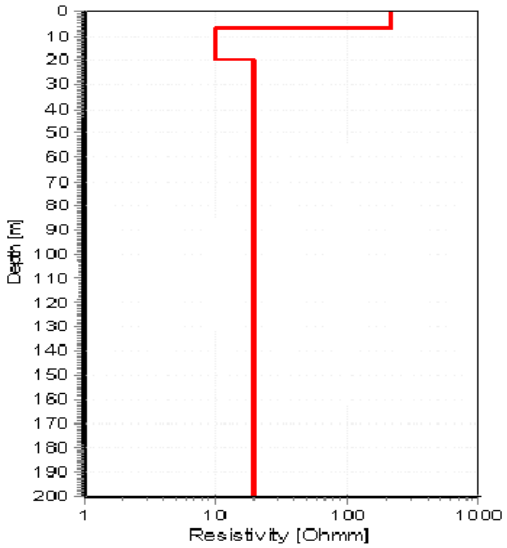

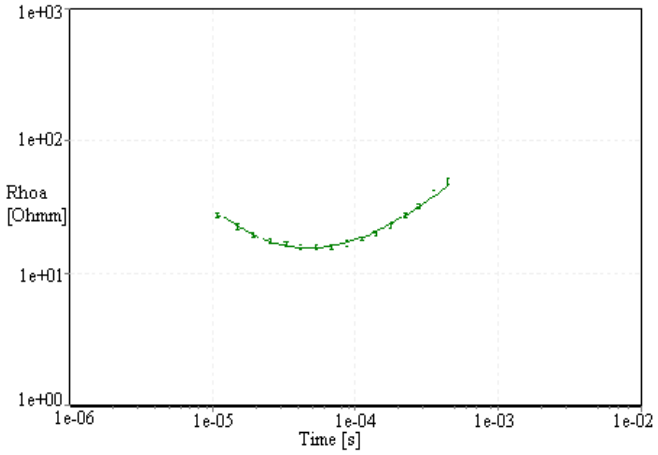

MT026: 3-Layered Model

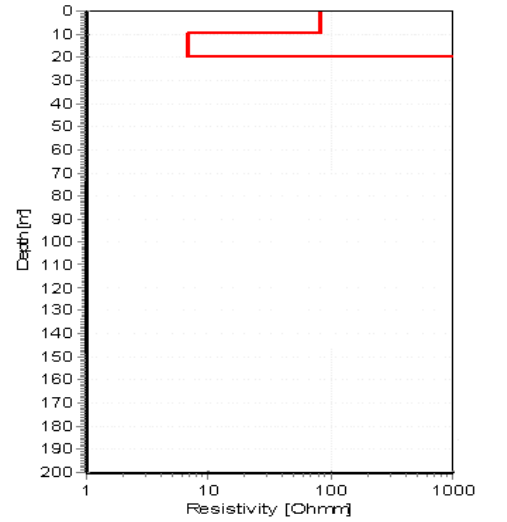

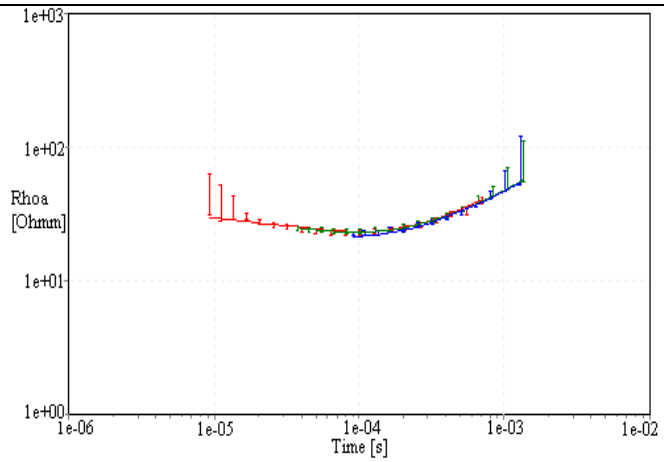

SM005T: 3-Layered Model

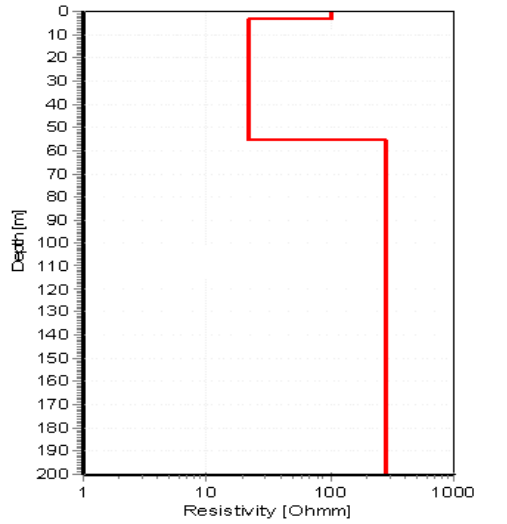

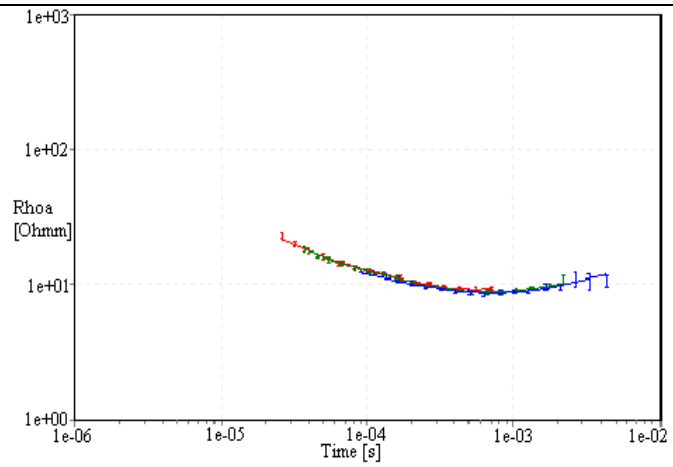

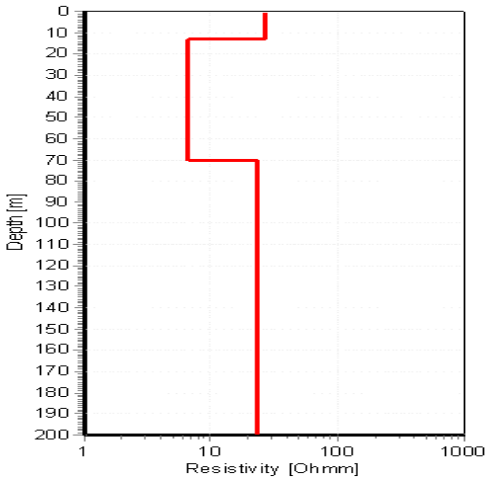

SM009T: 3-Layered Model

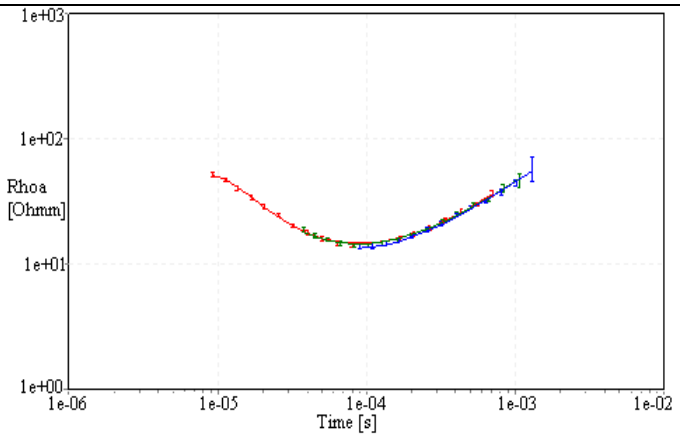

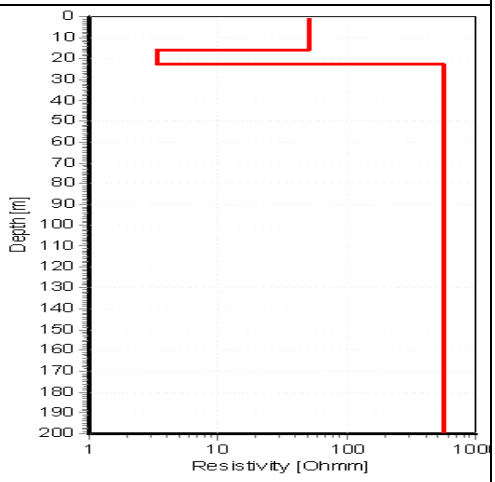

SM011T: 3-Layered Model

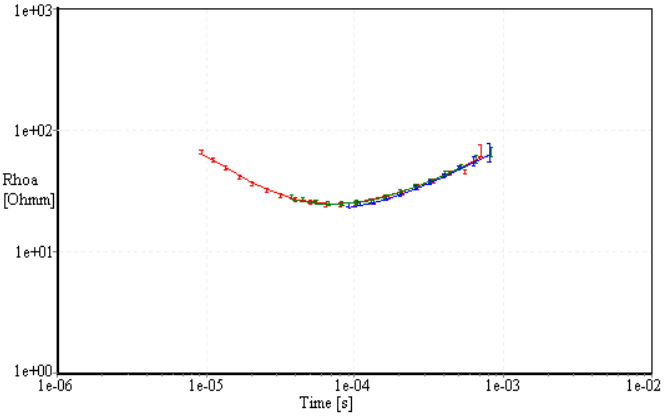

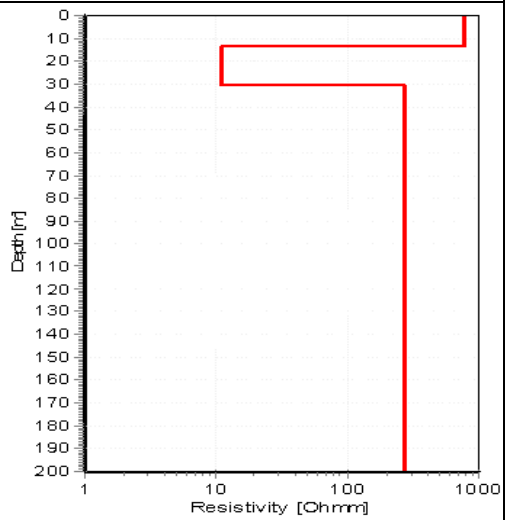

SM012T: 3-Layered Model

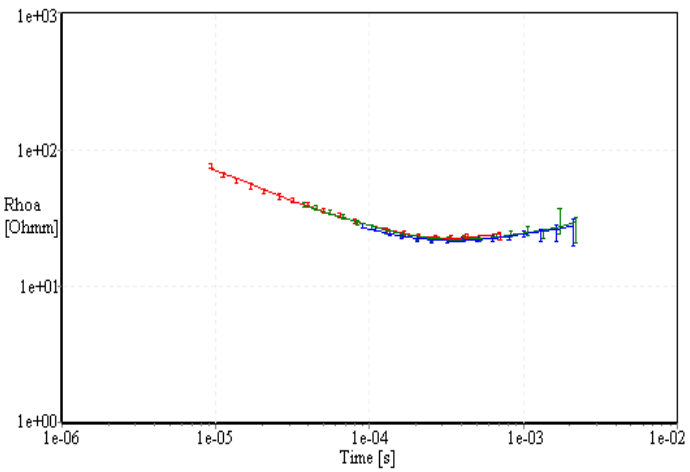

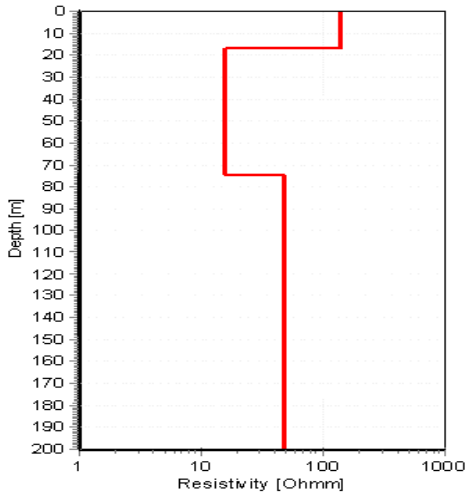

SM023T: 3-Layered Model

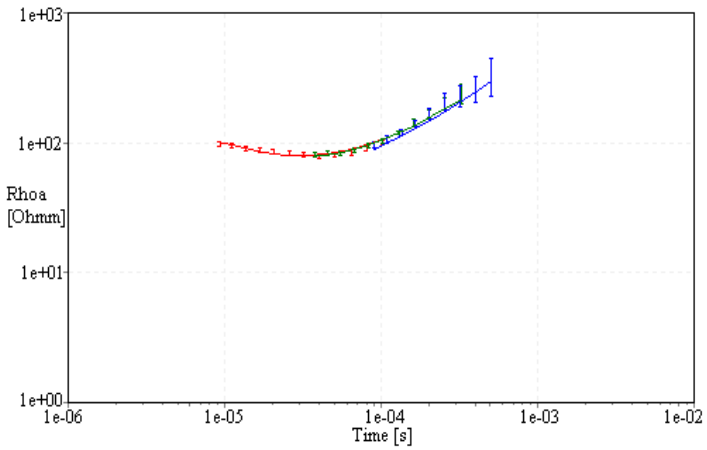

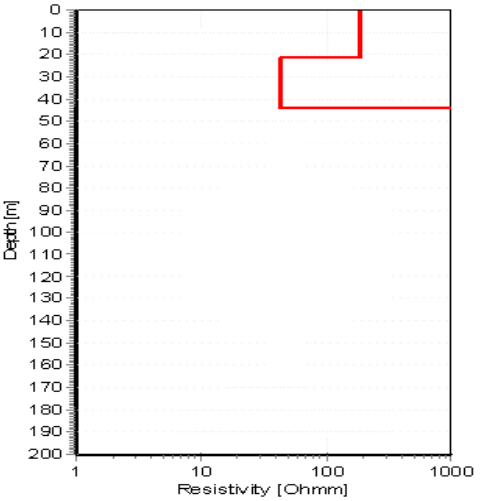

SM027T: 3-Layered Model

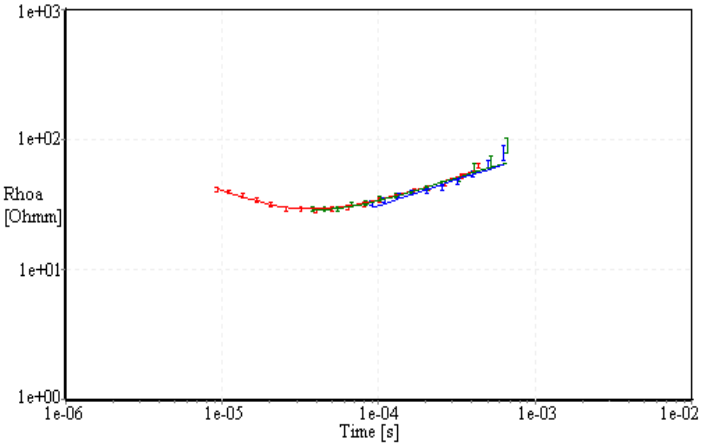

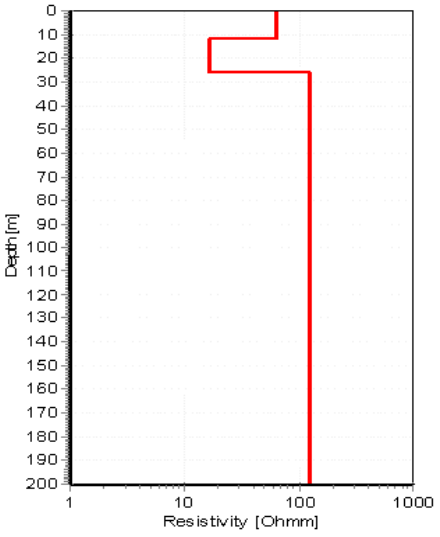

SM034T: 3-Layered Model

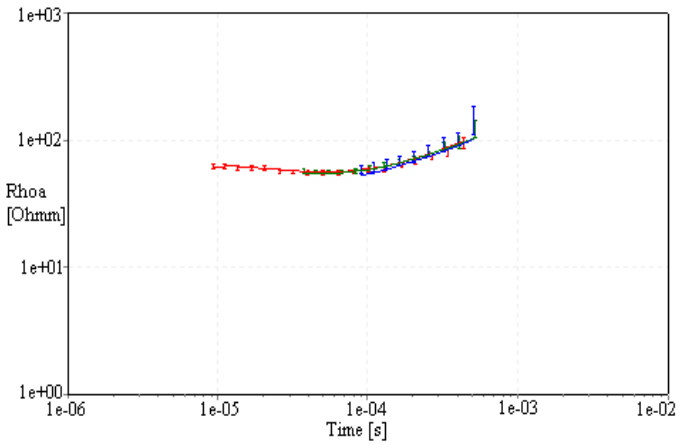

SM036T: 3-Layered Model

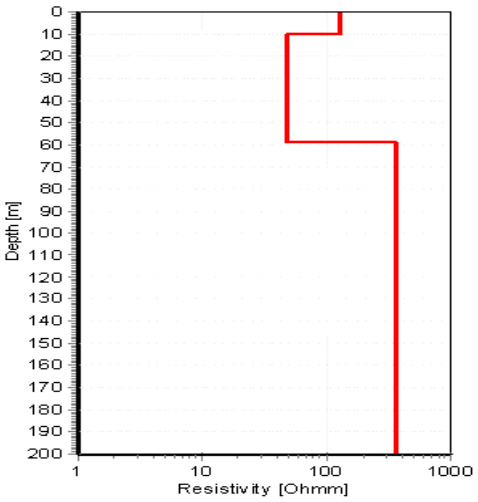

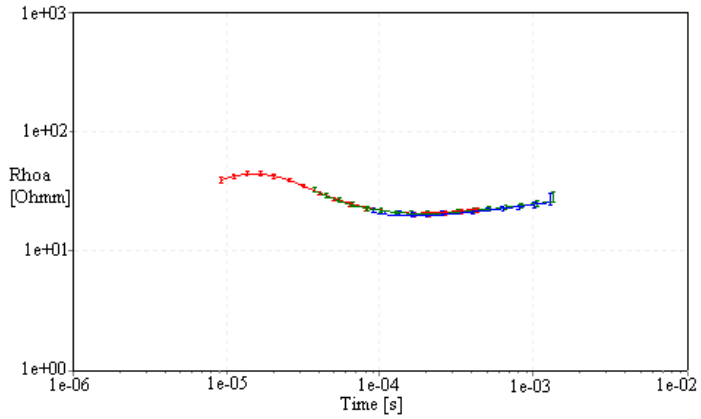

SM045T: 3-Layered Model

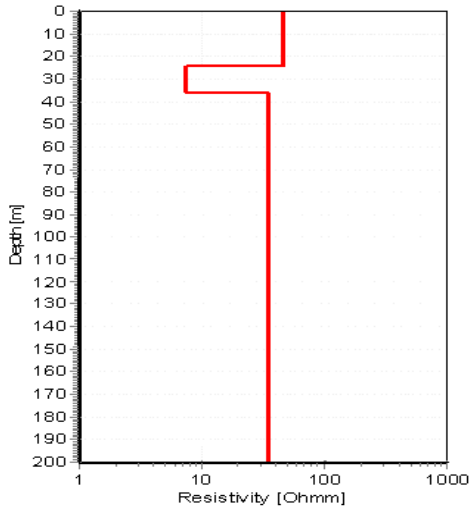

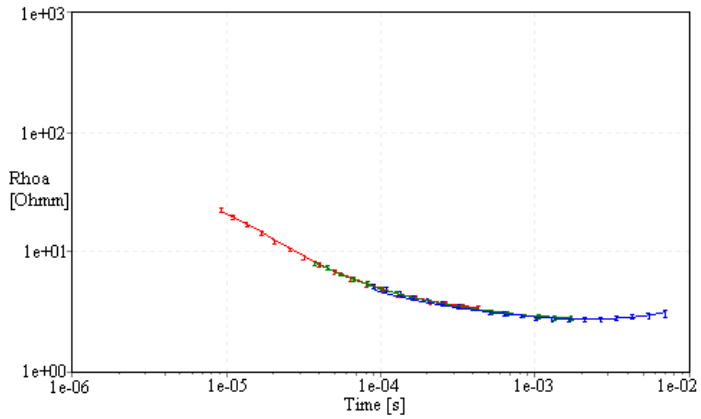

SM049T: 3-Layered Model

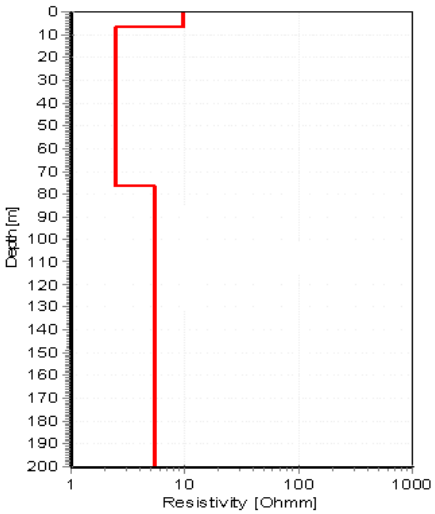

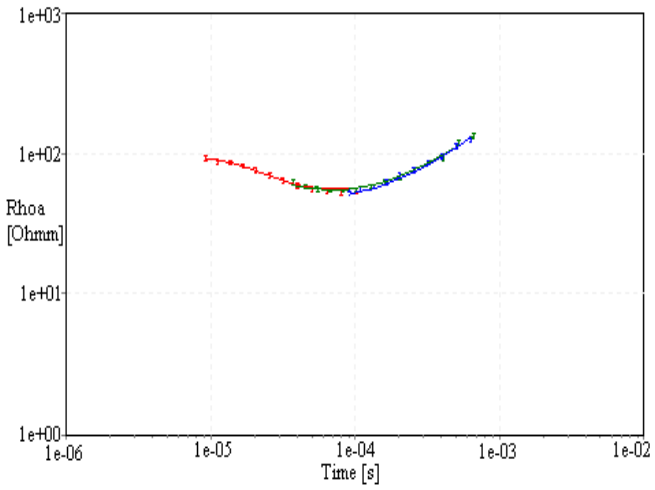

SM060T: 3-Layered Model

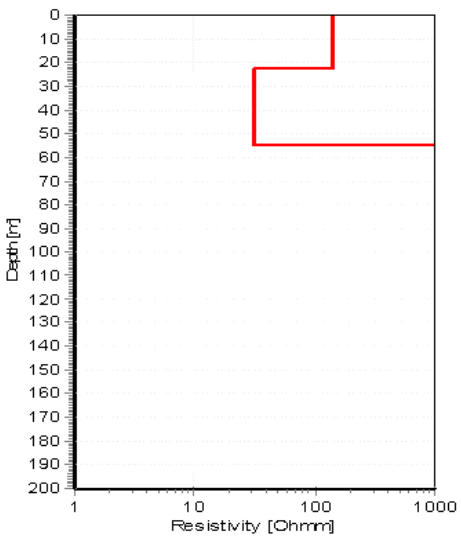

Appendix 6: Apparent Resistivity Data (in error bars) and Line Model (right panel) for a 4-layered Model in the Machile River Basin, South-Western, Zambia

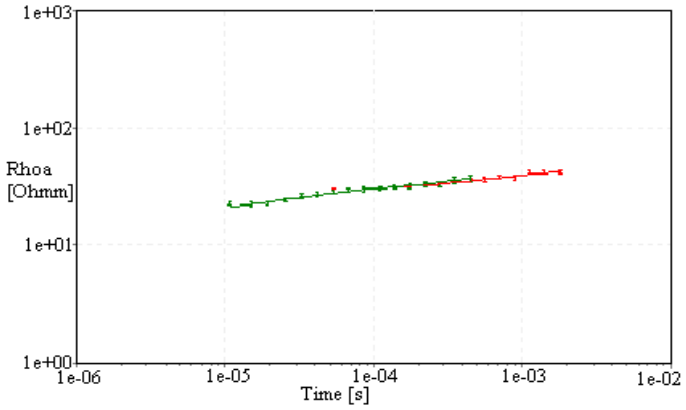

MT001: 4_Layered Model

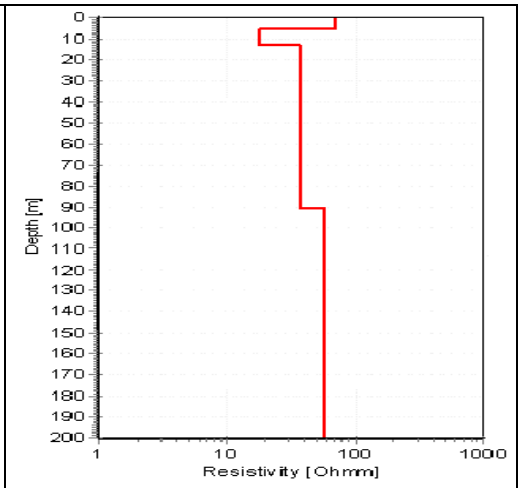

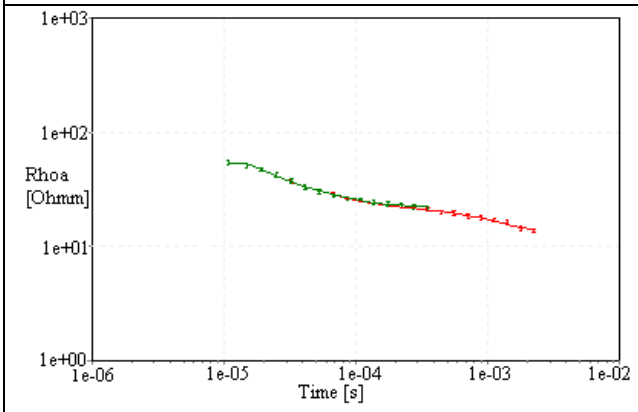

MT004: 4-Layered Model

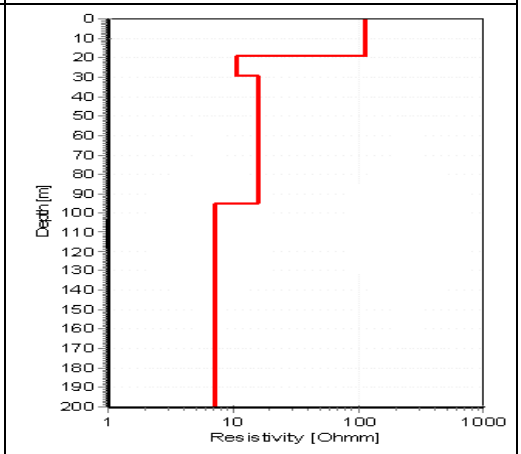

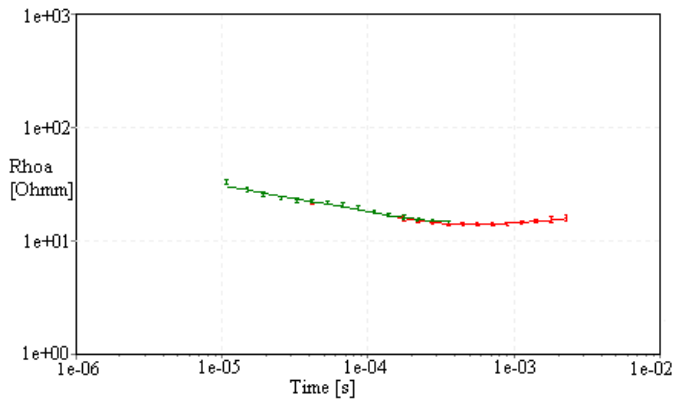

MT006: 4-Layered Model

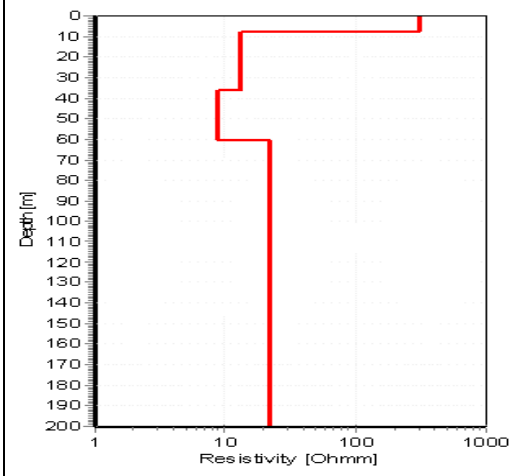

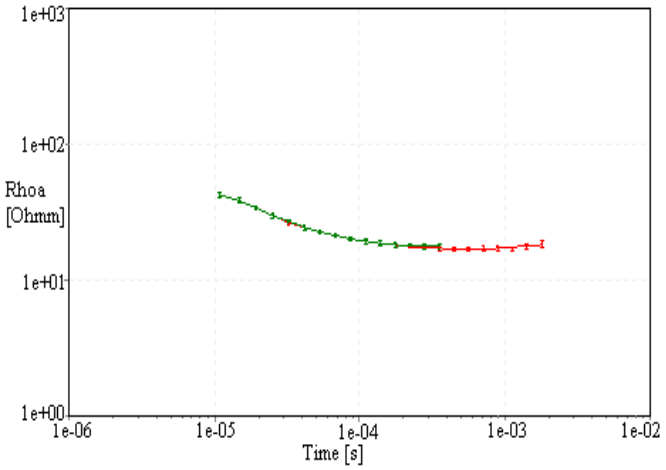

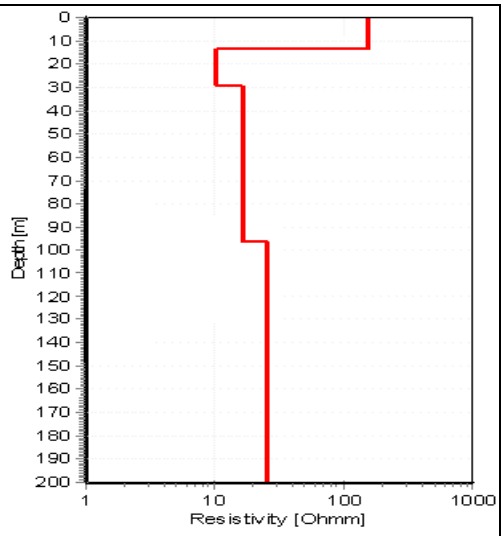

MT007: 4-Layered Model

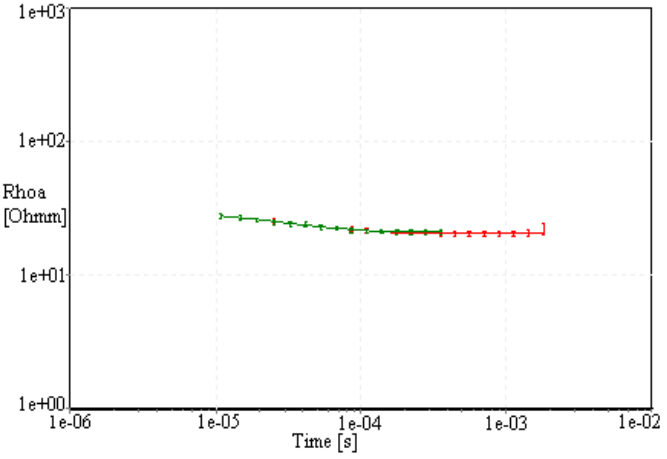

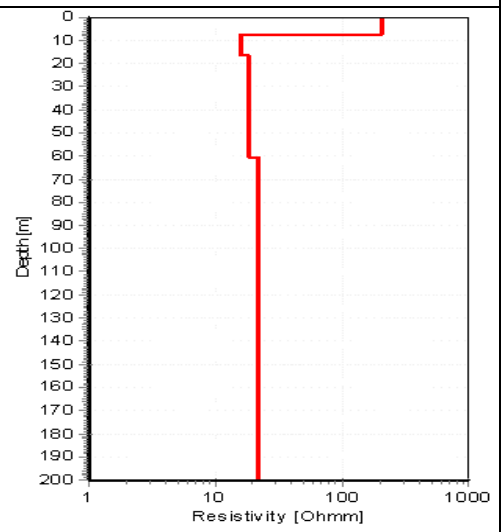

MT008: 4-Layered Model

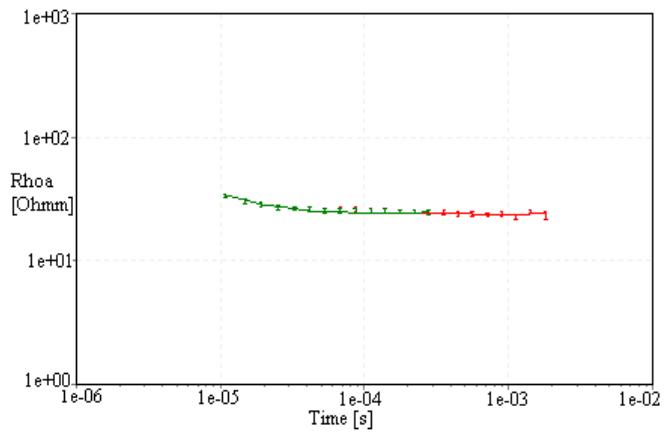

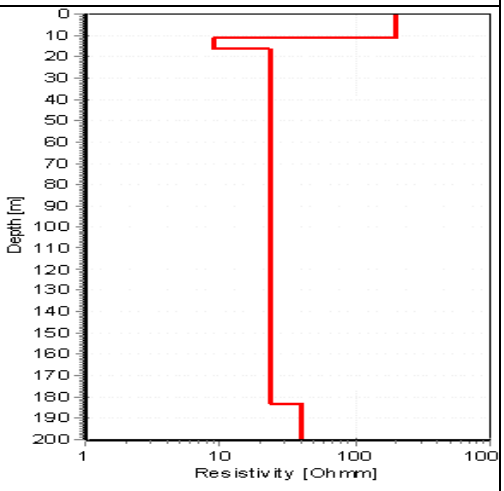

MT009: 4-Layered Model

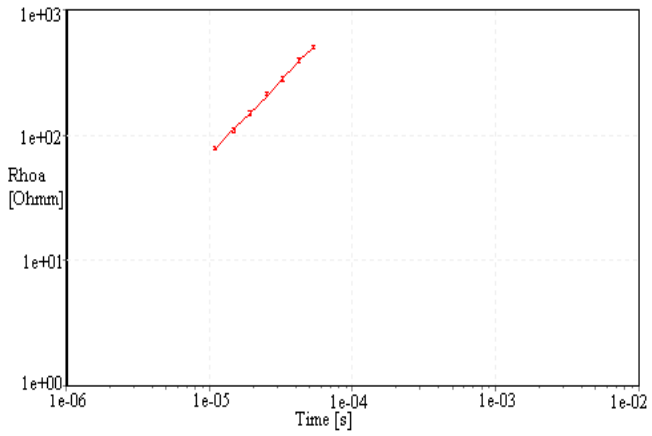

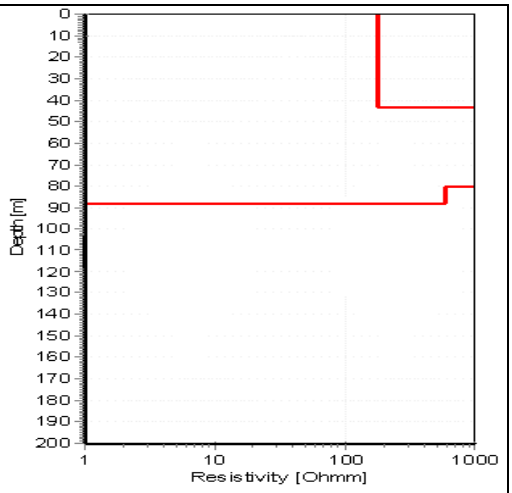

MT011: 4-Layered Model

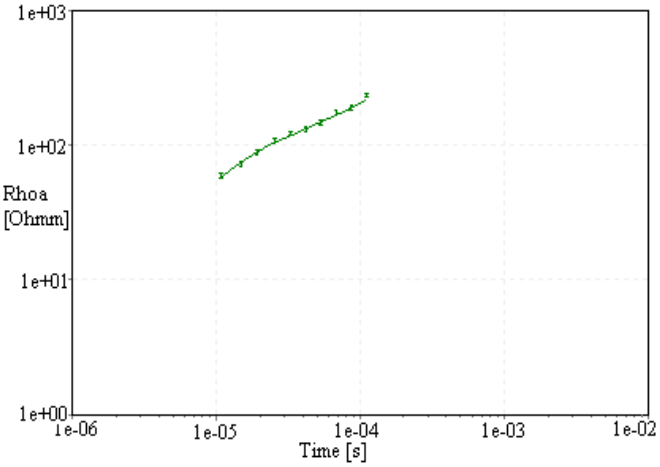

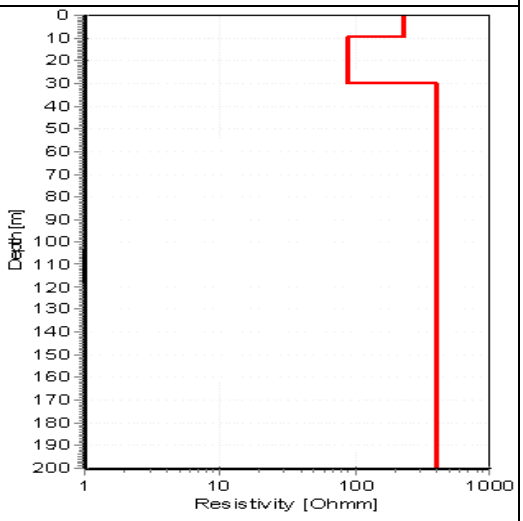

MT013: 4-Layered Model

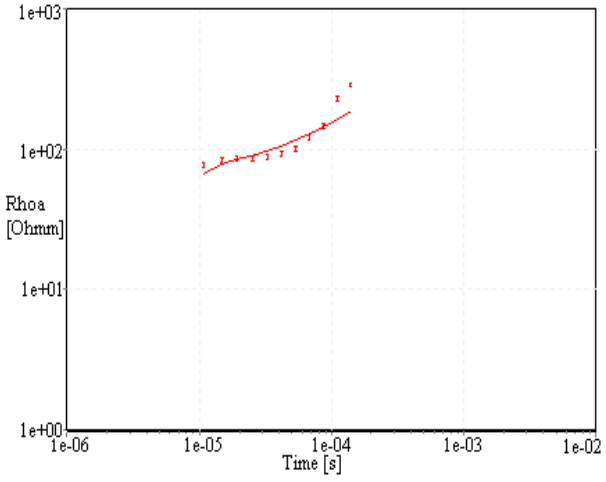

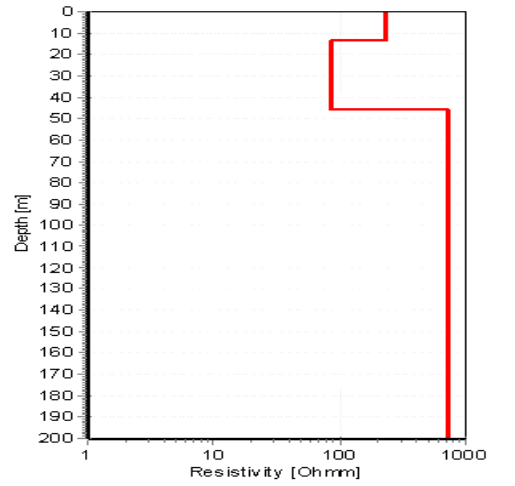

MT020: 4-Layered Model

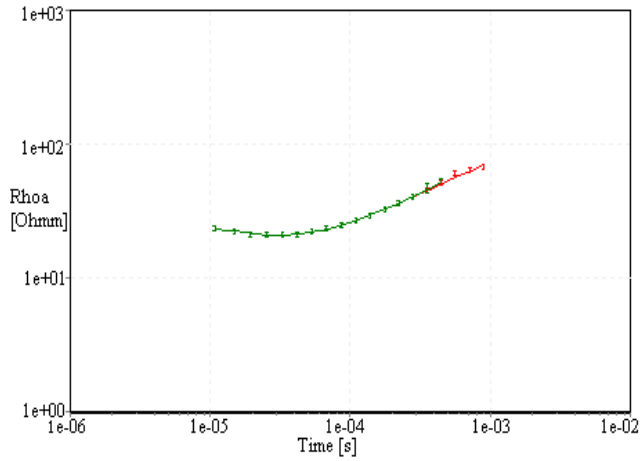

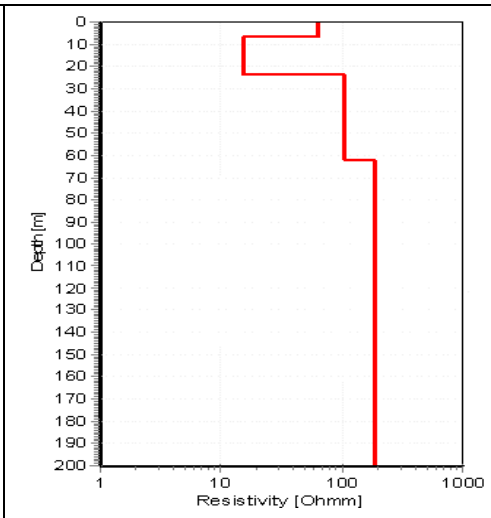

MT021: 4-Layered Model

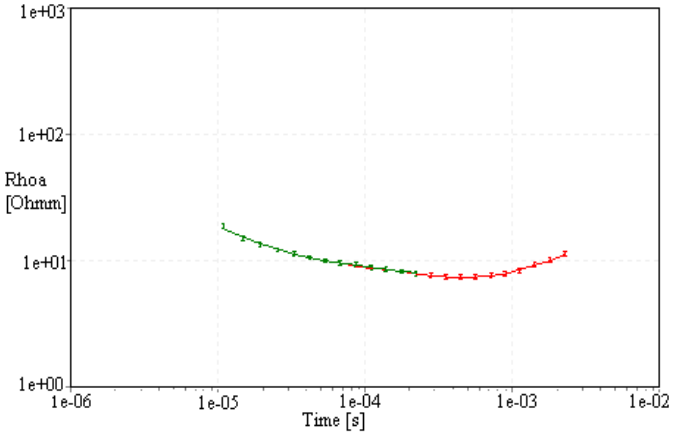

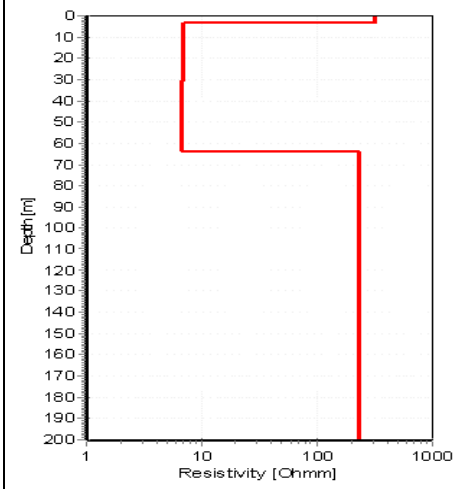

MT022: 4-Layered Model

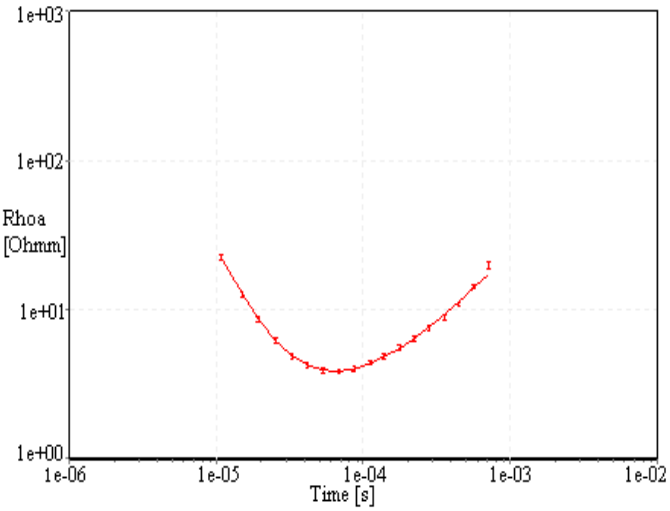

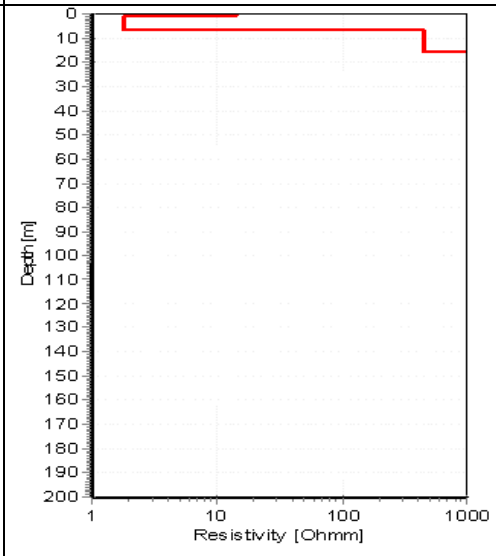

MT023: 4-Layered Model

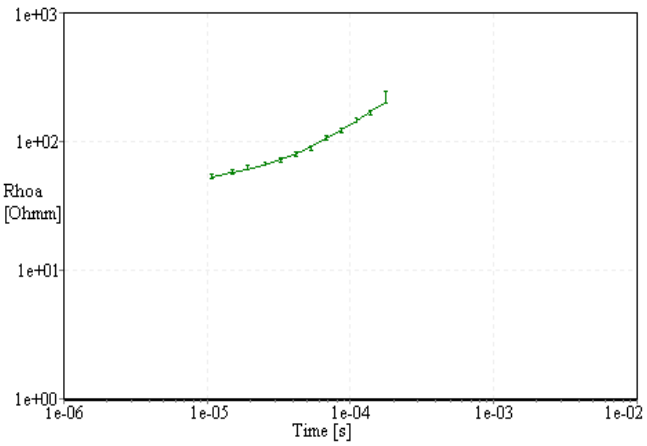

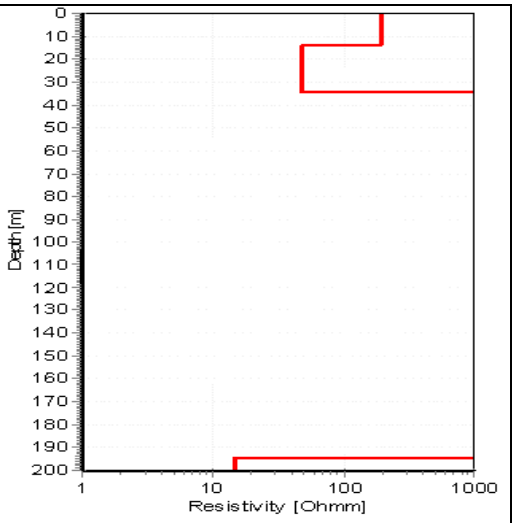

MT024: 4-Layered Model

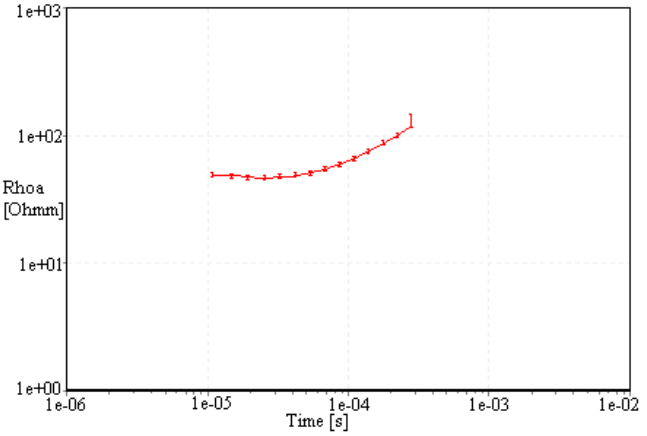

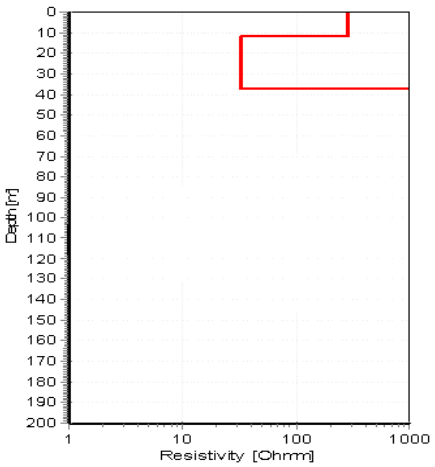

MT025: 4-Layered Model

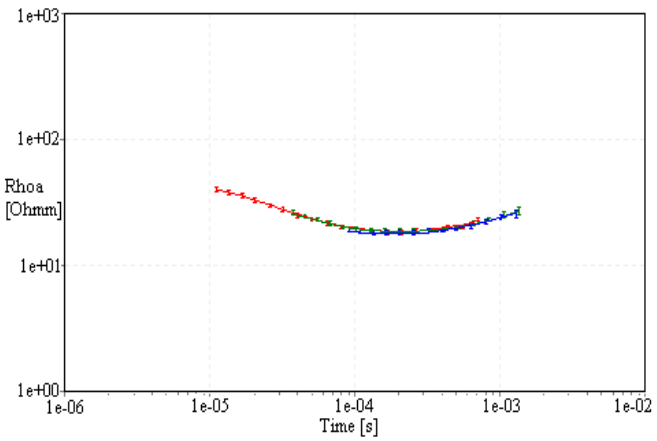

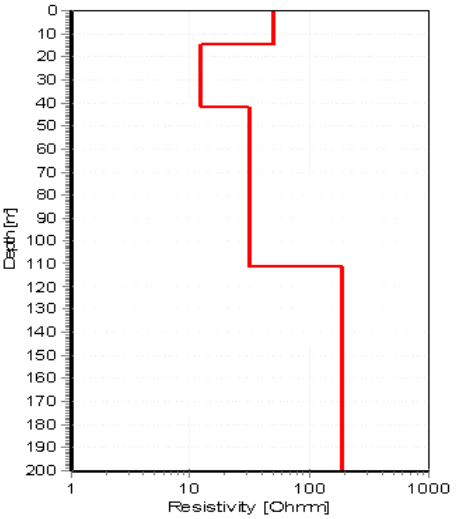

SM003T: 4-Layered model

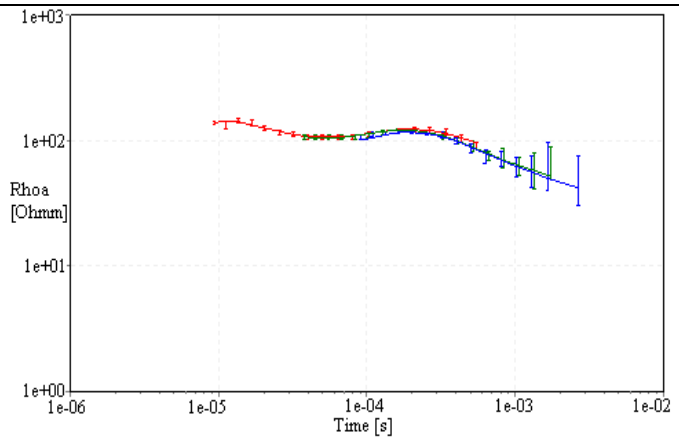

SM004T: 4-Layered Model

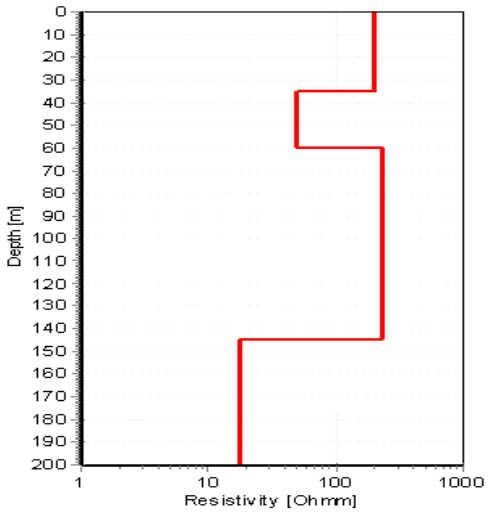

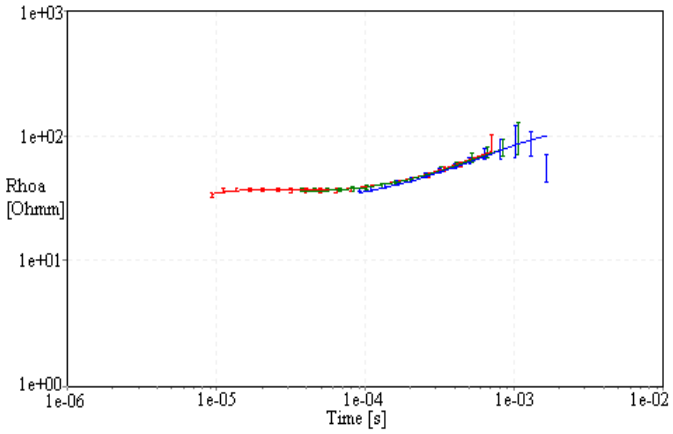

SM013T: 4-Layered Model

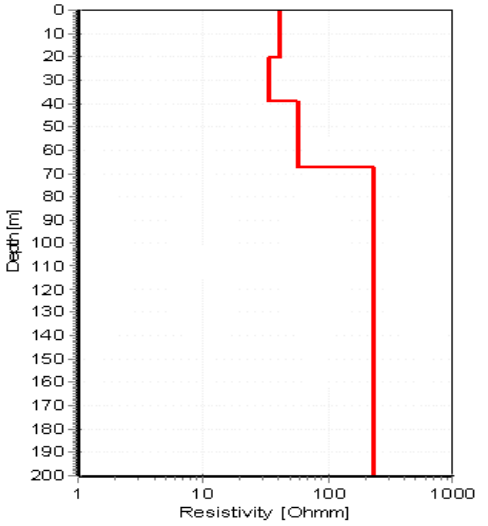

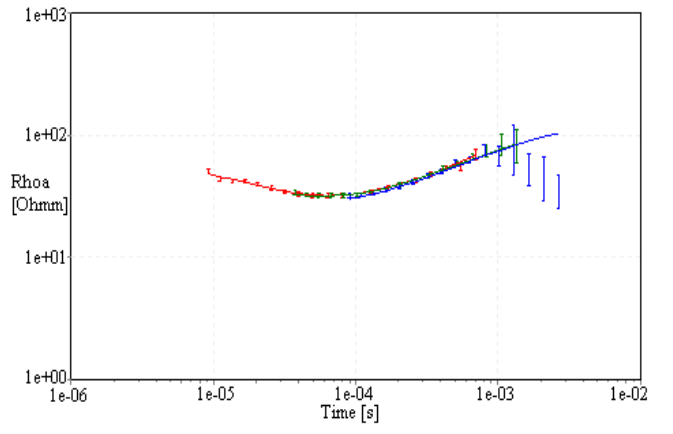

SM014T: 4-Layered Model

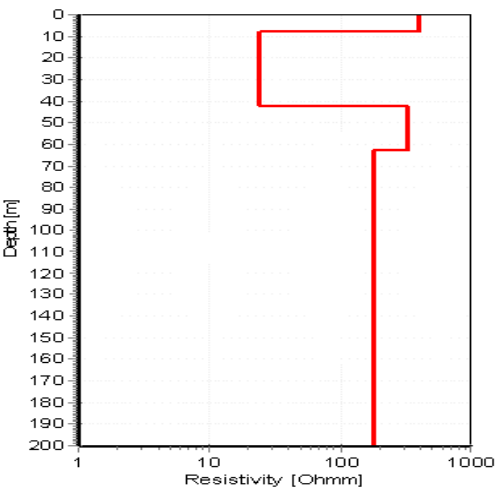

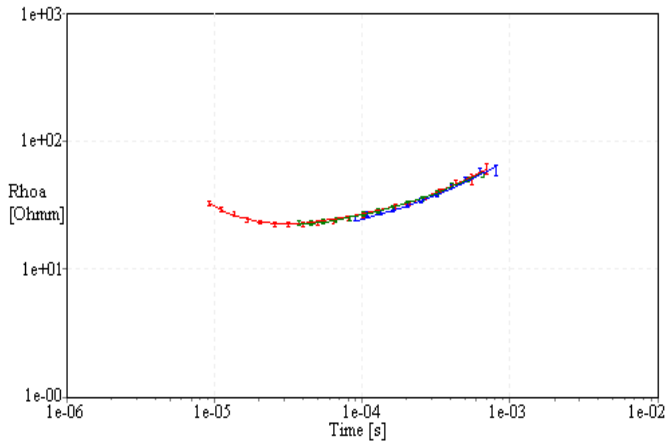

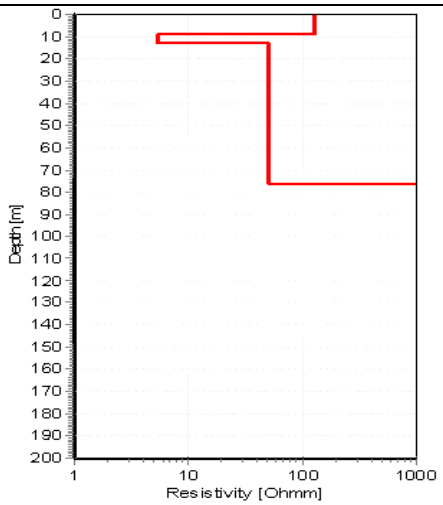

SM015T: 4-Layered Model

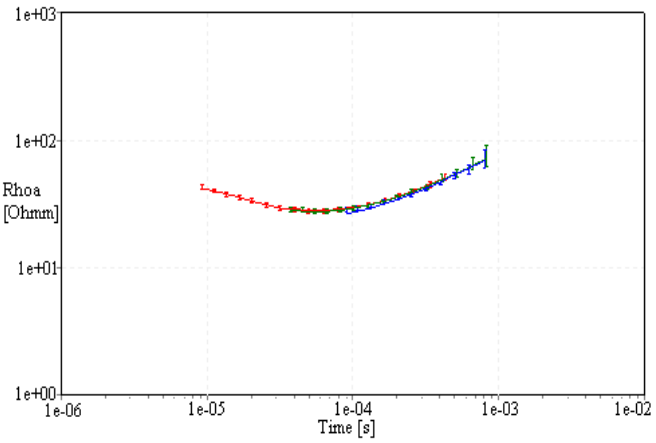

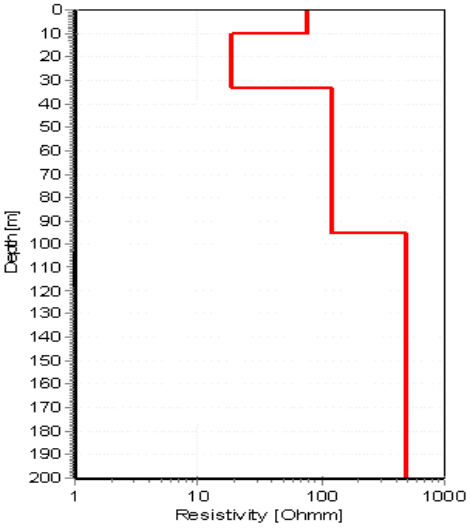

SM021T: 4-Layered Model

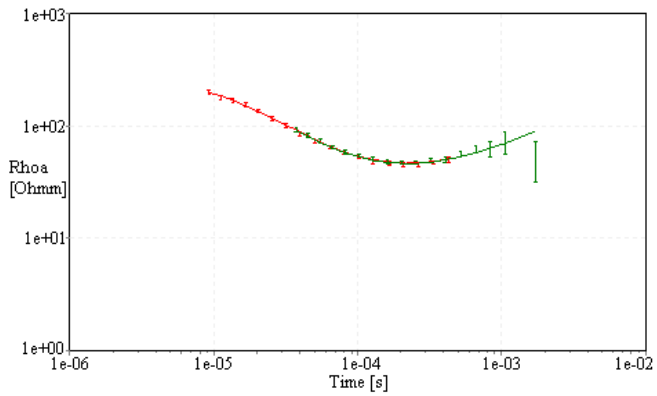

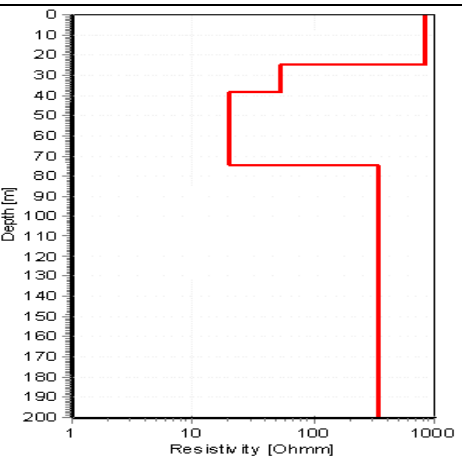

SM025T: 4-Layered Model

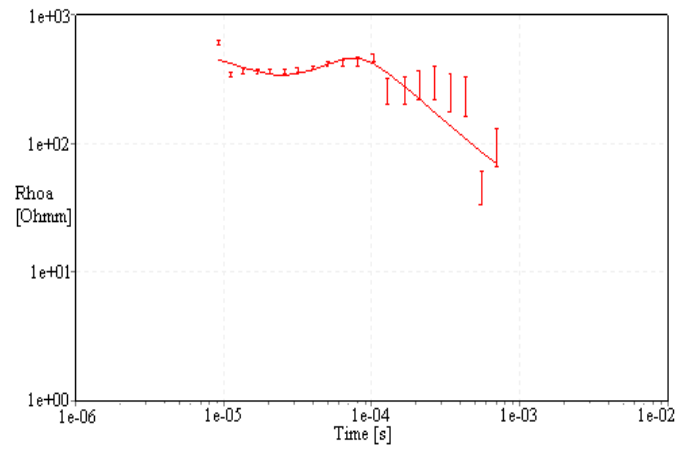

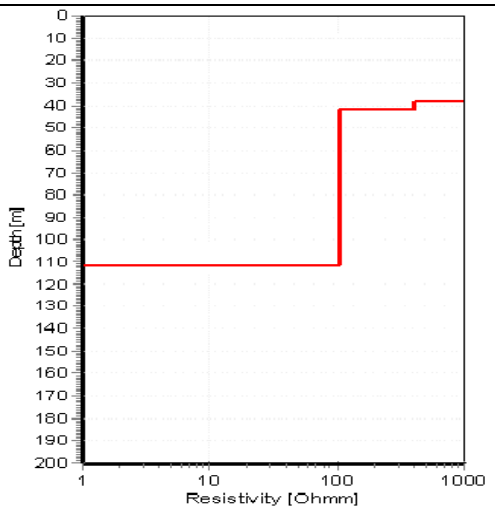

SM028T: 4-Layered Model

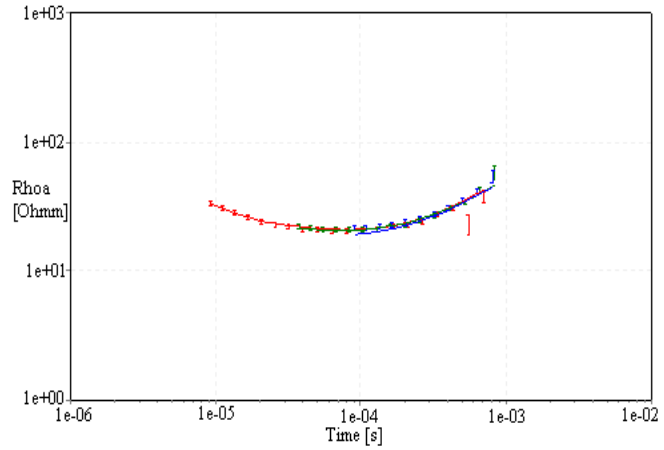

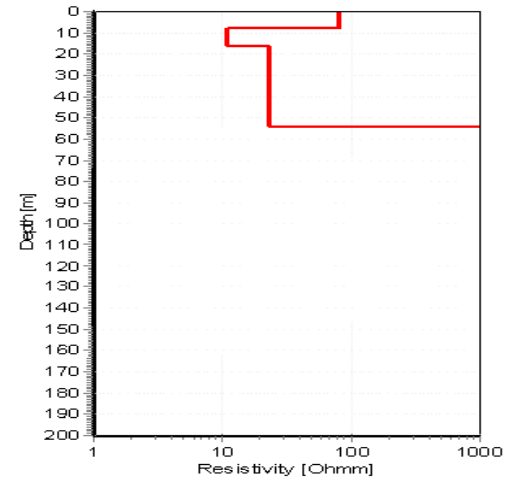

SM029T: 4-Layered Model

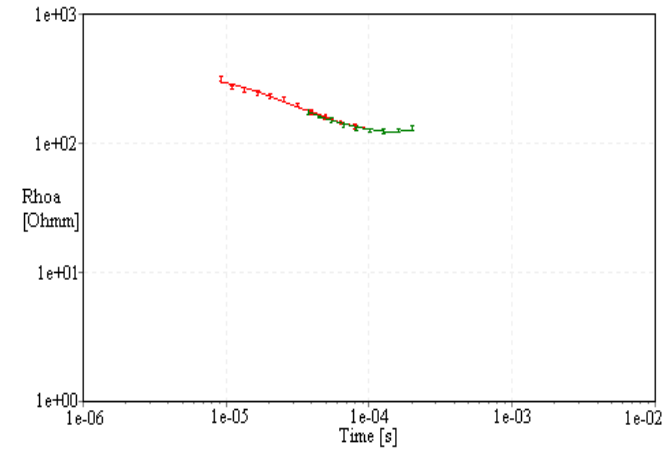

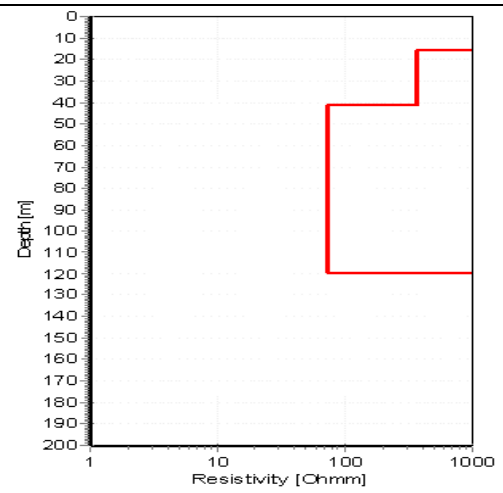

SM032T: 4-Layered Model

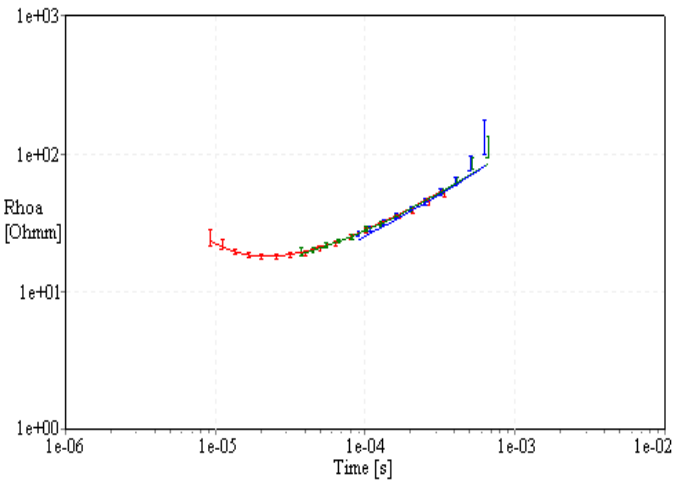

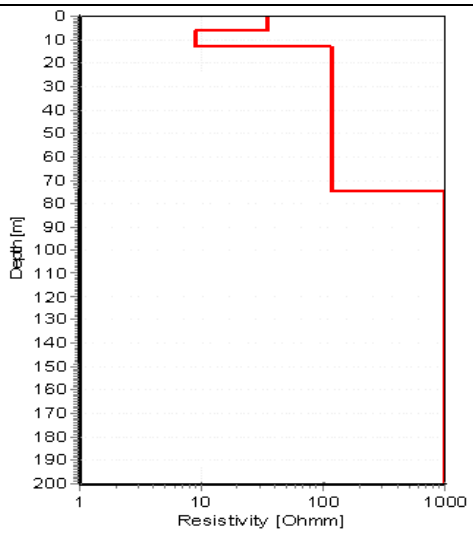

SM033T: 4-Layered Model

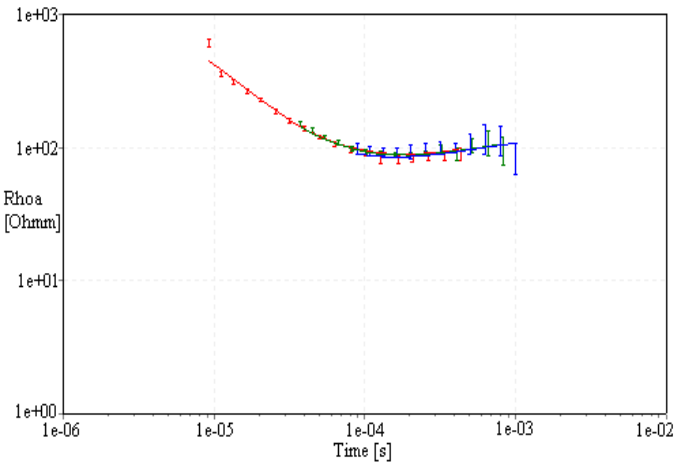

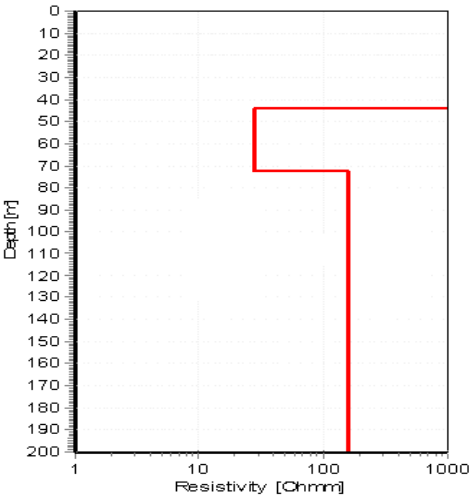

SM035T: 4-Layered Model

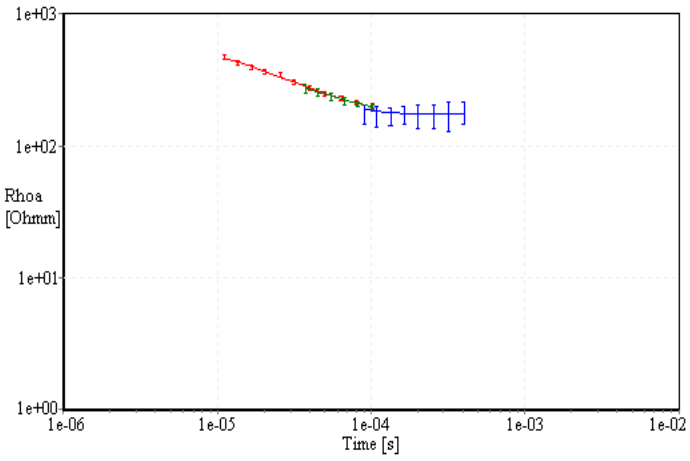

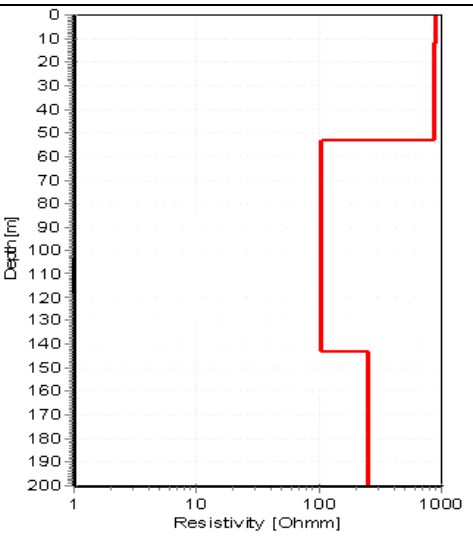

SM037T: 4-Layered Model

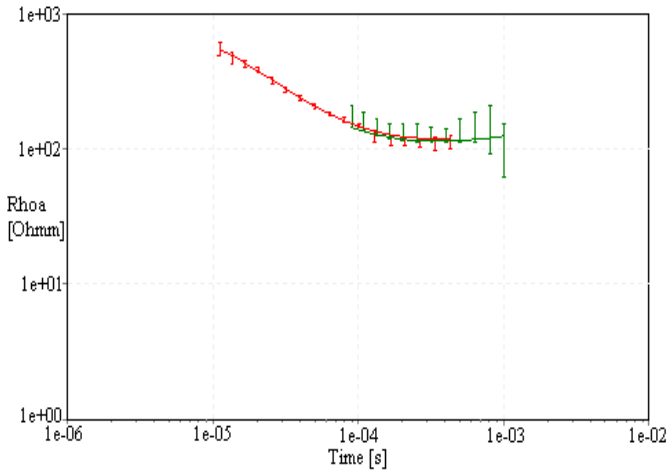

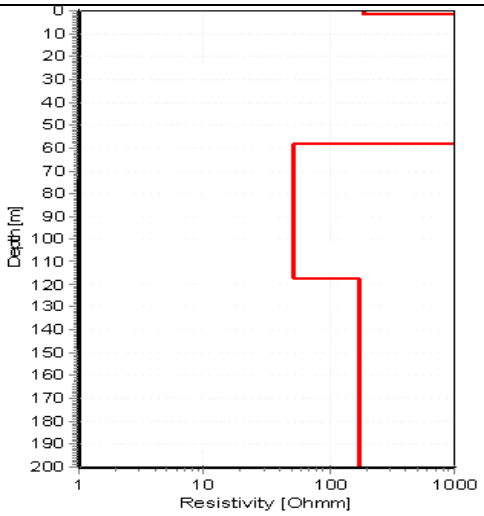

SM038T: 4-Layered Model

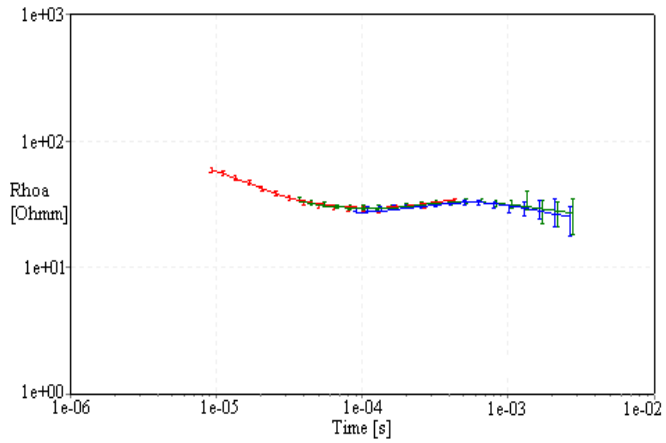

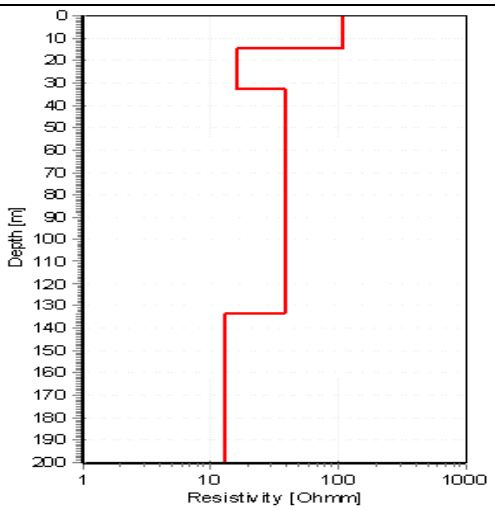

SM043T: 4-Layered Model

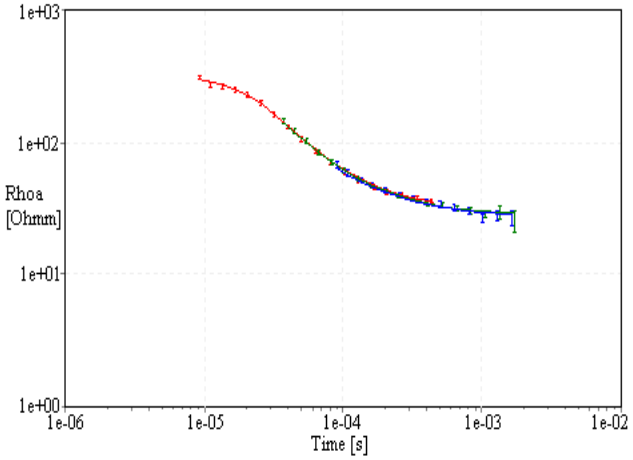

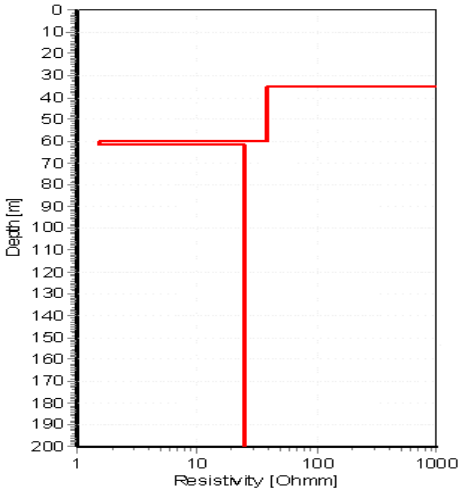

SM044T: 4-Layered Model

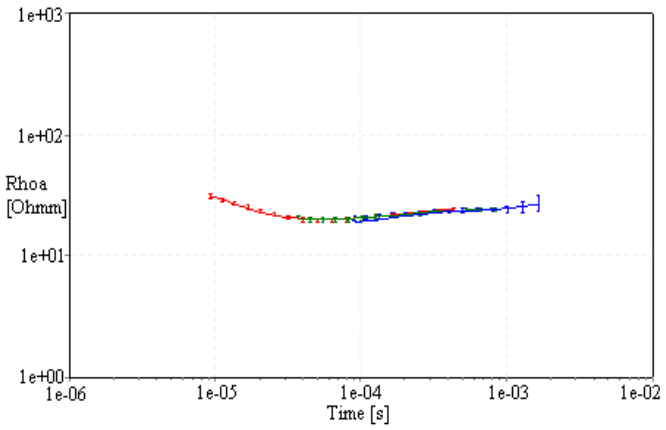

SM046T: 4-Layered Model

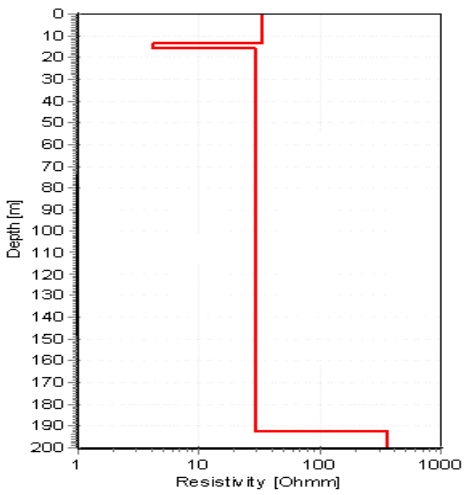

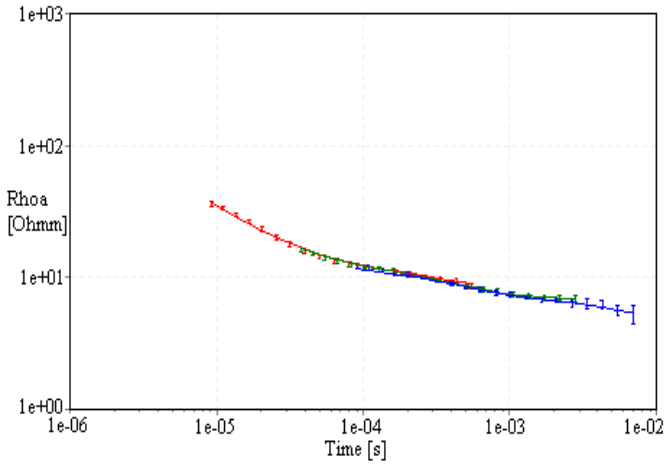

SM047T: 4-Layered Model

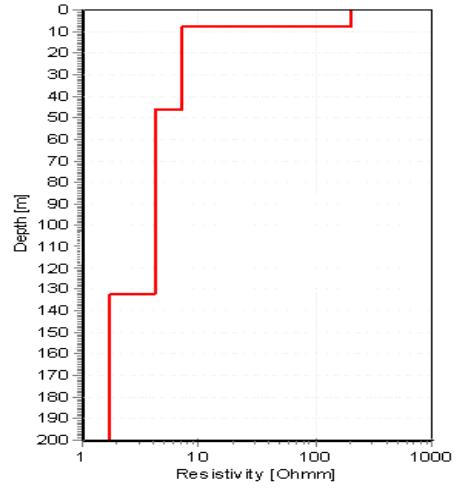

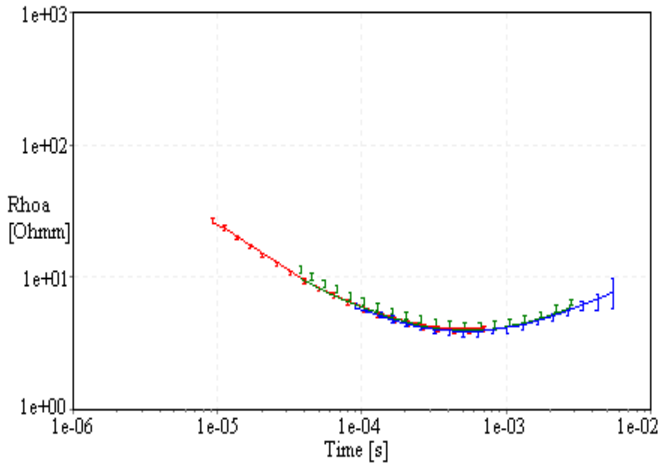

SM051T: 4-Layered Model

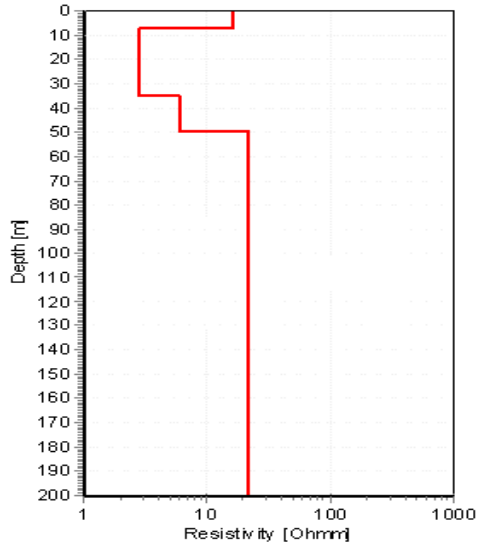

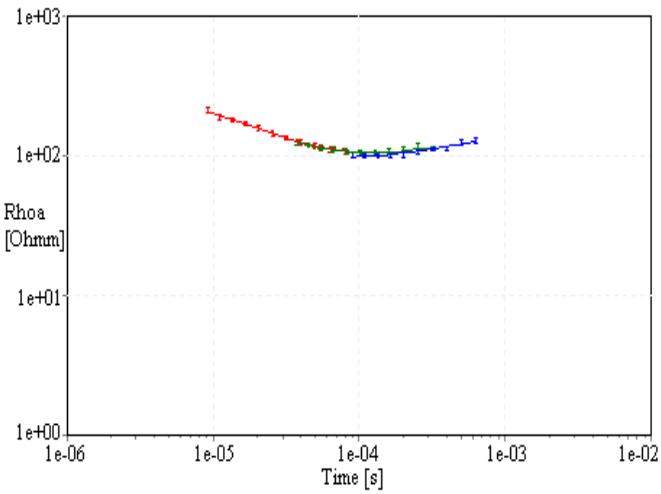

SM055T: 4-Layered Model

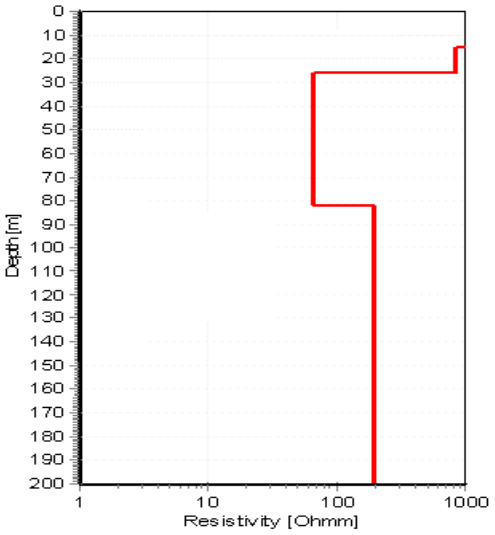

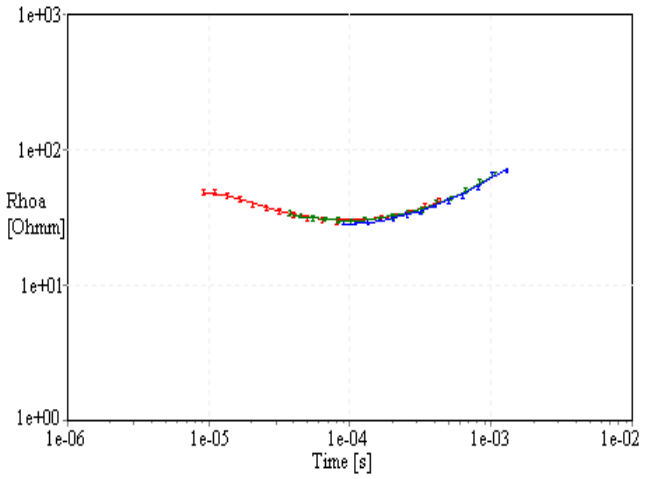

SM056T: 4-Layered Model

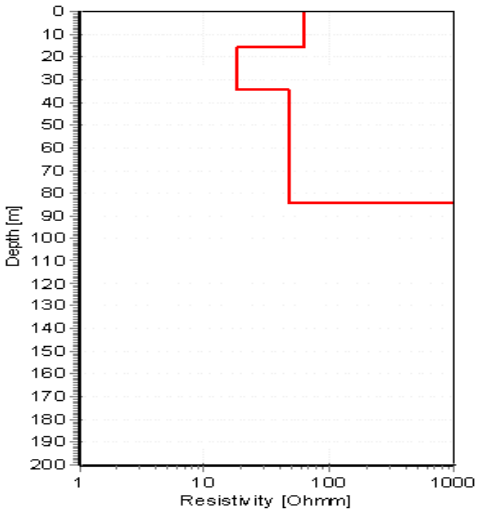

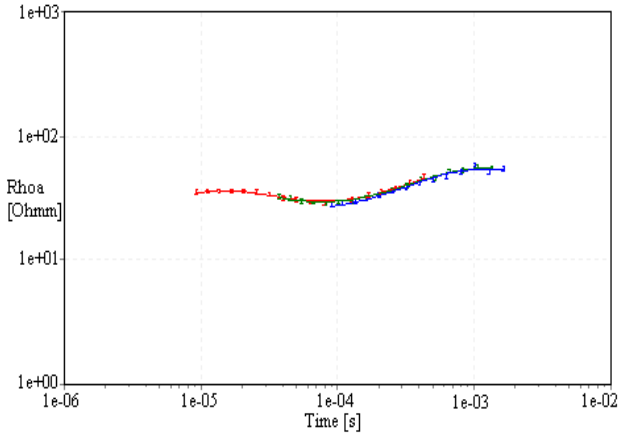

SM057T: 4-Layered Model

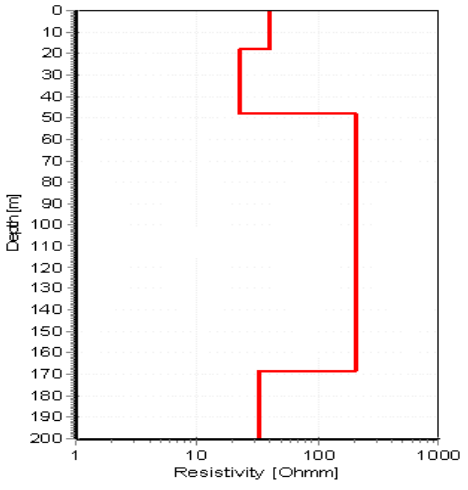

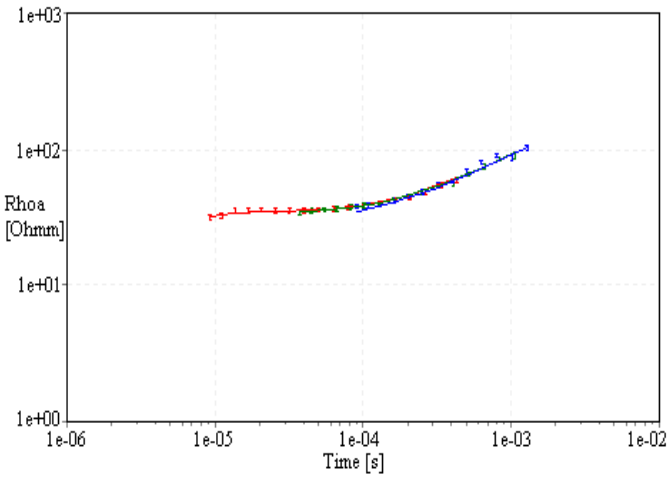

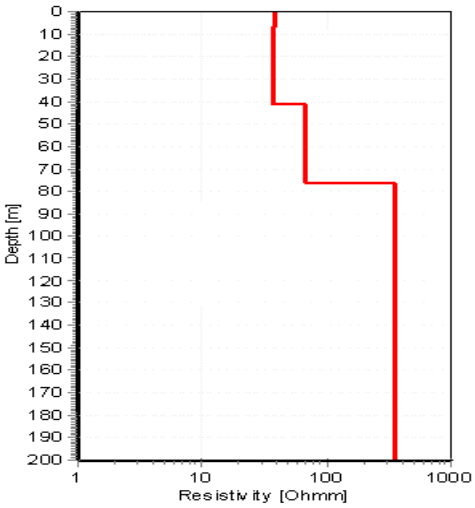

SM058T: 4-Layered Model

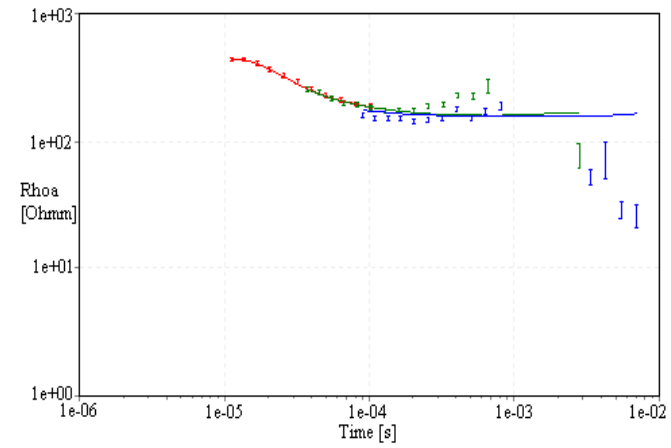

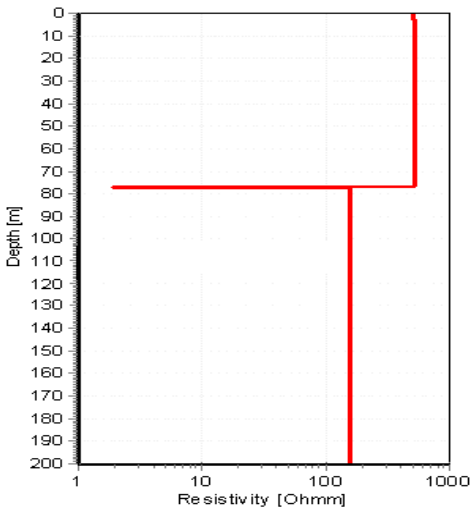

SM061T: 4-Layered Model

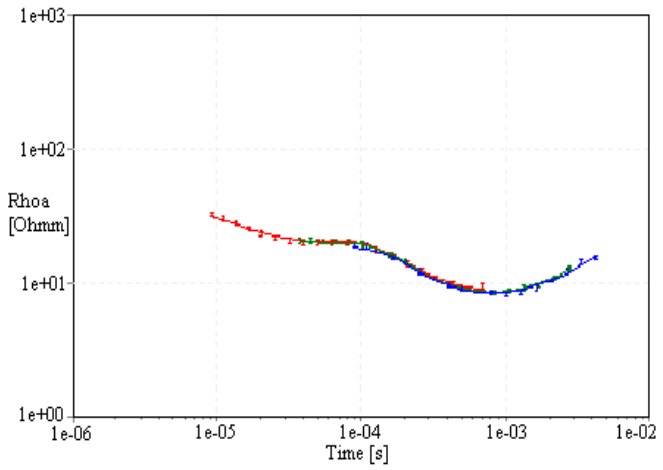

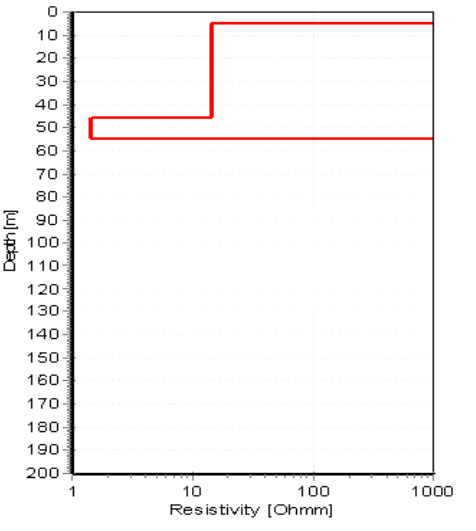

SM062T: 4-Layered Model

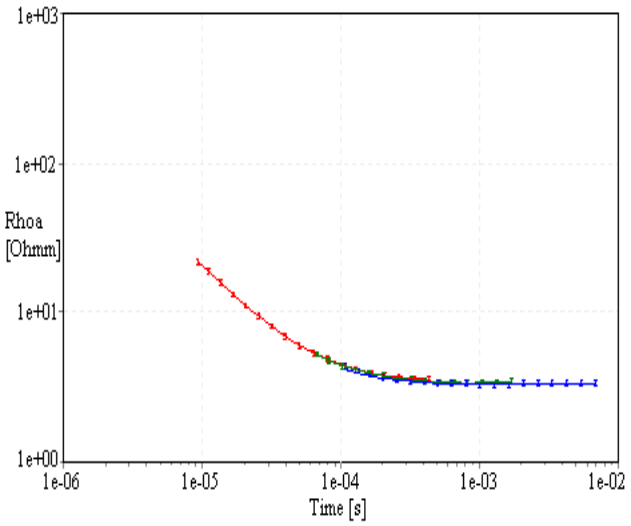

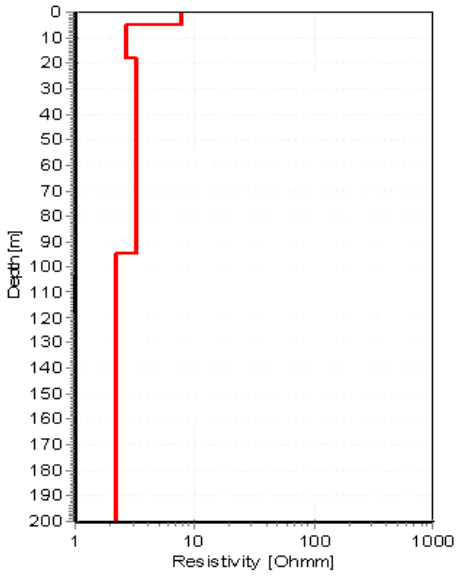

SM066T: 4-Layered Model

Appendix 7: Apparent Resistivity Data (in error bars) and Line Model (right panel) for a 5-layered Model in the Machile River Basin, South-Western, Zambia

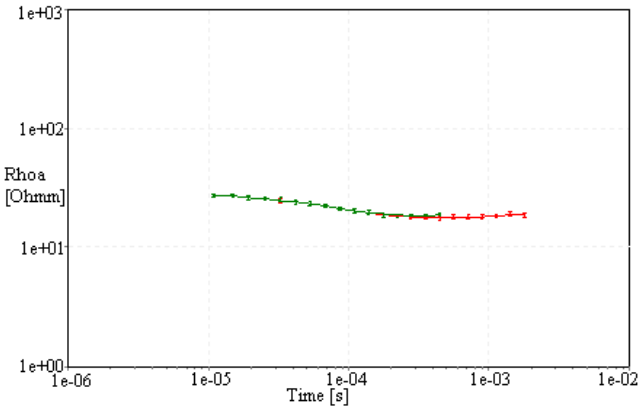

MT003: 5-Layered Model

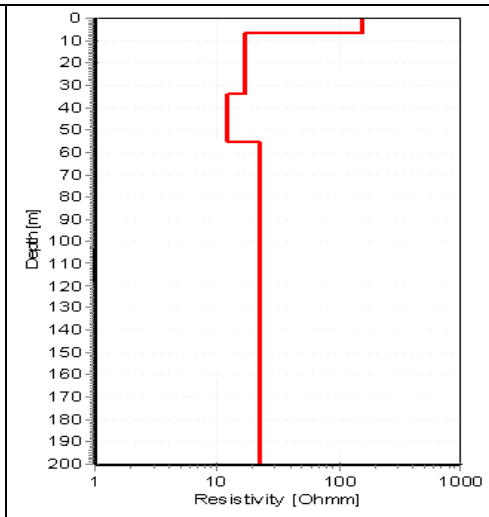

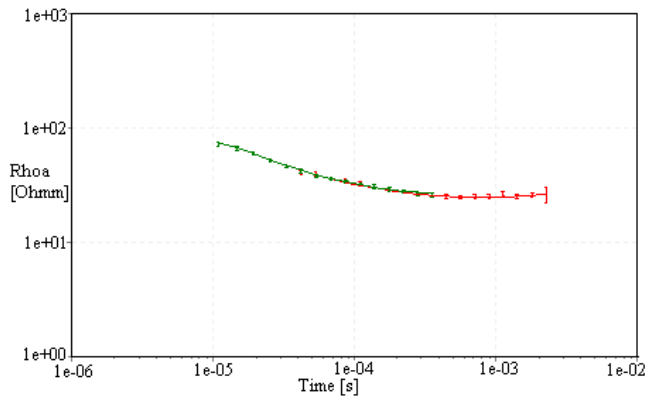

MT005: 5-Layered Model

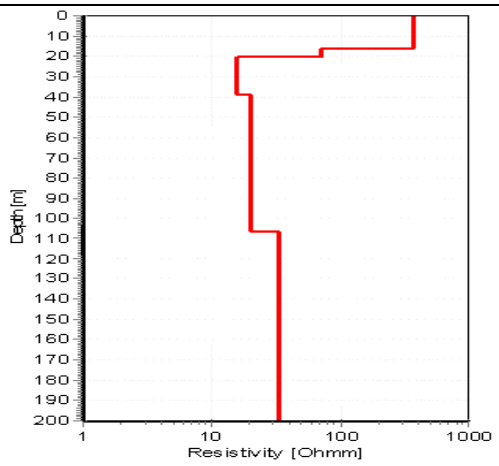

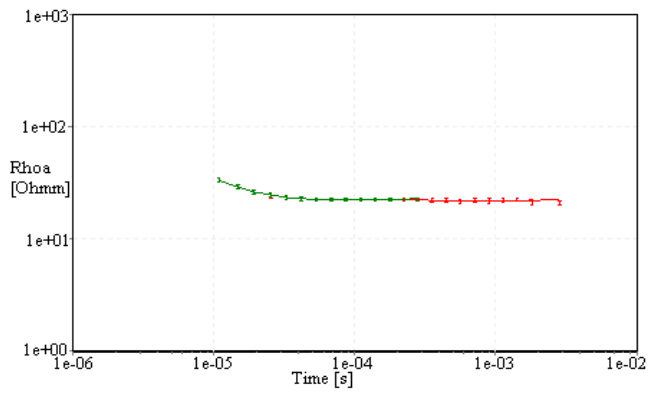

MT017: 5-Layered Model

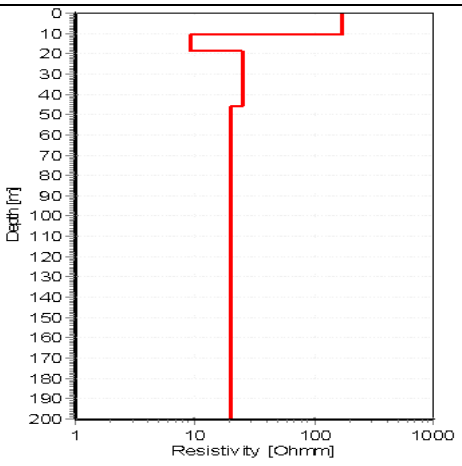

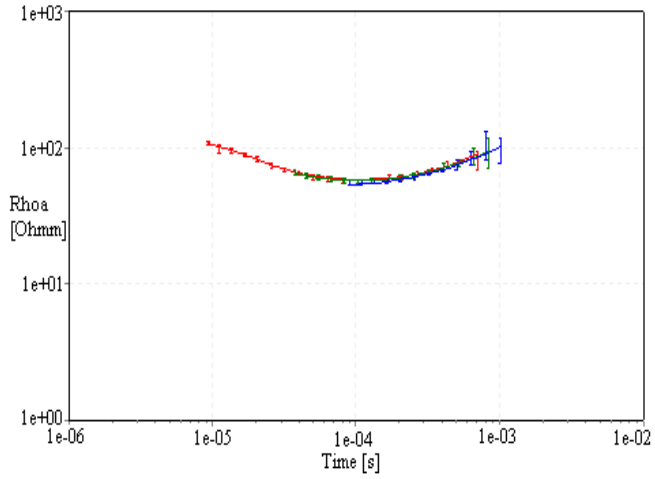

SM006T: 5-Layered Model

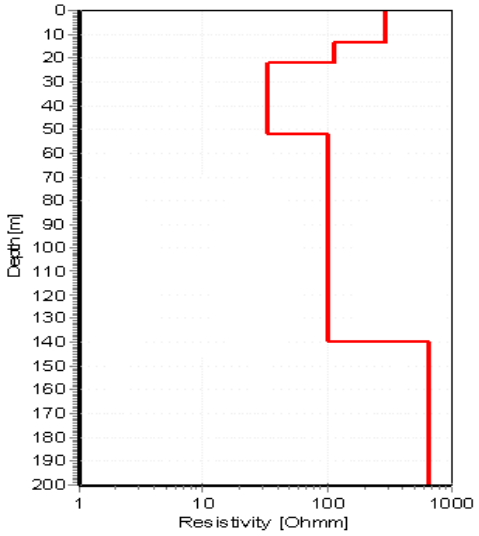

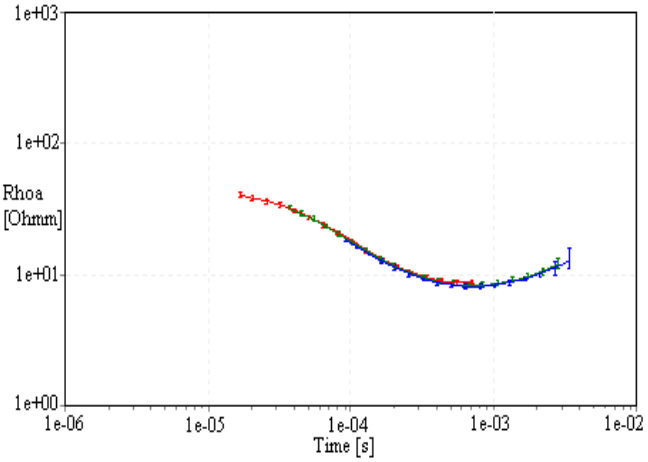

SM010T: 5-Layered Model

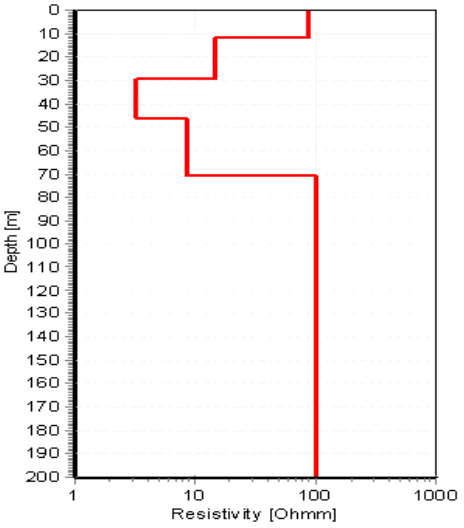

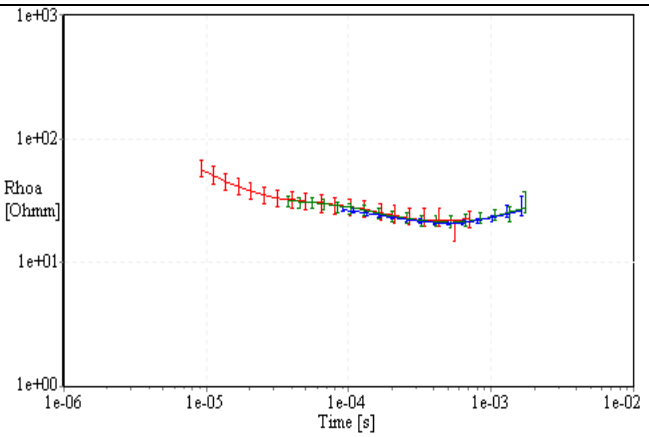

SM022T: 5-Layered Model

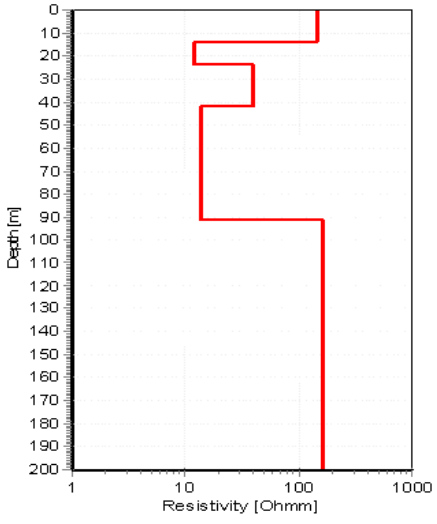

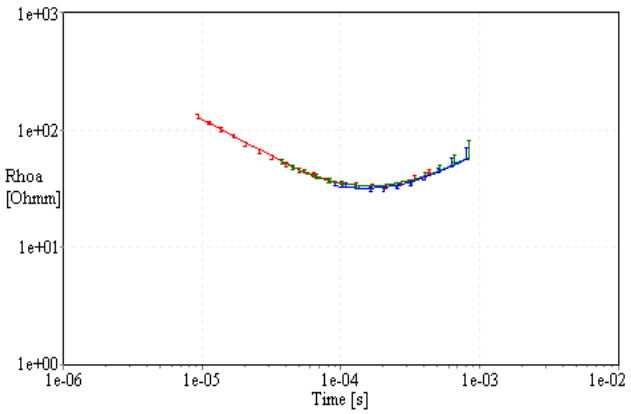

SM026T: 5-Layered Model

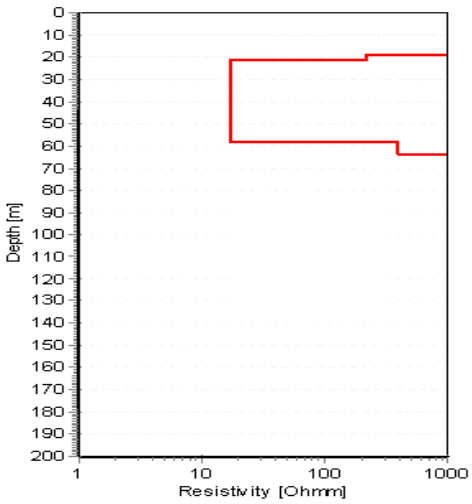

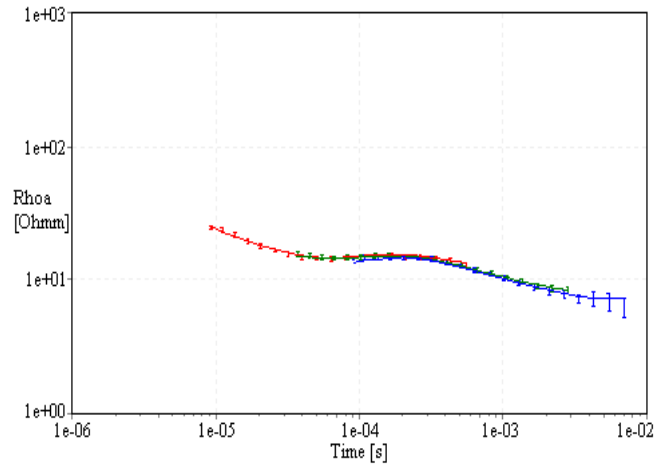

SM048T: 5-Layered Model

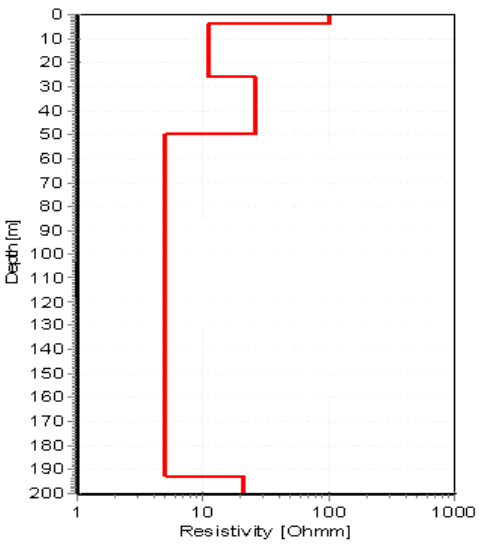

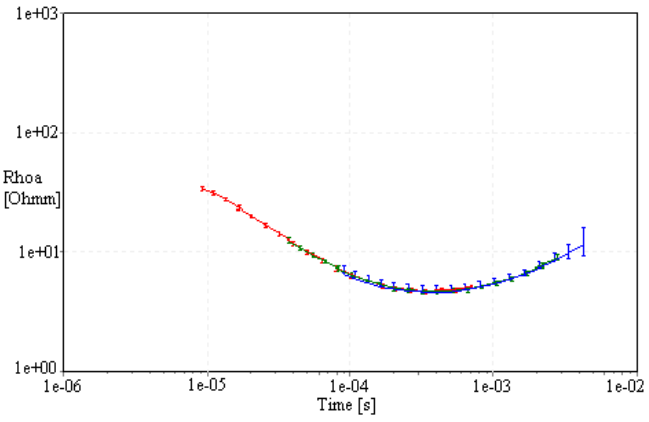

SM050T: 5-Layered Model

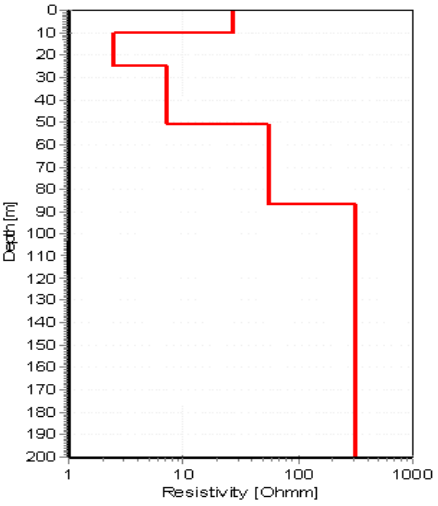

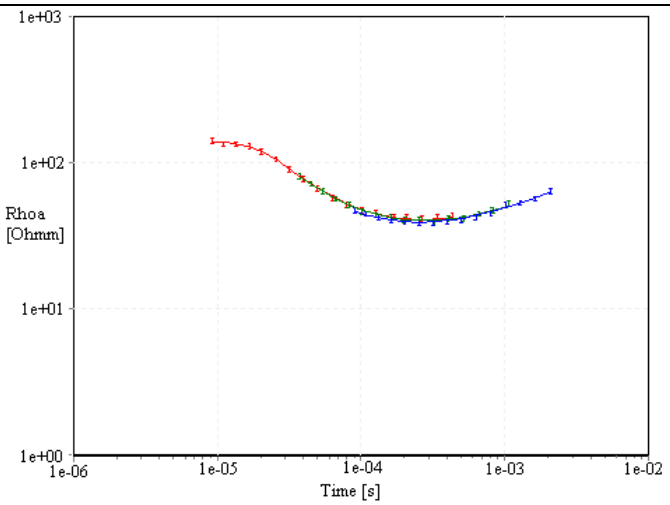

SM059T: 5-Layered Model

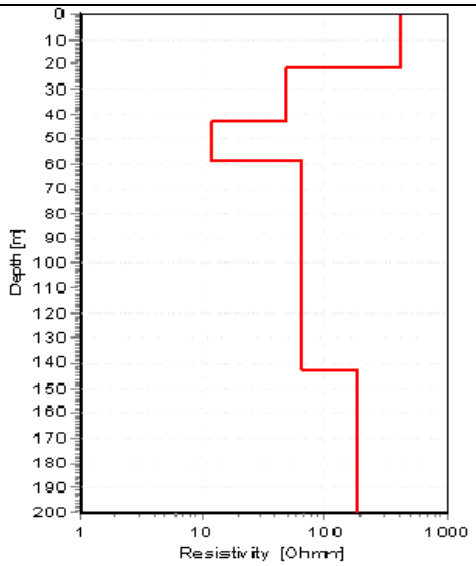

Appendix 8: Geological Data (243 to 256) for Machile River Basin in South-Western Zambia

IDENT	X	Y	ELEVTOP	ELEVBOT	SFC_ELEVATION
243	396661.535	8069678.019	1149	1147	1150
243	396661.535	8069678.019	1147	1144.5	1150
243	396661.535	8069678.019	1132	1106.5	1150
243	396661.535	8069678.019	1144.5	1132	1150
243	396661.535	8069678.019	1150	1149	1150
246	325020.9533	8164279.429	1015	1013	1015
246	325020.9533	8164279.429	1013	1007	1015
246	325020.9533	8164279.429	1007	997	1015
246	325020.9533	8164279.429	981	973	1015
246	325020.9533	8164279.429	973	955	1015
246	325020.9533	8164279.429	955	946.5	1015
246	325020.9533	8164279.429	997	981	1015
247	358539.5826	8047269.199	1023	1019	1023
247	358539.5826	8047269.199	1019	1017	1023
247	358539.5826	8047269.199	1017	920	1023
248	409989.3627	8114473.274	1221	1219	1221
248	409989.3627	8114473.274	1219	1118	1221
251	323028.3843	8104538.684	982	908	986
251	323028.3843	8104538.684	908	896	986
251	323028.3843	8104538.684	896	882	986
251	323028.3843	8104538.684	882	870.5	986
251	323028.3843	8104538.684	986	982	986
252	393686.9895	8065619.595	1195	1157	1197
252	393686.9895	8065619.595	1157	1145	1197
252	393686.9895	8065619.595	1129	1127	1197
252	393686.9895	8065619.595	1135	1129	1197
252	393686.9895	8065619.595	1127	1111	1197
252	393686.9895	8065619.595	1197	1195	1197
252	393686.9895	8065619.595	1145	1135	1197
254	390059.6632	8065477.391	1165	1151	1169
254	390059.6632	8065477.391	1151	1108	1169
254	390059.6632	8065477.391	1169	1165	1169
255	347211.4509	8028338.071	914	836	916
255	347211.4509	8028338.071	916	914	916
256	354205.7066	8047544.667	1010	1000	1010
256	354205.7066	8047544.667	980	974	1010
256	354205.7066	8047544.667	974	941	1010
256	354205.7066	8047544.667	1000	980	1010

ROCKVALUE	LID	DTOP	DBOT	VALSTRING	DESCRIPTION
4	2	1	3	c	clay
15	3	3	5.5	sc	schist
17	5	18	43.5	gra	granite
18	4	5.5	18	gne	gneiss
19	1	0	1	cwg	clay with gravel
1	1	0	2	fs	fine sand
3	2	2	8	ss	sandstone
3	3	8	18	ss	sandstone
3	5	34	42	ss	sandstone
3	6	42	60	ss	sandstone
3	7	60	68.5	ss	sandstone
12	4	18	34	mus	mudstone
1	1	0	4	fs	fine sand
3	2	4	6	ss	sandstone
6	3	6	103	ba	basalt
8	1	0	2	l	laterite
20	2	2	103	gra-gne	granite and gneiss
3	2	4	78	ss	sandstone
3	3	78	90	ss	sandstone
3	4	90	104	ss	sandstone
3	5	104	115.5	ss	sandstone
22	1	0	4	ms	medium sand
1	2	2	40	fs	fine sand
3	3	40	52	ss	sandstone
3	6	68	70	ss	sandstone
4	5	62	68	c	clay
6	7	70	86	ba	basalt
14	1	0	2	surfs	surface soil
22	4	52	62	ms	medium sand
3	2	4	18	ss	sandstone
3	3	18	61	ss	sandstone
14	1	0	4	surfs	surface soil
6	2	2	80	ba	basalt
14	1	0	2	surfs	surface soil
1	1	0	10	fs	fine sand
3	3	30	36	ss	sandstone
6	4	36	69	ba	basalt
10	2	10	30	swc	sand with clay
1	1	0	8	fs	fine sand
3	4	20	30	ss	sandstone
4	3	10	20	c	clay
6	5	30	55	ba	basalt
21	2	8	10	swg	sand and gravel

Appendix 9: Geological data (258 to 271) for Machile River Basin in South-Western Zambia

IDENT	X	Y	ELEVTOP	ELEVBOT	SFC_ELEVATION
258	357742.1694	8047509.224	1006	994	1012
258	357742.1694	8047509.224	994	963	1012
258	357742.1694	8047509.224	1012	1006	1012
259	356249.412	8060421.755	1046	1036	1046
259	356249.412	8060421.755	1032	983	1046
259	356249.412	8060421.755	1036	1032	1046
260	321584.3503	8032615.513	937	931	937
260	321584.3503	8032615.513	931	915	937
260	321584.3503	8032615.513	915	884	937
261	339043.1499	8082600.437	1021	913.5	1023
261	339043.1499	8082600.437	1023	1021	1023
262	324639.4107	8088184.922	894	992	994
262	324639.4107	8088184.922	990	982	994
262	324639.4107	8088184.922	962	928	994
262	324639.4107	8088184.922	992	990	994
262	324639.4107	8088184.922	976	962	994
262	324639.4107	8088184.922	994	908	994
262	324639.4107	8088184.922	908	894	994
262	324639.4107	8088184.922	982	976	994
263	366651.3868	8091034.257	1103	1101	1103
263	366651.3868	8091034.257	1101	1031	1103
266	310195.0822	8153109.883	993	989	993
266	310195.0822	8153109.883	985	965	993
266	310195.0822	8153109.883	955	938	993
266	310195.0822	8153109.883	989	985	993
266	310195.0822	8153109.883	965	955	993
267	314274.7776	8162926.063	1012	976	1016
267	314274.7776	8162926.063	974	952	1016
267	314274.7776	8162926.063	976	974	1016
267	314274.7776	8162926.063	1016	1012	1016
270	354120.3694	8046587.907	986	982	994
270	354120.3694	8046587.907	994	986	994
270	354120.3694	8046587.907	982	960	994
270	354120.3694	8046587.907	960	936	994
270	354120.3694	8046587.907	936	924	994
271	298497.343	8160609.377	1011	1007	1011
271	298497.343	8160609.377	979	948	1011
271	298497.343	8160609.377	1007	1001	1011
271	298497.343	8160609.377	1001	991	1011

ROCKVALUE	LID	DTOP	DBOT	VALSTRING	DESCRIPTION
3	2	6	18	ss	sandstone
6	3	18	49	ba	basalt
10	1	0	6	swc	sand with clay
1	1	0	10	fs	fine sand
6	3	14	63	ba	basalt
22	2	10	14	ms	medium sand
1	1	0	6	fs	fine sand
3	2	6	22	ss	sandstone
6	3	22	53	ba	basalt
17	2	2	109.5	gra	granite
19	1	0	2	cwg	clay with gravel
4	3	2	100	c	clay
6	5	4	12	ba	basalt
12	8	32	66	mus	mudstone
21	4	2	4	swg	sand and gravel
22	7	18	32	s	Sand
24	1	0	86	mro	metamorphic rock
25	2	86	100	sla	Slate
25	6	12	18	sla	Slate
14	1	0	2	surfs	surface soil
17	2	2	72	gra	granite
1	1	0	4	fs	fine sand
3	3	8	28	ss	sandstone
3	5	38	55	ss	sandstone
10	2	4	8	swc	sand with clay
12	4	28	38	mus	mudstone
3	2	4	40	ss	sandstone
3	4	42	64	ss	sandstone
12	3	40	42	mus	mudstone
21	1	0	4	swg	sand and gravel
3	2	8	12	ss	sandstone
10	1	0	8	swc	sand with clay
17	3	12	34	gra	granite
17	4	34	58	gra	granite
17	5	58	70	gra	granite
1	1	0	4	fs	fine sand
3	6	32	63	ss	sandstone
4	2	4	10	c	clay
10	3	10	20	swc	sand with clay

Appendix 10: Geological Data (271 to 283) for Machile River Basin in South-Western Zambia

IDENT	X	Y	ELEVTOP	ELEVBOT	SFC_ELEVATION
271	298497.343	8160609.377	987	979	1011
271	298497.343	8160609.377	991	987	1011
272	334375.4046	8172392.322	1051	1049	1051
272	334375.4046	8172392.322	1045	1037	1051
272	334375.4046	8172392.322	1021	1007	1051
272	334375.4046	8172392.322	995	987	1051
272	334375.4046	8172392.322	1031	1021	1051
272	334375.4046	8172392.322	1049	1045	1051
272	334375.4046	8172392.322	1007	995	1051
272	334375.4046	8172392.322	1037	1031	1051
273	298737.9266	8167818.085	1048	1038	1048
273	298737.9266	8167818.085	1028	1008	1048
273	298737.9266	8167818.085	1006	967	1048
273	298737.9266	8167818.085	1008	1006	1048
273	298737.9266	8167818.085	1038	1028	1048
274	383607.5845	8061165.748	1129	1099	1131
274	383607.5845	8061165.748	1099	1066	1131
274	383607.5845	8061165.748	1131	1129	1131
275	383539.0424	8060902.003	1133	1131	1133
275	383539.0424	8060902.003	1131	1077.5	1133
276	324094.6793	8162983.671	1015	1011	1015
276	324094.6793	8162983.671	1003	997	1015
276	324094.6793	8162983.671	981	961	1015
276	324094.6793	8162983.671	1011	1003	1015
276	324094.6793	8162983.671	997	981	1015
276	324094.6793	8162983.671	961	952	1015
278	337872.2246	8069480.244	983	979	983
278	337872.2246	8069480.244	947	909.5	983
278	337872.2246	8069480.244	971	955	983
278	337872.2246	8069480.244	955	947	983
278	337872.2246	8069480.244	979	973	983
278	337872.2246	8069480.244	973	971	983
280	406451.6557	8112134.243	1239	1237	1239
280	406451.6557	8112134.243	1229	1225	1239
280	406451.6557	8112134.243	1237	1229	1239
280	406451.6557	8112134.243	1225	1207	1239
280	406451.6557	8112134.243	1207	1199	1239
280	406451.6557	8112134.243	1199	1178	1239
283	414659.0255	8121290.449	1259	1251	1269

ROCKVALUE	LID	DTOP	DBOT	VALSTRING	DESCRIPTION
10	5	24	32	swc	sand with clay
26	4	20	24	sws	sand with silt
1	1	0	2	fs	fine sand
1	3	6	14	fs	fine sand
3	6	30	44	ss	sandstone
3	8	56	64	ss	sandstone
4	5	20	30	c	clay
8	2	2	6	l	laterite
12	7	44	56	mus	mudstone
22	4	14	20	s	sand
1	1	0	10	fs	fine sand
3	3	20	40	ss	sandstone
3	5	42	81	ss	sandstone
12	4	40	42	mus	mudstone
26	2	10	20	sws	sand with silt
6	2	2	32	ba	basalt
6	3	32	65	ba	basalt
14	1	0	2	surfs	surface soil
4	1	0	2	c	clay
6	2	2	55.5	ba	basalt
1	1	0	4	fs	fine sand
3	3	12	18	ss	sandstone
3	5	34	54	ss	sandstone
12	2	4	12	mus	mudstone
12	4	18	34	mus	mudstone
12	6	54	63	mus	mudstone
4	1	0	4	c	clay
6	6	36	73.5	ba	basalt
21	4	12	28	swg	Sand with gravel
21	5	28	36	sg	sand and gravel
22	2	4	10	ms	medium sand
26	3	10	12	sws	sand with silt
4	1	0	2	c	clay
5	3	10	14		meta quartzites
15	2	2	10	sc	schist
	4	14	32		
	5	32	40		
	6	40	61		
10	3	10	18	swc	sand with clay

Appendix 11: Geological Data (283 to 292) for Machile River Basin in South-Western Zambia

IDENT	X	Y	ELEVTOP	ELEVBOT	SFC_ELEVATION
283	414659.0255	8121290.449	1269	1267	1269
283	414659.0255	8121290.449	1251	1225	1269
283	414659.0255	8121290.449	1267	1259	1269
283	414659.0255	8121290.449	1225	1196	1269
284	384401.756	8096932.108	1166	1164	1166
284	384401.756	8096932.108	1164	1144	1166
284	384401.756	8096932.108	1144	1138	1166
284	384401.756	8096932.108	1138	1117	1166
287	304817.9759	8163957.436	995	989	1007
287	304817.9759	8163957.436	989	983	1007
287	304817.9759	8163957.436	983	959	1007
287	304817.9759	8163957.436	959	939.5	1007
287	304817.9759	8163957.436	1007	995	1007
289	331913.3028	8069972.917	973	971	977
289	331913.3028	8069972.917	949	941	977
289	331913.3028	8069972.917	971	967	977
289	331913.3028	8069972.917	941	935	977
289	331913.3028	8069972.917	977	973	977
289	331913.3028	8069972.917	967	963	977
289	331913.3028	8069972.917	957	953	977
289	331913.3028	8069972.917	963	957	977
289	331913.3028	8069972.917	953	949	977
290	358908.0884	8081920.683	1085	1083	1085
290	358908.0884	8081920.683	1083	1075	1085
290	358908.0884	8081920.683	1075	1071	1085
290	358908.0884	8081920.683	1071	1055	1085
290	358908.0884	8081920.683	1055	1047	1085
290	358908.0884	8081920.683	1047	1029	1085
290	358908.0884	8081920.683	1029	1005.5	1085
291	376229.1528	8100650.021	1178	1152	1180
291	376229.1528	8100650.021	1152	1142	1180
291	376229.1528	8100650.021	1142	1114	1180
291	376229.1528	8100650.021	1180	1178	1180
292	374363.2317	8100518.133	1176	1174	1176
292	374363.2317	8100518.133	1174	1172	1176
292	374363.2317	8100518.133	1172	1146	1176
292	374363.2317	8100518.133	1146	1143	1176
292	374363.2317	8100518.133	1143	1126	1176

ROCKVALUE	LID	DTOP	DBOT	VALSTRING	DESCRIPTION
14	1	0	2	surfs	surface soil
15	4	18	44	sc	schist
22	2	2	10	ms	medium sand
	5	44	73		
1	1	0	2	fs	fine sand
6	2	2	22	ba	basalt
6	3	22	28	ba	basalt
6	4	28	49	ba	basalt
3	2	12	18	ss	sandstone
3	3	18	24	ss	sandstone
3	4	24	48	ss	sandstone
12	5	48	67.5	mus	mudstone
26	1	0	12	sws	sand with silt
4	2	4	6	c	clay
4	8	28	36	c	clay
10	3	6	10	swc	Sand with Clay
10	9	36	42	swc	sand with clay
19	1	0	4	cwg	clay with gravel
19	4	10	14	cwg	clay with gravel
19	6	20	24	cwg	clay with gravel
	5	14	20	c	clay
28	7	24	28	grv	gravel
14	1	0	2	surfs	surface soil
19	2	2	10	cwg	clay with gravel
20	3	10	14	gra-gne	granite and gneiss
20	4	14	30	gra-gne	granite and gneiss
20	5	30	38	gra-gne	granite and gneiss
20	6	38	56	gra-gne	granite and gneiss
20	7	56	79.5	gra-gne	granite and gneiss
17	2	2	28	gra	granite
17	3	28	38	gra	granite
17	4	38	66	gra	granite
14	1	0	2	surfs	surface soil
14	1	0	2	surfs	surface soil
20	2	2	4	gra-gne	granite and gneiss
20	3	4	30	gra-gne	granite and gneiss
20	4	30	33	gra-gne	granite and gneiss
20	5	33	50	gra-gne	granite and gneiss

Appendix 12: Geological Data (292 to 302) for Machile River Basin in South-Western Zambia

IDENT	X	Y	ELEVTOP	ELEVBOT	SFC_ELEVATION
292	374363.2317	8100518.133	1126	1122	1176
292	374363.2317	8100518.133	1122	1106	1176
293	374952.6595	8100315.905	1181	1161	1181
293	374952.6595	8100315.905	1161	1131	1181
293	374952.6595	8100315.905	1131	1114	1181
294	387279.0256	8068689.733	1122	1109	1134
294	387279.0256	8068689.733	1130	1126	1134
294	387279.0256	8068689.733	1126	1122	1134
294	387279.0256	8068689.733	1134	1130	1134
294	387279.0256	8068689.733	1088	1074	1134
294	387279.0256	8068689.733	1109	1094	1134
294	387279.0256	8068689.733	1094	1088	1134
295	387296.9693	8068136.586	1147	1145	1147
295	387296.9693	8068136.586	1145	1141	1147
295	387296.9693	8068136.586	1141	1107	1147
295	387296.9693	8068136.586	1107	1092	1147
299	329654.8891	8065932.194	922	906.5	972
299	329654.8891	8065932.194	972	922	972
300	368074.3313	8093787.668	1107	1105	1107
300	368074.3313	8093787.668	1105	1095	1107
300	368074.3313	8093787.668	1095	1077	1107
300	368074.3313	8093787.668	1077	1059	1107
300	368074.3313	8093787.668	1059	1051.5	1107
301	397267.0999	8069840.426	1133	1129	1151
301	397267.0999	8069840.426	1121	1103	1151
301	397267.0999	8069840.426	1089	1085	1151
301	397267.0999	8069840.426	1081	1048	1151
301	397267.0999	8069840.426	1147	1143	1151
301	397267.0999	8069840.426	1143	1133	1151
301	397267.0999	8069840.426	1129	1121	1151
301	397267.0999	8069840.426	1103	1089	1151
301	397267.0999	8069840.426	1085	1081	1151
301	397267.0999	8069840.426	1151	1147	1151
302	396907.1926	8069819.79	1141	1135	1145
302	396907.1926	8069819.79	1145	1143	1145
302	396907.1926	8069819.79	1143	1141	1145
302	396907.1926	8069819.79	1135	1127	1145
302	396907.1926	8069819.79	1127	1101	1145
302	396907.1926	8069819.79	1101	1089	1145

ROCKVALUE	LID	DTOP	DBOT	VALSTRING	DESCRIPTION
20	6	50	54	gra-gne	granite and gneiss
20	7	54	70	gra-gne	granite and gneiss
17	1	0	20	gra	granite
17	2	20	50	gra	granite
17	3	50	67	gra	granite
3	4	12	25	ss	sandstone
4	2	4	8	c	clay
12	3	8	12	mus	mudstone
14	1	0	4	surfs	surface soil
15	7	46	60	sc	Schist
20	5	25	40	gra-gne	granite and gneiss
20	6	40	46	gra-gne	granite and gneiss
1	1	0	2	fs	fine sand
1	2	2	6	fs	fine sand
1	3	6	40	fs	fine sand
6	4	40	55	ba	basalt
1	2	50	65.5	fs	fine sand
10	1	0	50	cws	clay with sand
1	1	0	2	fs	fine sand
17	2	2	12	gra	granite
17	3	12	30	gra	granite
17	4	30	48	gra	granite
17	5	48	55.5	gra	granite
5	4	18	22		meta quartzites
5	6	30	48		meta quartzites
5	8	62	66		meta quartzites
5	10	70	103		meta quartzites
15	2	4	8	sc	schist
15	3	8	18	sc	schist
15	5	22	30	sc	schist
15	7	48	62	sc	schist
15	9	66	70	sc	schist
21	1	0	4	sg	sand and gravel
5	3	4	10		meta quartzites
14	1	0	2	surfs	surface soil
20	2	2	4	gra-gne	granite and gneiss
20	4	10	18	gra-gne	granite and gneiss
20	5	18	44	gra-gne	granite and gneiss
20	6	44	56	gra-gne	granite and gneiss

Appendix 13: Geological Data (302 to 325) for Machile River Basin in South-Western Zambia

IDENT	X	Y	ELEVTOP	ELEVBOT	SFC_ELEVATION
302	396907.1926	8069819.79	1089	1085	1145
302	396907.1926	8069819.79	1085	1075	1145
303	361756.0464	8083366.537	1040	1006	1088
303	361756.0464	8083366.537	1086	1040	1088
303	361756.0464	8083366.537	1088	1086	1088
305	400041.6313	8114255.228	1226	1222	1232
305	400041.6313	8114255.228	1222	1153	1232
305	400041.6313	8114255.228	1232	1230	1232
305	400041.6313	8114255.228	1228	1226	1232
305	400041.6313	8114255.228	1230	1228	1232
306	400269.5192	8108248.529	1187	1185	1187
306	400269.5192	8108248.529	1183	1177	1187
306	400269.5192	8108248.529	1177	1114	1187
306	400269.5192	8108248.529	1185	1183	1187
312	382336.3522	8100134.729	1141	1135	1167
312	382336.3522	8100134.729	1135	1107	1167
312	382336.3522	8100134.729	1093	1087	1167
312	382336.3522	8100134.729	1167	1141	1167
312	382336.3522	8100134.729	1107	1093	1167
312	382336.3522	8100134.729	1087	1076	1167
313	386955.6822	8074312.221	1055	1047	1075
313	386955.6822	8074312.221	1075	1073	1075
313	386955.6822	8074312.221	1073	1063	1075
313	386955.6822	8074312.221	1063	1055	1075
313	386955.6822	8074312.221	1047	982	1075
314	355972.4872	8074138.474	1021	1015	1021
314	355972.4872	8074138.474	1015	963	1021
318	358380.9771	8063934.819	1059	1057	1059
318	358380.9771	8063934.819	1055	990.5	1059
318	358380.9771	8063934.819	1057	1055	1059
319	359765.8814	8063280.512	1062	1052	1062
319	359765.8814	8063280.512	1052	1048	1062
319	359765.8814	8063280.512	1048	981	1062
320	310326.653	8069763.744	951	949	951
320	310326.653	8069763.744	949	847.5	951
325	316137.6796	8113955.805	919	901	973
325	316137.6796	8113955.805	937	933	973
325	316137.6796	8113955.805	955	945	973

ROCKVALUE	LID	DTOP	DBOT	VALSTRING	DESCRIPTION
20	7	56	60	gra-gne	granite and gneiss
20	8	60	70	gra-gne	granite and gneiss
12	3	48	82	mus	mudstone
17	2	2	48	gra	granite
19	1	0	2	cwg	clay with gravel
17	4	6	10	gra	granite
17	5	10	79	gra	granite
22	1	0	2	ms	medium sand
22	3	4	6	ms	medium sand
	2	2	4	sco	sand core
10	1	0	2	cws	clay with sand
20	3	4	10	gra-gne	granite and gneiss
20	4	10	73	gra-gne	granite and gneiss
27	2	2	4	s	silt
5	2	26	32		meta quartzites
5	3	32	60		meta quartzites
5	5	74	80		meta quartzites
17	1	0	26	gra	granite
17	4	60	74	gra	granite
17	6	80	91	gra	granite
5	4	20	28		meta quartzites
10	1	0	2	cws	clay with sand
17	2	2	12	gra	granite
20	3	12	20	gra-gne	granite and gneiss
20	5	28	93	gra-gne	granite and gneiss
10	1	0	6	cws	clay with sand
17	2	6	58	gra	granite
1	1	0	2	fs	Fine sand
6	3	4	68.5	ba	basalt
21	2	2	4	sg	Sand and Gravel
1	1	0	10	fs	Fine sand
3	2	10	14	ss	sandstone
6	3	14	81	ba	basalt
4	1	0	2	c	clay
17	2	2	103.5	gra	granite
3	6	54	72	ss	sandstone
10	4	36	40	cws	clay with sand
21	2	18	28	sg	Sand and Gravel

Appendix 14: Geological Data (325 to 346) for Machile River Basin in South-Western Zambia

IDENT	X	Y	ELEVTOP	ELEVBOT	SFC_ELEVATION
325	316137.6796	8113955.805	933	919	973
325	316137.6796	8113955.805	973	955	973
325	316137.6796	8113955.805	945	937	973
326	357072.0537	8077312.218	1051	1049	1051
326	357072.0537	8077312.218	1031	1025	1051
326	357072.0537	8077312.218	991	987	1051
326	357072.0537	8077312.218	1049	1031	1051
326	357072.0537	8077312.218	1025	991	1051
326	357072.0537	8077312.218	987	971	1051
332	334376.0949	8072258.611	984	980	984
332	334376.0949	8072258.611	974	868.5	984
332	334376.0949	8072258.611	980	974	984
333	383976.7849	8080151.009	1132	1130	1132
333	383976.7849	8080151.009	1126	1072	1132
333	383976.7849	8080151.009	1130	1126	1132
335	387040.8352	8083868.274	1123	1121	1123
335	387040.8352	8083868.274	1121	1075	1123
335	387040.8352	8083868.274	1075	1062	1123
336	379901.1591	8072160.547	1047	1031	1055
336	379901.1591	8072160.547	1055	1053	1055
336	379901.1591	8072160.547	1031	1005.5	1055
336	379901.1591	8072160.547	1053	1047	1055
340	314715.257	8129567.324	981	975	981
340	314715.257	8129567.324	975	967	981
340	314715.257	8129567.324	967	937	981
340	314715.257	8129567.324	909	889.5	981
340	314715.257	8129567.324	937	909	981
341	382626.1824	8117892.964	1139	1057	1139
342	337933.9944	8026810.159	924	922	924
342	337933.9944	8026810.159	922	821	924
343	336572.7301	8027229.502	922	920	922
343	336572.7301	8027229.502	920	819	922
344	358523.6884	8044864.39	1040	1034	1040
344	358523.6884	8044864.39	1030	972.5	1040
344	358523.6884	8044864.39	1034	1030	1040
345	409879.4828	8114533.649	1220	1117	1220
346	409869.0665	8114235.988	1206	1188	1214
346	409869.0665	8114235.988	1144	1134	1214

ROCKVALUE	LID	DTOP	DBOT	VALSTRING	DESCRIPTION
21	5	40	54	sg	Sand and Gravel
27	1	0	18	sws	Silt with Sand
27	3	28	36	sws	Silt with Sand
1	1	0	2	fs	Fine sand
6	3	20	26	ba	basalt
6	5	60	64	ba	basalt
17	2	2	20	gra	granite
17	4	26	60	gra	granite
17	6	64	80	gra	granite
4	1	0	4	c	clay
6	3	10	115.5	ba	basalt
21	2	4	10	sg	Sand and Gravel
4	1	0	2	c	clay
20	3	6	60	gra-gne	granite and gneiss
	2	2	6	basc	Basement complex
14	1	0	2	surfs	surface soil
17	2	2	48	gra	granite
	3	48	61		Meta-Volcanics
6	3	8	24	ba	basalt
14	1	0	2	surfs	surface soil
20	4	24	49.5	gra-gne	granite and gneiss
21	2	2	8	sg	Sand and Gravel
1	1	0	6	fs	Fine sand
1	2	6	14	fs	Fine sand
3	3	14	44	ss	sandstone
3	5	72	91.5	ss	sandstone
12	4	44	72	mus	mudstone
17	1	0	82	gra	granite
4	1	0	2	c	clay
6	2	2	103	ba	basalt
4	1	0	2	c	clay
6	2	2	103	ba	basalt
4	1	0	6	c	clay
6	3	10	67.5	ba	basalt
28	2	6	10	grv	gravel
20	1	0	103	gra-gne	granite and gneiss
5	3	8	26		meta quartzites
5	5	70	80		meta quartzites

Appendix 15: Geological Data (346 to 370) for Machile River Basin in South-Western Zambia

IDENT	X	Y	ELEVTOP	ELEVBOT	SFC_ELEVATION
346	409869.0665	8114235.988	1214	1212	1214
346	409869.0665	8114235.988	1212	1206	1214
346	409869.0665	8114235.988	1188	1144	1214
346	409869.0665	8114235.988	1134	1110.5	1214
347	412914.4842	8115355.338	1231	1225	1231
347	412914.4842	8115355.338	1225	1101	1231
351	347166.6952	8028368.713	917	913	917
351	347166.6952	8028368.713	913	837	917
352	345882.288	8027374.915	915	913	915
352	345882.288	8027374.915	913	812	915
353	345803.7527	8027251.461	913	911	913
353	345803.7527	8027251.461	911	828	913
354	346316.9976	8027494.495	910	812	915
354	346316.9976	8027494.495	915	910	915
355	346248.255	8027611.272	914	836	916
355	346248.255	8027611.272	916	914	916
356	398920.7366	8129694.059	1221	1215	1225
356	398920.7366	8129694.059	1223	1221	1225
356	398920.7366	8129694.059	1225	1223	1225
356	398920.7366	8129694.059	1215	1121.5	1225
357	399241.8483	8130027.522	1222	1220	1222
357	399241.8483	8130027.522	1218	1118.5	1222
357	399241.8483	8130027.522	1220	1218	1222
359	338951.0491	8082688.246	1026	1024	1026
359	338951.0491	8082688.246	1024	910.5	1026
360	324492.1948	8087869.346	987	979	991
360	324492.1948	8087869.346	971	911	991
360	324492.1948	8087869.346	991	987	991
360	324492.1948	8087869.346	979	971	991
368	403052.9376	8122155.854	1261	1259	1261
368	403052.9376	8122155.854	1251	1157.5	1261
368	403052.9376	8122155.854	1259	1251	1261
369	403049.3559	8121780.772	1183	1180	1257
369	403049.3559	8121780.772	1255	1253	1257
369	403049.3559	8121780.772	1257	1255	1257
369	403049.3559	8121780.772	1253	1183	1257
369	403049.3559	8121780.772	1180	1153.5	1257
370	387624.5275	8103462.567	1195	1193	1195
370	387624.5275	8103462.567	1193	1074	1195

ROCKVALUE	LID	DTOP	DBOT	VALSTRING	DESCRIPTION
10	1	0	2	cws	clay with sand
20	2	2	8	gra-gne	granite and gneiss
20	4	26	70	gra-gne	granite and gneiss
20	6	80	103.5	gra-gne	granite and gneiss
5	1	0	6		meta quartzites
20	2	6	130	gra-gne	granite and gneiss
4	1	0	4	c	clay
6	2	4	80	ba	basalt
6	1	0	2	ba	basalt
6	2	2	103	ba	basalt
1	1	0	2	fs	fine sand
6	2	2	85	ba	basalt
6	2	5	103	ba	basalt
14	1	0	5	surfs	surface soil
6	2	2	80	ba	basalt
19	1	0	2	cwg	clay with gravel
4	3	4	10	c	clay
8	2	2	4	l	laterite
14	1	0	2	surfs	surface soil
17	4	10	103.5	gra	granite
14	1	0	2	surfs	surface soil
17	3	4	103.5	gra	granite
19	2	2	4	cwg	clay with gravel
14	1	0	2	surfs	surface soil
17	2	2	115.5	gra	granite
3	2	4	12	ss	sandstone
3	4	20	80	ss	sandstone
10	1	0	4	cws	clay with sand
25	3	12	20	sla	Slate
1	1	0	2	fs	fine sand
17	3	10	103.5	gra	granite
21	2	2	10	sg	Sand and Gravel
5	4	74	77		meta quartzites
10	2	2	4	cws	clay with sand
14	1	0	2	surfs	surface soil
17	3	4	74	gra	granite
17	5	77	103.5	gra	granite
14	1	0	2	surfs	surface soil
20	2	2	121	gra-gne	granite and gneiss

Appendix 16: Geological Data (371 to 387) for Machile River Basin in South-Western Zambia

IDENT	X	Y	ELEVTOP	ELEVBOT	SFC_ELEVATION
371	387775.422	8102317.099	1196	1194	1196
371	387775.422	8102317.099	1146	1144	1196
371	387775.422	8102317.099	1194	1146	1196
371	387775.422	8102317.099	1144	1093	1196
372	383662.4281	8060859.561	1132	1056	1136
372	383662.4281	8060859.561	1136	1132	1136
375	409901.8268	8112816.647	1227	1223	1227
375	409901.8268	8112816.647	1223	1123.5	1227
376	409826.1975	8112588.405	1230	1228	1230
376	409826.1975	8112588.405	1228	1126.5	1230
377	310133.2632	8054515.087	877	861	941
377	310133.2632	8054515.087	941	915	941
377	310133.2632	8054515.087	915	887	941
377	310133.2632	8054515.087	887	877	941
378	310052.0515	8054458.978	940	930	940
378	310052.0515	8054458.978	916	910	940
378	310052.0515	8054458.978	910	895	940
378	310052.0515	8054458.978	930	916	940
379	381668.7746	8095997.095	1154	1152	1154
379	381668.7746	8095997.095	1152	1050.5	1154
380	381668.7746	8095997.095	1050.5	1152	1154
380	381668.7746	8095997.095	1152	1051	1154
382	331996.5389	8069927.125	971	967	977
382	331996.5389	8069927.125	977	975	977
382	331996.5389	8069927.125	975	971	977
382	331996.5389	8069927.125	959	921	977
382	331996.5389	8069927.125	967	959	977
382	331996.5389	8069927.125	921	911	977
383	349409.4653	8077677.522	1035	1033	1035
383	349409.4653	8077677.522	1029	931.5	1035
383	349409.4653	8077677.522	1033	1029	1035
384	349563.8254	8077638.824	1033	955	1035
384	349563.8254	8077638.824	931.5	1033	1035
385	363321.7743	8102676.524	1143	1141	1143
385	363321.7743	8102676.524	1141	1011	1143
386	362843.8174	8104004.533	1126	1124	1126
386	362843.8174	8104004.533	1124	1023	1126
387	373539.8178	8097940.466	1158	1156	1158

ROCKVALUE	LID	DTOP	DBOT	VALSTRING	DESCRIPTION
4	1	0	2	c	clay
5	3	50	52		meta quartzites
20	2	2	50	gra-gne	granite and gneiss
20	4	52	103	gra-gne	granite and gneiss
6	2	4	80	ba	basalt
14	1	0	4	surfs	surface soil
10	1	0	4	cws	clay with sand
20	2	4	103.5	gra-gne	granite and gneiss
8	1	0	2	l	laterite
20	2	2	103.5	gra-gne	granite and gneiss
1	4	64	80	fs	fine sand
4	1	0	26	c	clay
10	2	26	54	cws	clay with sand
21	3	54	64	swg	sand with gravel
4	1	0	10	c	clay
4	3	24	30	c	clay
10	4	30	45	cws	clay with sand
19	2	10	24	cwg	clay with gravel
14	1	0	2	surfs	surface soil
17	2	2	103.5	gra	granite
14	3	0	2	surfs	surface soil
17	4	2	103	gra	granite
1	3	6	10	fs	fine sand
4	1	0	2	c	clay
10	2	2	6	cws	clay with sand
10	5	18	56	cws	clay with sand
19	4	10	18	sg	clay with gravel
28	6	56	66	grv	gravel
10	1	0	2	cws	clay with sand
17	3	6	103.5	gra	granite
21	2	2	6	sg	sand and gravel
17	5	2	80	gra	granite
19	4	103.5	2	cwg	clay with gravel
3	1	0	2	ss	sandstone
17	2	2	132	gra	granite
1	1	0	2	fs	fine sand
17	2	2	103	gra	granite
1	1	0	2	fs	fine sand

Appendix 17: Geological Data (387 to 406) for Machile River Basin in South-Western Zambia

IDENT	X	Y	ELEVTOP	ELEVBOT	SFC_ELEVATION
387	373539.8178	8097940.466	1156	1152	1158
387	373539.8178	8097940.466	1152	1056	1158
388	373732.9782	8097312.046	1162	1160	1162
388	373732.9782	8097312.046	1160	1074	1162
389	374121.4517	8097437.247	1152	1150	1152
389	374121.4517	8097437.247	1150	1056	1152
390	374249.5508	8100671.245	1181	1179	1181
390	374249.5508	8100671.245	1179	1078	1181
391	367808.7218	8093752.766	1105	1103	1105
391	367808.7218	8093752.766	1095	1093	1105
391	367808.7218	8093752.766	1103	1095	1105
391	367808.7218	8093752.766	1093	1003	1105
392	367922.0635	8093655.012	1109	1107	1109
392	367922.0635	8093655.012	1107	1007	1109
393	361492.6938	8083489.797	1088	1010	1096
393	361492.6938	8083489.797	1096	1094	1096
393	361492.6938	8083489.797	1094	1088	1096
396	400041.6313	8114255.228	1232	1230	1232
396	400041.6313	8114255.228	1230	1228	1232
396	400041.6313	8114255.228	1228	1128.5	1232
397	399698.0337	8108276.75	1202	1076	1202
399	382297.533	8099295.797	1165	1163	1165
399	382297.533	8099295.797	1161	1153	1165
399	382297.533	8099295.797	1163	1161	1165
399	382297.533	8099295.797	1153	1091	1165
399	382297.533	8099295.797	1091	1044	1165
400	382332.0864	8099391.151	1168	1166	1168
400	382332.0864	8099391.151	1166	1047	1168
401	381242.7363	8100728.173	1175	1173	1175
401	381242.7363	8100728.173	1171	1169	1175
401	381242.7363	8100728.173	1173	1171	1175
401	381242.7363	8100728.173	1169	1072	1175
402	381872.5075	8100154.207	1169	1167	1169
402	381872.5075	8100154.207	1167	1066	1169
403	387463.6829	8074076.039	1072	1060	1086
403	387463.6829	8074076.039	1086	1084	1086
403	387463.6829	8074076.039	1060	983	1086
403	387463.6829	8074076.039	1084	1072	1086
406	330185.4069	8070557.269	975	971	975

ROCKVALUE	LID	DTOP	DBOT	VALSTRING	DESCRIPTION
3	2	2	6	ss	sandstone
17	3	6	102	gra	granite
1	1	0	2	fs	fine sand
17	2	2	88	gra	granite
3	1	0	2	ss	sandstone
17	2	2	96	gra	granite
14	1	0	2	surfs	surface soil
20	2	2	103	gra-gne	granite and gneiss
1	1	0	2	fs	fine sand
5	3	10	12		meta quartzites
17	2	2	10	gra	granite
17	4	12	102	gra	granite
1	1	0	2	fs	fine sand
17	2	2	102	gra	granite
17	3	8	86	gra	granite
19	1	0	2	cwg	clay with gravel
28	2	2	8	grv	gravel
4	1	0	2	c	clay
10	2	2	4	cws	clay with sand
17	3	4	103.5	gra	granite
17	1	0	126	gra	granite
4	1	0	2	c	clay
5	3	4	12		meta quartzites
17	2	2	4	gra	granite
17	4	12	74	gra	granite
17	5	74	121	gra	granite
4	1	0	2	c	clay
17	2	2	121	gra	granite
3	1	0	2	ss	sandstone
5	3	4	6		meta quartzites
17	2	2	4	gra	granite
17	4	6	103	gra	granite
8	1	0	2	l	laterite
17	2	2	103	gra	granite
5	3	14	26		meta quartzites
10	1	0	2	cws	clay with sand
20	4	26	103	gra-gne	granite and gneiss
22	2	2	14	ms	medium sand
10	1	0	4	cws	clay with sand

Appendix 18: Geological Data (406 to 449) for Machile River Basin in South-Western Zambia

IDENT	X	Y	ELEVTOP	ELEVBOT	SFC_ELEVATION
406	330185.4069	8070557.269	971	900	975
411	380306.2304	8075522.306	1085	1083	1085
411	380306.2304	8075522.306	1083	982	1085
412	380078.1738	8075643.785	1081	1077	1081
412	380078.1738	8075643.785	1077	978	1081
413	357379.0412	8077627.537	1051	973	1053
413	357379.0412	8077627.537	1053	1051	1053
415	334467.1323	8072038.011	983	979	983
415	334467.1323	8072038.011	973	867	983
415	334467.1323	8072038.011	979	973	983
416	334692.1765	8071929.173	984	980	984
416	334692.1765	8071929.173	964	914	984
416	334692.1765	8071929.173	980	964	984
417	384239.8029	8080238.81	1119	1115	1135
417	384239.8029	8080238.81	1133	1131	1135
417	384239.8029	8080238.81	1135	1133	1135
417	384239.8029	8080238.81	1131	1119	1135
417	384239.8029	8080238.81	1115	1032	1135
419	375002.8807	8060220.21	1114	1013	1115
419	375002.8807	8060220.21	1115	1114	1115
420	374979.2805	8060259.899	1111	1010	1112
420	374979.2805	8060259.899	1112	1111	1112
421	387607.1536	8084471.105	1118	1116	1118
421	387607.1536	8084471.105	1116	1015	1118
424	379664.5997	8072288.609	1058	1037	1059
424	379664.5997	8072288.609	1059	1058	1059
424	379664.5997	8072288.609	1037	956	1059
426	382759.3985	8117866.052	1074	1072	1144
426	382759.3985	8117866.052	1144	1142	1144
426	382759.3985	8117866.052	1142	1074	1144
426	382759.3985	8117866.052	1072	1041	1144
448	393901.7233	8064963.477	1170	1146	1202
448	393901.7233	8064963.477	1142	1129	1202
448	393901.7233	8064963.477	1146	1142	1202
448	393901.7233	8064963.477	1129	1110	1202
448	393901.7233	8064963.477	1200	1180	1202
448	393901.7233	8064963.477	1202	1200	1202
448	393901.7233	8064963.477	1180	1170	1202
449	387226.1738	8069600.081	1064	1059	1120

ROCKVALUE	LID	DTOP	DBOT	VALSTRING	DESCRIPTION
19	2	4	75	cwg	clay with gravel
14	1	0	2	surfs	surface soil
20	2	2	103	gra-gne	granite and gneiss
10	1	0	4	scl	sand and clay
20	2	4	103	gra-gne	granite and gneiss
17	2	2	80	gra	granite
19	1	0	2	cwg	clay with gravel
4	1	0	4	c	clay
6	3	10	116	ba	Basalt
21	2	4	10	sg	Sand and Gravel
4	1	0	4	c	clay
6	3	20	70	ba	Basalt
10	2	4	20	scl	sand and clay
5	4	16	20		meta quartzites
8	2	2	4	l	laterite
14	1	0	2	surfs	surface soil
15	3	4	16	sc	schist
20	5	20	103	gra-gne	granite and gneiss
6	2	1	102	ba	basalt
22	1	0	1	ms	medium sand
6	2	1	102	ba	basalt
22	1	0	1	ms	medium sand
14	1	0	2	surfs	surface soil
17	2	2	103	gra	granite
6	2	1	22	ba	basalt
14	1	0	1	surfs	surface soil
20	3	22	103	gra-gne	granite and gneiss
5	3	70	72		meta quartzites
14	1	0	2	surfs	surface soil
17	2	2	70	gra	granite
17	4	72	103	gra	granite
1	4	32	56	fs	fine sand
3	6	60	73	ss	sandstone
4	5	56	60	c	clay
6	7	73	92	ba	basalt
10	2	2	22	swc	sand with clay
14	1	0	2	surfs	surface soil
21	3	22	32	sg	sand and gravel
5	4	56	61		meta quartzites

Appendix 19: Geological Data (449 to 459) for Machile River Basin in South-Western Zambia

IDENT	X	Y	ELEVTOP	ELEVBOT	SFC_ELEVATION
449	387226.1738	8069600.081	1118	1096	1120
449	387226.1738	8069600.081	1120	1118	1120
449	387226.1738	8069600.081	1096	1064	1120
453	378952.4955	8080582.119	1140	1128	1140
453	378952.4955	8080582.119	1128	1122	1140
453	378952.4955	8080582.119	1122	1119	1140
453	378952.4955	8080582.119	1119	1113	1140
453	378952.4955	8080582.119	1113	1101	1140
453	378952.4955	8080582.119	1101	1095	1140
453	378952.4955	8080582.119	1095	1092	1140
454	387252.6723	8084382.849	1129	1120	1129
454	387252.6723	8084382.849	1114	1105	1129
454	387252.6723	8084382.849	1105	1099	1129
454	387252.6723	8084382.849	1120	1114	1129
455	385852.8767	8110884.933	1187	1181	1187
455	385852.8767	8110884.933	1181	1172	1187
455	385852.8767	8110884.933	1172	1151	1187
457	356253.0958	8064081.367	1054	1048	1054
457	356253.0958	8064081.367	1048	1042	1054
457	356253.0958	8064081.367	1042	1027	1054
457	356253.0958	8064081.367	1027	1018	1054
458	382552.7074	8099683.413	1163	1160	1163
458	382552.7074	8099683.413	1160	1129	1163
458	382552.7074	8099683.413	1129	1112	1163
459	374652.4524	8100183.515	1173	1122	1177
459	374652.4524	8100183.515	1177	1173	1177

ROCKVALUE	LID	DTOP	DBOT	VALSTRING	DESCRIPTION
6	2	2	24	ba	basalt
14	1	0	2	surfs	surface soil
15	3	24	56	sc	schist
17	1	0	12	gra	granite
17	2	12	18	gra	granite
17	3	18	21	gra	granite
17	4	21	27	gra	granite
17	5	27	39	gra	granite
17	6	39	45	gra	granite
17	7	45	48	gra	granite
6	1	0	9	ba	basalt
6	3	15	24	ba	basalt
6	4	24	30	ba	basalt
	2	9	15		
17	1	0	6	gra	granite
17	2	6	15	gra	granite
17	3	15	36	gra	granite
6	1	0	6	ba	basalt
6	2	6	12	ba	basalt
6	3	12	27	ba	basalt
6	4	27	36	ba	basalt
14	1	0	3	surfs	surface soil
15	2	3	34	sc	schist
17	3	34	51	gra	granite
3	2	4	55	ss	sandstone
14	1	0	4	surfs	surface soil

Appendix 20: Geological Data (S1 toS9) for Machile River Basin in South-Western Zambia

IDENT	X	Y	ELEVTOP	ELEVBOT	SFC_ELEVATION
S1	266791.8559	8123892.324	1056	1041	1056
S1	266791.8559	8123892.324	1041	1038	1056
S1	266791.8559	8123892.324	1038	998	1056
S2	304925.1421	8112135.49	965	961	965
S2	304925.1421	8112135.49	961	959	965
S2	304925.1421	8112135.49	959	943	965
S2	304925.1421	8112135.49	943	913	965
S2	304925.1421	8112135.49	913	910	965
S2	304925.1421	8112135.49	910	870	965
S3	218941.922	8085112.313	1024	1006	1024
S3	218941.922	8085112.313	1006	962	1024
S3	218941.922	8085112.313	962	922	1024
S4	222586.4937	8083953.051	1020	992	1020
S4	222586.4937	8083953.051	992	920	1020
S5	202173.3919	8074571.172	963	961.5	963
S5	202173.3919	8074571.172	961.5	960	963
S5	202173.3919	8074571.172	960	920	963
S6a	221334.7355	8070046.635	975	965	975
S6a	221334.7355	8070046.635	965	954	975
S6a	221334.7355	8070046.635	954	952	975
S6a	221334.7355	8070046.635	952	944	975
S6a	221334.7355	8070046.635	944	929	975
S6a	221334.7355	8070046.635	929	925	975
S6a	221334.7355	8070046.635	925	922	975
S6a	221334.7355	8070046.635	922	882	975
S6b	220774.0554	8069592.84	965	953	965
S6b	220774.0554	8069592.84	953	947	965
S6b	220774.0554	8069592.84	947	934	965
S6b	220774.0554	8069592.84	934	926	965
S6b	220774.0554	8069592.84	926	886	965
S7a	279607.9587	8119818.636	988	958	988
S7a	279607.9587	8119818.636	958	952	988
S7a	279607.9587	8119818.636	952	940	988
S7a	279607.9587	8119818.636	940	900	988
S7b	279274.835	8119984.26	990	978	990
S7b	279274.835	8119984.26	978	938	990
S7b	279274.835	8119984.26	938	898	990
S9	289266.4151	8120272.1	980	976	980
S9	289266.4151	8120272.1	976	974	980

ROCKVALUE	LID	DTOP	DBOT	VALSTRING	DESCRIPTION
1	1	0	15	fs	fine sand
2	2	15	18	lg	laterite and gravel
3	3	18	58	ss	sandstone
1	1	0	4	fs	fine sand
4	2	4	6	c	clay
7	3	6	22	fss	fine sand and silt
3	4	22	52	ss	sandstone
5	5	52	55	q	quartzite
3	6	55	95	ss	sandstone
1	1	0	18	fs	fine sand
3	2	18	62	ss	sandstone
6	3	62	102	ba	basalt
1	1	0	28	fs	fine sand
3	2	28	100	ss	sandstone
1	1	0	1.5	fs	fine sand
8	2	1.5	3	l	laterite
6	3	3	43	ba	basalt
1	1	0	10	fs	fine sand
9	2	10	21	ls	limestone
3	3	21	23	ss	sandstone
9	4	23	31	ls	limestone
3	5	31	46	ss	sandstone
5	6	46	50	q	quartzite
3	7	50	53	ss	sand stone
6	8	53	93	ba	basalt
1	1	0	12	fs	fine sand
3	2	12	18	ss	sandstone
9	3	18	31	ls	limestone
3	4	31	39	ss	sandstone
6	5	39	79	ba	basalt
1	1	0	30	fs	fine sand
10	2	30	36	cfs	clayed fine sand
3	3	36	48	ss	sandstone
6	4	48	88	ba	basalt
16	1	0	12	cs	course sand
3	2	12	52	ss	sandstone
6	3	52	92	ba	basalt
7	1	0	4	fss	fine sand and silt
10	2	4	6	cfs	clayed fine sand

Appendix 21: Geological Data (S9 to S26) for Machile River Basin in South-Western Zambia

IDENT	X	Y	ELEVTOP	ELEVBOT	SFC_ELEVATION
S9	289266.4151	8120272.1	974	968	980
S9	289266.4151	8120272.1	968	928	980
S10	225751.3689	8069239.35	948	935	948
S10	225751.3689	8069239.35	935	918	948
S10	225751.3689	8069239.35	918	917	948
S10	225751.3689	8069239.35	917	877	948
S12	277031.8202	8141460.425	1057	1041	1057
S12	277031.8202	8141460.425	1041	1011	1057
S12	277031.8202	8141460.425	1011	971	1057
S16	205549.1485	8071555.914	960	954	960
S16	205549.1485	8071555.914	954	941	960
S16	205549.1485	8071555.914	941	901	960
S17	210216.0852	8066568.23	963	955	963
S17	210216.0852	8066568.23	955	949	963
S17	210216.0852	8066568.23	949	868	963
S18	266465.5581	8167736.563	1114	1110	1114
S18	266465.5581	8167736.563	1110	1098	1114
S18	266465.5581	8167736.563	1098	1082	1114
S18	266465.5581	8167736.563	1082	1070	1114
S18	266465.5581	8167736.563	1070	1042	1114
S18	266465.5581	8167736.563	1042	1002	1114
S19a	231613.0794	8171363.922	1020	984	1020
S19a	231613.0794	8171363.922	984	944	1020
S19b	231668.5101	8171672.214	1027	1023	1027
S19b	231668.5101	8171672.214	1023	985	1027
S19b	231668.5101	8171672.214	985	945	1027
S20	274139.4211	8155519.138	1122	1108	1122
S20	274139.4211	8155519.138	1108	1056	1122
S20	274139.4211	8155519.138	1056	1016	1122
S23	251084.5331	8112236.554	1014	1002	1014
S23	251084.5331	8112236.554	1002	962	1014
S23	251084.5331	8112236.554	962	922	1014
S24	272639.0007	8106948.467	968	956	968
S24	272639.0007	8106948.467	956	920	968
S24	272639.0007	8106948.467	920	880	968
S25	213438.2395	8076135.73	1005	997	1005
S25	213438.2395	8076135.73	997	959	1005
S25	213438.2395	8076135.73	959	919	1005
S26	272390.2654	8111260.074	976	948	976

ROCKVALUE	LID	DTOP	DBOT	VALSTRING	DESCRIPTION
7	3	6	12	fss	fine sand and silt
3	4	12	52	ss	sandstone
1	1	0	13	fs	fine sand
3	2	13	30	ss	sandstone
12	3	30	31	mus	mudstone
3	4	31	71	ss	sandstone
1	1	0	16	fs	fine sand
3	2	16	46	ss	sandstone
6	3	46	86	ba	basalt
1	1	0	6	fs	fine sand
3	2	6	19	ss	sandstone
6	3	19	59	ba	basalt
1	1	0	8	fs	fine sand
3	2	8	14	ss	sand stone
6	3	14	95	ba	basalt
1	1	0	4	fs	fine sand
1	2	4	16	sf	fine sand
7	3	16	32	fss	fine sand and silt
10	4	32	44	cfs	clayed fine sand
3	5	44	72	ss	sand stone
15	6	72	112	sc	Schist
1	1	0	36	fs	fine sand
6	2	36	76	ba	basalt
1	1	0	4	fs	fine sand
7	2	4	42	fss	fine sand and silt
6	3	42	82	ba	basalt
1	1	0	14	fs	fine sand
3	2	14	66	ss	sandstone
15	3	66	106	sc	Schist
1	1	0	12	fs	fine sand
3	2	12	52	ss	sandstone
6	3	52	92	ba	basalt
1	1	0	12	fs	fine sand
3	2	12	48	ss	sandstone
6	3	48	88	ba	basalt
1	1	0	8	fs	fine sand
3	2	8	46	ss	sandstone
6	3	46	86	ba	basalt
1	1	0	28	fs	fine sand

Appendix 22: Geological Data (S26 to U241) for Machile River Basin in South-Western Zambia

IDENT	X	Y	ELEVTOP	ELEVBOT	SFC_ELEVATION
S26	272390.2654	8111260.074	948	942	976
S26	272390.2654	8111260.074	942	940	976
S26	272390.2654	8111260.074	940	918	976
S26	272390.2654	8111260.074	918	878	976
S27	195811.2956	8134662.405	983	960	983
S27	195811.2956	8134662.405	960	959	983
S27	195811.2956	8134662.405	959	919	983
S28	221363.5273	8068167.439	948	940	948
S28	221363.5273	8068167.439	940	885	948
S28	221363.5273	8068167.439	885	845	948
S29	249553.0766	8087312.039	978	959	978
S29	249553.0766	8087312.039	959	954	978
S29	249553.0766	8087312.039	954	929	978
S29	249553.0766	8087312.039	929	889	978
U141	229623.5883	8082256.991	1009	981	1009
U141	229623.5883	8082256.991	981	937	1009
U141	229623.5883	8082256.991	937	897	1009
U211	284363.8283	8069248.967	936	935	936
U211	284363.8283	8069248.967	935	934	936
U211	284363.8283	8069248.967	934	932	936
U211	284363.8283	8069248.967	932	926	936
U211	284363.8283	8069248.967	926	922	936
U211	284363.8283	8069248.967	922	920	936
U211	284363.8283	8069248.967	920	914	936
U211	284363.8283	8069248.967	914	910	936
U211	284363.8283	8069248.967	910	870	936
U221	288005.5883	8068992.242	934	930	934
U221	288005.5883	8068992.242	930	922	934
U221	288005.5883	8068992.242	922	916	934
U221	288005.5883	8068992.242	916	912	934
U221	288005.5883	8068992.242	912	910	934
U221	288005.5883	8068992.242	910	906	934
U221	288005.5883	8068992.242	906	898	934
U221	288005.5883	8068992.242	898	858	934
U23	250962.9917	8112256.576	1015	1011	1015
U23	250962.9917	8112256.576	1011	967	1015
U23	250962.9917	8112256.576	967	927	1015
U241	272638.6814	8106948.464	968	966	968

ROCKVALUE	LID	DTOP	DBOT	VALSTRING	DESCRIPTION
3	2	28	34	ms	medium sand
7	3	34	36	fss	fine sand and silt
3	4	36	58	ss	sandstone
6	5	58	98	ba	basalt
1	1	0	23	fs	fine sand
3	2	23	24	ss	sandstone
6	3	24	64	ba	basalt
3	1	0	8	ms	mudstone
3	2	8	63	ss	sandstone
6	3	63	103	ba	basalt
1	1	0	19	fs	fine sand
12	2	19	24	mus	mudstone
3	3	24	49	ss	sandstone
6	4	49	89	ba	basalt
1	1	0	28	fs	fine sand
3	2	28	72	ss	sandstone
6	3	72	112	ba	basalt
1	1	0	1	fs	fine sand
4	2	1	2	c	clay
10	3	2	4	cfs	clayed fine sand
1	4	4	10	fs	fine sand
10	5	10	14	cfs	clayed fine sand
4	6	14	16	c	clay
3	7	16	22	ms	medium sand
10	8	22	26	cfs	clayed fine sand
1	9	26	66	fs	fine sand
4	1	0	4	c	clay
1	2	4	12	fs	fine sand
10	3	12	18	cfs	clayed fine sand
1	4	18	22	fs	fine sand
4	5	22	24	c	clay
1	6	24	28	fs	fine sand
9	7	28	36	ls	limestone
4	8	36	76	c	clay
3	1	0	4	ms	medium sand
3	2	4	48	ss	sandstone
6	3	48	88	ba	basalt
14	1	0	2	surfs	surface soil

Appendix 23: Geological Data (U241 to S8) for Machile River Basin in South-Western Zambia

IDENT	X	Y	ELEVTOP	ELEVBOT	SFC_ELEVATION
U241	272638.6814	8106948.464	966	958	968
U241	272638.6814	8106948.464	958	934	968
U241	272638.6814	8106948.464	934	894	968
U251	214005.8714	8076940.571	1006	986	1006
U251	214005.8714	8076940.571	986	982	1006
U251	214005.8714	8076940.571	982	976	1006
U251	214005.8714	8076940.571	976	946	1006
U251	214005.8714	8076940.571	946	906	1006
U142	228307.5601	8080803.021	1009	987	1009
U142	228307.5601	8080803.021	987	957	1009
U142	228307.5601	8080803.021	957	917	1009
U19b	231624.582	8171631.693	1026	1024	1026
U19b	231624.582	8171631.693	1024	983	1026
U19b	231624.582	8171631.693	983	943	1026
U212	284393.1664	8069267.766	936	935	936
U212	284393.1664	8069267.766	935	934	936
U212	284393.1664	8069267.766	934	932	936
U212	284393.1664	8069267.766	932	926	936
U212	284393.1664	8069267.766	926	922	936
U212	284393.1664	8069267.766	922	920	936
U212	284393.1664	8069267.766	920	914	936
U212	284393.1664	8069267.766	914	910	936
U212	284393.1664	8069267.766	910	870	936
U222	287952.3417	8069003.973	934	928	934
U222	287952.3417	8069003.973	928	922	934
U222	287952.3417	8069003.973	922	900	934
U222	287952.3417	8069003.973	900	884	934
U222	287952.3417	8069003.973	884	878	934
U222	287952.3417	8069003.973	878	874	934
U222	287952.3417	8069003.973	874	872	934
U222	287952.3417	8069003.973	872	832	934
U242	272648.0465	8106628.744	968	960	968
U242	272648.0465	8106628.744	960	932	968
U242	272648.0465	8106628.744	932	892	968
U252	213613.9605	8077085.799	1007	989	1007
U252	213613.9605	8077085.799	989	949	1007
S8	257003.464	8086430.002	969	957	969
S8	257003.464	8086430.002	957	931	969
S8	257003.464	8086430.002	931	891	969

ROCKVALUE	LID	DTOP	DBOT	VALSTRING	DESCRIPTION
1	2	2	10	fs	fine sand
3	3	10	34	ss	sandstone
6	4	34	74	ba	basalt
1	1	0	20	fs	fine sand
3	2	20	24	ss	sandstone
9	3	24	30	ls	limestone
3	4	30	60	ss	sandstone
6	5	60	100	ba	basalt
1	1	0	22	fs	fine sand
3	2	22	52	ss	sandstone
6	3	52	92	ba	basalt
14	1	0	2	surfs	surface soil
1	2	2	43	fs	fine sand
6	3	43	83	ba	basalt
1	1	0	1	fs	fine sand
4	2	1	2	c	clay
10	3	2	4	cfs	clayed fine sand
1	4	4	10	fs	fine sand
10	5	10	14	cfs	clayed fine sand
4	6	14	16	c	clay
1	7	16	22	fs	fine sand
10	8	22	26	cfs	clayed fine sand
1	9	26	66	fs	fine sand
4	1	0	6	c	clay
1	2	6	12	fs	fine sand
10	3	12	34	cfs	clayed fine sand
1	4	34	50	fs	fine sand
10	5	50	56	cfs	clayed fine sand
1	6	56	60	fs	fine sand
10	7	60	62	cfs	clayed fine sand
1	8	62	102	fs	fine sand
1	1	0	8	fs	fine sand
3	2	8	36	ss	sandstone
6	3	36	76	ba	basalt
1	1	0	18	fs	fine sand
6	2	18	58	ba	basalt
1	1	0	12	fs	fine sand
3	2	12	38	ss	sandstone
6	3	38	78	ba	basalt

Appendix 24: Geological Data (MT001 to MT009) for Pseudo Boreholes based on TDEM data in the Machile River Basin in South-Western Zambia

IDENT	X	Y	ELEVTOP	ELEVBOT	SFC_ELEVATION
MT001	389468.6373	8153831.411	1072.1899	1067.7899	1072.1899
MT001	389468.6373	8153831.411	1067.7899	1057.9899	1072.1899
MT001	389468.6373	8153831.411	1057.9899	980.2899	1072.1899
MT002	361638.9269	8155106.968	1024.36	1006.66	1024.36
MT002	361638.9269	8155106.968	1006.66	922.66	1024.36
MT003	338322.2059	8161028.886	1029.09	1017.99	1029.09
MT003	338322.2059	8161028.886	1017.99	967.39	1029.09
MT006	334406.7492	8180397.73	1041.96	1032.56	1041.96
MT006	334406.7492	8180397.73	1032.56	944.16	1041.96
MT007	348943.9717	8195154.693	1103.5601	1091.8601	1103.5601
MT007	348943.9717	8195154.693	1091.8601	1068.5601	1103.5601
MT008	334091.5081	8138587.149	989.14697	982.74697	989.14697
MT008	334091.5081	8138587.149	982.74697	953.64697	989.14697
MT009	349523.0995	8144623.085	1008.74	998.14	1008.74
MT009	349523.0995	8144623.085	992.64	992.64	1008.74

ROCKVALUE	LID	DTOP	DBOT	VALSTRING	DESCRIPTION
1	1	0	4.4	fs	fine sand
3	2	4.4	14.2	ss	sandstone
3	3	14.2	91.9	ss	sandstone
1	1	0	17.7	fs	fine sand
3	2	17.7	101.7	ss	sandstone
1	1	0	11.1	fs	fine sand
3	2	11.1	61.7	ss	sandstone
3	1	0	9.4	ss	sandstone
3	2	9.4	97.8	ss	sandstone
1	1	0	11.7	ss	sand
3	2	11.7	35	ss	sandstone
3	1	0	6.4	ss	sandstone
3	2	6.4	35.5	ss	sandstone
3	1	0	10.6	ss	sandstone
3	2	16.1	16.1	ss	sandstone

Appendix 25: Contents of the Computer Disc (CD)

The CD submitted together with this thesis contains the following information:

(i) Electronic copy of the thesis;

(ii) Geological modelling data to be opened in GeoScene3D software; and

(iii) The TDEM data for both the Sesheke and Kazungula sides of the Machile River Basin.